AXINTERNATIONAL JOURNAL OF COMPUTATIONAL ENGINEERING RESEARCH (IJCER)

ISSN: 2250-3005

VOLUME 2 Jan-Feb 2012 ISSUE 1

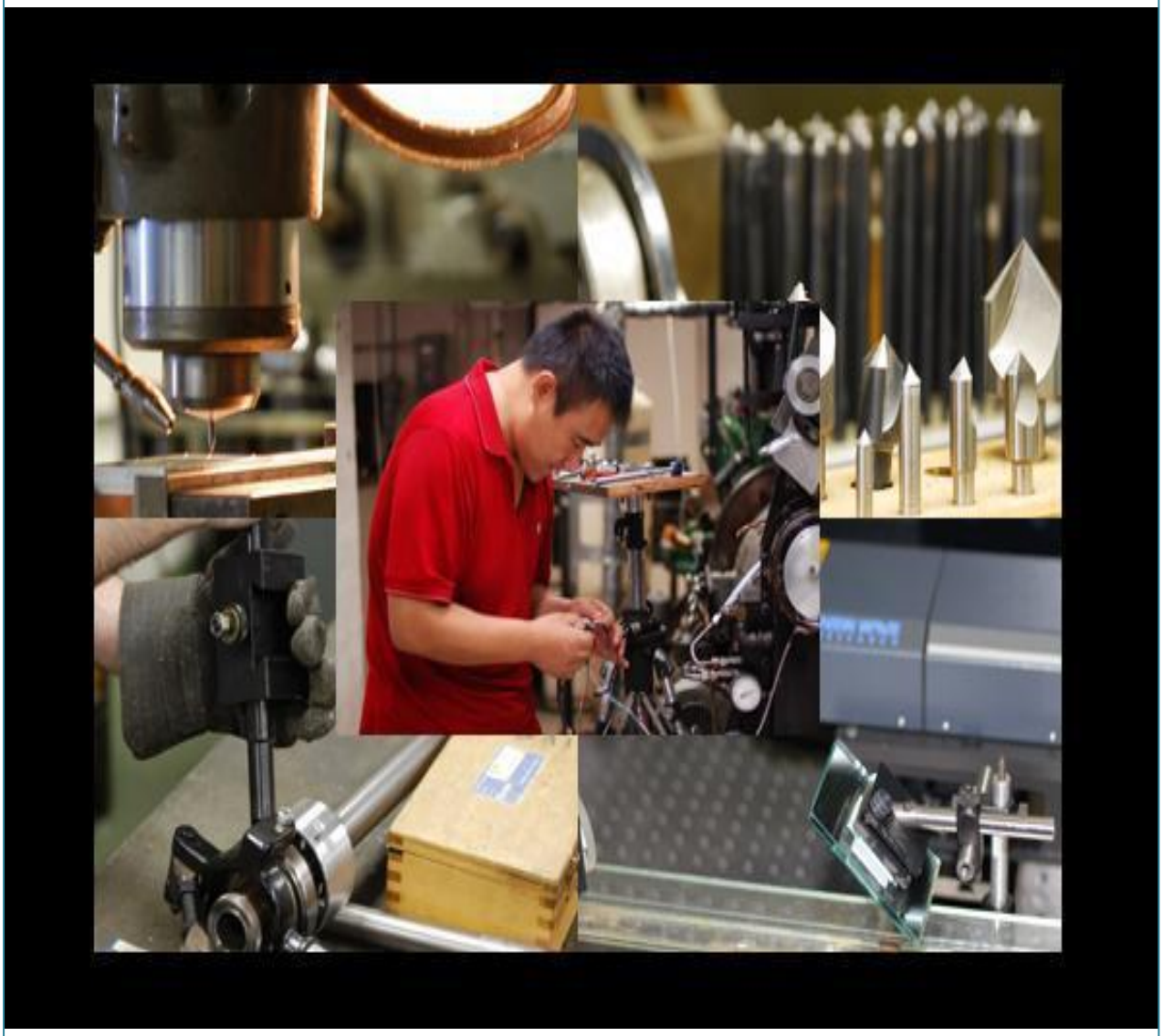

Email : ijceronline@gmail.com Url : www.ijceronline.com

INTERNATIONAL JOURNAL OF COMPUTATIONAL ENGINEERING RESAERCH (IJCER)

EDITORIAL BOARD

CONTENTS :

Development of an Optimal Routing Algorithm for MANET using Neural Networks

Anuj Kumar Chauhan[1], Sohan Garg[2]
1. Department of IT, RKGIT Ghaziabad (U.P.)
2. Department of MCA, RKGIT Ghaziabad (U.P.)

Abstract:
This paper evaluates a self-organizing routing protocol for Ad Hoc network, called the Neuron Routing Algorithm (NEURAL). NEURAL has been designed taking into ac- count the learning and self-organizing abilities of the brain. More precisely, it was inspired by the synapses process between neurons, when a signal is propagated. Basically, the most significant characteristic of NEURAL is the uniform distribution of the information around the node's location based on the current changes in its neighborhood. Using a 2-hop acknowledgment mechanism, local information is monitored in order to be used for route selection method, classification procedures and learning algorithms.

1 Introduction:

Inspired by the biological nervous system, Artificial Neural System (ANS) and neural networks are being applied to study a wide variety of problems in the areas of engineering and business [7, 22, and 18]. A neuron is the individual computational element that makes up most artificial neural system models [11]. A neuron presents three major parts called *dendrites*, the cell *body* and a single *axon*. *Dendrites* are nerve fibers that are connected to the cell *body* or soma, where the nucleus is located. Extending from the cell body is a single long fiber called the *axon*. At the ends of the neuron, terminal branches, synaptic junctions or *synapses* connect the axon with the dendrites of the following neurons [16]. In a ANS system, the information is propagated between neurons using electrical stimulation along dendrites. High stimulation signal produces an out- put to the other neighbor neurons and so the information takes the right way to the destination, where a reaction will occur. Otherwise, low stimulation signal will be blocked by the neurons and the information will be not transported. The *synapse* is defined as the communication process between neurons, when a signal is propagated. This means that the information is forwarded using electrical stimulations along dendrites. The modification of synaptic weights provides the traditional method for the design of neural networks. Such an approach is the closest to linear adaptive filter theory, which is already well established and successfully applied in such diverse fields as communications, control radar, sonar, seismology and biomedical engineering [14].

The characteristics described above are desirable in the context of Ad Hoc networks. The first association is the *synapse* process between neurons as the capacity of a processing element to communicate with others (Routing). Thus, the amount of neighbors around a node can be represented as a probabilistic weight value or "synaptic weight". Nodes are free to move randomly and organize themselves arbitrarily. This means that the ad hoc network's topology changes rapidly and unpredictably as well as synaptic weights are changed in the local environment. The advantage of Artificial Intelligent algorithms for control problem in complex systems is that the weights can be found by examining the performance of a network as controller rather than by providing correct control signals for various input data [24].

The goal behind this paper is described a novel routing Algorithm called Neuron Routing Algorithm (NEURAL), which it has been inspired by the synapses process. The design of NEURAL is based on three main phases, which apply some algorithms used in the area of neural networks. The *Pre-processing* phase involves a classification rule for Pattern Recognition called the K-Nearest Neighbor Rule. Afterwards, the *Route Discovery* phase considers an self- organizing algorithm based on the Kohonen model. And finally, the *Learning* phase employs a Trust and Reputation mechanism, which it has been integrated to the extension of the Kohonen model.

The rest of the paper is organized as follows: Section 2 introduces a background about Classification, Self-organizing and Artificial Intelligent System theory. The NEURAL architecture was developed in section 3 using the performance of three main modules. The conjunction of these modules provides tools to accomplish the implementation for a network simulator in section 4, and finally, conclusions in section 5.

2 Background of Artificial Neural Systems:

2.1 Preprocessing for Pattern Recognition:

The K-Nearest Neighbor Rule (K-NNR) [4] is proposed as simple classifiers algorithm which it is usually applied in the pattern recognition area. K-NNR assigns an object of unknown class to the plurality class among the *K* labeled "training" objects that are closer to it. Closeness is usually defined in terms of a metric distance on the Euclidean space with the input measurement variables as axes [14]. K-NNR Rule definition is enhanced as follows: Let *x* denote the center point of a small hyper sphere with volume V, which its radius grows until contains exactly *K* points irrespective of their class label. Based on this sample of *K* points, K_d points belong for example to the class C_d . So that the calculation of the class-conditional density for the point *x* is given by

$$p\,(x \text{ I } C_d) = K_d / (M_d \,.\, V) \qquad (1)$$

The unconditional density can be similarly estimated from

$$p\,(x) = K / (M \,.\, V) \qquad (2)$$

While the prior can be estimated using

$$p\,(C_d) = (M_d / M) \qquad (3)$$

Finally based on the Baye's theorem to give

$$p\,(C_d \text{ I } x) = p\,(x \text{ I } C_d)\,.\,p\,(C_d) / p\,(x) = K_d / K \qquad (4)$$

The eqn. 4 is known as the K-nearest-neighbor classification rule. It involves finding a hyper sphere around the point **x** which contains K points (independent of their class), and then assigning **x** to the class according to the largest number of representatives inside the hyper sphere [4].

2.2 Kohonen Model for Self-Organizing Systems:

The Kohonen model [17] employs a two-dimensional neuron layer. This layer is innervated by *d* input fibers (axons), which carry the input signal. This signal excites or inhibits the neurons of the layer via synaptic connections. We consider conditions under which the excitation of the neurons is restricted to a spatially localized region in the layer. The location of this region is then determined by those neurons that respond most intensively to the given stimulus. The mathematical formulation of the kohonen model is shown taking into account the three processes to define a Self-organizing system such as: *broadcasting of the input, selection of the winner, and adaptation* of the models in the spatial neighborhood of the winner.

2.2.1 Broadcasting of the input:

An incoming signal pattern or input vector **x** ($\mathbf{x} = x_1, x_2, ..., x_m$) represents the average activities x_l of the individual incoming fibers $l = 1, 2..., m$. The *strength* of the synapse or synaptic weight vector **w** between the neuron ***i*** and *m* neighbors is denoted by $\mathbf{w}_{i,j} = w_{i,1}, w_{i,2}, ..., w_{i,m}$. Suppose a incoming stimulus in neuron *i*. This neuron forms in its dendritic tree a weight sum as

$$\mathbf{net}_i = \sum_{j=1}^{m} wij.xj \qquad (5)$$

2.2.2 Selection of the "winner"

The above equations describe an active neuron ***i***, in which the total excitation is concentrated within a singles and connected *cluster* of ***j*** consecutive neurons. Kohonen suggests an approximation (*net*i) for eqn. 5 using the position of the maximum excitation on the basis external signal *xl* alone. More precisely, *net*i is determined from

$$\mathbf{net}_i = \sum_{j=1}^{m} wim.x\,m = \max\left(\sum_{j=1}^{m} \mathbf{w}\,ij\,.\,\mathbf{xj}\right) \qquad (6)$$

2.2.3 Adaptation procedure:

Helge et al. [15] enhanced an adaptation step for the kohonen model, in which every synaptic change is limited to a neighborhood zone about the excitation center (neuron *i*). In this zone, the synaptic connections are changed such that a subsequent re-occurrence of the same or a similar stimulus will lead to an increased excitation in the neighborhood.

2.3 Learning Process in Neural Networks:

Fischler et al. [8] defined learning as follows: *Learning is a process by which the free parameters of a neural network are adapted through a process of stimulation by the environment in which the network is embedded. The type of learning is determined by the manner in which the parameter changes take place*. In other words an effective learning process has a close relationship with the interaction between environment and neurons, which are ideally part of the medium.

Sensing trust and local reputation allows calculation of the control output variable that it was described by Ritter et al. [15] in the extended model of Kohonen. The implementation of a reputation management framework is enhanced for computing system in order to facilitate a distributed and efficient mechanism for resource selection and learning such as in the research area of Grid computing systems [10, 9]. For example, Alunkal et al. [1] applied a reputation management service based on community experiences to classify, select, and tune the allocation of entities, including resources and services provided by people. Grid systems introduce the term of Trust or Reputation such as defined Azzedin [2]: *"Trust is the firm belief in the competence of an entity to act as expected such that this firm belief is not a fixed value associated with the entity but rather it is subject to the entity's behavior and applies only within a specific context at a given time"*. On the other hand, reputation's definition is assumed as follows: *"the reputation of an entity is an expectation of its behavior based on other entities' observations or information about the entity's past behavior within a specific context at a given time"*.

3 Evaluating a modular architecture for NEURAL:

The conjunction of three phases, which consider algorithms normally applied in the area of neural networks, pro- vide robust and efficient tools to be implemented in NEU- RAL. The modular architecture in figure 1 shows these modules as *Pre-processing*, *Route Discovery* and *Learning*. In the Pre-processing module, the K-Nearest-Neighbors Rule (K-NNR) is employed in order to provide classification rule to sense continuous changes in the network. The Route Discovery module computes a self-organizing routing algorithm using the Kohonen model. Finally, the performance of a trust mechanism is carried up in the learning module.

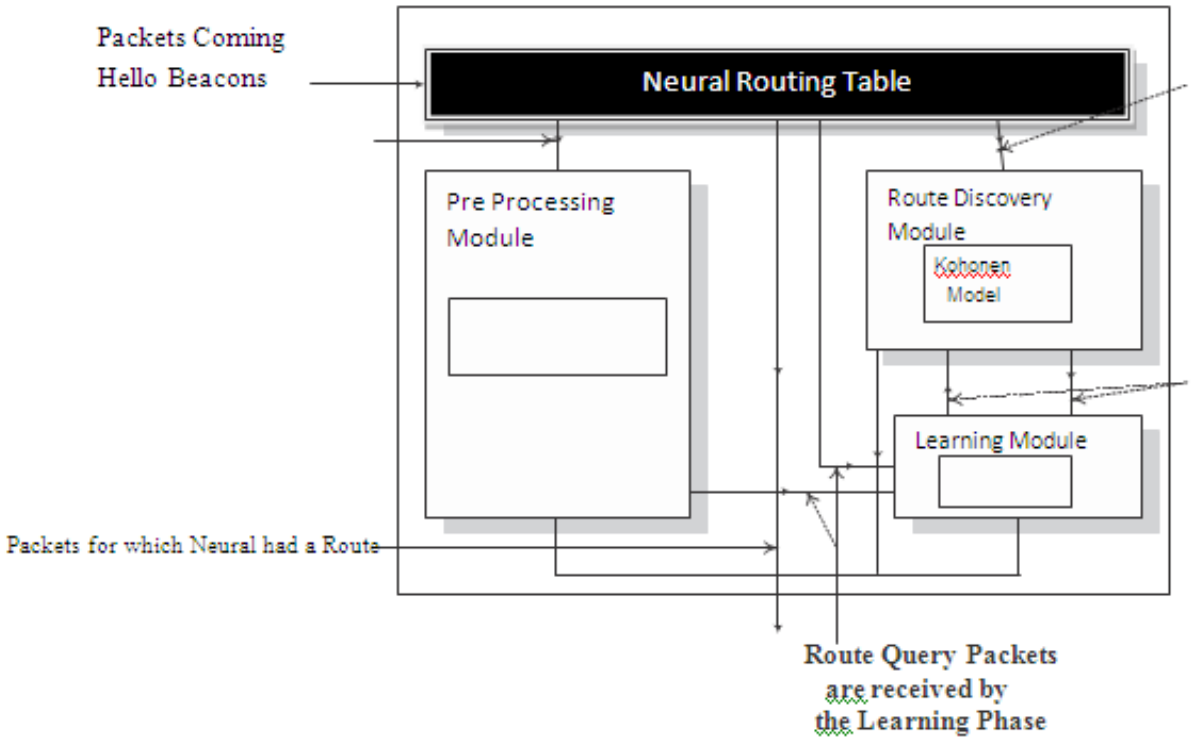

Figure 1. Schematic modular Architecture for NEURAL

3.1 Preprocessing Module:
Based on sending hello request and reply packets during an interval of time (pre-processing interval), the pre-processing module adapts the K-Nearest-Neighbors Rule sensing the continuous topology changes of the network. K-NNR disseminates environmental changes using the activation stage (A_S). The activation stage, which it is configured using the *activation threshold* (*K* value from K-NNR), represents an estimation of the local density based on the
1-hop information. The value of this stage consists in two behaviors such as

Excitatory Behavior: nodes belonging to excitatory class are in a crowded area with high probability of interconnection (synapses). In our protocol, nodes in the excitatory class are identified by the activation stage (A_S) equal to +1.

Inhibitory Behavior: In the case of an inhibitory class, areas are identified in Ad Hoc networks by isolated clusters. Nodes present a low synaptic capacity (*synaptic weight*) or poor communication ability with their neighbors. The activation stage (A_S) is set to -1.

For the pre-processing phase in NEURAL, we propose as flooding technique the "Post-synapse" schema, where this name is related with the communication process between neurons after that a signal arrived to the receptor neuron. Post-synapse describes the combination of a probabilistic schema applied in a generic epidemic protocol [12] together with the random query processing delay from the ZRP [13]. For example, nodes with an excitatory behavior present high local density, thereby they should manage low values of broadcasted probability (ProbBrcst) in order to avoid flooding due to useless broadcast packets. Otherwise, nodes, which belong to the inhibitory class, need to improve their connectivity in the environment using high values of ProbBrcst to spread their location for other neighbors. In sum, each nodes performs the post-synapse algorithm as follows

if* (*A*s = +1) *then ProbBrcst = Excitatory Brcst

else ProbBrcst = Inhibitory Brcst **(7)**

where *Excitatory Brcst* < *Inhibitory Brcst*

3.2 Route Discovery Module:
NEURAL applies in the discovery phase a self-organized feature map called the Kohonen model, which it is used to select the next route in the MANET network based on a *competitive learning* procedure. In order to be consequent with the mathematical formulation of the Kohonen model in sec 2.2, the Route Discovery phase in NEURAL is sub- divided in three steps.

3.2.1 Broadcasting:
In this step, signals or inputs are broadcasted around MANET with the purpose of configuring input vectors from the Kohonen model. Suppose that the *processing element "i"* is going to select the following route between *j* neighbor nodes ($j \in \mathbb{N} : j > 0$). First, the two inputs vectors (the input vector x_i and synaptic vector $w_{i,j}$) are initialized based on the information of the *local activation zone*. The local activation zone represent the diameter of a 2-hop distance (Neighborhood around the node *"i"*). The neighborhood is defined by "first" neighbors (n_j), which are *j* nodes around the *processing element i*, and "second" neighbors (N_m) that are *m* neighbors from the "first" neighbors. So that the information about the *local activation zone* is obtained by the node *i* broadcasting *"Stimulus"* messages to the "first" and "second" neighbors, respectively. Node *i* take into account the relationship between distance with neighbors and the communication capacity of its neighbors. In NEURAL, the round trip time (RTT) is represented as the input vector x_i and the synaptic weight (w_{ij}) is assigned to the number of "second" neighbors (N_m). The capacity of node to communicate with others neighbors is called *synaptic weight*. With the purpose of normalize vectors x_i and w_{ij} the following expressions are implemented for the node *i*.

$$x_i = \exp\left(RTT_j / T_j\right), \quad m=1,2,3,\ldots\ldots\ldots\ldots\ldots j \qquad (8)$$

$$w_{ij} = Nm / Tn, \quad m= 1,2,3\ldots\ldots\ldots\ldots\ldots j \qquad (9)$$

Where RTT_j is the Round Trip Time vector of the *j*th "first" neighbors and the vector N_m denotes the number of

"second" neighbors for the each *j*th node. In addition, τ_j and τ_N are the maximal values of the RTT and N_m observed in the *local activation zone* of the neuron *i*.

3.2.2 Selection of the "winner":
The "winner" is the node with the optimal "properties" to forward a packet to the destination. The node, which is searching a route, represents the central "stimulus" in the *local activation* zone. Thus, "first" neighbors initiate a competition to be selected as "winner". So that rules of this The best-matching neuron (winner) is selected by the maximum excitation signal $net_{i,j}$, which it is given by eqn. 6 considering input vectors (x_i and w_{ij}) from the broadcasting action.

3.2.3 Adaptation:
Nodes that are topographically close in the array up to a certain geometric distance will activate each other to learn something from the neighborhood. With the purpose of implementing a control output variable, an trust mechanism is adapted in the *learning* phase based on the extension of Kohonen's model.

3.3 Learning module:
The goal of this module is provide a learning parameter to be applied for control actions. It provides a *learning* system architecture for NEURAL. Trust calculation is processed into three **layers.**

4 NEURAL performance using a network simulator:
In this section, we address the issue for configuring the NEURAL routing protocol to provide the best performance for particular networks. For this purpose, the network simulator *ns-2* [3] was employed to simulate the NEURAL module architecture described in the section 3. The network simulator *ns-2* is an object-oriented and discrete even-drive network simulator that in the recent year it has incorporated powerful tools, protocols and modules in the area of ad hoc networks as well as wireless networks.

4.1 Simulation scenario configuration:
To make effective the convergence of Route Discovery and Learning phases in NEURAL, the optimal configuration of the pre-processing phase was evaluated using different scenarios. First, each mobile host has an omni-directional antenna having unity gain with a nominal radio range of 250 m. The random waypoint model [5] is selected as mobility model in a rectangular field with nodes' speed uniformly between cero and a maximum value of 20 $m.s^{-1}$. Number of sources and the sending rate are varied to study different loads for each configuration. To evaluate metrics, we consider the study of the packet delivery ratio, routing overhead and the average delay such as in [13, 20, 5]. Packet delivery ratio represents the fraction of control packet delivered to the destination. In addition, the total of routing packets transmitted in the simulation are measured using the routing overhead. And finally, the aver- age delay shows the average one-way latency observed between transmitting and receiving a packet. It is important to mention that for each configuration, reported measurements are the mean of 10 runs with different random seeds.

4.2 Evaluating the impact of useless broadcast in NEURAL:
To evaluate the performance of the Post-synapse algorithm, 20 nodes are configured using 20 seconds of pause time and a pre-processing interval of 5 seconds. So that every 5 seconds a hello packets is broadcasted for each nodes to start the pre-processing phase. Simulation was run during 150 seconds taking into account 5 different transition times: 15, 25, 50, 75 and 100 seconds.
The efficiency of the Post-synapse algorithm is first examined based on the delivery ratio for reply packets during diverse transition times. Figure 2 shows the delivery ratio for reply packets when the Post-synapse algorithm is applied to broadcast the hello messages of the pre-processing phase. So that percentages in the figure represent the "ProbBrcst" from the Post-synapse algorithm. For example, considering a ProbBrcst of 100% means that 100% of the hello messages were broadcasted to neighbors.

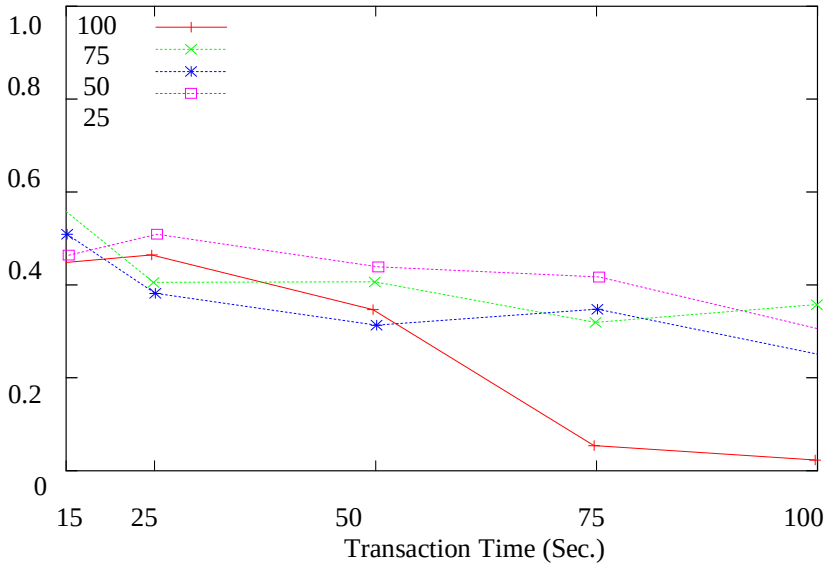

Figure 2. Delivery ratio for reply packets using Post-synapse algorithm

The real performance of the algorithm can be checked when the transition time is over 50 seconds. I.e., broadcasting all the hello messages in the pre-processing phase (ProbBrcst=100%), the control traffic (represented by hello and reply packets) introduces more collisions and packets loss into the wireless channel. Thus, the delivery ratio is abruptly decreased under 0,1 when the transition time rises. Otherwise, the packet delivery ratio show stable behavior with values between 0.38 and 0.4, when the broadcast probabilities were set to 25% and 75%, respectively. In this study, the routing overhead is related to the control traffic generated by the hello messages and reply packets in the pre-processing phase. Based on results depicted in figure 3, we observe that the pre-processing phase overloads the network performing without a broadcast query algorithm. As ex- ample, metrics with 100% of Broadcast Probability shown around 2400, 2100 and 1300 routing packets for 100, 75 and
50 seconds of transition time, respectively. Thus, routing protocols that involve ack/nack mechanism to improve reliability, unfortunately, also tend to compromise their scalability by heavily loading the network. However, the performance of the Post-synapse algorithm as query mechanism allows avoiding query implosion in the network. In our case, Figure 3 demonstrates that the overhead can be reduced until around 30% for the different transition times.
Taking into account the efficient performance of the Post-synapse algorithm over the control overhead (Figure 3) in the network, we concentrate on improving the delivery ratio observed in the figure 2. For this purpose, a random query processing delay (RQPD) was employed within the configuration of the Post-synapse algorithm. More precisely, RQPD mechanism addressed the problem of "simultaneous" reply messages by spreading out the packet with a random delay. Specifically, each node schedules a random delay prior to broadcast the packet [13].

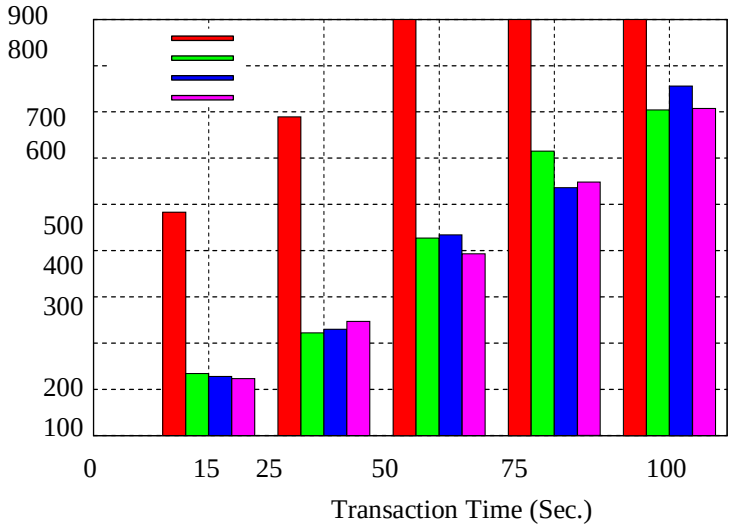

Figure 3. Number of routing packet sent using the Post-synapse algorithm

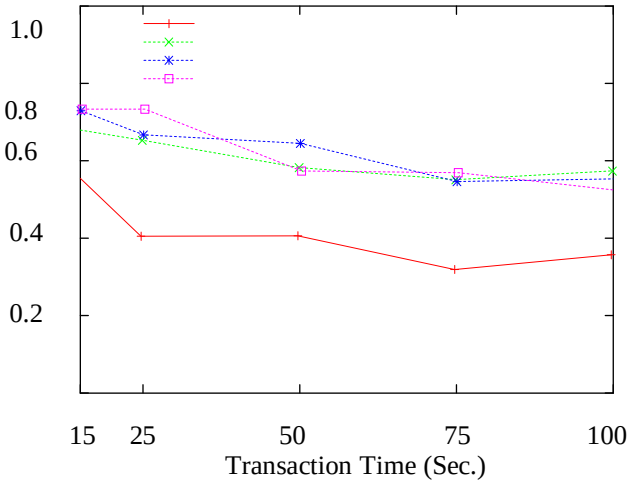

Figure 4. Delivery ratio for reply packets using the modified Post-synapse algorithm

Furthermore, we investigate the performance of the Post-synapse algorithm in the process of sending back a reply packets. In this case, nodes that receive a hello packet response to the source according to acknowledged probability (ProbAck). To verify the above modification in our algorithm, we consider the last simulation scenario with the following configuration parameters: a RQPD of 100 ms such proposed in [13] and ProbBrcst of 75%. With almost the same delivery ratio, the modified Post-synapse algorithm improved over 50% the performance for diverse transition times. For example in figure 4, using 50 secs of transition time the best delivery ratio (0.65) was achieved with a acknowledged probability of 50%. Otherwise, when nodes response each received hello message (ProbAck=100%), redundancy appears as well as collisions increased in the wireless channel. For this case the delivery ratio was 0.4.In sum, the modified Post-synapse algorithm that applies a probabilistic behavior to send and response hello messages allows to increase the delivery ratio with a low total routing overhead such as figure 5 illustrated.

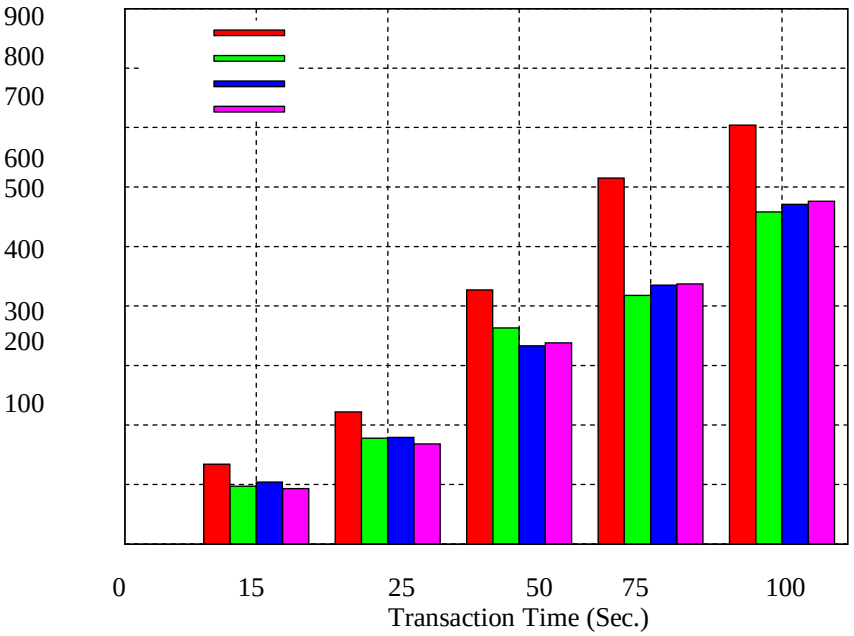

Figure 5. Number of routing packets sent using the modified Post-synapse algorithm

4.3 Study of the scalability of the preprocessing phase in NEURAL:

In this section is furthermore proposed to improve scalability by segmenting the network into clusters, which are each managed by the performance of the K-Nearest- Neighbors Rule (K-NNR) in NEURAL. More precisely, we investigate the optimal configuration of the *activation threshold* or K value based on the algorithm described in section 2.1. For this configuration, 50, 100 or 200 nodes were placed in a field of 1300 x 500 meters. Pre-processing interval of 10 secs and pause time of 20 seconds. Based on broadcasting *Hello* messages, nodes compare the number of acknowledgments (N_{ack}) with the *activation threshold* (A_t). After this initial procedure each node presents an activation state according to the number of neighbors. Nodes belong to the excitatory class employ broadcast probabilities (ProbBrcst) of 25 % and acknowledged probability (ProbAck) of 50% for the hello and reply packets, respectively. Otherwise, a probability of 75% was applied in both cases for nodes in the inhibitory class. Simulations was run varying the activation threshold as 0, 1,3, 5, 7 and 10. These values have been applied considering the performance of the Weighted Clustering Algorithm (WCA) in Ad Hoc networks. WCA [6] is a weight based distributed clustering algorithm which takes into consideration the number of nodes a clusterhead can handle ideally (without any severe degradation in the performance), trans- mission power, mobility, and battery power of the nodes. Studies (such as [18]) related to the optimal configuration of WCA proposed that each clusterhead can at most handle ten nodes as ideal degree. The load handled by a clusterhead is essentially the number of nodes supported by it. As we mention before, the maximal activation threshold to classify cluster belonging to the inhibitory class is 10 nodes.

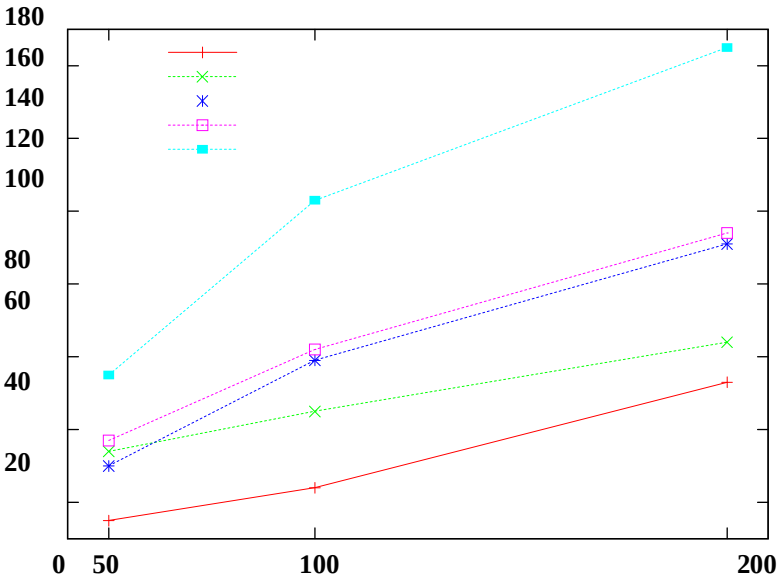

Figure 7. Scalability of the activation thresh- old

Figure 6 illustrates the average of routing packets (hello and reply packets) per node. Metrics using activation threshold (A_t) equals cero represents that the K-Nearest-Neighbors Rule is not applied in the pre-processing modules. For this case, the lowest control overhead was obtained due to the algorithm considered that all nodes were within a crowded region. So that only 25% of the total hello packets were broadcasted to neighbors. Otherwise, based on a activation threshold of ten ($A_t = 10$), the K-Nearest-Neighbors Rule achieved to disseminate clusters with less than 10 nodes. These clusters were related with an inhibitory behavior broadcasting packets with a high probability (75%). For this reason, high control overhead results were obtained for each topology configuration using $A_t = 10$. Based on results for $A_t = 5$ and $A_t = 7$, the control packet loads the network with the same proportion. For these values, figure 6 shows that the mean routing packets converged to 38, 59 and 95 packets per node for each configuration topology conformed with 50, 100 and 200 nodes, respectively. Finally, we note that the performance of the K-Nearest- Neighbors Rule has a better behavior when the activation threshold is seven ($A_t = 7$). Using this threshold the algorithm allows to classify clusters or inhibitory regions integrated with max. 7 nodes. Furthermore, results shown less overhead than $A_t = 10$ as the number of nodes increases. Metrics were compared with the performance of the weight clustering algorithm (WCA). Nuevo et. al reported in [18] around 32 routing packets using 50 nodes. In our case, the overhead was around 35 and 38 routing packets based on an activation threshold of 5 and 7, respectively

Conclusion:

In this paper, the design of a self-organizing routing algorithm called NEURAL is achieved using classification, adaptive and learning algorithms from the Artificial Neural System. This routing protocol is inspired by the synapses in the brain, in which neighbors neurons compete to propagate the signal. We contribute with the design of a modular architecture for the NEURAL protocol. Afterwards, simulations were carried up to provide the optimal configuration for the Pre-processing module in NEURAL. The pre- processing phase is related with a classification rule which operates broadcasting packets to a local region. Broadcast is widely used in sensor and ad hoc networks to disseminate information about environmental changes in the network. Therefore, it is essential to develop efficient broad- cast protocols that are optimized for energy consumption and low control overhead. Thus, the "Post-synapse" algorithm was introduced in this paper as a query mechanism to avoid flooding due to useless broadcast packets in the NEURAL protocol.

The Pre-processing requires selection of the following parameters: periodic update interval (pre-processing interval), configuration of the K-Nearest-Neighbors Rule (activation threshold) and searching of the optimal transient time to update routing tables in the simulations. These parameters will likely represent a tradeoff between the latency of the control information, delivery ratio for control packets and excessive communication overhead.

Our simulation results show improved performance for the pre-processing module of the NEURAL protocol in

terms of low control overhead and high delivery radio for control packets as the Post-synapse algorithm was employed. When evaluating scalability of the pre-processing phase, the control overhead was managed taking into ac- count the efficient performance of the K-Nearest-Neighbors Rule as classification rule. We finally conclude that by focusing in these configuration parameters, the NEURAL routing protocol can be hopefully improved in the performance of the Route Discovery and Learning phases. The above results conduce to further researches such as evaluating NEURAL based on the performance of all its modules and comparison with the current routing algorithms.

References

[1] B. Alunkal, I. Veljkovic, and G. von Laszewski. Reputation- based grid resource selection. In *Workshop on Adaptive Grid Middleware*, New Orleans, USA, 1999.

[2] F. Azzedin and M. Maheswaran. Towards trust-aware re- source management in grid computing systems.In *In Second IEEE/ACM International Symposium on Cluster Computing and the Grid (CCGRID'02)*, pages 452–457, Berlin,Germany, May 2002.

[3] U. Berkeley and U. ISI. The network simulator ns- 2, 1998. Part of the VINT project. Available from [4] C. Bishop. *Neural Network for Pattern Recognition*. Oxford University Press, Great Britain, 2000.

[5] J. Broch, D. Maltz, D. Johnson, Y. Hu, and J. Jetcheva. A performance comparison of multi-hop wireless ad hoc networks routing protocols. In *Fourth annual ACM/IEEE inter- national conference on Mobile computing and networking*, pages 85–97. ACM Press, 1998.

[6] M. Chatterjee, S. Das, and D. Turgut. Wca: A weighted clustering algorithm for mobile ad hoc networks. In *Journal of Cluster Computing (Special Issue on Mobile Ad hoc Networks)*, volume 5 N2, pages 193–204, april 2002.

[7] I. Cloete and A. Skabar. Feature selection for financial trading rules. In *Proceedings of 13th. European Simulation Symposium: Simulation in Industry*, pages 713–717, Marseille, France, 2001.

[8] M. Fischler and O. Firschein. *Intelligence: The eye, The brain, and The computer*. Addison-Wesley, Reading, Massachusetts, 1987.

[9]I. Foster and C. Kesselman. The grid: Blueprint for a new computing infrastructure. *Morgan Kaufmann Publisher*,1999.

[10] I. Foster, C. Kesselman, and S. Tuecke. The anatomy of the grid: Enabling scalable virtual organizations. *Int'l Journal on Supercomputer Applications*, 2001.

[11] J. Freeman and D. Skapura. *Neural Networks: Algorithms, applications, and programming techniques*. Addison- Wesley, Reading, Massachusetts, 1992.

[12] D. Ganesan, B. Krishnamachari, A. Woo, D. Culler, D. Estrin, and S. Wicker. An empirical study of epidemic algorithms in large scale multihop wireless networks, march 2002. Intel Research, IRB-TR-02-003.

[13] Z. Hass and M. Pearlman. The performance of query control schemes for the zone routing protocol. In *IEEE/ACM Transactions on networking*, volume 9 N4, pages 427–438, Aug. 2001.

[14] S. Haykin. *Adaptive Filter Theory*. Pretice-Hall, Englewood Cliffs, NJ, 1991.

[15] R. Helge, T. Martinetz, and K. Schulten. *Neural Computation and Self-Organizing Maps- An Introduction*. Addisonn- Wesley, New York, 1992.

[16] J. Hertz, A. Krogh, and R. Palmer. *Introduction to the theory of neural computation*. Addison-Wesley, Santa Fe Institute, USA, 1992.

[17] D. Turgut, S. Das, R. Elmasri, and B. Turgut. Optimizing clustering algorithm in mobile ad hoc networks using genetic algorithmic approach. In *Proceeding of GLOBECOM 2002*, Taipei, Taiwan, november 2002.

[18] E. Weeks and J. Burgess. Evolving artificial neural networks to control chaotic systems. *Physical Review E, The American Physical Society*, 56:1531–1540, Aug. 1997.

Molecular Dynamics of Heat Transfer and Quantum Mechanics

Thomas Prevenslik*
QED Radiations
Discovery Bay, Hong Kong, CHINA

Abstract
Molecular Dynamics (MD) is used in computational heat transfer to determine the thermal response of nanostructures. Finding basis in classical statistical mechanics, MD relates the thermal energy of the atom to its momentum by the equipartition theorem. Momenta of atoms in an ensemble are determined by solving Newton's equations with inter-atomic forces derived from Lennard-Jones potentials. Statistical mechanics always assumes the atom has thermal energy, or equivalently the capacity to absorb heat. Otherwise, the temperature of the atoms cannot be related to its thermal energy, the consequence of which is atoms in nanostructures have the same heat capacity as those at the macroscale. For bulk materials, MD heat transfer is performed for an ensemble of atoms in submicron computation boxes under periodic boundary conditions. Consistent with statistical mechanics, MD simulations of the bulk are valid because atoms having heat capacity in discrete submicron boxes under periodic boundary conditions are equivalent to those in the bulk that do indeed have heat capacity. Quantum mechanics (QM) differs. Unlike MD simulations of the bulk with atoms having heat capacity, QM precludes atoms in discrete nanostructures from having heat capacity. Nevertheless, the literature is replete with MD simulations of discrete nanostructures with atoms having heat capacity. Although consistent with statistical mechanics, MD of discrete nanostructures is invalid by QM. By QM, atoms in discrete nanostructures lacking heat capacity cannot conserve heat by an increase in temperature, and therefore the classical modes of heat transfer – convection, radiation, and conduction that depend on temperature have no meaning. Instead, conservation at the nanoscale proceeds by the creation of non-thermal QED induced EM radiation that charges the discrete nanostructures by the photoelectric effect, or is emitted to the surroundings. QED stands for quantum electrodynamics and EM for electromagnetic. Examples of MD simulations are presented that by QM are valid or invalid and recommendations made for how invalid MD heat transfer of discrete nanostructures may be consistent with QM. For interacting nanostructures, MD heat transfer simulations consistent with QM are computationally intractable, and therefore finite element (FE) simulations are proposed using estimates of QED radiation from the nanostructures in programs such as ANSYS and COMSOL

Keywords: Molecular dynamics, nanostructures, heat transfer, statistical mechanics, quantum mechanics, quantum electrodynamics

I. Introduction

MD is commonly used to simulate heat transfer in discrete nanostructures, but MD was actually developed to determine the macroscopic transport properties of bulk liquids [1-3]. Finding theoretical basis in statistical mechanics, MD derives the momenta of an ensemble of atoms in submicron computational boxes based on the solution of Newton's equations. Historically, MD simulations were in fact preceded in the 1950's by Monte Carlo (MC) simulations, e.g., the virial coefficients were derived [4] with MC simulations of spherical particles in submicron 2D computational square boxes under periodic boundary conditions. Later, MC simulations [5] were based on atomic interactions given by Lennard-Jones potentials that allowed thermodynamic data for liquid argon to be compared with computer generated MC solutions. About this time, MD solutions of bulk liquids using hard spheres [6] were first proposed. In the 1960's, the MD simulation [7] of liquid argon was later followed by the seminal MD paper [8].

Since 1950, MD simulations [4-8] imposed periodic boundary conditions on the submicron computation boxes allowing the bulk properties of the liquid to be derived with a small number of atoms. Otherwise, the solution of Newton's equations for the large number of atoms in macroscopic volumes was intractable. However, in MD simulations of heat transfer, periodic boundaries assure the fundamental premise of statistical mechanics is satisfied, i.e., the atoms have macroscopic heat capacity. Not only is this consistent with statistical mechanics, but also with the fact that in the bulk liquid being simulated, all atoms do indeed have heat capacity. By statistical mechanics, MD solutions under periodic boundaries with all atoms having heat capacity are valid even though the computation boxes are submicron.

Today, MD simulations of heat transfer are not performed to derive bulk properties. Exceptions include MD to determine the thermal conductivity of nanofluids [9] comprising nanoparticles (NPs) in liquid argon. Indeed, the literature is replete with MD simulations of discrete nanostructures that are unambiguously not periodic [10-12]. Consistent with statistical mechanics, the atoms in the nanostructures are assumed to have macroscopic heat capacity, the MD simulations of which are thought to provide precise atomic descriptions of nanoscale heat transfer when in fact they are invalid because QM precludes atoms in discrete nanostructures from having heat capacity. In effect, MD simulations that assume atoms have heat capacity derive the thermal response of the nanostructure as if it were a scaled down macroscopic body, and therefore

are meaningless in the understanding of heat transfer at the nanoscale. Clearly, QM invalidates MD heat transfer of discrete nanostructures, but

What can be done to make discrete MD heat transfer consistent with QM?

II. Purpose

Clarify the QM validity of MD simulations of heat transfer under periodic boundary conditions and invalidity of MD for discrete nanostructures. Provide recommendations for performing MD heat transfer simulations in discrete nanostructures that are consistent with QM.

III. Theory

Classical heat transfer assumes atoms have heat capacity and conserve absorbed heat from EM sources (lasers, molecular collisions, electrical resistance, etc.) by an increase in temperature. Because of this, conduction, radiation, and convection have meaning in dissipating absorbed heat. QM differs in that the heat capacity of atoms in nanostructures (NPs, thin films, nanowires, etc.) vanishes, and therefore temperature changes do not occur. Hence, classical conduction, radiation, and convection that depend on temperature are meaningless. Heat transfer for an isolated NP is illustrated in Fig. 1.

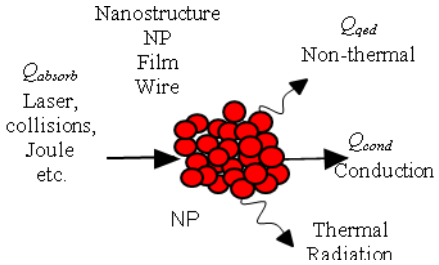

Figure 1 Heat transfer at the nanoscale showing a NP conserving heat from EM sources

Lacking changes in temperature, the NP conserves absorbed heat flow Q_{absorb} by the emission of QED induced radiation Q_{qed}. However, some conduction Q_{cond} may occur if the NP is in contact with a surface. Unlike thermal radiation by the Stefan-Boltzmann law important at high temperatures, QED induced emission is non-thermal EM radiation at the NP temperature. The heat flow balance is,

$$Q_{abs} - Q_{qed} = Q_{cond} \qquad (1)$$

QM Restrictions

Unlike statistical mechanics, QM restricts the heat capacity of atoms in nanostructures. The Einstein-Hopf relation [13] for the harmonic oscillator giving the dispersion of Planck energy E with the EM confinement wavelength λ is the measure of the capacity of the atom to absorb heat,

$$E = \frac{\frac{hc}{\lambda}}{\exp\left(\frac{hc}{\lambda kT}\right) - 1} \qquad (2)$$

where, h is Planck's constant, c the speed of light, k Boltzmann's constant and T absolute temperature. The QM relation for the Planck energy in relation to the classical oscillator by statistical mechanics is illustrated in Fig. 2.

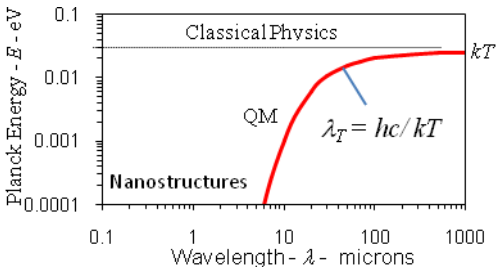

Figure 2 The Atom as a Harmonic Oscillator at 300 K.

By the equipartition theorem of statistical mechanics, the thermal energy of the classical oscillator is always kT allowing the atom to have the same heat capacity in nanostructures as at the macroscale. QM oscillators differ in that kT energy is only available for $\lambda > \lambda_T$ while kT energy is restricted for $\lambda < \lambda_T$. At ambient temperature, $\lambda_T \sim 50$ microns. Hence, Fig. 2 shows the heat capacity of the atom is less than kT for $\lambda < 50$ microns with full kT energy available only for $\lambda > 50$ microns. By QM, atoms in nanostructures having $\lambda_T < 1$ micron have virtually no heat capacity to conserve heat from any EM source by an increase in temperature.

TIR Confinement

Lack of heat capacity by QM precludes heat from EM sources to be conserved in nanostructures by an increase in temperature. However, the absorbed heat must still be conserved, and therefore conservation proceeds during TIR confinement by creating QED induced radiation *inside* the nanostructure. TIR stands for total internal reflection. TIR has a long history beginning with Tyndall in 1870 who observed if the refractive index of a body is greater than that of the surroundings, absorbed light is trapped at its surface. In nanostructures, TIR has an important significance and need not be limited to light absorption. Unlike macrostructures, nanostructures have high surface to volume ratios, and therefore heat from any EM source (lasers, molecular collisions, electrical resistance, etc.) is absorbed almost totally in the NP surface. Since the nanostructure surface corresponds to the TIR wave function of the absorbed heat, QED induces the absorbed heat to undergo the spontaneous creation of photons *inside* the nanostructure. However, TIR confinement is not permanent, but rather sustains itself only during heat absorption, i.e., absent heat absorption, there is no TIR confinement and QED radiation is not created.

Taking the spherical NP as the idealized shape of the most common nanostructure, the TIR confinement of heat creates QED photons at frequency f having Planck energy E,

$$f = \frac{c/n}{\lambda}, \qquad \lambda = 2D, \qquad E = hf \tag{3}$$

where, n is the refractive index and D the diameter of the NP. Unlike macrostructure QED emission at phonon frequencies, nanostructures have $\lambda < 1$ micron with QED emission occurring at frequencies f beyond the UV.

QED Induced Heat Transfer

QED induced heat transfer is the consequence of the QM requirement that the heat capacity of the atom vanishes in nanostructures. Consider the NP resting on a surface as depicted in Fig. 3.

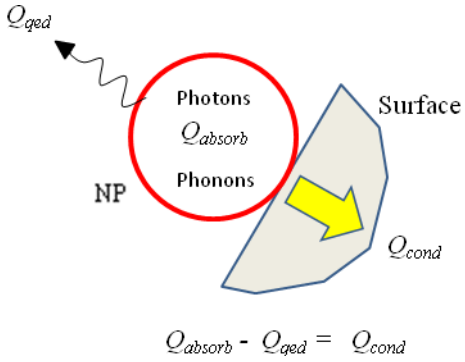

Figure 3 QED Induced Heat Transfer

Since absorbed heat Q_{absorb} cannot be conserved by an increase in NP temperature, conservation occurs by another path. One path is conductive flow Q_{cond} into the surface by phonons, and the other by emission of QED radiation Q_{qed} from QED photons. However, phonons respond to absorbed heat at acoustic velocities while QED photons move at the speed of light. Hence, absorbed heat Q_{absorb} is conserved promptly by QED emission before phonons respond, and therefore conductive heat transfer does not occur, i.e., $Q_{qed} \sim Q_{absorb}$. If the NP is isolated from the surface, the prompt QED emission occurs before the phonons in the NP respond.

In QED induced heat transfer, absorbed heat Q_{absorb} is conserved almost totally by creating number N of QED photons *inside* the nanostructure that produce electrical charge by the photoelectric effect. The QED photons are created at the rate dN/dt,

$$\frac{dN}{dt} = \frac{Q_{absorb}}{E} \qquad (4)$$

However, if the nanostructure sis in contact with a surface, conductive heat Q_{cond} must be considered. In nanoscale thin-films attached to macroscopic substrates, electrical current through the film produces Joule heat Q_{absorb} that is conserved by Q_{qed} emission to the surroundings and conduction Q_{cond} into the substrate. Typically, the effective conductivity for thin-films is found [14] reduced from the bulk as the film thickness is reduced below 100 nm. However, the QED emission was excluded [15] from the heat balance, which if included, the conductivity does not decrease, but remains at bulk as the film thickness is decreased. If Q_{qed} is not included in the heat balance, Q_{cond} is thought [14] to be higher than actual, and therefore the thermal conductivity K is reduced from bulk to satisfy the heat balance. Excluding Q_{qed} from the heat balance is understandable because the QED emission from thin films having thickness $d < 100$ nm occurs at Planck energy $E > 6.2$ eV, which is beyond the UV and would not be normally observed. Because of this, the reduced thermal conductivity was explained [14] by scattering of phonons. However, prompt QED emission conserves absorbed Joule heat without conduction, making meaningless the notion of reduced conductivity by scattering of phonons when in fact conduction does not occur.

IV. Review of MD Simulations

The MD simulations [9-12] in the literature are reviewed in relation to the QM restriction that the atoms in discrete nanostructures do not have heat capacity, thereby invalidating any MD simulations claiming temperature changes, thermal conduction, and heat currents.

Nanofluids

Nanofluids comprising NPs in solvents are claimed to surpass the thermal performance of traditional heat transfer liquids. MD simulations following procedures using the Green-Kubo method [1-3] were used [9] to determine the thermal conductivity of a nanofluid consisting of copper NPs in liquid argon. Consistent with QM, periodic boundaries with atoms having heat capacity were assumed. For a Cu nanofluid, the NP diameter is about 2 nm in a cubic computational box of 4 nm on a side having a total of 2048 atoms as depicted in Fig. 4.

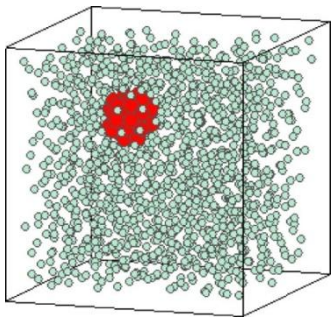

Figure 4 Nanofluid in Computation Box – Periodic Boundaries

Lennard Jones potentials were used to simulate the interactions between Cu atoms in the NP and between the Cu and Ar atoms. Results suggest enhanced thermal conductivity is caused by the increased movement of liquid argon atoms by Brownian motion in the presence of NPs. However, the long-range interactions between the NP and its image neighbors that should be significant at 4 nm spacing were not included. Larger computational boxes that capture NP interactions with neighbors would reduce the increased Brownian movement of liquid atoms and decrease any enhanced thermal conductivity found for the shorter computational boxes. Classical physics assumed in MD should not give higher conductivity than that given by standard mixing rules, but otherwise the MD solution is valid and consistent with QM.

Nanocars

Nanocars including molecular motors are nanostructures [10] comprised of ordered atoms and molecules that convert heat into mechanical motion. The heat may take various EM forms including light, Joule heat, and electron beams, e.g., nanocars are observed to move by simply heating the substrate. In a typical experiment, a large number of nanocars are laid down at random on a gold surface. Upon heating the gold surface, the cars are observed to move. For clarity, only a single car is shown in Fig. 5

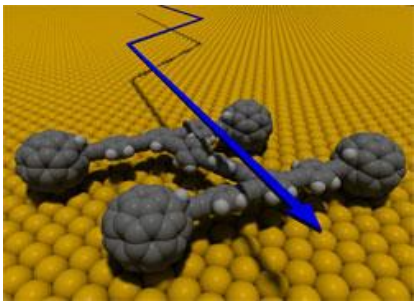

Figure 5 Discrete Nanostructure - Nanocar

The mechanism by which heat is converted into nanocar motion is not well understood. MD simulations [10] of heat transfer were performed to explain observed motions. However, MD heat transfer of nanocars is invalid because QM restricts the heat capacity of atoms. Hence, absorption of heat by the nanocar from the substrate cannot be conserved by an increase in temperature. It is not surprising therefore, the MD simulations show the cars to distort, but not move.

However, this MD result is expected in our macroscopic world. If you park your car with the brakes off in a flat parking lot on a hot day, you would not expect it to move and collide with other cars. Macroscopic results are found in MD simulations because atoms in nanocars are assumed to have heat capacity as in our macroscopic cars. For classical physics by statistical mechanics, Fig. 2 shows the Planck energy of the atom in a macroscopic car under EM confinement at long wavelengths is the same as that in nanocars at short wavelengths, and therefore neither car would be expected to move.

QM differs. Conservation proceeds by the QED induced frequency up-conversion of absorbed heat to the TIR confinement frequency of the nanocar that at UV or higher levels charges the nanocar positive by the photoelectric effect. Similarly, other nanocars charge positive. Observed nanocar motion is therefore caused by random electrostatic repulsions between nanocars.

Carbon Nanotube (CNT) Actuator

MD simulations [11] have been used in attempts to explain how thermal gradients drive linear actuators consisting of the concentric CNTs shown in Fig. 6. By heating the ends of the fixed CNT, the outer CNT is found to move toward the cold end of the fixed CNT. The thermal driving force is found proportional to the temperature gradient.

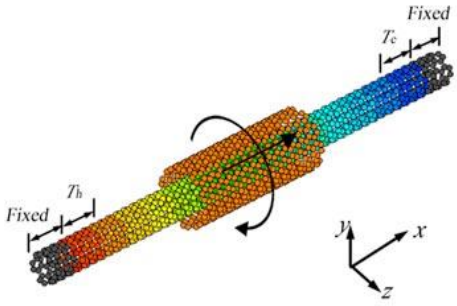

Figure 6 Discrete Nanostructure – Concentric CNTs

However, MD simulations did not show any motion of the outer CNT. By adding a thermophoretic spring, motion was observed in the MD response, but then only a thermophoretic analysis having nothing to do with MD is required. The MD simulation showing the outer CNT did not move under the temperature gradient across the fixed CNT is consistent with our macroscopic world, e.g., heating a macroscopic equivalent of the CNT nanostructures, say concentric pipes would obviously not cause motion of the outer pipe. Similar to nanocars, the problem is atoms in the MD simulation of the CNTs and those in macroscopic pipes have the same heat capacity as shown in Fig. 2. What this means is the mechanism of CNT linear actuators cannot be explained by MD based on classical statistical mechanics.

The QM explanation of CNT motion is simple. More QED radiation is produced at the hot end of the fixed CNT than at the cold end. By the photoelectric effect, the hot end is therefore charged positive more than the cold end. The outer CNT then moves by repulsion to the cold end under the charge gradient. MD simulations cannot explain the CNT motion because charge is necessary and classical physics does not produce charge.

Sputtering

The Kinetic Monte Carlo technique (KMC) is a procedure for solving kinetic equations in non-equilibrium processes. Unlike traditional MC, real time is included in the evolution of the system. The KMC simulation [12] of 5 keV argon atoms impacting a Cu (111) crystal is shown in Fig. 7. The KMC simulation shows the emission of large clusters of Cu atoms from the crystal. The color coding temperature of the atoms: white - black 300K - 1400K; blue 1400K - 2800K; green 2800K - 4200K; red above 4200K.

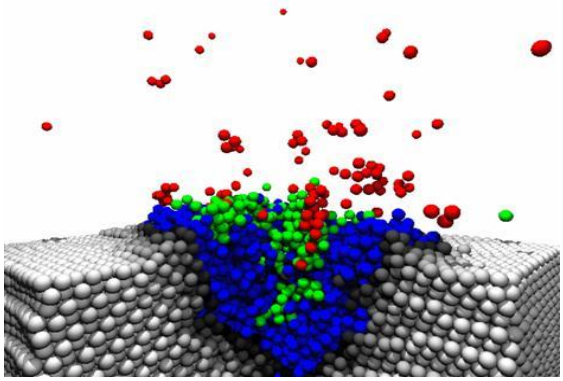

Figure 7 Discrete Nanostructure – Sputtering

The extent of the KMC model is observed to be submicron, and therefore the temperatures found that exceed melting of copper are proof the KMC simulation is invalid by QM. However, the KMC solution may be made at least consistent with QM by holding the temperature constant with the Nose-Hoover thermostat [1-3] during the solution run. The QED emission may then be estimated from the saved history of thermostat heat and input into a FE simulation of melting over larger regions of the crystal.

V. Summary and Conclusions

MD simulations of heat transfer based on statistical mechanics that assume atoms have heat capacity are valid only for periodic boundaries.

Unlike statistical mechanics, QM precludes atoms in discrete nanostructures from heat capacity, the consequence of which is that heat from EM sources (lasers, molecular collisions, Joule heat, etc.) absorbed in nanostructures is conserved by the creation of charge or the emission of QED induced radiation. Classical heat transfer by radiation, convection, and conduction that depend on the temperature of the nanostructure are no longer valid. Similarly, Fourier's heat conduction equation is not valid for discrete nanostructures.

MD simulations of discrete nanostructures reported in the literature are invalid by QM. Arguments that MD is consistent with statistical mechanics may be dismissed as QM governs heat transfer at the nanoscale.

In discrete MD simulations, absorbed heat is conserved by the creation of QED photons that produce charge by the photoelectric effect. Conversely, discrete MD simulations based on classical physics having heat capacity do not produce charge and erroneously conserve absorbed heat by an increase in temperature.

The common belief that MD simulations provide a precise description of heat transfer in nanostructures not possible with classical physics using FE programs such as ANSYS or COMSOL is erroneous. MD and FE give equivalent results, but both are invalid by QM.

VI. Recommendations

Given the MD of discrete nanostructures is invalid by QM, the following procedure [16] is recommended to make the MD heat transfer simulation of nanostructures at least consistent with QM.

1. During the MD simulation, use the Nose-Hoover thermostat [1-3] to hold the temperature constant as required by QM. The QED radiation created in a nanostructure is its thermostatic heat.
2. At each time step, use the QED induced radiation to compute the thermal response of the surroundings and the charge in the nanostructures by the photoelectric effect.
3. Compute the thermal and dynamic response of the system of nanostructures.

Since the MD solution of heat transfer for even a few interacting nanostructures is computationally intractable, an alternative is to forego MD simulations altogether and instead make a FE simulation of the nanostructures and the

surroundings. Estimate the QED radiation for each nanostructure based on the heat absorbed from EM sources. Simple hand-calculations suffice. Input the QED radiation in a FE simulation to determine the macroscopic thermal and dynamic response consistent with QM. Include the charge created from QED radiation in generating electrostatic forces between nanostructures to determine their dynamic response.

References

[1] C. G. Gray, K. E. Gubbins, *Theory of Molecular Fluids*, Oxford, Clarendon Press, 1985.

[2] J-P Hansen, I. R. McDonald, *Theory of Simple Liquids*, London, Academic Press, 1986.

[3] M. P. Allen, D. J. Tildesley, *Computer Simulations of Liquids*, Oxford, Clarendon Press, 1987.

[4] N. Metropolis, A. W. Rosenbluth, M. N. Rosenbluth, A.H. Teller, E. Teller, Equation of state calculations by fast computing machines, J. Chem. Phys., 1953, Vol 21, pp 1087-1092

[5] W. W. Wood, F. R. Parker, Monte Carlo equation of state of molecules interacting with the Lennard-Jones potential, J. Chem. Phys., 1957, Vol 27, pp 720-33.

[6] B. J. Alder, T. E. Wainwright, Studies in Molecular Dynamics. I General Method, J. Chem. Phys., 1959, Vol 31, pp 459-66.

[7] A. Rahman, Correlations in the Motions of Atoms in Liquid Argon, Phys. Rev, 1964, Vol 136A, pp 405-11.

[8] J. J. Nicolas, K. E. Gubbins, W. B. Streett, D. J. Tildesley, Equation of State for the Lennard-Jones fluid, Mol. Phys., 1979, Vol 37, pp 1429-54.

[9] S. Sarkar, S. P. Selvam, Molecular dynamics simulation of effective thermal conductivity and study of enhanced thermal transport in nanofluids, J. Appl. Phys, 2007, Vol 102, pp 074302.

[10] V. Akimov, A. V. Nemukhin, A. A. Moskovsky, A. B. Kolomeisky, J. M. Tour, Molecular Dynamics of Surface-Moving Thermally Driven Nanocars, J. Chem. Theory Comput 2008, Vol 4, pp 652-6.

[11] Q-W Hou, B-Y Cao, Z-Y Guo, Thermal gradient induced acuuation of double-walled carbon nanostubes, Nanotechnology, 2009, Vol 20, pp 495503.

[12] Surface and Plasma Technology, Vienna University of Technology, http://www.iap.tuwien.ac.at/www/opt/parasol.php

[13] A. Einstein, L. Hopf, Statistische Untersuchung der Bewegung eines Resonators in einem Strahlungsfeld, *Ann. Physik*, 1910, Vol 33, pp 1105-10.

[14] W. Liu and M. Aseghi, Thermal Conductivity Measurements of Ultra-Thin Single Crystal Silicon Layers, J. Heat Transfer, 2006, Vol 128, pp 75-83.

[15] T. Prevenslik, Heat Transfer in Thin Films, Third Int. Conf. on Quantum, Nano and Micro Technologies, ICQNM, Cancun, February 1-6, 2009.

[16] T. Prevenslik, Validity of Heat Transfer by Molecular Dynamics, Tribochemistry - HAGI 2011 - HAGI, See PPT Presentation at HAGI http:// www.nanoqed.org , 2011.

Author Information

Thomas Prevenslik is a retired American living in Hong Kong and Berlin. He is a graduate of Carnegie Institute of Technology and the University of Pittsburgh. He spent most of his career as a Mechanical engineer in the nuclear power industry working on advanced reactors at Westinghouse. Later as a consultant, he worked for American and Japanese companies in computer simulations of structural dynamics and heat transfer in the diverse areas of optical telescopes, gas bearings, turbine engines, and molecular dynamics of chemical reactions. He became involved in nanoscale heat transfer because classical physics based on phonon theories by Einstein and Debye failed to provide rational explanations of observations. In contrast, he has promoted QED induced heat transfer based on the quantum mechanical requirement that the heat capacity of the atom vanishes at the nanoscale. Conservation of absorbed energy therefore cannot proceed by an increase in temperature, and instead QED creates photons *inside* the nanostructure that produce charge, or are emitted to the surroundings. QED heat transfer by photons avoids the numerous unphysical explanations of observations at the nanoscale based on phonons that suggests changing the mixing rules for nanofluids; reduced bulk thermal conductivity depending on film thickness; the fourth circuit element of memristors; molecular signaling by the lock and key mechanism in olfaction; and so forth. QED induced heat transfer by photons not only offers a rational approach inaccessible to nanoscale heat transfer by phonons, but in the far more diverse areas of nanostructure interaction with macroscopic systems.

Process Optimization for Laser Cladding Operation of Alloy Steel using Genetic Algorithm and Artificial Neural Network

Subrata Mondal[1], Bipan Tudu[2], Asish Bandyopadhyay[3], Pradip K. Pal[3]

[1]School of Laser Science & Engineering, Jadavpur University, India

[2]Instrumentation and Electronics Engineering Department, Jadavpur University, India

[3]Mechanical Engineering Department, Jadavpur University, India

Abstract:

This paper presents an investigation on single objective optimization for CO_2 laser cladding process considering clad height (H) and clad width (W) as performance characteristics. This optimization of multiple quality characteristics has been done using Genetic Algorithm (GA) approach. The aim of this work is to predict the performance characteristics (H and W) at optimized condition by applying back propagation method of artificial neural network (ANN). The essential input process parameters are identified as laser power, scan speed of work table and powder feed rate. In order to validate the predicted result, an experiment as confirmatory test is carried out at the optimized cladding condition. It is observed that the confirmatory experimental result is showing a good agreement with the predicted one. It has also been found that the optimum condition of the cladding parameters for multi performance characteristics varies with the different combinations of weighting factors.

Keywords: Laser cladding, Taguchi method, Optimization, GA, ANN

1. Introduction:

Laser surface cladding is a popular non-traditional coating technology in recent days. This is because of the superior surface uniqueness of the coat in which the surface with resistance to wear, corrosion and hardness can be resulted. In fact, from the application point of view, the coating on any component produced by laser is highly comparable to other coating processes such as plasma coating and spray coating. Laser cladding is one of the thermal type techniques in which laser is used as heat source to deposit a thin layer of a desired metal (by melting) on the substrate surface. Laser cladding using powder can be performed in two distinct ways. In the first process, powder is pasted on the surface by some adhesive and then the clad is formed by laser beam. In the second process, powder is pneumatically fed into the melt pool on a substrate surface so that powder jet and laser beam are focused on the same area and the clad is formed on the surface; the second process is called 'blown powder method'[1]. Some of the important process parameters are- laser power, scan speed of work table, stand-off distance and powder mass flow rate. Generally, the effect of laser cladding process performance is evaluated on the basis of clad bead dimension such as clad height, clad width and depth of penetration [2, 3]. The powder injection method has been applied in the present study. The present work is performed to study laser cladding process on 20MnCr5 substrate as they are potentially used in automobile and mechanical industries.

A lot of experimental investigations have been done to analyze the effect of process parameters on clad bead geometry and clad quality by varying one factor at a time [4-6]. But a large number of experiments need more time and money. To overcome this drawback, many researchers [7-9] were applied design of experiments (DOE) technique to analyze their experimental data and optimize the process parameters for desired response(s). In recent years, Taguchi method has become a powerful tool for improving the productivity during research and development state so that quality of product can be obtained in the economical way. It is found that the traditional Taguchi method was applied to optimize a single quality characteristic in the literature. However, single-objective optimization method is easier than multi-objective optimization technique.

In the present investigation, single-objective optimization has been applied for two quality characteristics such as clad width (W) and clad height (H) during CO_2 laser cladding for manganese steel surface using Genetic Algorithm. Nature of one objective is larger-the-better for clad width and smaller the better for other one (clad height). After finding the optimum condition the optimum results are predicted by developing ANN model and compared with confirmation test.

2. Experimental Approach

The equipment used for laser cladding is a 3.5 kW continuous wave CO_2 Laser Rapid Manufacturing (LRM) system. The LRM set-up consists of a high power laser system integrated with the beam delivery system, powder feeding system and job/beam manipulation system [13]. Fig. 1 depicts the schematic arrangement of the LRM machine. Ni-Cr-Mo powder has been fed into the molten pool using a volumetric-controlled powder feeder through a co-axial powder feeding nozzle. Argon gas is used as a shielding gas and powder carrier. The key process parameters are selected from the literature survey and those are laser power, scan speed and powder feed rate. First, a number of single tracks are deposited at various machining conditions to obtain continuous and uniform tracks which lead to facilitate to determine the range of process parameters for control levels in Taguchi method (Table.3). Then the actual experiments are performed as per the L_9 Taguchi orthogonal array. Focal length (f=2 mm) and stand-off-distance (SOD=16 mm) have been kept constant throughout the experimentation. Experiments are performed by expecting to obtain the aspect ratio (W/H) of clad bead nearby 15.

The experiments are performed on Φ 3 inch x 0.5 inch thick specimens of 20MnCr5 steel. The surfaces of the substrate are sand blasted prior to laser cladding. The powder (feeding material) used in laser cladding is Inconel-625 powder. The powder particles are of globe-shaped with size of 45-106 µm. Chemical composition of the powder is shown in Table 1. In order to improve the surface characteristics of this substrate an anticorrosive powder material is used as the clad material. It is a non-magnetic, corrosion and oxidation resistant. Nickel and chromium provide resistance to oxidizing environment, while nickel and molybdenum to non-oxidizing environment. Pitting and crevice corrosion are prevented by molybdenum [10].

Table1: composition of Inconel-625

Elements	Chromium	Molybdenum	Nickel
Percentage in weight	20%	5%	Balance

The design of experiment is a statistical tool which helps to minimize the number of experiments so that appropriate data will be collected [11]; the minimum number of experiments will be performed to acquire the necessary technical information and suitable statistical methods will be used to analyze the collected data. Taguchi's method for experimental design is straightforward and easy to apply to many engineering situations, making it a powerful yet simple tool [12, 13]. The initial task of this stage is to find out the key process control parameters with their ranges and performance evaluation parameter (output) that is to be measured. The levels of each variable represent the range for which the effect of that variable is desired to be known.

In order to minimize the number of experiments, the experiments are planned against a three level Taguchi's Orthogonal Array that required 9 runs in total to be carried out. The process parameters of laser power, scan speed of the table and powder feed rate have been varied to investigate the process responses of clad quality. The selected L_9 orthogonal array in the present analysis is presented in Table 2.

Table 2: L_9 Taguchi orthogonal array

Experiment No.	Laser Power-P (kW)	Scan speed-V (mm/min)	Powder eed rate-C (mm^3/m
1	1.0	0.3	5
2	1.0	0.5	8
3	1.0	0.8	11
4	1.25	0.3	8
5	1.25	0.5	11
6	1.25	0.8	5
7	1.5	0.3	11
8	1.5	0.5	5
9	1.5	0.8	8

2.1 Collecting the experimental data

The quality characteristics of clad bead are determined by measuring clad width (W) and clad depth (D) [Fig.1]. For each of the clad beads three measurements at different location have been taken and averages of them are considered. The measured values of two responses H and W using L_9 orthogonal array are shown in Table 3.

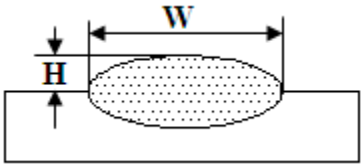

Fig.1 Geometry of cross-section of a single layer and single bead clad

Table 3: Experimental Observations using L_9 OA

Trials Run	Clad Height (H)-mm	Clad Width (W)-mm
1	0.39	0.94
2	0.34	0.88
3	0.47	0.99
4	0.81	1.33
5	0.41	0.97
6	0.16	0.75
7	1.22	1.97
8	0.24	1.3
9	0.25	0.92

3. Application of Genetic Algorithm to the Laser Cladding Process

The genetic algorithm (GA) is a stochastic searching method which searches throughout the solution space to find the best solution for a given optimization criteria, mimicking the process of natural evolution, the principle of survival of the fittest. The evolution usually starts from a population of randomly generated chromosomes and happens in generations. In each generation, the fitness of every individual chromosome in the population is evaluated. This fitness function is always problem dependent. Depending on the problem in hand, one has to select or design a suitable fitness function. The chromosome having the best fitness value is included in a new population for the next generation directly without any modification. Such chromosomes are called elite chromosomes. Thereafter, from the rest of the parent chromosomes for that generation, multiple ones are stochastically selected based on their fitness (selection) and recombined (crossover) and randomly mutated (mutation) to be included in the new population. The new population is then used in the next iteration of the algorithm. Generally, the algorithm terminates when a pre-defined number of generations have been produced, or a satisfactory fitness level has been reached by the population. However, if the algorithm has terminated due to a pre-defined number of generations, a satisfactory solution may or may not have been reached. Also, a satisfactory fitness level may require a huge number of generations to be executed. Hence, a trade-off between the maximum of number of generations and the desired fitness level is often called for. A pseudo-code for a Simple Genetic Algorithm (SGA) is presented in Fig.2.

```
Begin
Initialize population;
Evaluate population;
        repeat
                Reproduction;
                Crossover;
                Mutation;
                Evaluate population;
until (termination criteria);
end.
```

Fig. 2 A pseudo-code for a Simple Genetic Algorithm (SGA)

Here, we have used single objective real coded genetic algorithm for obtaining the combination of laser power, scan speed and powder feed rate at optimized condition. The optimization is done twice: once for minimizing the clad height and once for maximizing the clad width. The initial population in both cases was a set of randomly generated real numbers in the given range. The maximum number of chromosomes in the population was fixed to be 100. Each chromosome size is three numbers long, one number for each of the laser power, scan speed and powder feed rate.
The following equations of clad height and clad width, obtained for given values of laser power, scan speed and powder feed rate by multiple regression analysis, were used as the objective functions respectively for minimizing clad height and maximizing clad width.

$$Clad\ Height(mm) = 2.5141 - 4.4317 * A - 4.9585 * B + 0.4663 * C - 0.6222 * A * B - 0.1962 * A * C - 0.2862 * B * C + 2.5143 * A^2 + 6.0714 * B^2 \quad \ldots\ldots(i)$$

$$Clad\ Width(mm) = 4.3322 - 6.5057 * A + 0.8294 * B + 0.0156 * C - 3.2 * A * B + 0.061 * A * C - 0.1095 * B * C + 3.3486 * A^2 + 2.8651 * B^2 \quad \ldots\ldots(ii)$$

The maximum number of generations was fixed to 500. The parametric values of crossover probability and mutation probability were chosen to be 0.8 and 0.001 respectively. The number of elite chromosomes to be preserved was fixed to 2.

Since GA is a heuristic search process sometimes it may get stuck at local minima or maxima during optimization. So, optimization for minimizing clad height and maximizing clad width is executed 10 times each. Table 4 presents the optimized process parameters for the minimum value of clad height and maximum value of clad width along with the respective standard deviations.

Table 4: Optimized Process Parameters using GA

Responses	Optimized Control Factors			Optimized Value	Standard Deviatio (%)
	Laser Power	Scan Speed	Powder Feed Rate		
Clad Height	1.2252	0.6205	5.3475	0.0951	1.06
Clad Width	1.4970	0.3024	10.9668	1.9710	1.92

4. Process Prediction through ANN during Optimization

Neural networks are composed of simple elements operating in parallel. These elements are inspired by biological nervous systems [14]. As in nature, the network function is determined largely by the connections between elements. One can train a neural network to perform a particular function by adjusting the values of the connections (weights) between elements. Commonly neural networks are adjusted, or trained, so that a particular input leads to a specific target output. There, the network is adjusted, based on a comparison of the output and the target, until the network output matches the target. Typically many such input/target pairs are used, in this supervised learning, to train a network [15].

There are various algorithms in the artificial neural network (ANN). In the present study the back propagation training algorithm is used. The aim of the ANN modeling is to establish a correlation of input process variables such as laser power, scan speed and powder feed rate with output parameters namely clad width and clad depth. The back propagation neural networks are usually referred to as feed forwarded and multi layered perceptron (MLP) with number of hidden layers. The error back-propagation process consists of two passes through the different layer of the network: a forward pass and a backward pass. In the forward pass an activity pattern (input vector) is applied to the sensory nodes of the network and its effect propagates through the network layer by layer. Finally, a set of output is produced as the actual response of the network. During the backward pass, all synaptic weights are adjusted in accordance with the error correction rule with the following formula.

$$\Delta\Omega(t) = \beta\delta_i O_i + \alpha\Delta w_{ij}(t-1) \qquad \text{.....(iii)}$$

Where, β = learning rate, α = momentum coefficient and δ= local error gradient, O_i= output of the i^{th} unit, w_{ij}= weighting factor connecting the i^{th} neuron of the input vector to the j^{th} neuron of the output vector.

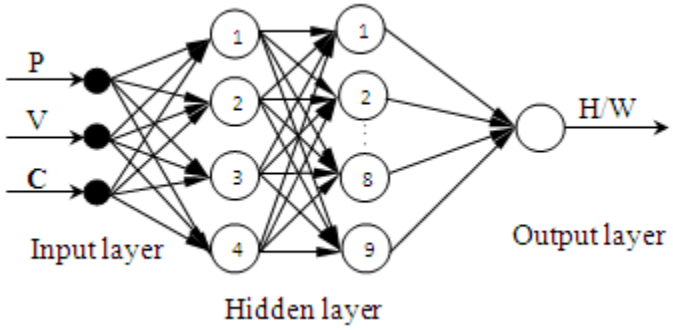

P = Laser power
V = Scan velocity
C = Powder mass flow rate
H = Clad height
W = Clad width

Fig.3: Structure of 4 layered ANN model for clad width

4.1 Training phase of neural network

To increase the accuracy and speed of the network the normalized data set obtained from Equation (iv) is used in the training and testing phase. Out of total available data set, 70% data set was used for training the network and remaining used for testing the network. There are two responses considered in the present process, one model for clad width (W) and another model for clad depth (D) formed separately. Therefore the number of neurons in the input and output layer has been set to three and one respectively in the present neural network architecture. Several network structures are formed by keep on changing the number of neurons in the hidden layers and finally 3-4-9-1 configuration is selected for clad width and 3-8-11-1 is selected for clad depth. The error plot for clad width is shown in Fig.4 and same kind of trend is also obtained in case of clad depth. The selected values of model parameters for clad width are shown in Table 5.

$$\eta_i = \frac{D_{ij}}{D_i^*} \qquad \text{.....(iv)}$$

Where D_{ij} = Experimental valu at i-th number of experiment for j-th response, D_i^* = Maximum value for j-th response.

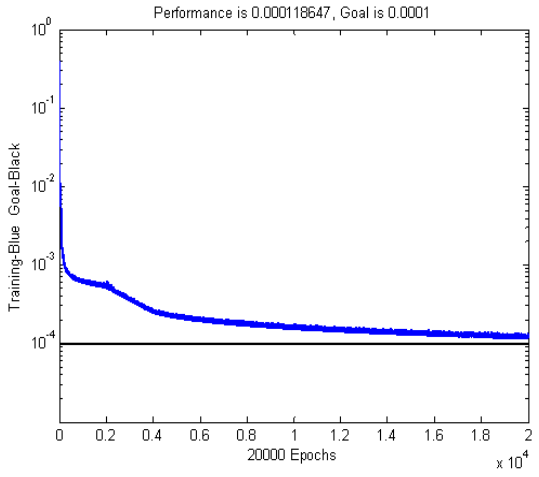

Fig.4: Variation of total error with number of Epochs in 3-4-9-1 network for clad width

Table 5: Selected Training Parameters of ANN for Clad Width

No. of epochs	20000
Goal	0.0001
Learning rate	0.05
Max_fail	5
Mu_max	10^{10}
Transfer function	Log sigmoid

5. Confirmatory test

For validation of the predicted results at optimum condition, experiments are conducted as per the optimum condition and observed that the average results are fairly close to the predicted results.

The estimated clad height or clad width $\bar{\eta}$ at the optimal level can be calculated as follows.

$$\bar{\eta} = \eta_m + \sum_{i=1}^{o} (\eta_i - \eta_m) \qquad \text{..... (v)}$$

Where, η_m is the total mean clad height, η_i is the mean clad height at the optimal level and o is the number of main design parameters that affect the quality characteristics. Table 6 shows the comparison of the estimated responses (calculated using equation (v)) with the actual responses obtained from the experiment using the optimal process parameter combination. The absolute prediction error (APE) in percentage has been calculated using the following formulae.

$$\text{APE} = \left| \frac{\text{Experimental - Predicted}}{\text{Experimental}} \right| \text{X100\%} \qquad \text{..... ..(vi)}$$

Table 6: Validation of the ANN Predicted Results

Responses	Experimental Value (mm)	Predicted Value (mm)	APE (%)
Clad Height	0.121	0.0872	27.94
Clad Width	2.124	2.3211	9.28

6. Conclusion

In the context of CO_2 laser cladding process performance for 20MnCr5 substrate using Inconel-625 powder as cladding material, an attempt is made to determine the optimum combination of laser power, scan speed and powder feed rate to maximize clad width as well as to minimize clad height at a time using Genetic Algorithm approach. From optimization method using GA, the optimum values obtained for H and W are 0.0951 mm and 1.9710 mm respectively which are showing great improvement in performance characteristics.

The artificial neural network model using BP-MLP technique has been developed specially for predicting the clad bead characteristics at optimum cladding condition. This model also helps to find the responses at other combinations of process variables. It is observed that developed ANN model shows a good agreement with the experimental results.

References:

1. Hans Gedda, Laser surface cladding a literature survey, 2000:07. ISSN: 1402-1536. ISRN: LTU-TR—00/07—SE
2. J. Paulo Davim, Carlos Oliveira, A. Cardoso, 2008, "Predicting the geometric form of clad in laser cladding by powder using multiple regression analysis (MRA)", Materials and Design 29 , pp 554 – 557
3. Oliveira U, Ocelı´k V, De Hosson J. "Analysis of coaxial laser cladding processing conditions" Surface & Coatings Technology 2005; 197:127–36
4. Godfrey C.Onwubolu, J. Paulo Davim, Carlos Oliveria, A. Cardoso "Prediction of clad angle in laser cladding by powder using response surface methodogy and scatter search" Optics & Laser technology 39 (2007) 1130-1134
5. Kathuria Y.P., "Laser-cladding process: a study using stationary and scanning CO_2 laser beams". Surf Coat Technol 1997; 97:442–7
6. L. Shepeleva, B. Medres, W.D. Kaplan, M. Bamberger, A. Weisheit, "Laser cladding of turbine blades", Surface and Coatings Technology 125 (2000) 45-48
7. S.M. Karazi, A.Issa,D.Brabazon, "Comparison of ANN and DoE for the prediction of laser-machined micro-channel dimensions" Optics and Lasers in Engineering 47 (2009) 956–964
8. K.Y. Benyounis, A.G. Olabi, "Optimization of different welding processes using statistical and numerical approaches – A reference guide", Advances in Engineering Software 39 (2008) 483–496
9. Aman Aggarwal, Hari Singh, Pradeep Kumar, Manmohan Singh, "Optimizing power consumption for CNC turned parts using response surface methodology and Taguchi's technique—A comparative analysis", journal of materials processing technology 2 0 0 (2 0 0 8) 373–384
10. C.P. Paul, P. Ganesh, S.K. Mishra, P. Bhargavaa, J. Negib, A.K. Nath, "Investigating laser rapid manufacturing for Inconel-625 components" Optics & Laser Technology 39 (2007) 800–805
11. Madhav S. Phadke "Quality Engineering Using Robust Design", Prentice Hall, Englewood Cliffs, New Jersery 07632
12. Kun-Lin Hsieh, Lee-Ing Tong, Hung-Pin Chiu, Hsin-Ya Yeh, "Optimization of a multi-response problem in Taguchi's dynamic system", Computers & Industrial Engineering 49 (2005) 556–571
13. Ozcan Tan, A. Sahin Zaimoglu, Sinan Hinislioglu, Selim Altun, "Taguchi approach for optimization of the bleeding on cement-based grouts", Tunnelling and Underground Space Technology 20 (2005) 167–173
14. Hasan Okuyucu, Adem Kurt, Erol Arcaklioglu, "Artificial neural network application to the friction stir welding of aluminum plates", Materials and Design 28 (2007) 78–84
15. Hany El Kadi, "Modeling the mechanical behavior of fiber-reinforced polymeric composite materials using artificial neural networks—A review", Composite Structures 73 (2006) 1–23

Fuzzy Programming approach for Fractional Multi-objective Transportation Problem with Impurity Constraints

Madhuri[*] P.K. Saksena[1]
[*]Department of Mathematics
GLA University, Mathura, India
[1]Retired Professor, Faculty of Engineering
Dayalbagh Educational Institute
Dayalbagh, Agra, India

Abstract
In this paper, a Fractional Multi-objective Transportation Problem with Impurity Constraints having demand and supply constraints somewhat uncertain imprecise and vague in nature is formulated as Fractional Multi-objective Transportation Problem with Impurity Constraints with extreme tolerances. By using suitable transformation, an equivalent Multi-objective Linear Transportation Problem with Impurity Constraints is formulated which is transformed into an equivalent crisp model to determine an optimal solution of Fractional Multi-objective Transportation Problem with Impurity Constraints.

Keywords: Fractional Transportation Problem, Fuzzy Programming, Crisp Model, Membership Function, Multi-objective Decision Making.

1. Introduction

Conventional optimization methods assume that all parameters and goals of an optimization model are precisely known. But for many practical problems there are incompleteness and unreliability of input information. This is caused to use fuzzy multi-objective optimization method with fuzzy parameters. Bit et al. [2] presented an application of fuzzy linear programming to the linear multi-objective transportation problem, a special type of vector minimum problem in which constraints were all equality type and the objectives were conflicting in nature. Li and Lai [4] presented a fuzzy compromise programming approach to multiobjective transportation problems. A characteristic feature of the approach proposed was that various objectives were synthetically considered with the marginal evaluation for individual objectives and the global evaluation for all objectives. Verma et al. [7] used a special type of non-linear (hyperbolic and exponential) membership functions to solve the multi-objective transportation problem. Sakawa et al. [5] discussed a two objective transportation problem, minimizing the transportation cost and minimizing the opportunity loss with respect to transportation time, in a housing material manufacturer and derived a satisfactory solution to the problem using interactive fuzzy programming method.

This paper presents a Fuzzy Programming approach to solve Fractional Multi-objective Transportation Problem with Impurity Constraints. The fractional multi-objective transportation problem with impurity constraints having demand and supply constraints somewhat uncertain imprecise and vague in nature is formulated as fractional multi-objective transportation problem with impurity constraints with extreme tolerances. By using suitable transformation, an equivalent multi-objective linear transportation problem with impurity constraints is formulated which is transformed into an equivalent crisp model to determine an optimal solution of fractional multi-objective transportation problem with impurity constraints.

2. Mathematical Formulation

The mathematical formulation of Fractional Multi-objective Transportation Problem with Impurity Constraints is written as:

P_1 Maximize $$Z^G(x) = \frac{N^G(x)}{D^G(x)} = \frac{\sum_{i=1}^{m}\sum_{j=1}^{n} c_{ij}^G x_{ij}}{\sum_{i=1}^{m}\sum_{j=1}^{n} d_{ij}^G x_{ij}}$$

subject to $\sum_{j=1}^{n} x_{ij} = \tilde{a}_i \qquad (i = 1,2,\ldots\ldots,m)$

$$\sum_{i=1}^{m} x_{ij} = \tilde{b}_j \qquad (j = 1,2,\ldots\ldots,n)$$

$$\sum_{i=1}^{m} f_{ijk} x_{ij} \le \tilde{q}_{jk} \qquad (j = 1,2,\ldots\ldots,n; k = 1,2,\ldots\ldots,P)$$

$$x_{ij} \ge 0 \qquad (i = 1,2,\ldots\ldots,m; j = 1,2,\ldots\ldots,n)$$

where

$Z^G(x) = [Z^1(x), Z^2(x), \ldots\ldots, Z^g(x)]$, is a vector of g fractional objective functions and the superscript on both fractional objective functions $Z^G(x)$, numerator $N^G(x)$ and denominator $D^G(x)$ are used to identify the number of fractional objective functions $(G = 1,2,\ldots\ldots,g)$

$\tilde{a}_i$ = amount available is somewhat uncertain/non-stochastic imprecise and vague in nature at the i^{th} supply point

$\tilde{b}_j$ = requirement is somewhat uncertain/non-stochastic imprecise and vague in nature at the j^{th} demand point

x_{ij} = amount of commodity to be transported from the i^{th} supply point to the j^{th} demand point

f_{ijk} = units of P impurities $(k = 1,2,\ldots\ldots,P)$ in one unit of the commodity when it is transported from the i^{th} supply point to the j^{th} demand point

$\tilde{q}_{jk}$ = units of greatest quantity of impurity k that can be received by demand point j is uncertain, imprecise and vague in nature

c_{ij}^G / d_{ij}^G = the proportional contribution to the value of G^{th} fractional objective function of transporting one unit of commodity from the i^{th} supply point to the j^{th} demand point.

Assumptions:

1. Without loss of generality it will be assumed that $\tilde{a}_i > 0 \ \forall \ i$; $\tilde{b}_j > 0 \ \forall \ j$.
2. For consistency, total demand requirement equals the total supply capacity.
3. Positive Triangular Numbers

- $\tilde{a}_i = (a_i - a_i^l, a_i, a_i + a_i^r)$ with tolerances $a_i^l (< a_i)$, $a_i^r (> 0)$.
- $\tilde{b}_j = (b_j - b_j^l, b_j, b_j + b_j^r)$ with tolerances $b_j^l (< b_j)$, $b_j^r (> 0)$.
- $\tilde{q}_{jk} = (q_{jk} - q_{jk}^l, q_{jk}, q_{jk} + q_{jk}^r)$ with tolerances $q_{jk}^l (< q_{jk})$, $q_{jk}^r (> 0)$.

4. $\sum_{i=1}^{m}\sum_{j=1}^{n} d_{ij}^G x_{ij} > 0$, for all feasible solution.

In this context, it may be noted that the impurity constraints of P_1 can be written as:

$$\sum_{i=1}^{m} f_{ijk} x_{ij} + x_{M+k,j} = \tilde{q}_{jk}$$

$$x_{M+k,j} \ge 0$$

where $x_{M+k,j}$ are the slack variables to the impurity constraints.

P_1 can be modified as the Fractional Multi-objective Transportation Problem with Impurity Constraints with extreme tolerances:

P_2 Maximize $Z^G(x) = \dfrac{N^G(x)}{D^G(x)} = \dfrac{\sum_{i=1}^{m}\sum_{j=1}^{n} c_{ij}^G x_{ij}}{\sum_{i=1}^{m}\sum_{j=1}^{n} d_{ij}^G x_{ij}}$

subject to

$$\sum_{j=1}^{n} x_{ij} \geq a_i - a_i^l$$

$$\sum_{j=1}^{n} x_{ij} \leq a_i + a_i^r$$

$$\sum_{i=1}^{m} x_{ij} \geq b_j - b_j^l$$

$$\sum_{i=1}^{m} x_{ij} \leq b_j + b_j^r$$

$$\sum_{i=1}^{m} f_{ijk} x_{ij} + x_{M+k,j} \geq q_{jk} - q_{jk}^l$$

$$\sum_{i=1}^{m} f_{ijk} x_{ij} + x_{M+k,j} \leq q_{jk} + q_{jk}^r \qquad x_{ij} \geq 0\,, x_{M+k,j} \geq 0$$

With the help of transformation $y = tx$, $(t > 0)$ [1], an equivalent Multi-objective Linear Transportation Problem with Impurity Constraints may be written as:

P_3 Maximize $[t \cdot N^G(y/t)]$

subject to

$$t \cdot D^G(y/t) \leq 1$$

$$\frac{1}{t}\sum_{j=1}^{n} y_{ij} \geq a_i - a_i^l$$

$$\frac{1}{t}\sum_{j=1}^{n} y_{ij} \leq a_i + a_i^r$$

$$\frac{1}{t}\sum_{i=1}^{m} y_{ij} \geq b_j - b_j^l$$

$$\frac{1}{t}\sum_{i=1}^{m} y_{ij} \leq b_j + b_j^r$$

$$\frac{1}{t}\left[\sum_{i=1}^{m} f_{ijk} y_{ij} + y'\right] \geq q_{jk} - q_{jk}^l$$

$$\frac{1}{t}\left[\sum_{i=1}^{m} f_{ijk} y_{ij} + y'\right] \leq q_{jk} + q_{jk}^r$$

$$y \geq 0, \quad y' \geq 0\,,\ t > 0$$

The fuzzy objective functions and constraints are characterized by their membership functions. To optimize the objective functions and the constraints, a decision in a fuzzy environment is defined in analogy to nonfuzzy environments as the selection of activities which simultaneously satisfy objective functions and constraints. Therefore, the decision in a fuzzy environment can be viewed as the intersection of fuzzy constraints and fuzzy objective functions.

The membership function of each objective functions and constraints can be written as:

$$\mu_G(t\cdot N^G(y/t)) = \begin{cases} 0 & \text{if } t\cdot N^G(y/t) \le 0, \\ \dfrac{t\cdot N^G(y/t)-0}{\tilde{Z}^G-0} & \text{if } 0 < t\cdot N^G(y/t) < \tilde{Z}^G, \\ 1 & \text{if } t\cdot N^G(y/t) \ge \tilde{Z}^G \end{cases}$$

$$\mu(\tilde{a}_i) = \begin{cases} 0 & \text{if } a_i > \dfrac{1}{t}\sum_{j=1}^{n} y_{ij} + a_i^l \\ \dfrac{\frac{1}{t}\sum_{j=1}^{n} y_{ij} + a_i^l - a_i}{a_i^l} & \text{if } \dfrac{1}{t}\sum_{j=1}^{n} y_{ij} < a_i \le \dfrac{1}{t}\sum_{j=1}^{n} y_{ij} + a_i^l \\ \dfrac{a_i - \frac{1}{t}\sum_{j=1}^{n} y_{ij} + a_i^r}{a_i^r} & \text{if } \dfrac{1}{t}\sum_{j=1}^{n} y_{ij} - a_i^r \le a_i < \dfrac{1}{t}\sum_{j=1}^{n} y_{ij} \\ 0 & \text{if } a_i \le \dfrac{1}{t}\sum_{j=1}^{n} y_{ij} - a_i^r \end{cases}$$

$$\mu(\tilde{b}_j) = \begin{cases} 0 & \text{if } b_j > \dfrac{1}{t}\sum_{i=1}^{m} y_{ij} + b_j^l \\ \dfrac{\frac{1}{t}\sum_{i=1}^{m} y_{ij} + b_j^l - b_j}{b_j^l} & \text{if } \dfrac{1}{t}\sum_{i=1}^{m} y_{ij} < b_j \le \dfrac{1}{t}\sum_{i=1}^{m} y_{ij} + b_j^l \\ \dfrac{b_j - \frac{1}{t}\sum_{i=1}^{m} y_{ij} + b_j^r}{b_j^r} & \text{if } \dfrac{1}{t}\sum_{i=1}^{m} y_{ij} - b_j^r \le b_j < \dfrac{1}{t}\sum_{i=1}^{m} y_{ij} \\ 0 & \text{if } b_j \le \dfrac{1}{t}\sum_{i=1}^{m} y_{ij} - b_j^r \end{cases}$$

$$\mu(\tilde{q}_{jk}) = \begin{cases} 0 & \text{if } q_{jk} > \dfrac{1}{t}\left[\sum_{i=1}^{m} f_{ijk}y_{ij} + y'\right] + q_{jk}^l \\ \dfrac{\frac{1}{t}\left[\sum_{i=1}^{m} f_{ijk}y_{ij} + y'\right] + q_{jk}^l - q_{jk}}{q_{jk}^l} & \text{if } \dfrac{1}{t}\left[\sum_{i=1}^{m} f_{ijk}y_{ij} + y'\right] < q_{jk} \le \dfrac{1}{t}\left[\sum_{i=1}^{m} f_{ijk}y_{ij} + y'\right] + q_{jk}^l \\ \dfrac{q_{jk} - \frac{1}{t}\left[\sum_{i=1}^{m} f_{ijk}y_{ij} + y'\right] + q_{jk}^r}{q_{jk}^r} & \text{if } \dfrac{1}{t}\left[\sum_{i=1}^{m} f_{ijk}y_{ij} + y'\right] - q_{jk}^r \le q_{jk} < \dfrac{1}{t}\left[\sum_{i=1}^{m} f_{ijk}y_{ij} + y'\right] \\ 0 & \text{if } q_{jk} \le \dfrac{1}{t}\left[\sum_{i=1}^{m} f_{ijk}y_{ij} + y'\right] - q_{jk}^r \end{cases}$$

3. Crisp Model

By introducing an auxiliary variable λ, P_3 can be transformed into the following Crisp Model [3]:

P_4 Max λ

subject to $\mu_G(t\cdot N^G(y/t)) \ge \lambda$

$$\mu(\tilde{a}_i) \ge \lambda$$
$$\mu(\tilde{b}_j) \ge \lambda$$
$$\mu(\tilde{q}_{jk}) \ge \lambda$$
$$t\cdot D^G(y/t) \le 1$$
$$0 \le \lambda \le 1,\ t > 0$$

The constraints in P_4 containing cross product terms λt which are not convex. Therefore the solution of this problem requires the special approach adopted for solving general non-convex application problems and therefore is solved by fuzzy decisive set method [6].

4. Algorithm

The steps of the algorithm are as follows:

Step 1: Formulate Problem P_1 as P_2.

Step 2: Obtain an equivalent Multi-objective Linear Transportation Problem with Impurity Constraints: P_3 using transformation $y = tx$, $(t > 0)$.

Step 3: Determine maximum aspiration level $\overline{Z}^G$ by maximizing each objective function of P_3.

Step 4: Define membership function of each objective function, constraints and impurity constraints of P_3.

Step 5: Transform P_3 into an equivalent crisp model P_4 by introducing an auxiliary variable λ.

Step 6: Solve the transformed crisp model: P_4 by using fuzzy decisive set method and obtain the optimal value λ^* of λ.

Step 7: Obtain optimal solution of P_1 with the help of the maximum value λ^* of P_4.

5. Numerical Example

Consider the following Fractional Multi-objective Transportation Problem with Impurity Constraints. Here supplies and demands are trapezoidal fuzzy numbers. If x_{ij} be the tonnage sent from source i to destination j, then it is required to

$$\text{Max } Z^G(x) = \frac{\sum_{i=1}^{3}\sum_{j=1}^{3} c_{ij}^G x_{ij}}{\sum_{i=1}^{3}\sum_{j=1}^{3} d_{ij}^G x_{ij}}$$

subject to,

$$\sum_{j=1}^{3} x_{ij} = \tilde{a}_i$$

$$\sum_{i=1}^{3} x_{ij} = \tilde{b}_j$$

$$\sum_{i=1}^{3} p_i x_{ij} \le L_j \tilde{b}_j$$

$$x_{ij} \ge 0$$

$$(i = 1,2,3;\ j = 1,2,3; G = 1,2,3)$$

Source i	Destination j			a_i	p_i
	$[c_{i1}\ \ d_{i1}]$	$[c_{i2}\ d_{i2}]$	$[c_{i3}\ d_{i3}]$		
1	$\begin{bmatrix}1\\5\\10\end{bmatrix}\begin{bmatrix}4\\4\\12\end{bmatrix}$	$\begin{bmatrix}2\\6\\3\end{bmatrix}\begin{bmatrix}4\\5\\7\end{bmatrix}$	$\begin{bmatrix}7\\2\\4\end{bmatrix}\begin{bmatrix}3\\3\\5\end{bmatrix}$	(7, 8, 10)	0.4
2	$\begin{bmatrix}1\\11\\1\end{bmatrix}\begin{bmatrix}5\\7\\7\end{bmatrix}$	$\begin{bmatrix}9\\3\\16\end{bmatrix}\begin{bmatrix}8\\8\\14\end{bmatrix}$	$\begin{bmatrix}3\\12\\1\end{bmatrix}\begin{bmatrix}9\\6\\1\end{bmatrix}$	(10,11,13)	0.8
3	$\begin{bmatrix}8\\4\\3\end{bmatrix}\begin{bmatrix}6\\1\\6\end{bmatrix}$	$\begin{bmatrix}9\\10\\4\end{bmatrix}\begin{bmatrix}2\\3\\8\end{bmatrix}$	$\begin{bmatrix}4\\2\\3\end{bmatrix}\begin{bmatrix}5\\12\\2\end{bmatrix}$	(8, 9, 11)	0.6
b_j	(6, 7, 9)	(4, 5, 7)	(15, 16, 18)		
L_j	0.7	0.7	0.7		

An equivalent multi-objective linear transportation problem with impurity constraints using transformation $y = tx$, $(t > 0)$ is:

$$\text{Max}\left\{\begin{aligned} z^1(y,t) &= y_{11} + 2y_{12} + 7y_{13} + y_{21} + 9y_{22} + 3y_{23} + 8y_{31} + 9y_{32} + 4y_{33},\\ z^2(y,t) &= 5y_{11} + 6y_{12} + 2y_{13} + 11y_{21} + 3y_{22} + 12y_{23} + 4y_{31} + 10y_{32} + 2y_{33},\\ z^3(y,t) &= 10y_{11} + 3y_{12} + 4y_{13} + y_{21} + 16y_{22} + y_{23} + 3y_{31} + 4y_{32} + 3y_{33} \end{aligned}\right\}$$

subject to

$$4y_{11} + 4y_{12} + 3y_{13} + 5y_{21} + 8y_{22} + 9y_{23} + 6y_{31} + 2y_{32} + 5y_{33} \le 1$$
$$4y_{11} + 5y_{12} + 3y_{13} + 7y_{21} + 8y_{22} + 6y_{23} + y_{31} + 3y_{32} + 12y_{33} \le 1$$
$$12y_{11} + 7y_{12} + 5y_{13} + 7y_{21} + 14y_{22} + y_{23} + 6y_{31} + 8y_{32} + 2y_{33} \le 1$$
$$y_{11} + y_{12} + y_{13} - 7t \ge 0$$
$$y_{11} + y_{12} + y_{13} - 10t \le 0$$
$$y_{21} + y_{22} + y_{23} - 10t \ge 0$$
$$y_{21} + y_{22} + y_{23} - 13t \le 0$$
$$y_{31} + y_{32} + y_{33} - 8t \ge 0$$
$$y_{31} + y_{32} + y_{33} - 11t \le 0$$
$$y_{11} + y_{21} + y_{31} - 6t \ge 0$$
$$y_{11} + y_{21} + y_{31} - 9t \le 0$$
$$y_{12} + y_{22} + y_{32} - 4t \ge 0$$
$$y_{12} + y_{22} + y_{32} - 7t \le 0$$
$$y_{13} + y_{23} + y_{33} - 15t \ge 0$$
$$y_{13} + y_{23} + y_{33} - 18t \le 0$$
$$4y_{11} + 8y_{21} + 6y_{31} + y_{41} - 49t \ge 0$$
$$4y_{11} + 8y_{21} + 6y_{31} + y_{41} - 70t \le 0$$

$$4y_{12}+8y_{22}+6y_{32}+y_{42}-28t\geq 0$$
$$4y_{12}+8y_{22}+6y_{32}+y_{42}-49t\leq 0$$
$$4y_{13}+8y_{23}+6y_{33}+y_{43}-105t\geq 0$$
$$4y_{13}+8y_{23}+6y_{33}+y_{43}-126t\leq 0$$
$$y_{11},y_{12},y_{13},y_{21},y_{22},y_{23},y_{31},y_{32},y_{33},y_{41},y_{42},y_{43}\geq 0,\ t>0.$$

The following maximum aspiration levels are obtained by maximizing each objective function :

$$z^1(y,t)\underset{\sim}{>}1.363057,\ z^2(y,t)\underset{\sim}{>}2.100775 \text{ and } z^3(y,t)\underset{\sim}{>}1.054341.$$

Using the membership functions, the above fuzzy model reduces to the following Crisp Model:

Max λ

subject to

$$y_{11}+2y_{12}+7y_{13}+y_{21}+9y_{22}+3y_{23}+8y_{31}+9y_{32}+4y_{33}-1.363057\ \lambda\geq 0$$
$$5y_{11}+6y_{12}+2y_{13}+11y_{21}+3y_{22}+12y_{23}+4y_{31}+10y_{32}+2y_{33}-2.100775\ \lambda\geq 0$$
$$10y_{11}+3y_{12}+4y_{13}+y_{21}+16y_{22}+y_{23}+3y_{31}+4y_{32}+3y_{33}-1.054341\ \lambda\geq 0$$
$$4y_{11}+4y_{12}+3y_{13}+5y_{21}+8y_{22}+9y_{23}+6y_{31}+2y_{32}+5y_{33}\leq 1$$
$$4y_{11}+5y_{12}+3y_{13}+7y_{21}+8y_{22}+6y_{23}+y_{31}+3y_{32}+12y_{33}\leq 1$$
$$12y_{11}+7y_{12}+5y_{13}+7y_{21}+14y_{22}+y_{23}+6y_{31}+8y_{32}+2y_{33}\leq 1$$
$$y_{11}+y_{12}+y_{13}\geq (7+\lambda)t$$
$$y_{11}+y_{12}+y_{13}\leq (10-2\lambda)t$$
$$y_{21}+y_{22}+y_{23}\geq (10+\lambda)t$$
$$y_{21}+y_{22}+y_{23}\leq (13-2\lambda)t$$
$$y_{31}+y_{32}+y_{33}\geq (8+\lambda)t$$
$$y_{31}+y_{32}+y_{33}\leq (11-2\lambda)t$$
$$y_{11}+y_{21}+y_{31}\geq (6+\lambda)t$$
$$y_{11}+y_{21}+y_{31}\leq (9-2\lambda)t$$
$$y_{12}+y_{22}+y_{32}\geq (4+\lambda)t$$
$$y_{12}+y_{22}+y_{32}\leq (7-2\lambda)t$$
$$y_{13}+y_{23}+y_{33}\geq (15+\lambda)t$$
$$y_{13}+y_{23}+y_{33}\leq (18-2\lambda)t$$
$$4y_{11}+8y_{21}+6y_{31}+y_{41}\geq (49+\lambda)t$$
$$4y_{11}+8y_{21}+6y_{31}+y_{41}\leq (70-2\lambda)t$$
$$4y_{12}+8y_{22}+6y_{32}+y_{42}\geq (28+\lambda)t$$
$$4y_{12}+8y_{22}+6y_{32}+y_{42}\leq (49-2\lambda)t$$
$$4y_{13}+8y_{23}+6y_{33}+y_{43}\geq (105+\lambda)t$$
$$4y_{13}+8y_{23}+6y_{33}+y_{43}\leq (126-2\lambda)t$$
$$\lambda\geq 0, t>0$$

Solve the crisp model by using the fuzzy decisive set method. The following values of λ are obtained in the next 30 iterations:

λ = 0.50; λ = 0.75; λ = 0.625; λ = 0.6875;
λ = 0.65625; λ = 0.671875; λ = 0.6796875; λ = 0.67578125;
λ = 0.677734375 λ = 0.676757812; λ = 0.676269531; λ = 0.67602539;
λ =0.67596332; λ = 0.675842285; λ = 0.675872802; λ =0.675857543;
λ =0.675849914; λ = 0.675846099; λ = 0.675848007; λ = 0.675847053;
λ = 0.67584753; λ = 0.675847291; λ = 0.675847172; λ = 0.675847113;
λ = 0.675847083; λ = 0.675847098; λ = 0.675847105; λ = 0.675847102;
λ = 0.675847103; λ = 0.675847104.

Consequently, the maximum value λ^* = 0.675847104 is obtained at the 31st iteration and solution of Crisp Model is:

y_{11}^* = 0.02474367, y_{13}^* = 0.03316893, y_{21}^* = 0.009168814, y_{22}^* =0.003489797,
y_{23}^* = 0.05883124, y_{31}^* = 0.01079152, y_{32}^* = 0.03433357, y_{33}^* = 0.01297173,
y_{41}^* = 0.09557549, y_{42}^* = 0.08515277, y_{43}^* = 0.1535401, t^* = 0.00669641,
λ^* = 0.675847104.

The optimal solution of the original problem is obtained as:

x_{11}^* = 3.695064968, x_{13}^* = 04.953240617, x_{21}^* = 1.369213355, x_{22}^* = 0.521144464,
x_{23}^* = 8.785489538, x_{31}^* = 1.611538123, x_{32}^* = 5.127160673, x_{33}^* = 1.937117052,
x_{41}^* = 14.27264609, x_{42}^* = 12.71618225, x_{43}^* = 22.92871852, Z^{1^*} = 0.921218109,
Z^{2^*} = 1.555058607, Z^{3^*} = 0.712573308.

6. Conclusion

To generate total transportation solutions for Fractional Multi-objective Transportation Problems with Impurity Constraints, an algorithm has been developed in this paper using Fuzzy Programming approach. Solving fractional multi-objective transportation models offers a more universal apparatus for a wider class of real life decision priority problems than the multi-objective transportation problems. The fractional multi-objective transportation problems results in a subset of feasible solutions from which a transportation system decision maker is sure of a most preferred solution.

References

[1] A. Charnes and W.W. Cooper. "Programming with linear fractional functional", Naval Research Logistic Quarterly, 1962, Vol.9, pp.181–186.
[2] A.K. Bit, M.P. Biswal, S.S. Alam. "Fuzzy programming approach to multicriteria decision making transportation problem", Fuzzy Sets and Systems, 1992, Vol. 50, pp. 135–141.
[3] H.J. Zimmermann. "Fuzzy programming and linear programming with several objective functions", Fuzzy Sets and System, 1978, Vol. 1, pp. 45–55.
[4] L. Li and K.K. Lai. "A fuzzy approach to the multiobjective transportation problem", Computers & Operations Research, 2000, Vol. 27, pp. 43–57.
[5] M. Sakawa, I. Nishizaki and Y. Uemura. "A decentralized two-level transportation problem in a housing material manufacturer: Interactive fuzzy programming approach", European Journal of Operational Research, 2002, Vol. 141, pp. 167–185.
[6] R.N. Gasimov and K. Yenilmez. "Solving fuzzy linear programming with linear membership functions", Turk. J. Math., 2002, Vol. 26, pp. 375–396.
[7] R. Verma, M.P. Biswal and A. Biswas. "Fuzzy programming technique to solve multi-objective transportation problems with some non-linear membership functions", Fuzzy Sets and Systems, 1997, Vol. 91, pp. 37–43.

Design and Development of Quad Band Rectangular Microstrip Antenna with Ominidirectional Radiation Characteristics

M. Veereshappa and S. N. Mulgi
Department of PG Studies and Research in Applied Electronics,
Gulbarga University, Gulbarga – 585 106, Karnataka, India.

Abstract:
This paper presents the design and development of slotted rectangular microstrip antenna for quad band operation and ominidirectional radiation characteristics. The quad bands are achieved between 4.81 to 16 GHz. The magnitude of operating bandwidth has been enhanced to a maximum value of 3.29, 17.22, 36.44 and 43.33% by varying the width of vertical slots on the patch. This enhancement does not affect the nature of ominidirectional radiation characteristics. The proposed antenna is simple in its geometry and has been constructed from conventional rectangular microstrip antenna by placing vertical slots on the patch and a ground plane of height equal to the length of microstripline on the top and bottom surface of the substrate. Experimental results are in close agreement with the simulated results. The proposed antenna may find application in microwave communication system**.**

Keywords: Bandwidth, Microstrip antenna, Ominidirectional and Slot

1. Introduction

Microstrip antennas (MSAs) are finding increasing applications in microwave communication systems because of their diversified uses such as low profile, light weight, planar configurations, easy to fabricate and low cost [1]. The MSA operating at more than one band of frequencies is quite useful because each band can be used independently for transmit receive applications. Number of investigations have been reported in the literature for the realization of dual, triple and multi band operation of microstip antenna [3-9]. But design of quad band operation realized from conventional rectangular microstrip antenna with ominidirectional radiation characteristics is an additional advantage of the device. Further the construction of quad band slotted rectangular microstrip antenna (QSRMSA) does not alter its size when compared to the size of conventional rectangular microstrip antenna (CRMA) designed for the same resonant frequency.

2. Description of antenna geometry

The art work of the proposed antenna is sketched by using computer software Auto-CAD to achieve better accuracy and is fabricated on low cost FR4-epoxy substrate material of thickness h = 1.6 mm and permittivity ε_r = 4.4 using photolithography process. Figure 1(a) shows the top view geometry of QSRMSA. The bottom view geometry of this antenna is as shown in Fig. 1(b). In Fig. 1(a) the selected area A of the substrate is $L \times W$ cm. On the top surface of the substrate a ground plane of height which is equal to the length of microstripline feed L_f is used. A gap of 1 mm is used between the top ground plane and microstripline feed. On the bottom of the substrate a continuous copper layer of height L_f is used below the microstripline which is bottom ground plane. The QSRMSA is designed for 3 GHz using the equations available for the design of conventional rectangular microstrip antenna in the literature [2]. The length and width of the rectangular patch are L_p and W_p respectively. The feed arrangement consists of quarter wave transformer of length L_t and width W_t which is connected as a matching network between the patch and the microstripline feed of length L_f and width W_f. A Semi miniature-A (SMA) connector is used at the tip of the microstripline feed for feeding the microwave power.

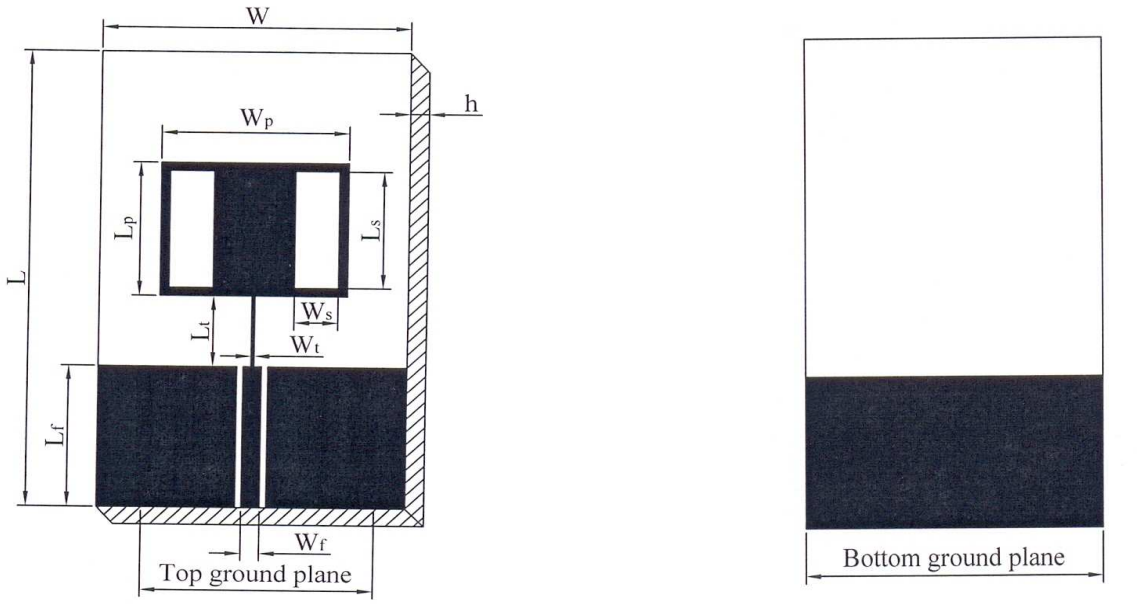

(a) Top view geometry of QSRMSA (b) Bottom view geometry of QSRMSA

Fig. 1 Geometry of QSRMSA when W_s = 6.1 mm

In Fig.1 (a) the vertical rectangular slots are placed on the patch. These slots treated as wide slots as their width is comparable to the length. The wide slots are selected because they are more effective in enhancing the bandwidth when compared to narrow slots. The length and width of vertical rectangular slots are L_s and W_s respectively. Both the slots are kept at a distance of 1.5 mm from the non resonating edges (L_p) of the patch. The design parameter of the proposed antenna is given in Table 1.

TABLE 1 Design Parameters of Proposed Antenna

L_p = 23.4 mm	W_p = 30.4 mm
L_f = 24.8 mm	W_f = 3.0 mm
L_t = 12.4 mm	W_t = 0.5 mm
L = 80.0 mm	W = 50.0 mm
Ls = 20.4mm	Ws = 6.1 mm

3. Experimental results

For the QSRMSA, the bandwidth over return loss less than -10 dB is simulated using HFSS simulating software and then tested experimentally on the Vector Network Analyzer (Rohde & Schwarz, Germany make ZVK model 1127.8651). The variation of return loss frequency of QSRMSA is as shown in Fig. 2. From this graph the experimental bandwidth (BW) is calculated using the equations,

$$BW = \left[\frac{f_2 - f_1}{f_C} \right] \times 100\ \%$$

were, f_1 and f_2 are the lower and upper cut of frequencies of the band respectively when its return loss reaches – 10 dB and f_c is the center frequency of the operating band. From this figure, it is found that, the antenna operates between 4.81 to 16 GHz.

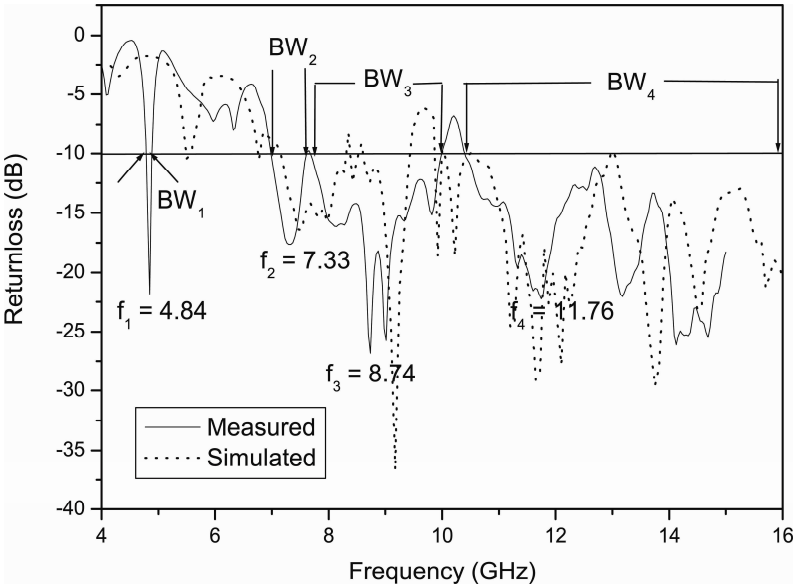

Fig. 2 Variation of return loss versus frequency of QSRMSA when W_s = 6.1 mm

In Fig. 2 it is seen that, the antenna gives four resonant frequency modes. The resonant frequency mode at f_1=4.84 GHz is due to the fundamental resonant frequency of the patch and others modes at f_2 = 7.33 GHz, f_3 = 8.74 GHz and f_4 = 11.76 GHz are due to the novel geometry of QSRMSA. The magnitude of experimental -10 dB bandwidth measured at BW_1 to BW_4 are 60 MHz (4.78-4.84 GHz) 1.24 %, 580 MHz (6.97-7.55 GHz) 7.98 %, 2.27 GHz (7.67-9.94 GHz) 25.78 % and 5.59 GHz (10.41-16 GHz) 42.33% respectively. Since the QSRMSA has been designed for 3 GHz. The fundamental resonant frequency mode (4.84 GHz) shifts from 3 GHz to 4.84 GHz. This shift of resonant mode towards higher frequency side is due to the coupling effect of microstripline feed and top ground plane. Simulated results of QSRMSA are also shown in Fig. 2.

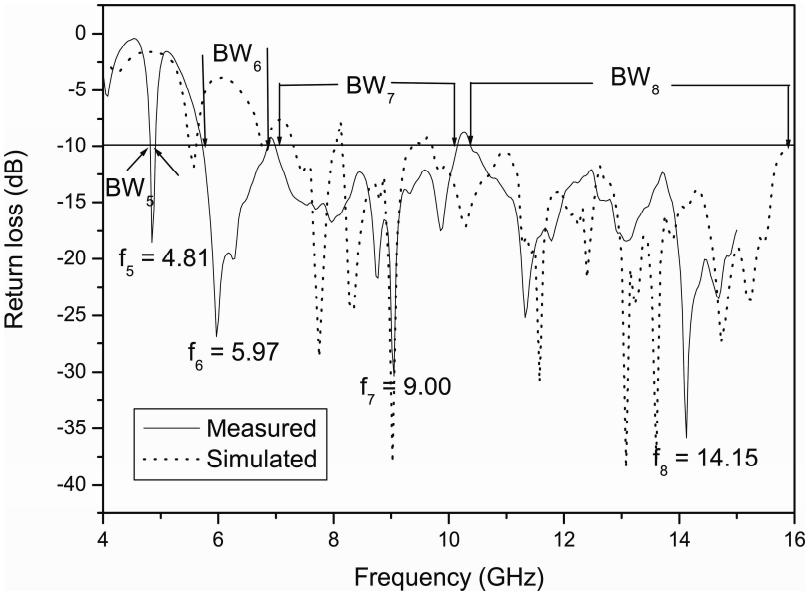

Fig. 3 Variation of return loss versus frequency of QSRMSA when W_s = 7.1 mm

Figure 3 shows the variation of return loss verses frequency of QSRMSA when W_s = 7.1 mm. It is clear from this figure that, the antenna again operates for four resonant frequency modes retaining the fundamental resonant mode at f_5 = 4.81 GHz and other modes at f_6 = 5.9 GHz, f_7 = 9.00 GHz and f_8 = 14.15 GHz. The magnitude of experimental bandwidth measured at BW_5 to BW_8 are 160 MHz (4.78-4.94 GHz) 3.29 %, 1.08 GHz (5.73-6.81 GHz) 17.22 %, 3.12 GHz (7-

10.12 GHz) 36.44 % and 5.59 GHz (10.41- 16 GHz) 43.33 % respectively. By comparing Fig. 2 and 3 it is clear that BW_5, BW6 and BW_7 increases in their magnitude respectively by 3.29 %, 17.22 % and 36.44 % when compared to BW_1, BW_2 and BW_3 by changing the width W_s to 7.1 mm in QSRMSA.This enhancement of bandwidth does not affect much the fundamental resonant frequency mode f_5 of QSRMSA when compared to f_1.The experimental and simulated results shown in Fig. 3 are in close agreement with each other.

The co-polar and cross-polar radiation pattern of QSRMSA is measured in its operating bands when W_s =. 7.1 mm. The typical radiation patterns measured at 5.97 GHz and 11.32 GHz are as shown in Fig. 4 and 5 respectively. The patterns are ominidirectional in nature

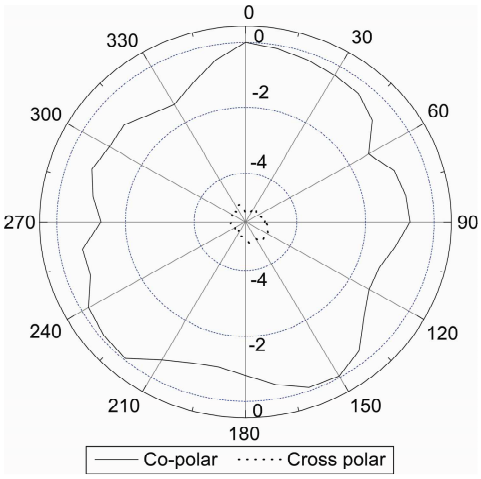

Fig. 4 Radiation pattern of QSRMSA measured at 5.97 GHz.

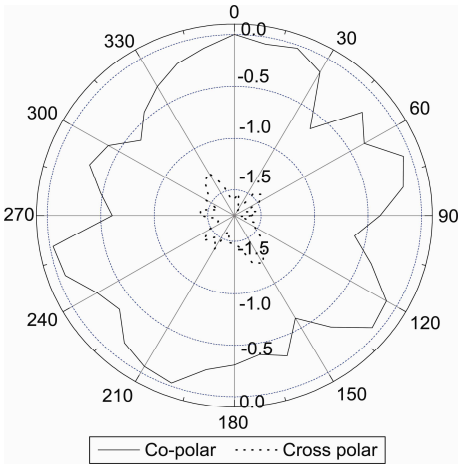

Fig. 5 Radiation pattern of QSRMSA measured at 11.32 GHz

The gain of the proposed antenna is measured by absolute gain method [1] using the formula

$$(G)dB = 10\ \log\left(\frac{P_r}{P_t}\right) - (G_t)dB\ -\ 20\log\left(\frac{\lambda_0}{4\pi R}\right)dB$$

where, P_t is the power transmitted by pyramidal horn antenna, P_r the power received by antenna under test (AUT), G_t the gain of the pyramidal horn antenna and R the distance between transmitting antenna and AUT. The variation of

experimental gain versus frequency of QSRMSA when W_s = 7.1 mm is as shown in Fig. 6. It is seen that, the antenna shows maximum gain of 14.95 dB at 4.85 GHz.

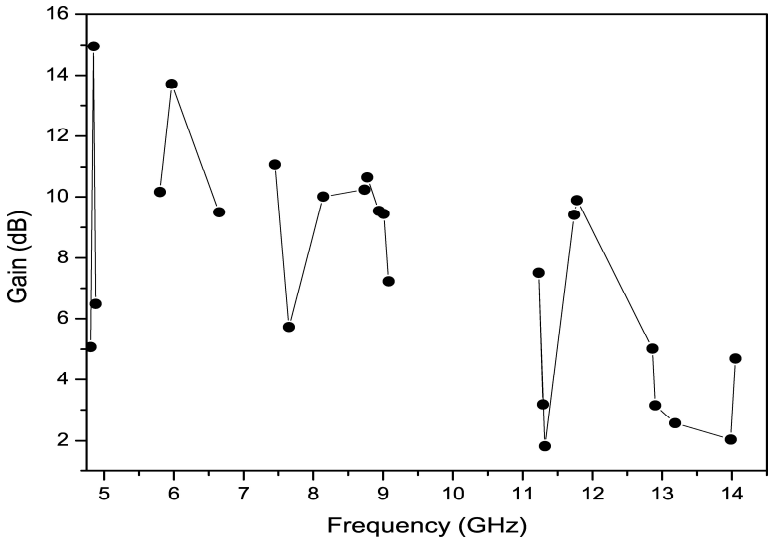

Fig. 6 Variation of gains versus frequency of QSRMSA when W_s = 7.1 mm

4. Conclusion

From the detailed experimental study it is concluded that, the QSRMSA constructed from CRMA is quite capable in producing quad band operation. The antenna operates between 4.81 to 16 GHz of frequency and gives ominidirectional radiation characteristics at each operating band. The magnitude of operating bandwidth has been enhanced to a maximum value of 3.29, 17.22, 36.44 and 43.33% by varying the width of vertical slots on the patch. The enhancement of bandwidth does not affect the nature of ominidirectional radiation characteristics. The simulated and experimental return loss results of QSRMSA are in close agreement with each other. The proposed antenna is simple in its design and fabrication. The antenna is fabricated using low cost FR4 substrate material. With these features the antenna may find any applications in microwave communication system.

Acknowledgements

The authors would like to thank Dept. of Sc. & Tech. (DST), Govt. of India, New Delhi, for sanctioning Vector Network Analyzer to this Department under FIST project. The authors also would like to thank the authorities of Aeronautical Development Establishment (ADE), DRDO, and Bangalore for providing their laboratory facility to make antenna measurements on Vector Network Analyzer.

References

1 Constantine A. Balanis, Antenna theory: analysis and design, John Wiley, New York, 1997.
2 I. J. Bahl and P. Bharatia, Microstrip antennas, Dedham, MA: Artech House, New Delhi, 1981.
3 H. K. Kan. Waterhouse. A. Y. J. Lee and Pavlickovski. 2005, "Dual frequency stacked shorted patch antenna." Electron lett.Vol.41, No.11, pp. 624-626.
4 C.-H. Cai, J. –S Row and K. –L. Wong. 2006, "Dual frequency microstip antenna with dual circular polarization." Electron lett. Vol. 42, No. 22, pp. 1261-1262.
5 J. Y . Sze and K .L Wong. 2000, " Slotted rectangular microstrip antenna for bandwidth enhancement", IEEE Trans. Antennas Propagat, Vol. 48, 1149-1152.
6 K. P. Ray and Y. Ranga. 2006, "Printed rectangular monopole antenna", Proc. IEEE APS Int. Symp. New Mexico, USA pp. 1636-1639.
7 Jia- Yi Size, Kin-lu Wong. 2000, "Slotted rectangular microstrip antenna for bandwidth enhancement", *IEEE* Trans Antennas Propagat 48, 1149-1152
8 W. C. Liu and H. –J. Liu. 2006, "Compact triple band slotted monopole antenna with asymmetrical CPW ground", Electron. Lett. Vol. 42 No. 15
9 K. G. Thomas and M. Sreenivasan. 2009,"Compact triple band antenna for WLAN, WiMAX applications," Electron lett.Vol.45, No.16, pp.811-813.

Location Management using Genetic Algorithm Tuned Neural Network in Mobile Networks

J. Amar Pratap Singh[1], Dr. S. Nirmala[2]
[1] Research Scholar, CSE, Anna University of Technology, Coimbatore
[2] Professor & Head, ECE, Muthayammal Engineering College, Rasipuram

Abstract:
Future mobile systems will be characterized by high user density and high mobility enabling users to communicate regardless of their geographical location. Large number of handovers and registrations will place great demands on radio links. One of the major issues in mobile wireless systems is location management, which is the process that allows a network to identify the exact location of a mobile terminal (MT) for call delivery. In this paper, we present a user pattern learning (UPL) strategy using genetic algorithm tuned artificial neural network (GAANN) to reduce the location update cost. the system maintains a list of places where each user is most likely to be in at each time interval. The intelligence of the location management procedure is increased by updating the profile of each user by users past calling history. Unless the MT detects that it has moved out of the registered profile, it does not perform any other location update. Paging is also done selectively as in the registered profile upon a call arrival for the MT. Experimental results shows that the profile based intelligent system using GAANN performs well than other well known strategies.

Keywords: location management, location update, paging, neural network, genetic algorithm, mobility management.

1 INTRODUCTION

The next generation mobile communications networks should provide not only voice and low-speed data services but also multimedia services requiring high data rate to the users of high density. In a wireless network user can move from place to place while maintaining communication with others. This property is called Mobility of the user. As well known, one of the key issues in cellular mobile communications is how to deliver incoming calls appropriately to the called user roaming from place to place. In the future mobile communications, this issue (especially, the location management) will become more important because of high user mobility [1]. To keep the mobile terminals connected in spite of mobility, the network has to keep track of mobile terminals which will be used to find mobile terminals when incoming calls have to be forwarded towards the mobile terminals.

A network is divided into geographical areas, called location areas (LA) and the location management system keeps track of current LA of a mobile terminal (MT). A location area may contain one or more cells. The location information is stored in the network database for location management. To maintain the consistency of the location information, an update process is triggered whenever a mobile terminal crosses LA boundaries. When a call arrives, a query to the location database is done to obtain the location information of the called MT. Then the location management system pages all the cells in the corresponding LA simultaneously. The same location management system is not possible in present generation mobile communication system, because of the fast growing population.

Location management methods are classified into two major groups: Memory-based and non-memory-based methods. The first group includes methods based on learning processes, which require knowledge of mobile user behavior, while the second group includes methods based on specific algorithms and network architectures. The strategy proposed in this paper belongs to the first group. In North America, the IS-41 standard is used for both the location update and call delivery procedures. This standard deploys a two-level database architecture consisting of a single home location register (HLR) and several visitor location registers (VLR). The HLR for a given network contains the network's subscriber profiles, while a VLR stores the profiles of the users that are currently roaming within LAs associated with that specific VLR. Third-generation mobile networks are characterized by high user density and high mobility (like current 2G systems) and small cell sizes, which will increase the number of location updates and handoff messages, thus limiting the switching capacity and available bandwidth. Reducing the signaling and database access costs of location management introduces significant technical challenges which have to be dealt with and constitutes an important research area. Therefore, more sophisticated schemes were proposed to make the location update and terminal paging operations more efficient. These schemes include the time-based, movement-based [6, 8] and distance-based schemes which locate an MT by paging the LA's ring by ring from its last updated location. Several alternative strategies have recently been proposed to improve the performance of the location management scheme [2-6].

Chien-Hsing Wu et al. [9], used a markov model for Location management. A probabilistic selective paging strategy concept is used for generalizing the selective paging scheme. S.Dasbit et al. (2002) [10], developed a probabilistic location management strategy in a cellular mobile environment. In this scheme the mobile switching center (MSC) maintains an indexed database to keep the frequency of traversals of all the visiting mobile units under it. When a call arrives for a particular mobile unit the MSC performs a location probability of the called MT and performs the best first search to find the cells where the desired MT may be located.

Lo and Chen (2002) [11], describes a dynamic region based location management system for personal communication services system. The strategy described makes use of the users' movement pattern from the set of regions the users is most likely to visit in a time interval. A distributed HLR is used to balance the workload. The call arrival rate and the mobility rate are considered for reducing the registration cost. The strategy used dynamically changes based on the number of regions, the degree of user mobility, and the system parameters such as the signaling cost between HLR and VLR. Yuguang [12], investigated an analytical model for calculating the total cost for pointer forwarding scheme and two-location algorithm. A general model involving various time variables are considered for analyzing the signaling cost. The cost analysis for the move and find are analyzed more analytically for many general cases.

Goo and Yong [13], developed a time based location registration scheme. The MT sends its location update information for every T units of time. If a call arrival occurs within T interval, the system pages the MT and the MT restarts its timer. A ring structure is considered. The inner most ring is ring 0 which is the center cell and it has only one cell. Ring 0 is surrounded by ring 1 and then by ring 2 and so on. When the system routes an incoming call to an MT, it first pages the center cell which is the recently registered location of the MT. If it does not succeed in finding the MT, it pages next surrounded ring. The paging goes on until it finds the MT.

Alejandro Quintero and Oscar Garcia [14], has developed a profile based strategy for managing user mobility in 3G mobile systems. In the 3G mobile systems the power of mobility on network performance must be reduced, mainly due to the huge number of mobile hosts in combination with the small cell size. A profile based strategy is presented to reduce the signaling traffic thereby increasing the intelligence of the location update procedure. User's moving information can be used to assists the user's mobility management, manage network resources and congestion control.

The increasing population of mobile subscribers, smaller sized cells has been used to accommodate the large number of mobile terminals (MT's). Sending paging signals to all cells within a location area (LA) to locate an MT may result in an excessive amount of network bandwidth. In current mobile networks, most users follow regular routines during business hours, residing mostly at their place of work. For these users, it is possible to predict with significant accuracy their location at a particular time of day. The aim of profile-based location prediction schemes is to leverage off this information to reduce location and paging requests [7]. Based on the profile of the user during the last observation period, the location management system generates a list of LA's. When there is a call for the MT, the location management system pages the call to the MT based on the profile of the user.

In this paper, a user pattern learning strategy is followed [8] for location management and the profile of the user is learned using genetic algorithm tuned neural network. In this approach, the MT updates its location only when it's moving direction changes. To locate an MT, paging can be carried out along its moving direction, and hence the paging cost is reduced. Moreover, the MT's moving direction can be determined by simple numerical calculations.

2. OVERVIEW OF THE PROPOSED APPROACH

2.1 Mobility Management in UMTS

In standard UMTS, Mobile Switching Centers (MSCs) are responsible for the circuit switched location management, while Serving GPRS Support Nodes (SGSNs) assume the packet switched location management. Both domains are linked over some interfaces, but the information is kept in separate network entities: The HLR is a common location information database for both domains. Several area types have been defined in UMTS to handle the location information:

- Location Areas (LA) is dividing the network into geographical areas
- A Routing Area (RA) is composed of a group of cells that belong to only one RA. Several RAs can be included in the same LA, but an RA cannot span more than one LA. The PS domain to track the MT's location when in idle mode uses the RAs.
- UMTS Registration Areas (URAS) are an intermediate level between cells and RAs (or LAs). They are similar to RAs

and LAs, but are used by the UTRAN to set trade-offs between the MT's location accuracy and signaling load. Furthermore, they are used to track the MT's location while it is in connected mode without using a logical channel. This concept is optional in UTRAN.
Cells are related to the provision of radio coverage. The idea of having this diversity is to allow a trade-off between location accuracy and paging

2.2 User Profile Learning Strategy
A user pattern learning strategy (UPL) associates with each user a list of location areas (LA) where she is most likely to be located within a given time interval. When a call arrives for an MT, each location within the list is paged sequentially until the MT is found. When a user moves between locations within the list, no location update is required. The list is stored at an intermediate location database (ILD) associated with a Mobile Switching Centers (MSC) as well as within the user's MT. The cost reduction depends on the behavior of each class of user. It can be assumed that, when the user follows its expected behavior, the cost of a location update is reduced.

In the UPL, if the position of a user is always known in advance, then no explicit registration is necessary. Thus, the optimal location area is given by a single cell, which, in turn, minimizes paging costs. Stationary users on fixed schedules exhibit this type of behavior. If mobile users are classified into categories, as was done in [15], the system could treat each category differently to minimize system costs. Furthermore, user mobility information can be used to assist mobility management (traffic routing), to manage network resources (resource allocation, call admission control, congestion, and flow control), and to analyze handoff algorithms in integrated wired/wireless networks.

2.3 GA Tuned ANN
Pattern recognition is one of the fields where neural networks (ANNs) have been strongly applied from many years. Pattern learning and classification can be stated as the problem of labeling test patterns derived by a particular application domain. In general, ANN systems are capable of "learning" trends in a given data set and establishing input-output relationships based strictly on a "test" set of data using back propagation algorithm. In particular, the BP is entirely dependent on the initial (weight) settings and most likely gets trapped into a local minimum. In order to address such deficiencies and drawbacks, in this paper, we propose Genetic Algorithm (GA) optimization technique, which automatically designs the optimal ANNs [both network structure and connection weights with respect to the training mean squared error (MSE)] specifically for each user profile.

GA is used to evolve traditional ANNs, and so the focus is particularly drawn on automatic design of the multilayer perceptrons (MLPs). This evolutionary operator makes the proposed system generic, i.e., no assumption is made about the number of (hidden) layers, and in fact, none of the network properties (e.g., feedforward or not, differentiable activation function or not, etc.) is an inherent constraint. The optimum dimension found corresponds to a distinct ANN architecture where the network parameters (connections, weights, and biases) can be resolved from the positional optimum reached on that dimension. Above all, using standard ANNs such as traditional MLPs, instead of specific architectures further contributes to the generic nature of the proposed system, and in short, all these objectives are meant to make it applicable to location management for any user profile without any modifications.

Neural networks derive their computing power through their ability to learn and then generalize; generalization refers to the ability of the neural network to produce reasonable outputs for inputs not encountered during training. It is this quality that we utilize to predict the movement of mobile users so that we can predict the position of a user in advance and reduce the paging cost based on the predicted destination cell. Finally, the impact on the performance of location management with GAANN is reduced. The cost of the UPL is decomposed into four components: training procedure, maintenance and update of the user's profile, location update, and call delivery. Although GAANN learning times are relatively long, evaluating the learned network in order to apply it to a subsequent instance (maintenance and update of the user's profile, location update and call delivery) is very fast. In GAANN, performance is improved over time by iteratively updating the weights in the network as compared to conventional ANN algorithms.

3. GAANN OPTIMAL DESIGN

Genetic algorithms are good at taking larger, potentially huge, search spaces and navigating them looking for optimal combinations of things and solutions which we might not find in a life time. For every mobile user there is a user pattern learning process associated to it. We may classify the users into three different categories depending the predictability of their daily routine: users who have a very high probability of being where the system expects them to be (deterministic users), users who have a certain likelihood of being where the system expects them to be (quasi-deterministic users), and users whose position at a given moment is unpredictable (random users), similar to the classification proposed in [7]. The predictability of deterministic and quasi-deterministic users can be used by the system to reduce the number of location update operations. So, after the learning process completes, we get the mobile user's behavior associated with known location areas. Then, a profile is built for the mobile user (Table 1). When a call arrives for a mobile, it is paged sequentially in each location within the list. When a user moves between location areas in this list, no location updates are required. The list is stored at the HLR in the information database (ID) as well as in the user's mobile terminal. The cost reduction depends on the behavior of each class of user. It can be assumed that, when the user follows its expected behavior, the location update cost is reduced, even if accesses to HLR are minimized when calls are received from relatively close areas. The proposed strategy increases the intelligence of the location update procedure and utilizes replication and locality to reduce the cost incurred from the paging procedure.

Examples	Di(Day)	Ti(Time)	Ci (Cell Id)	Probability (%)
E1	Monday	02.15	5,1,6	90,50,10
E2	Monday	11.45	5,2,1	95,50,10
E3	Sunday	12.00	5,6,3	40,90,15
E4	Thursday	14.15	5,2,1	95,50,10
E5	Thursday	05.30	5,1,6	90,50,10

Table 1. Sample User Profile

In this problem, the learning process aims to derive a list with which we can find the cell in which the MT locates at any time of every day with high accuracy after observing the behavior of the mobile user for a period, for example, a month.
There are three layers in the Neural Networks: input layer, hidden layer, and output layer. The role of the hidden layer is to remap the inputs and results of previous layers to achieve a more separable or classifiable representation of the data and allow attachment of semantics to certain combinations of layer inputs.
By observing the mobile user's daily behavior, we use the GAANN algorithm to learn the behavior. With some useful data from observation of the mobile user as the input nodes, we can obtain the output as the result we want, which is the cell information of the mobile user on observation, that is to say, the cell list for a mobile user.

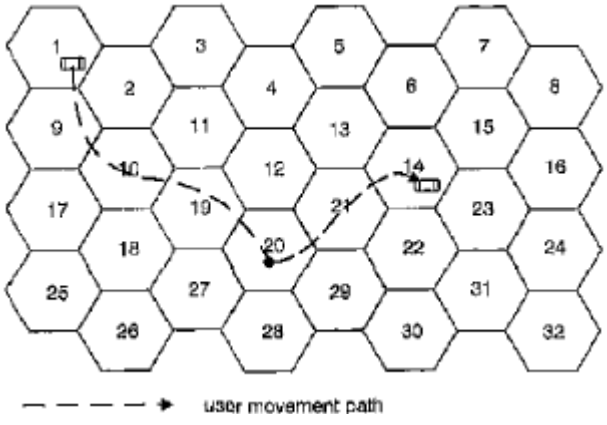

Fig.1 User Movement Path

3.1. GA Optimality Evaluation

In this case, there are three layers, the input layer that contains the values for Day and Time, a hidden layer is optimally designed, and two output units that gives the value of the output values, it's the probability that reside each cell in the user profile i.e Cell ID and probability. In order to determine which network architectures are optimal (whether it is global or local) for a particular problem, we apply exhaustive BP training over every network configuration in the architecture space defined. The number of neurons in the hidden layer in the ANN is determined optimally by the genetic algorithm. As mentioned earlier, BP is a gradient-descent algorithm, and thus, for a single run, it is susceptible to getting trapped to the nearest local minimum. However, performing it a large number of times with randomized initial parameters eventually increases the chance of converging to (a close vicinity of) the global minimum of the fitness function. The fitness function for the Neural Network optimization problem is taken as, $E = MSE$, where MSE is the mean square error between the desired target and actual output of the Neural Network Design.

The optimization of GAANN for the Location Management of MT is performed with the learning rate and the momentum constant varied from 0 to 1 and the hidden neurons varied from 31 to 200. For this training a maximum of 200 generations in GA are performed with a population size of 20 and with 500 training epochs. The crossover rate is 0.8 and mutation rate is 0.01. Using the proposed algorithm an optimized ANN is achieved with Nh =121, Lr = 0.00152 and Mc = 0.8972. Thus, the GAANN algorithm yields a compact network configuration in the architecture space rather than the complex ones as long as optimality prevails.

4. Simulation results

To assess the accuracy of the presented analytical model, in this section a performance evaluation of the Location Management System as well as a detailed model, which captures all relevant aspects of our approach in a concise way is presented. The simulation models both the call delivery and mobility behavior of users offering the ability to consider different service types and different MT groups over a range of cell-layout scenarios. Three different cell layout scenarios have been investigated. The first assumes macrocells only (9 Km^2), the second medium-size cells (1 Km^2), while the third small-size microcells (0.1 Km^2).

In this experiments, 1,000 MTs are simulated and we generated 1,000 samples for each cell layout scenario assuming normal distributions using the statistics estimated from the real data. The simulations are rub for the probability of a user being roaming within his associated list from 0.5 to 0.99. Assuming that a user is within that area covered by its list at least half of time. In practice, it would not do for a performer to have a list of likely positions in which a user is not found at least half of the time. In the case of users whose position at a given moment is unpredictable and the past knowledge of their location cannot predict their future location, our strategy is not applicable.

Assuming that link costs and database access costs are defined by message transmission delays and updating or query delays, respectively. For each mobile terminal, we define the following quantities:

A: average number of calls (i.e., voice or data) to a target MT per time unit;
fi: average number of times the user changes LA per time unit;
UT: average total cost of the location updates procedure;
ST: average total cost of the location search procedure; and
CG: average total cost per time unit for the location update and the location search.

The total cost per time unit for the location search and location update procedures of the proposed scheme is $C_G = \mu U_T + \lambda S_T$

4.1 Cost Comparison

Cayirci and Akyildiz [16] proposed a strategy for location management, which we call Cayirci, while the GPRS/ UMTS standard proposed another strategy, which we call UMTS, for solving the same problem. To be able to compare our strategy to UMTS, we have to compute the costs for the location update and location search operations. We define the following costs for the UMTS location management procedure:

S: cost for a location update operation according to the GPRS/UMTS standard;
SUMTS: cost for a location search operation according to the GPRS/UMTS standard; and
CUMTS: total cost per time unit for the location search and location update operations.

The total cost per time unit for the location search and location update procedures is given by $C_{UMTS} = \mu U_{UMTS} + \eta S_{UMTS}$

relative cost of the proposed scheme is defined as the ratio of the total cost of our scheme (per time unit) on the total cost of the standard UMTS procedures. Furthermore, this relative cost is a function of the call-to-mobility ratio (CMR):

$$\frac{C_G}{C_{UMTS}} = \frac{\mu U_T + \lambda S_T}{\mu U_{UMTS} + \lambda S_{UMTS}}$$

$$\frac{C_G}{C_{UMTS}} = \mu \left(\frac{U_T + (\lambda / \mu) S_T}{U_{UMTS} + (\lambda / \mu) S_{UMTS}} \right)$$

Where $CMR = \lambda / \mu$

The method proposed by Cayirci and Akyildiz is based on a profile similar to the one used in our scheme. There are some differences between the two, but they are mainly structural differences. For example, the short-term events leading to registration are not reflected as they are in our scheme. Furthermore, our profile is more likely to find the user in fewer trials due to the "next nodes" field that provides information on the next visited areas. Both factors compensate each other. Another important difference is the fact that [6] sets up a list of cells where no updates are performed while the user roams within this set of cells. Otherwise, a new record is created and another classical location update method is used (i.e., IS-41 or standard GPRS/UMTS). The total cost per time unit for the location search and location update procedures is given by $C_{Cayirci} = \mu U_{Cayirci} + \eta S_{Cayirci}$

As we did for the UMTS standard, we define the relative cost of our scheme compared to Cayirci's scheme as:

$$\frac{C_G}{C_{Cayirci}} = \frac{\mu U_T + \lambda S_T}{\mu U_{Cayirci} + \lambda S_{Cayirci}}$$

$$\frac{C_G}{C_{Cayirci}} = \mu \left(\frac{U_T + (\lambda / \mu) S_T}{U_{Cayirci} + (\lambda / \mu) S_{Cayirci}} \right)$$

Where $CMR = \lambda / \mu$

Users regularity is taken as (K), is the probability that an MT moves to the next node from the current node according to its current movement pattern. We have categorized the users into three classes by observing the users regularities.

1. All of the people who belong to the deterministic class have regularity close to 1.
2. The regularity Quasi-deterministic users are varying between 0.5 and 0.8.
3. Random users cannot be assigned a list and, thus, their values are below 0.5

Fig. 2 shows the results for a simulation of the scheme that belong to the deterministic users having a roaming probability of 0.9. When considering deterministic users that have a 99 percent probability of roaming within their profile, Cayirci's algorithm achieves a very low cost compared to our scheme. When the user is slightly less deterministic (i.e., a probability around 90 percent of roaming according to its profile), the location update costs for both schemes get closer and the location search procedure decides which algorithm has a smaller cost.

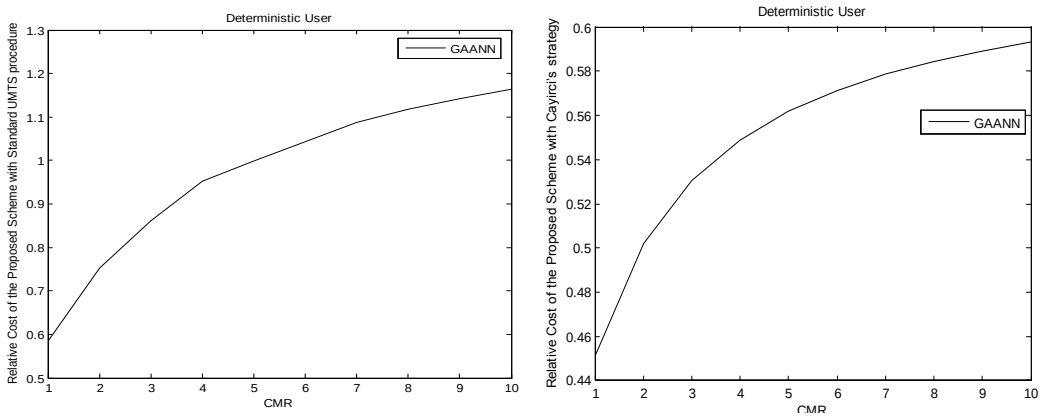

(a) (b)

Fig 2. Deterministic User (K=0.9) (a) Relative cost to standard UMTS (b) Relative cost to Cayrici's strategy

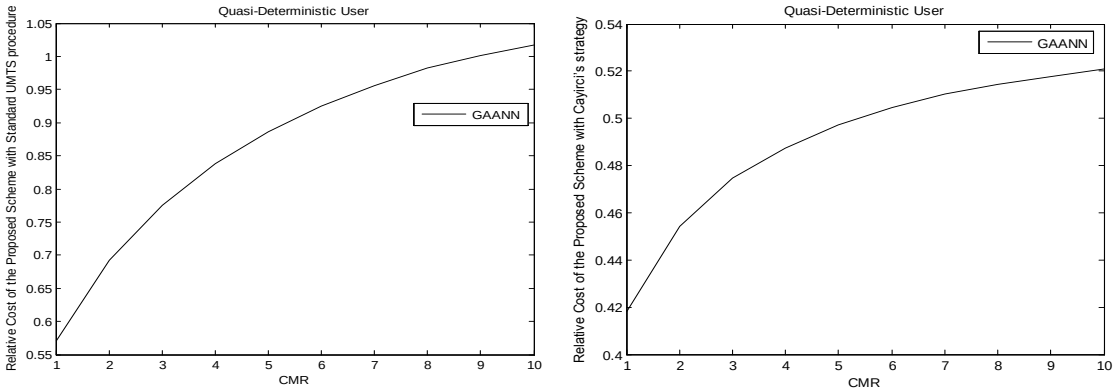

(a) (b)

Fig 3. Quasi- Deterministic User (K=0.7) (a) Relative cost to standard UMTS (b) Relative cost to Cayrici's strategy

Fig. 3 shows the relative cost for quasi deterministic users and this shows how the number of paging trials increases the cost of our scheme when compared to the UMTS standard where the user's location is always explicitly known. However, the proposed algorithm outperforms the UMTS standard for every CMR between 0 and 10 and for a value of n lower than 4. When n reaches 4, the cost of our scheme is higher than the cost for the UMTS standard for high values of CMRs (i.e., location search takes more importance). Nevertheless, for every paging trial that is not completed (from 3 to 2,2 to 1, etc.), the proposed scheme has a 20 percent cost reduction when compared to the UMTS standard.

5. Conclusion

In this paper, a user profile learning using GAANN is proposed to reduce location update signaling cost by increasing the intelligence of the location procedure in UMTS. This strategy associates to each user a list of cells where she is likely to be with a given probability in each time interval. The list is ranked from the most likely to the least likely place where a user may be found. When a call arrives for a mobile, it is paged sequentially in each location within the list. When a user moves between location areas in the list, no location updates are required. The results obtained from our performance evaluation confirm the efficiency and the effectiveness of UPL in comparison with the UMTS standard and other well-known strategy. This improvement represents a large reduction in location update and paging signaling costs.

References

[1] S. Tabbane, "Location management methods for third-generation mobile systems," *IEEE Commun. Mag.*, vol. 35, pp. 72–84, Aug. 1997.

[2] Y.-B. Lin, "Reducing location update cost in a PCS network," in *Proc. IEEE PIMRC'*, Taiwan, R.O.C., Oct. 1996.

[3] J. Li, Y. Pan, and X. Jia, "Analysis of Dynamic Location Management for PCS Networks," IEEE Trans. Vehicular Technology, pp. 1109-1119, Sept. 2002.

[4] Z. Mao and C. Douligeris, "A Location-Based Mobility Tracking Scheme for PCS Networks," Computer Comm., vol. 23, no. 18, pp. 1729-1739, Dec. 2000.

[5] A. Abutaleb and V.O.K. Li, "Location Update Optimization in Personal Communication Systems," ACM-Baltzer J. Wireless Networks, vol. 3, no. 3, pp. 205-217, Aug. 1997.

[6] I.F. Akyildiz, J. Ho, and Y. Lin, "Movement-Based Location Update and Selective Paging for PCS Networks," IEEE/ACM Trans. Networking, vol. 4, no. 4, pp. 629-638, Aug. 1996.

[7] G. Pollini and I. Chih-Lin, "A Profile-Based Location Strategy and Its Performance," *IEEE JSAC*, vol. 15, no.8, 1997, pp. 1415–24.

[8] S. Tabbane, "An Alternative Strategy for Location Tracking,"*IEEE JSAC*, vol. 13, no. 5, 1995, pp. 880–82.

[9] Chien-Hsing Wu, Huang-Pao Lin and Leu-Shing Lan, "A New Analytic Framework for Dynamic Mobility Management of PCS Networks", IEEE Transactions on Mobile Computing, Vol. 1, No. 3, July-September 2002, Pp: 208-220.

[10] S.Dasbit et al, "A probabilistic location management strategy in cellular mobile environment", Proceedings of IEEE TENCON 2002, pp: 1008-1011.

[11] Shou-Chih Lo and Arbee L. P. Chen, "Adaptive Region-Based Location Management for PCS Systems", IEEE Transactions on Vehicular Technology, Vol. 51, No. 4, July 2002, Pp: 667-676.

[12] Wenchao Ma and Yuguang Fang, "Two-Level Pointer Forwarding Strategy for Location Management in PCS Networks", IEEE Transactions on Mobile Computing, Vol. 1, No. 1, January-March 2002, Pp: 32-45.

[13] Goo Yeon Lee, "Numerical Analysis of Optimum Timer Value for Time-Based Location Registration Scheme", IEEE Communications Letters, VOL. 6, NO. 10, OCTOBER 2002, pp: 431-433.

[14] Alejandro Quintero and Oscar Garcia, "A Profile-Based Strategy for Managing User Mobility in Third-Generation Mobile Systems", IEEE Communications Magazine, September 2004, pp: 134-139.

[15] Alenjandro Quintero, "A User Pattern Learning Strategy for Managing Users' Mobility in UMTS Networks" IEEE trans. On Mobile Comuting, vol4. No.6, Nov/Dec 2005, pp 552-566.

[16] E. Cayirci and I.F. Akyildiz, "User Mobility Pattern Scheme for Location Update and Paging in Wireless Systems," IEEE Trans.Mobile Computing, vol. 1, no. 3, pp. 236-247, July-Sept. 2002.

Dynamic Classification of Power Systems via Kohonen Neural Network

S.F Mahdavizadeh
Iran University of Science & Technology, Tehran, Iran
M.A Sandidzadeh
Iran University of Science & Technology, Tehran, Iran
M. R. Aghamohammadi
Power & Water University of Technology, Tehran, Iran

Abstract- Dynamic security assessment is one of the most prominent behavioral attributes of power systems. It can be assessed and evaluated by means of various behavioral events. For dynamic analysis of power systems after faults, Critical Clearing Time (CCT) is one of the most important parameters to evaluate. Calculation of CCT requires solving complicated problems which usually involves solving time consuming non-linear equations during fault moments. In this paper we use Kohonen neural network for finding a new pattern. First some sample patterns are created, and this is done in such a way to cover the entire operating space of the system. Then parameters of this pattern are applied to the neural network in order to train it and gain the best input. After these patterns are classified (20 different classes) and based on neural network's outputs, attributes of each class is determined. Finally a program is developed to determine each new behavioral pattern's class and attribute by applying it.

Keywords: Dynamic Security, Kohonen Neural Network, Transient Stability

1. Introduction

Dynamic security assessment is one of the prominent behavioral features of power systems which can be assessed and appraised base on various behavioral phenomenon. Transient stability is one of the dynamic phenomenons which can be used for dynamic security assessment of power systems. Network and generators' stability depends on various parameters such as network structure, generators specifications, load levels and generation pattern of the generators. Generation pattern can be changed during operation of a system and can improve and increase the dynamic security level of that system via a suitable generation pattern [1]. Creating a procedure for dynamic security level assessment of power systems by finding attributes of generation patterns is the purpose of this paper. This can be done by pattern finding, neural network and other methods. Critical Clearing Time (CCT) is the stability and classification index of generation pattern in this paper, and based on that we can classify generation patterns according to their security levels [2].
CCT is the most prominent parameter that can be identified for dynamic analysis of power systems. Calculation of CCT requires complicated computations that include time consuming solving of nonlinear equations when fault occurs. In this paper we want to use Kohonen artificial neural network for pattern extraction. Therefore by using correct inputs and without calculation of CCT, we can assess the dynamic security via neural network [1].

2. Introduction to the Neural Network

2.1. Learning with Supervisor

In learning with supervisor, a set of data pairs called learning data $I(P_i,T_i)$ is assigned to the learning rule in which P_i is the input to the network and T_i is the desired network output for P_i input. After applying P_i input to the network, w_i (weight coefficients) is compared with T_i in network output and then the learning error is calculated and is used to tune network parameters[3]. So that when next time the same P_i input is applied to the network, network output gets closer to T_i, knowing that the teacher is a system with exclusive environmental control (for example it knows that for P_i input the proper output is T_i)

2.2 Unsupervised Learning

In unsupervised or self-organizing learning, neural network parameters are tuned and amended only via system answers. In other words, input vectors are transmitted to the network only via captured data. Compared to learning with supervisor, in this method the desired answer vector is not applied to the network. In other words, no sample of the function the network has to learn is given to it. We will see that in practice learning by supervisor in networks consisting of multiple neural layers is very slow, and in such cases a combination of supervised and unsupervised learning is recommended[3], [4].

2-3 Kohonen Neural Network

In most applications it is better to ask the network to classify the learning data by itself. For this purpose, it is better to have these two main hypotheses in mind: First, membership in a level generally means having shared attributes, and second, the network can discriminate these shared attributes in input data space. Self organizing Kohonen maps are one type of these networks based on the mentioned hypotheses and it uses unsupervised learning for changing inner network state and modeling highlighted attributes of training data. We will investigate this by taking a closer look at Kohonen training algorithm[3],[5].

***2.4* General Operation of Kohonen**

It is postulated that the brain uses local maps for modeling complex structures. Kohonen has used this to his own advantage because this helps Kohonen to compress information via a method called *vector quantization*. This also helps the network to save input data meaningfully while also keeping its topological features.

Compression of information means that data can be kept in a space much smaller than a previous one[6].

The brain cortex is mainly composed of two dimensional surfaces of neurotic connections though it can keep meanings of much higher dimensions inside itself. Application of Kohonen algorithm is also usually two dimensional.

As an example, you can take a look at figure 1. This network is composed of only one two-dimensional surface. The fact to be highlighted here is that neurons, unlike multi-layered perceptrons, are not located on different (input, hidden, output) surfaces; rather they are located on an even level surface. All inputs are connected to output nodes. It is shown that there is no separate output surface. Each node in the network is also an output node.

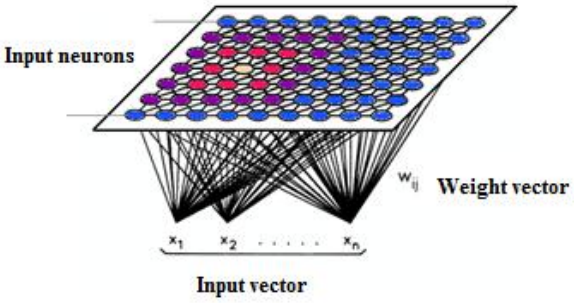

Figure (1): A Kohonen Network

2.5 Kohonen Algorithm

Kohonen training algorithm arranges network nodes as local neighbors, so that it can classify attributes of input information [7]. Network topography map is shaped automatically by periodically comparing inputs of each node with the vector saved by it in its connection lines. No desired answer is defined for training inputs. Whenever inputs of a node match the vector saved in that node, that area of the network is selectively optimized, so that it later represents the average training information of a data surface [8]. If the network is randomly shaped and adjusts itself slowly, it achieves a stable state.

This algorithm is like this:

1- Randomly determine primary weight coefficients and select the primary neighborhood radius (initially set t = 0)

Determine primary weight coefficient values which are the connectors between *n* input nodes to *j* output nodes by random values. $W_{ij}(t)$ presents weight coefficients at time *t* , which is the input, and *j* which is the output node. It should be noticed that at first we assign t = 0

Initially assign a large value to radius of neighborhood of output nodes ($N_j(0)$).

2- Select the input vector randomly from patterns selected for training.

Then apply input vector to the network. $X_i(t)$ is the input value of node *i* at time *t*

3- Determine neuron *c* so that its weight coefficients vector W_C has the shortest distance from the input vector.

Weight coefficient vector is selected as the following:

a) Distance d_j between input and output vector of each node *j* is determined via the following equation :

$$d_j = \sum_{i=0}^{n-1} ((x_i(t) - w_{ij}(t))^2 \qquad (1)$$

b) We Select the shortest distance *min{d_j}*
Correct weight coefficient W_C of winner neuron *c* and weight coefficients of its neighbor W_i.
These weight coefficients are corrected via the following equation:

$$w_{ij}(t+1) = w_{ij}(t) + \alpha(t)(x_i(t) - w_{ij}(t)) \qquad (2)$$

With these equations, weight coefficients of all neurons located in neighborhood of $N_C(t)$ are corrected.

Neighborhood function $\alpha(t,i)$ is decreased with time. This reduction rate is logarithmic.
As a result sharing coefficient of weight coefficients is slowed gradually. Consequently, radius of neighborhood is also reduced gradually.

4- Increase the time (t= t+1)
5- Repeat the algorithm by jumping to step 2. [4], [5], [9]
In this paper MATLAB functions are used for neural network simulation.

3. Methods for Creating Operation Patterns

One of the most important parts of dynamic security assessment - when done *offline* and via neural networks- is introducing the system entirely to the neural network[3]. For neural network training we need to define all the work space. Neural network only can interpolate in the work space, and for this reason defining the total performance condition of power system is really necessary. Therefore we tried to define this work apace. In order to produce this work space, minimum and maximum demands in load buses are determined. For example $P_{Lmin}{}^{i}$ *and* $P_{Lmax}{}^{i}$ are minimum demand and maximum demand of *i*th bus. Then this load limitation is divided into ten parts.
Total load of power system can be calculated with relation 3:

$$pload_{Sys}^{\ i} = \sum_{i=1}^{m} pload\,(i) \qquad (3)$$

In which $pload_{sys}^{i}$ is load's level of *i*th bus of power system.
After that, with the minimum and maximum power generation of each bus, the generation orders will be extracted.
Finally by taking random patterns into accounts we will have loads of 10 load levels and for each load level 10 random load patterns and 10 random production patterns for our desired network, meaning that 1000 operation patterns are taken into account.
We cannot use all these patterns for network training and the number of patterns used should be as low as possible (so that it won't impact the network training). This is because a high number of patterns will make the training process very time consuming and slow.
It is therefore necessary to select suitable sample patterns with optimal numbers from among all other patterns for this purpose. Our basis for selecting patterns was sample network's load level. So that 202 patterns were selected as primary patterns for network training and these patterns, when compared to the total patterns, have the same load levels. Figures (2) and (3) prove this. By comparing these two graphs it becomes clear that distribution of load levels of the selected patterns and the entire patterns is the same.

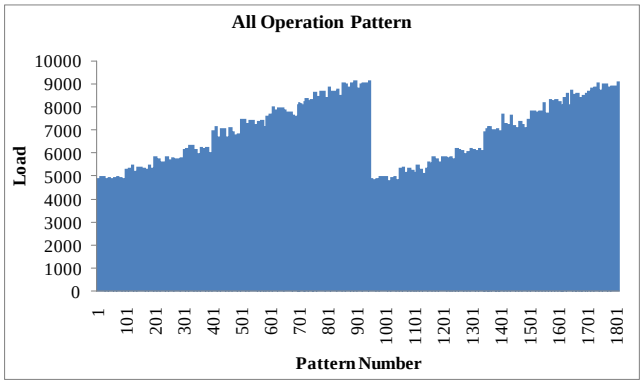

Figure (2) Load levels of all patterns (including 1817 operation patterns)

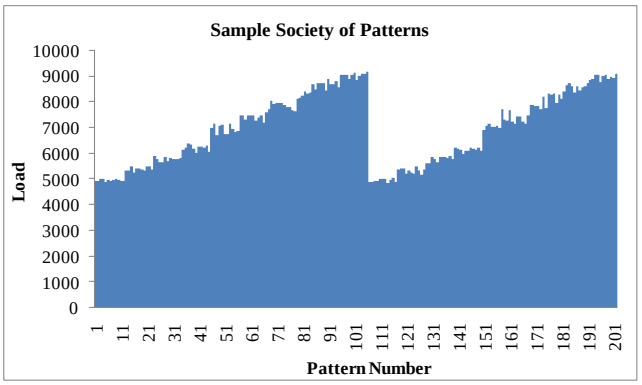

Figure (3) Load level of 202 sampled patterns (patterns with load level distribution similar to that of the entire patterns)

4. Sample Network Introduction

The questioned network in this article is IEEE network with 39 buses. This network comprises 10 buses with generator and 29 load buses. It also has 34 lines.

For simplicity, network lines in this article are displayed like figure 4. It is to be noticed that bus 31 is selected as the reference bus.

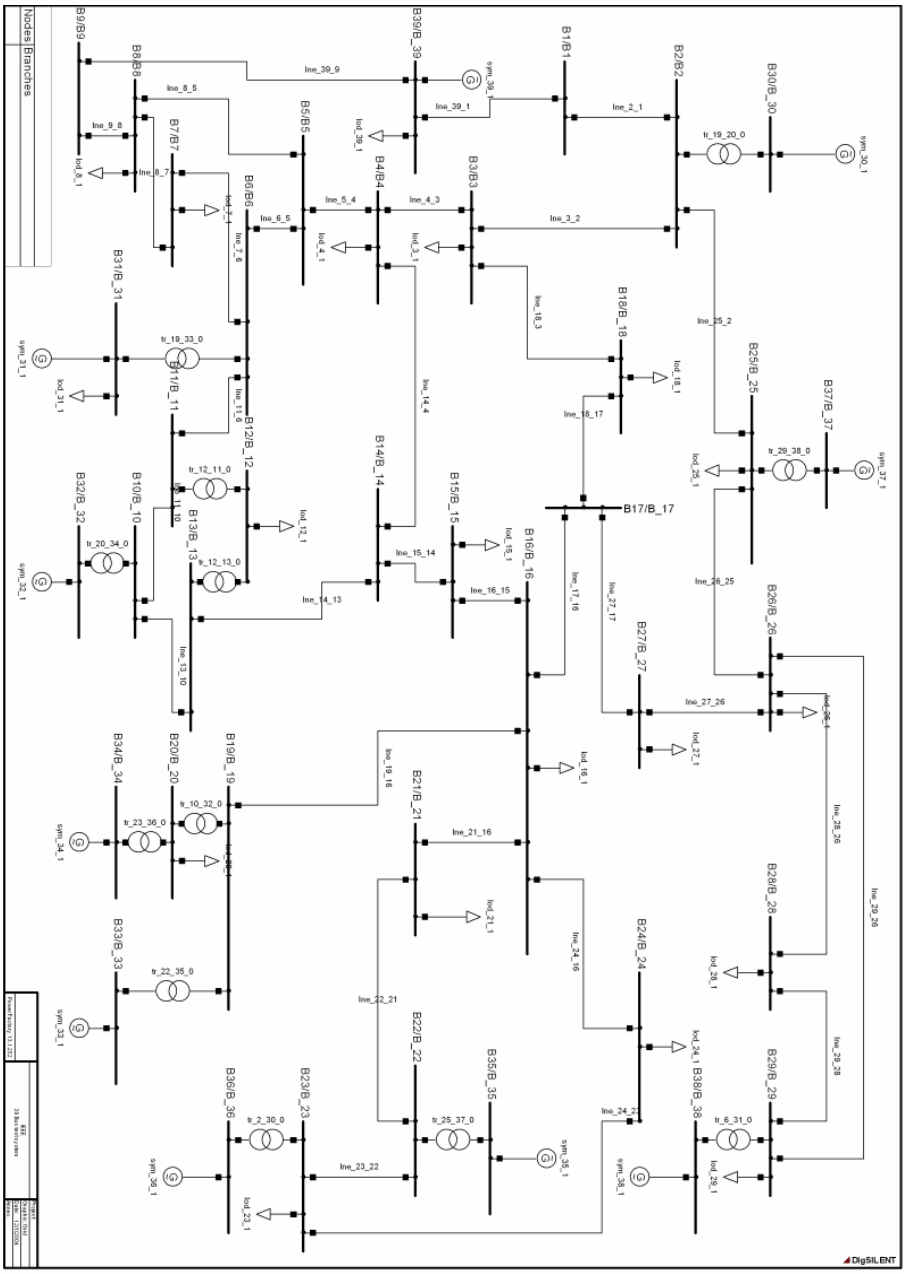

Figure (4): Sample Network with 39 buses

5. Combination of utilized parameters

Combination of inputs can be a better way for describing primary state of the system. So we decided to use various combinations of parameters. Since some parameters yield to analogous behaviors in the power system, we have not used combination of all of them. Here we have used 12 different combinations that include:

1) Lines active flow power (P_{Line})
2) Lines active flow power and each generator's active generation power (P_{Line} & P_G)
3) Lines active flow power, each generator's active generation power and voltage of buses (P_{Line} & P_G & V)
4) Lines active flow power, each generator's active generation power and inertia constant (P_{Line} & P_G &H)
5) Lines active flow power, each generator's active generation power and lines reactive flow power (P_{Line} & P_G &Q_{Line})

6) Lines active flow power, each generator's active generation power, lines reactive flow power and voltage amount (P_{Line} & P_G & Q_{Line} & V)
7) Lines active flow power and voltages of buses (P_{Line} & V)
8) Lines active flow power, voltages of buses and inertia constant (P_{Line} & V & H)
9) Lines active flow power, lines reactive flow power and voltages of buses (P_{Line} & Q_{Line} & V)
10) Lines active flow power, each generator's active generation power, lines reactive flow power, load of buses, voltage amount and inertia constant (H & P_{Line} & P_G & Q_{Line} & Q_G & P_{Load} & V)
11) Load active power and generators' generation power (*PLoad* & *PG*)
12) Active and reactive load power (*PLoad* & *QLoad*)

To indentify the best input combination we should first define a principle. Our principle here is classification based on behavioral patterns (dynamical or CCT). It means that we take one input load of the neural network as CCT of lines and after training we define it in form of classes. After this we classify the results gained from training of operation patterns. Notice that the number of classes in both classification methods (behavioral and operational) should be the same. Finally we compare equivalent classes and measure coordination percent of each class. By calculating average coordination percent of each class we achieve total coordination percent. Finally we take total coordination percent as the comparison principle for various inputs.
Coordination percent was achieved between each one of the mentioned combinations and CCT. The gained results are demonstrated in table (1). As it is shown in this table, the highest percents were achieved for (*PLine* & *QLine* & *V*) and (*PLine* & *V*) combinations. In table (1) total coordination percent is achieved by surveying each individual pattern's coordination. It means coordinated patterns in patterns classifications is determined based on operation neural network and is divided by the number of total patterns. Also coordination percent of each class is calculated separately and classes with the highest and lowest coordination are indicated in this table. Finally by calculating the average weight of coordination percent of the entire classes, the average weight coordination of classes is calculated.
We have used equation (4) for calculating the average coordination percent of classes:

$$CP_{av} = \frac{\sum_{k=1}^{k=7} CP_k \times N_k}{\sum_{k=1}^{k=7} N_k} \qquad (4)$$

CP_{av}: Coordination Percent Average
N_k: Number of Patterns in Kth class
CP_k: Coordination Percent in Kth class

Table (1): Coordination percent between classification by selected combinations and CCT

Parameter	P_{Line}	V	Q_{Line}	Q_G	P_G
Coordination percent to CCT of parameters	*43.4*	*15.7*	*25.2*	*7.21*	*6.18*

6. Selecting Optimal Combination by Correlation Coefficient Method

As previously mentioned, for optimal training of neural networks their inputs should be selected from those operation quantities that have the highest impact on changes of CCT values of lines. Correlation Coefficient method for determining these quantities is described in the following part.
In this method, correlation between one line's CCT values and each operation quantity of system is calculated via equation

(5):

$$r = \frac{S_{XY}}{S_Y S_X} = \frac{\sum XY - (1/n)\sum X \sum Y}{\sqrt{[\sum X^2 - (1/n)(\sum X)^2][\sum Y^2 - (1/n)(\sum Y)^2]}} \qquad (5)$$

In equation (5) we have:

X & Y: are quantities we want to find their correlation, which can represent CCT and the desired operation variable respectively.
n: Number of samples
Neural Network input is selected from those operation quantities that have the highest correlation with all lines CCT.
In table (2) total correlation percent of lines CCT to different parameters is presented.
It can be seen in this table that P_{Line}, V and Q_{Line} have a better condition and lines CCT have the highest correlations with these variables. Now by using the results from the two mentioned methods and by taking the experimented coordination percent into account, (P_{Line} & Q_{Line} & V) is selected as the optimized combination.

Table (2) Percent of Lines CCT correlation to different parameters

	Input Parameter	*Total coord. Percent*	*Max. Coord. Classes*	*Min. Coord. Classes*	*Average coord. Classes*
1	*Line*	*76.8*	*95*	*35*	*75*
2	*Line & P_G*	*74.8*	*100*	*36*	*76*
3	*Line & P_G & H*	*75.3*	*100*	*35*	*73*
4	*Line & P_G & V*	*72.8*	*100*	*35*	*74*
5	*Line & P_G & Q_{Line}*	*74*	*100*	*37*	*76*
6	*Line & P_G & Q_{Line} &*	*77.3*	*100*	*37*	*78*
7	*Line & V*	*82*	*100*	*55*	*83*
8	*Line & V & H*	*71.4*	*94*	*37*	*67*
9	*Line & Q_{Line}_V*	*79.8*	*100*	*50*	*79.5*
10	*Line & P_G & Q_{Line} & & P_{Load} & V*	*75.8*	*100*	*42*	*78*
11	*Load & P_G*	*61*	*95*	*32*	*61.5*
12	*Load & Q_Load*	*47.5*	*94*	*28*	*49.5*

7. Choosing the Best Number of Neurons

As it was previously mentioned, the exact number of security classes of sample network is not clear to us and therefore we can't estimate the exact number of neurons. Consequently we have to train the network for various numbers of neurons and find the results. We will compare each gained state of our selected operation patterns with their analogous dynamic parameters and select the optimal number of neuron from a state that has the highest coordination rate.
In table (3) we have the coordination results for states with 16, 25, 100, 196, 225, 256 and 400 neurons. It is seen that an increase in the number of neurons results in an increase in coordination percent. Since large a number of neurons extends the training time and also we observe no significant boost in coordination rate when this number exceeds 196, we have decided to choose 196 as the number of neurons. We also tested 100 neuron sets, though since there was a low coordination in neighborhood neurons, we decided not to use this configuration of neurons.

Table (3): Assessing the best configuration of neurons by comparing behavioral and working neural network classification

Number of Neurons	*inimum neur coordination*	*aximum neur coordination*	*Average neuron coordination in the first state*	*Average neuron coordination in the second state*	*inal average coordination*
16	*37*	*100*	*66*	*67*	*66..5*
25	*40*	*100*	*66*	*67.5*	*66.75*
100	*37*	*100 (34)*	*82*	*87*	*84.5*
196	*41*	*100 (34)*	*84*	*88*	*86.5*
225	*41*	*100 (61)*	*84*	*90*	*87.5*
256	*41*	*100 (61)*	*86*	*91*	*89*
400	*41*	*100*	*88*	*92*	*90*

8. Final Classification

By finding the appropriate combination and optimal number of neurons for neural network training we should now train the specified patterns.

We start network training by applying the resultant inputs and the optimal number of neurons. We have assumed 5000 iterations. It was consequently observed that 68 neurons won in the training process and a number of patterns were dedicated to them. Each one of these neurons can represent one class. The remaining (128) neurons were not excited enough in this process and they are considered dead neurons.

Since winning neurons are numerous and neighbor neurons might have similar behaviors, it might be possible to put some of them in the same classes. Therefore it is necessary to first study patterns located in each neuron and then define each neuron's characteristics. After defining characteristics of all neurons we study these characteristics' shared points in neighboring neurons, and if they have the same characteristics we put them in same classes.

The criterions for classification of patterns included in neurons are:

1- The amount of similarity of neurons' characteristics
2- Order of neighborhood of neurons

We classified the gained results with the aim of defined principles. Finally we have achieved 20 security classes for operation patterns.

9. Feature Extraction of Classes

Classification via neural network is not based on a specific physical context. In other words, Kohonen neural network classifies patterns only based on mathematical principles and in fact it is us that have to look for specific physical characteristics in classes created by neural network. Finding the mentioned characteristic(s) depends on our purpose of classifying the desired inputs. Since assessing dynamic security is our goal in this paper, then the basis for patterns classification is dynamic security. It is clear that CCT of lines is a clear indication of network dynamic security.

For investigating condition of patterns CCT we indentify lines with the lowest CCT in each pattern and record CCT value of these lines. Now we investigate CCT condition of patterns located inside each neuron.

It can be observed that patterns located inside neurons with the worst lines CCT are identical, and the amount of CCT in patterns of each neuron is in an identical range. It should be noticed that order of lines criticality is considered in all of them.

Hence after classification (or putting neighbor neurons with the same behavior in the same class), orders of the worst lines was also considered for patterns of each class; meaning that the patterns located in a class have the same worst lines and their CCT value is in the same range, though the amount of coordination in this case was reduced when compared to the previous case.

Another characteristic of the resulting classes is that all patterns located in a class have almost identical load levels.

In figure (5) conformity percent of each class is presented. Also number of patterns of each class is indicated as redundancy of each class:

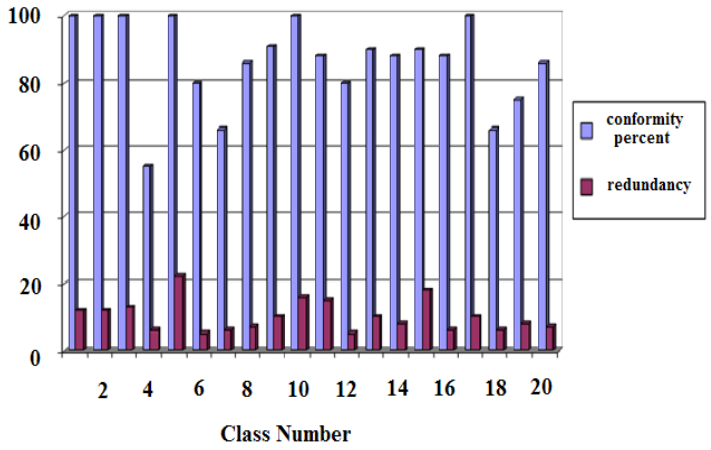

Figure (5): Conformity percent and redundancy of patterns of each class under training

To obtain the accuracy levels of each class we have calculated conformity levels of classes for experimental patterns presented in figure (6).
Classes displayed here with low accuracy have small number of patterns. It can be seen that we have attained the promised accuracy here.

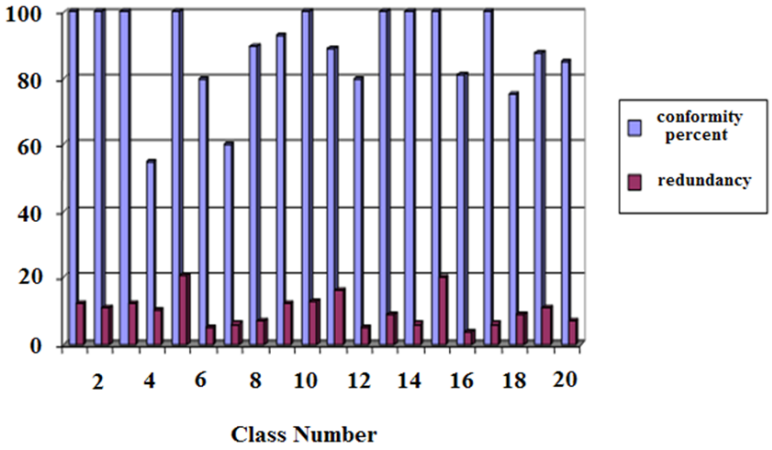

Figure (6): Conformity percent and number of patterns for each class for experimental patterns

Finally with the aim of equation (6), the total conformity degree of neural network turnover in assessment phase is achieved.

$$cd_{Test} = \frac{\sum_{k=1}^{k=20} cd_k \times N_k}{\sum_{k=1}^{k=20} N_k} = 0.91 \qquad (6)$$

In which:
CP_{Test} : Neural Network weigh coordination percent

N_k : Number of Patterns in kth class

CP_k : Weigh coordination percent in kth class

10. Neural Network Assessment

In order to make sure that the operation of neural network is valid we should investigate some examples here. We did select an overall of 200 samples from operation patterns and investigated the results after applying them to the network. It was observed that the neural network had correctly responded with the accuracy we expected from it.

11. Conclusion

With rapid expansion of the power network in Iran and its operational complexity, it has become necessary to identify this system's operation security limits. Time is of an ultimate significance when identifying these security limits. Having live data of network security status will help us to find better ways for operating the network. In this paper we did pursue these goals and a method for extracting these security borders and power system security classification was presented.

The proposed method helps to investigate limits of generators' generation order configurations in various operation patterns of power systems when compared to transient stability phenomenon. It should be noted that the aim of this method is not to estimate or calculate CCT; rather it helps to present an overall picture of system security status and also early detection of critical lines.

To reach the mentioned goals we used Kohonen neural network in this paper and it was shown that Kohonen neural network provides a solution for our mentioned goals. In this method by classifying patterns into various security groups we presented network security status by 20 different security classes.

Attributes of each class was identified as its characteristic. It was observed that patterns inside each class have identical worst lines and follow identical critical patterns. Also we found that patterns in each class have the similar load levels.

References

[1]. P. Kundur , "Power System Stability and Control" International Edition ed. California, McGraw Hill Inc., 1994.

[2]. Hiroshi Takada Yoshinori Kato Shinichi Iwamoto, "Transient Stability Preventive Control Using CCT and Generation Margin", Power Engineering Society Summer Meeting, IEEE 2001, Vol. 2, p. 881-886

[3]. Mahmoud B. Zayan, Mohamed A. El-Sharkawi and Nadipuram R. Prasad, "Comparative Study of Feature Extraction Techniques for Neural Network Classifier", IEEE Proc. of ISAP'96, Orlando, Florida, January-February 1996, p. 400-404

[4]. Alain J. Germond, "Power System Static Security Assesment Using The Kohonen Neural Network Classifier", IEEE Transactions on Power Systems, Vol. 7, No. 2, May 1992, p. 865-872

[5]. R.Beale, T.Jackson, "Neural Computing: An Introduction", Institute of Physics Publishing

[6]. M. Boudour, A. Hellal, "Large Scale Power System Dynamic Security Assessment using the Growing Hierarchical Self-organking Feature Maps", IEEE International Conference on Industrial Technology (ICIT), 2004.

[7]. E.S. Karapidakis and N.D. Hatziargyriou, "Application of Artificial Neural Networks for Security Assessment of Medium Size Power System", 10th Meditenmean Electrotechnical Conference, MEleCon 2000, Vol. 3.

[8]. Dejan J. Sobajic, Yoh-Han Pao, Artificial Neural-Net Based Dynamic Security Assessment for Electric Power Systems, IEEE Transactions on Power Systems, February 1989, Vol. 4, No. 1, p.220-228

[9]. K.W.Chan, A.R.Edwards, R.W.Dunn and ARDaniels, "On-line dynamic security contingency screening using artificial neural networks", IEE proc-Gener Transm Distrib, November 2000, Vol 147, No 6, p. 367-372.

Actionable Knowledge Discovery

Ambikavathi .V[1], Veeraiah.A[2] Prabhu.R[3]
[1]Department of Master of Computer Applications , [2,3] Department of Information Technology
P.S.R Engineering College, Sivakasi-626 140.

Abstract— The data mining process consists of a series of steps ranging from data cleaning, data selection and transformation, to pattern evaluation and visualization. One of the central problems in data mining is to make the knowledge actionable. Here the term actionable refers to the mined patterns suggest concrete and profitable actions to the decision-maker. In this paper, we present a formal view of actionable knowledge discovery (AKD) from the system and decision-making perspectives. AKD is a closed optimization problem- solving process from problem definition, framework/model design to actionable pattern discovery, and is designed to deliver operable business rules that can be seamlessly associated or integrated with business processes and systems. To support such processes, we correspondingly propose, formalize, and illustrate Multisource Combined-Mining-based AKD (MSCM-AKD). A real-life case study of MSCM-based AKD is demonstrated to extract debt prevention patterns from social security data. Substantial experiments show that the proposed frameworks are sufficiently general, flexible, and practical to tackle many complex problems and applications by extracting actionable deliverables for instant decision-making.

Keywords— Data Mining, Domain-Driven Data Mining, Actionable Knowledge Discovery, Decision Making.

I. INTRODUCTION

Data mining, as well as its synonyms knowledge discovery and information extraction, is frequently referred to the literature as the process of extracting interesting information or patterns from large databases. There are two major issues in data mining research and applications: patterns and interest. The identified patterns are then handed over business people for further employments. The business people cannot effectively take over and interpret the identified patterns for business use. This may result from several aspects of challenges besides the dynamic environment enclosing constraints. Many patterns mined but they are not informative and transparent to business people who do not know which are truly interesting and operable for their businesses. Business people feel confused by why and how they should care about the identified patterns may be either commonsense or of no particular interest to business needs. Business people often do not know, and are also not informed, how to interpret them and what straightforward actions can be taken on them to support business decision-making and operation.

Stating the AKD problem from system and micro- economy perspectives to define fundamental concepts of action ability and actionable patterns. Defining knowledge action ability by highlighting both technical significance and business expectations that need to be considered, balanced, and/or aggregated in AKD, proposing four general frameworks to facilitate AKD, and demonstrating the effectiveness and flexibility of the proposed frameworks in tackling real-life AKD.

The main idea of MSCM-AKD [3] such as handles AKD in either multiple data sources or large quantities of data, one of the data sets is selected for mining initial patterns, some learned patterns are then selected to guide feature construction and pattern mining on the next data set(s). The iterative mining stops when all data sets are mined, and the corresponding patterns are then merged/summarized into actionable deliverables

II. KNOWLEDGE MANAGEMENT

The knowledge management [5] is becoming a hotspot of the management research. Explicit knowledge is systematic and easy to communicate and share in the form of leaflet, scientific formula and software. Tacit knowledge is highly personal and difficult to formulize and communicate, it runs deeply in the personal action and understanding of the surrounding in the form of workmanship, special skill, product market and teamwork, including the informal technology in “know how”.

The knowledge management is the promotion of the flexible and creative competence with the team wisdom and a new method to share the explicit and tacit knowledge for the company.” The knowledge management is one kind of science to identify, obtain, evaluate, retrieve and share all of the company information through the promotion of the integration.” The development of the knowledge management must be faster with the more violent market competition.

The research of the basic tasks of the knowledge management can strengthen our understanding and promote the method and mode of the knowledge management for companies and organizations. The two basic tasks that are mentioned in the text are only one fundamental question of the knowledge management. Here it didn't go further how to complete the basic tasks and how to fulfill the other tasks of the knowledge sharing and management. However, it stays the necessary need and pressing task of the knowledge management to find the operable and systematic method of the knowledge management.

From the knowledge chain model [6], three aspects should be understood to grasp knowledge management: 1) The management is a process for companies to administer their owned knowledge resources, and the core object is knowledge. 2) Operated by the links of accumulation, sharing, learning, application and innovation, knowledge can guide enterprise's actions and continuously generate values. 3) Culture, management and technology are the three key elements in knowledge management.

The characteristics of KMS are knowledge management is the extension and development of information management. KMS and traditional management information system has the following differences: 1. The target of collection, processing and dissemination is different. The traditional management information system is for collecting, processing and dissemination the information that reflects the real world objects' attribute. But the target, what knowledge management systems have to collect, disseminate and dispose, is the knowledge that carried by human brain, and has implied characteristic. 2. Target object has different processing depth. Traditional management information systems treat the information most on the surface processing, such as calculation, merger, compilation, linking, etc. 3. Products are in different forms. Traditional management information system's output is usually in form of reports, documents, statements or other summary data. But knowledge management system's output is varied, which is multimedia output integrated text, graphics, audio and video. 4. The value orientation of system's product is different. The information products of the traditional management information system have higher demand of timeliness, accuracy. And the knowledge products provided by knowledge management system emphasize innovation, scientific, experience and skills. 5. Different measurement. The traditional management information system takes the computer hardware, software, network connectivity and enterprises' income as the measurement. But knowledge management system develops the knowledge investment, knowledge-intensive and the breadth and depth in excavating tacit knowledge as measurement.

III. RELATED WORK

Data mining and knowledge discovery has emerged to be one of the most vivacious areas in information technology during the last decade. It has boosted a major academic and industrial campaign crossing many traditional areas such as database, statistics, business as well as emergent disciplines.

In [1] have explained that action hierarchy which is defined as a tree of actions with patterns and pattern templates (data mining queries) assigned to its nodes. A method for discovering actionable patterns is presented and various techniques for optimizing the discovery process are proposed. To define actionability as a measure of interestingness of patterns based on the concept of action hierarchy.

In [2] presented that most data mining algorithms is to facilitate the discovery of concise and interpretable information from large amounts of data. However, many of the current formalizations of data mining algorithms have not quite reached this goal. One of the reasons for this is that the focus on using purely automated techniques has imposed several constraints on data mining algorithms.

In [3] have proposed that Domain-driven KDD represents a paradigm shift from a research-centered discipline to a practical tool for actionable knowledge. Despite many open issues, deployed systems are already showing ways to transmit reliable research in forms that satisfy business needs with direct support for decisions. It represents a paradigm shift from a research-centered discipline to a practical tool for actionable knowledge.

In [4] presented the current data mining algorithms and tools often stop at the delivery of patterns satisfying expected technical interestingness. Business people are not informed about how and what to do to take over the technical deliverables. D3M aims to construct next-generation methodologies, techniques and tools for a possible paradigm shift from data-centered hidden pattern mining to domain-driven actionable knowledge delivery.

Actionable Knowledge Discovery Applications [7] are Customer Relationship Management, Supplier Selection, Crime Identification and Business Intelligence.

Customer Relationship Management (CRM) consists of four dimensions: Customer identification, customer attraction, customer retention, and customer development. Customer satisfaction is the central concern for customer retention. Supplier selection is one of the most parts in supply chain management. Strategic partnership with better performing suppliers should be integrated into the manufacturing to improve the performance in various aspects including reducing costs by eliminating wastes, continuously improving quality to achieve zero defects, reducing lead time at different

stages of the manufacturing. Crime detection for credit applications is so popular in bank industry. Phua et al. [8] presented an updated adaptive Communal Analysis Suspicion Scoring (CASS) algorithm. CASS adaptively changes the appropriate parameter setting to trade off efficiency and effectiveness. Their approach is validated with three sets of experiments on real credit applications. Business Intelligence (BI) refers to skills, processes, technologies, applications and practices used to support decision-making. BI technologies provide historical, current, and predictive views of business operations. The approach uses domain knowledge to filter indicators, and enables incremental adjustment of underlying domain model thorough involving domain knowledge.

IV. PROPOSED METHODOLOGY

MSCM-AKD Enterprise applications often involve multiple-subsystems-based and heterogeneous data sources that cannot be integrated, or are too costly to do so. Another common situation is that the data volume is so large that it is too costly to scan the whole data set. Mining such complex and large volumes of data challenges existing data mining approaches

The MSCM-AKD framework can also be instantiated into a number of mutations. For instance, for a large volume of data, MSCD-AKD can be instantiated into data partition + unsupervised + supervised-based AKD by integrating data partition into combined mining. An example is as follows: First, the whole data set is partitioned into several data subsets based on the data/business understanding and domain knowledge jointly by data miners and domain experts, say data sets 1 and 2. Second, an unsupervised learning method is used to mine one of the preference data sets, say data set 1. Supervised learning is further conducted on data set 2 to generate actionable patterns by checking both technical and business interestingness. Finally, the individual patterns mined from both data subsets are combined into deliverables.

Table 1. MSCM-AKD Algorithm

INPUT: Target Data Sets DB, Business Problem Ψ, and Thresholds ($t_{o,0}$, $t_{s,0}$, $b_{o,0}$ and $b_{s,0}$)

OUTPUT: Actionable Patterns $\tilde{P}$ and business rules $\tilde{R}$.

Step 1: Identify or partition whole source data into N data sets DB_n (n = 1,..., N);

Step 2: *Data Set-n mining*: Extracting general patterns P_n on data set/subset DB_n;

FOR l = n to (N)

Develop modeling method m_n with technical interestingness $t_{i,n}()$ (i.e., $t_o()$, $t_b()$) or unified $i_{i,n}()$ Employ method m_n on the environment e and data DB_n engaging meta-knowledge Ω_m;

Extract the general pattern set P_n;

ENDFOR

Step 3: *Pattern merger*: Extracting actionable patterns $\tilde{P}$;

FOR l = n to N

Design the pattern merger functions $\oplus^N P_n$ to merge all patterns into $\tilde{P}$ by involving domain and meta knowledge Ω_d and Ω_m, and business interestingness $b_i()$;

Employ the method $\oplus P_n$ on the pattern set P_n;

Extract the actionable pattern set $\tilde{P}$;

ENDFOR

Step 4: Converting patterns $\tilde{P}$ to business rules $\tilde{R}$.

Finally, combined patterns can be transformed into operable business rules that may indicate direct actions for business decision-making. For instance, for the above combined association, it actually connects key business elements with segmented customer characteristics, and we can generate the following business rule by extending the Business Rule specification.

Table 2. Delivering Business Rules

For All customer i ($i \in I$ is the number of valid customers)
Condition:
satisfies S/he is a debtor aged 65 or plus;
relates
S/he is under arrangement of "withholding" and
"irregularly",
and
His/her favorite Repayment method is "withholding";
Operation:
Alert = "S/he has 'High' risk of paying off debt in a very long timeframe."
Action = "Try other arrangements and repayments in R_2, such as trying to persuade her/him to repay under 'irregular' arrangement with 'cash or post.'"
End-All

CONCLUSION

This framework is supporting the controlled data of employee's regarding withheld and payment process and it is very effective data from social welfare. The framework includes, collect and maintain the organizational and non-organizational data regarding their salary. Proposed system can be hardly applied in real cases if the service provider cannot protect the data it has acquired from competitors and selects the trusted parties from which it wants to receive information.

REFERENCES

[1] G. Adomavicius and A. Tuzhilin, "Discovery of Actionable Patterns in Databases: The Action Hierarchy Approach," Proc. Int'l Conf. Knowledge Discovery and Data Mining (KDD '97), pp. 111-114, 1997.

[2] C. Aggarwal, "Towards Effective and Interpretable Data Mining by Visual Interaction," ACM SIGKDD Explorations Newsletter, vol. 3, no. 2, pp. 11-22, 2002.

[3] L. Cao, "Domain-Driven Actionable Knowledge Discovery," IEEE Intelligent Systems, vol. 22, no. 4, pp. 78-89, July/Aug. 2007.

[4] L. Cao, "Domain-Driven Data Mining: Empowering Actionable Knowledge Delivery," Proc. Pacific-Asia Conference, 2008.

[5] J.F. Boulicaut and B. Jeudy, "Constraint-Based Data Mining," The Data Mining and Knowledge Discovery Handbook, pp. 399-416, Springer, 2005.

[6] S. Yoon, L. Henschen, E. Park, and S. Makki, "Using Domain Knowledge in Knowledge Discovery," Proc. Eighth Int'l Conf. Information and Knowledge Management, pp. 243-250, 1999.

[7] Jiying Li and Jianwu Dang "A Survey on Actionable Knowledge Discovery Applications," IEEE Conference, 2010.

[8] C. Phua, V. Lee, K. S. Miles and R. Gayler, "Adaptive communal detection in search of adversarial identity crime," Proceedings of the 2007 International Workshop on Domain Driven Data Mining, pp.1–10, San Jose, USA, August 2007.

Remote-Controlled Home Automation Systems with Different Network Technologies

[*]Subhashrahul Shekhar[1] , BV Sravan Kumar[2] , S Ramesh[3]
1.Department of ECE,KCG college of technology(Chennai)
2.Department of ECE,KCG college of technology(Chennai)
3.Department of ECE,KCG college of technology(Chennai)

Abstract
This paper describes an investigation into the potential for remote controlled operation of home automation systems. It considers problems with their implementation, discusses possible solutions through various network technologies and indicates how to optimize the use of such systems. The home is an eternal, heterogeneous, distributed computing environment which certainly requires a careful study before developing any suitable Home Automation System (HAS) that will accomplish its requirements. Nevertheless the latest attempts at introducing Home Automation Systems in actual homes for all kinds of users are starting to be successful thanks to the continuous standardization process that is lowering the prices and making devices more useful and easier to use for the end user. Even so several important issues are always to be handled strictly before developing and installing a Home Automation System; factors like security, reliability, usefulness, robustness and price are critical to determine if the final product will accomplish the expected requirements.

Keywords: Home Automation Systems, Home network, Domotics, Ubiquitous access, User- friendly interfaces, Standards.

1. Introduction: Evolution of Home Automation Systems.

The concept of "automation" has existed for many years. It began with a student connecting two electric wires to the hands of an alarm clock in order to close a circuit of a battery and light bulb. Later, companies developed automated systems of their own to control alarms, sensors, actuators and video cameras and, in so doing, created the first automated buildings. The term "intelligent home" followed. Due to the obvious advantages of these systems, their influence on the conventional home was predictable and finally, in 1988, the term *domotics* was coined. *"Domotics is the application of computer and robot technologies to domestic appliances. It is a portmanteau word formed from domus and robotics"*. A modern definition of Domotics could be the interaction of technologies and services applied to different buildings with the purpose of increasing security, comfort, communications and energy savings.
At the beginning automated devices were independent or, sometimes, grouped in small independent systems. But the idea of giving them interoperability using a common "language" keeps on growing up, consequently following such idea the first Home Automation Systems (HASs) appeared bringing a new concept of a home network full of possibilities, but this included also new factors to bear in mind.

In addition, a strong reason why of HASs are becoming popular is because they are plenty of attractive features that can easily lure companies to enter quickly this emerging market, also they represent a great research opportunity in creating new fields in engineering, architecture and computing . However, these new technologies are still in their early stages with a lack of robust standards creating compatibility issues affecting their reliability. Another problem is that these systems are not always fully accepted by final users, especially the old and disabled – arguably the ones that need it the most. It is the goal of researchers to find out how to introduce home automation into our lives so as to only affect us positively. As an example, one effort to make these systems usable and affordable by any user helped the use of old, cheap and simple technologies like the X-10 protocol to transfer data in the home-network, in relative terms this approach created low cost HASs taking the advantage that X-10 technology do not require additional wiring. Even though newest technologies are constantly coming and a constant migration from wired to wireless is gradually affecting technologies involved within the home network possibly corroborating what Myers, Brad A. et al said that the future home network will have ubiquitous embedded computation with an increasing number of appliances having wireless communication. In fact, there are many recent tendencies to integrate various kinds of embedded devices and consumer appliances into software systems, tendencies that have emerged from the ideas of pervasive computing. This evolution offers many useful possibilities in Domotics.

Lately, it is being proved that Domotics has many interesting fields, and among them using remote-Controlled HASs to control the home network is one of the most challenging. The possibility of having ubiquitous access to many devices within a building at any time, from anywhere, resolves many of the problems that users often face when they return home, saving a significant amount of time. It also notably increases the security in any kind of building and it may even provide a backup control system for local system breakdowns. This ubiquitous access could be achieved from many different digital devices and it is known that the network hierarchy has been rapidly moving lower in the chain towards smaller and more personal devices.Considering latest tendencies, everything points at

prompt remote control standardization in home networks.

2. Aims of the paper
This paper has several aims:

· Show usefulness of remote-controlled HASs in Domotics

· Indicate the path evolution is following in Domotics

· Illustrate different ways to control of a home network using standardized technologies.

· Demonstrate the possibility of an ubiquitous access to the home network using actual technologies

· Explain possible actual benefits for Home Automation Systems

· Discuss several issues that may affect a remote-controlled HASs

· Propose a standarized remote-controlled HASs architecture

· Encourage (modular) user- friendly interfaces development

· To note down that the citation "provide an easier way to manage consistent user interaction in heterogeneous Environments" fits completely in Domotics

These aims have to be achieved thanks to an extensive literature review about Domotics and other related fields including network technologies such as 802.11, X-10, GSM, IP (using UPnP package) and several programming languages such as XML, WML, Java, C++ and
.NET technologies. Additionally all contents in the paper must be backed by investigations
into the related social, ethical, legal issues and a meticulous investigation of the involved standards that may influence remote-controlled HAS in the actuality.

3. Why Remote Control?

Wireless technologies represent a rapidly emerging area of growth and importance for providing ubiquitous access to the network; WLANs based on the IEEE 802.11 standard are being implemented constantly in the houses and Broadband wireless (BW) is also an emerging wireless technology which is competing with Digital Subscriber Line (DSL). According to this, it makes sense that the logical direction about managing HASs in the near future is going to be by means of a remote control. But wireless technologies in domotics should be implemented carefully.

This paper aims to answer the following questions :

· What are the benefits of using remote control in domotics?

· What are the main issues of using remote control in domotics?

· After studying issues and benefits of remote controlling, is it still profitable to use remote controlled HASs?

3.1. Home network remote-controlling benefits

The increasing ubiquity of heterogeneous computing devices such as laptop computers, palms, mobiles etc. shows that users prefer a ubiquitous access of a system rather than to be uncomfortably forced to go physically to the nearest control point. Remote control saves time and everybody is aware of this, it also provides increased security and flexibility. For example, if the user receives a SMS saying that there was an intrusion, he/she can connect to the internet and watch the video cameras inside the house to see what happens, another example could be the possibility to turn on the heaters from the distance using a mobile, laptop or PDA so as soon as the user reaches the house it will be hot already, this could be really useful especially in cold countries. As a matter of fact security will always be a main priority in all families, and prevention is better than cure. By receiving alerts in a portable device user is informed of all possible issues occurring in the house and it gives the possibility to deal with it using different ways of control like instant messaging, since many users are already familiar with the concepts and user interfaces of instant messaging. Many computers and mobile devices also already have instant messaging clients installed.

Good scalability properties, independence of location or geographical distance, and high flexibility due to the different existing protocols make remote-controlling HASs suitable for most user needs.

3.2. Home network remote-controlling issues
Roychowdhury and Moyer (2001) identify four primary reasons:

1. Interoperability

2. Scalability

3. Security

4. limited services

Interoperability refers to the capability of devices of different types and from different manufacturers to communicate and cooperate. Scalability refers primarily to scalability in terms of geographical distance and location independence. In the context of offering remote access as a service, scalability in terms of capacity would also be an issue. Security is probably the most important issue among them and the hardest to deal with regarding the media used in wireless communications. Finally, Limited Services due to bandwidth limitations of wireless networks in comparison with other wired technologies.

In addition to Roychowdhury and Moyer (2001) reasons, two more important issues have to be mentioned:

5. Usability

6. Existence of multiple standards

HASs are not being well accepted by old or disabled users and, in some cases, users don't like computers controlling their lives. While appliances get more computerized with more features, their user interfaces get harder to use forcing users to come back to the old behaviour with their appliances again,this lack of acceptance is worse when users have to use complex hand-held/portable devices or small interfaces. And the existence of multiple standards is a major obstacle for deployment of wireless networks, while GSM is the only widely supported standard in Europe and Asia for mobile communications, multiple standards are in use in the U.S.

3.3. After considering benefits and issues
Even with all issues related to remote-controlled HASs it seems that the benefits are just good enough to continue advancing in this field, also just recently, organizations have been formed to ensure network and device interoperability. For example, the adoption of the 802.11b standard has made wireless data networks one of the hottest newcomers in the current wireless market. As a result, in one hand remote-controlled HASs represent in Domotics a great opportunity to improve human computer interaction thanks to its ubiquitous access, but in the other hand they represent one of the most challenging environments due to involved security issues and relative complexity of portable devices.

4. Architecture of the Remote -Controlled HAS

It is clearly necessary to have an organized and defined structure for HASs. Since their creation normally involves different areas of electronics, architecture and computing, there are many different ways to develop solutions and not all of them can be applied to all users. This makes them difficult to implement due to the high impact that they might have on the everyday user. Using an overall view, a Domotics project can be divided into three stages: *Study*, *Definition* and *Installation*. In the study section, it is very important to know which benefits the users are going to get with the project and which technologies are going to be used. An optimal study will help considerably at the definition stage where inputs, outputs and processes are more defined. The last two steps can be completed with the help of software tools, although not all HASs have to follow this model. A well defined domotics model is the one used in the project Amigo.This project is based in a semantic modelling of services that enables interoperability of heterogenous services. The ontology may facilitate clear description on how far each device is suitable for different kinds of information and different interaction demand.

Another important approach more oriented to the concept of the home network, and one of the most widespread, is to divide the whole network into three: *Data*, *Control* and *Multimedia*, making it easier to manage the whole system - optimizing technology applications and allocating them in different areas of the network with better purpose. In a remote controlled HAS the home-network will be approached differently depending on the selected protocol for the service and the required bandwidth. For example, control via a mobile using the SMS service can be achieved using the X-10 protocol, but advanced control of video cameras or appliances requiring video or heavy interfaces will fit better if it is used the Internet via TCP/IP and a web server. There are many ways of approaching a HAS but, if the final product contains a bad-structured network, it will make the project less secure, less useful and it could fail in its scalability.

Candidate technology to standardize the remote-Controlled HASs is the Internet Protocol (IP), using UPnP package which is totally compatible with strongly standardized technologies such as IP, XML, HTML and WML; while the

X-10 which includes RF (radio frequency) compatible devices that enables the use of remote controls inside the house, and the GSM (Global System for Mobile Communications) Digital standard provide an outstanding backup emergency control. Remote access will be achieved outside the building from the Internet and GSM networks and inside the building through the home network using the 802.11 standard and the X-10 protocol. Among other factors that will affect the final performance of the remote-controlled HAS we have the decision to select the programming language/s. Normally any programming language should be suitable to create the interfaces and to link the home-network with the outer networks but, when linking certain technologies and standards, some languages are more reliable than others, depending on their portability and library provision. Also other factors such as the global linking of the system or the usability and scalability of the final product will have to be considered at the time of the final binding.

The summarized schema of the HAS is shown below:

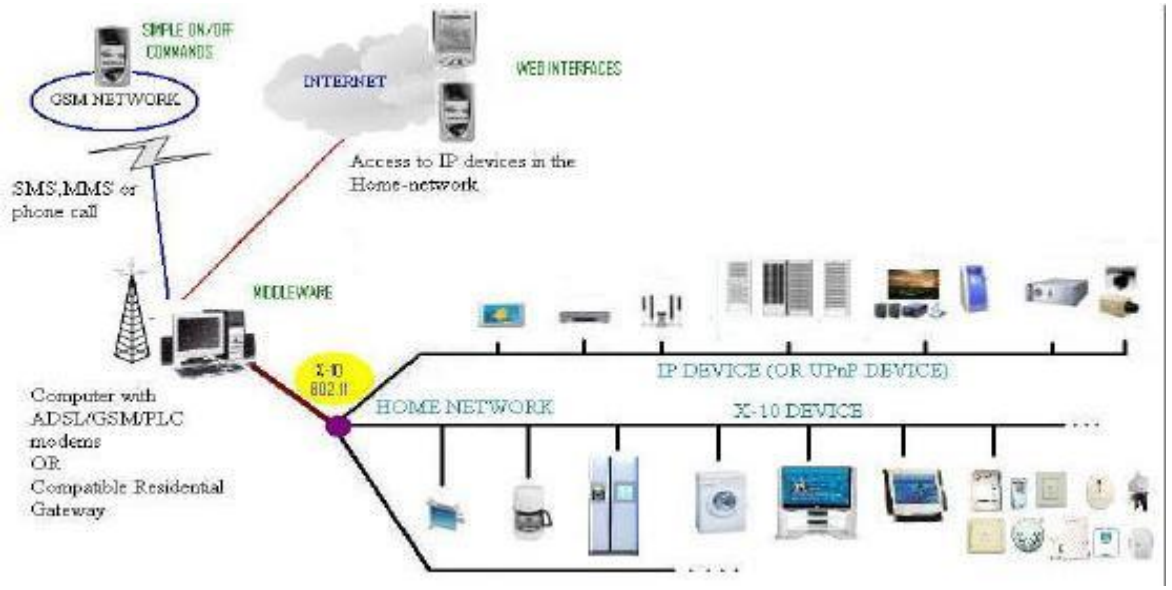

Figure 1. Remote-controlled HAS

In accordance with the objectives defined, the final system must achieve remote control, with practical interfaces involving different technologies and the different devices compatible with
the selected network protocols. A useful and scalable remote-controlled HAS is produced and its functionality tested using UPnP or X-10 compatible devices. Encouraging remote control, comparing actual standards and accelerating the process of standardisation in HASs are also important factors to consider and it is necessary to use low-price materials in order to make cheap HASs commercially available, sooner, for everyone. The whole control cycle must be complete from the user selecting a control action from their remote point until the target device realizes the desired action.

4.1. IP Remote control

UPnP is a lightweight architecture to extend the Plug & Play concepts to network devices and services UPnP defines two roles of devices: control points who act as clients and controlled devices who act as servers. It is very flexible and it comes with several helpful solutions for a Home-network. Controlled devices are containers which embed services and other controlled devices Services define the functionality offered by the device and control points use the services to control the device and monitor their status. The architecture do not defines an API, and is therefore language independent.

Figure 2. UPnP stack and stages

A brief definition of the different stages:

1. **Addressing** ensures that each device receives a valid IP-Address
2. In the **Discovery** stage defines how control points can find controlled devices.
3. During **Description** a control points receives the device and service descriptions (expressed in XML) of the controlled device. The device descriptions contain several standards and vendor specific device information and a list of embedded services and devices. The service description contains the actions and state variables of the service.
4. The **Control** stage uses SOAP (Simple Object Access Protocol) to invoke actions of services. SOAP is a RPC technique that uses HTTP as the transport protocol and XML for marshalling.
5. At the **Eventing** stage uses GENA (General Event Notification Architecture) to inform control points of state changes occurred at controlled devices.
6. A **presentation** page can be presented for user control. This step delivers a HTML (or WML) page to the control point. Better defined or specific interfaces could be required for special users perhaps even using flash.

UPnP package is directly connected to the Device and Service Descriptions defined by the UPnP Device Architecture. The descriptions are expressed in XML. The object model can be generated from a corresponding XML-File. Also the XML representation can be accessed by the object model. UPnP comes with a well defined and structured hierarchy of classes that makes implementation highly reliable.

IP remote control cycle is as follows:

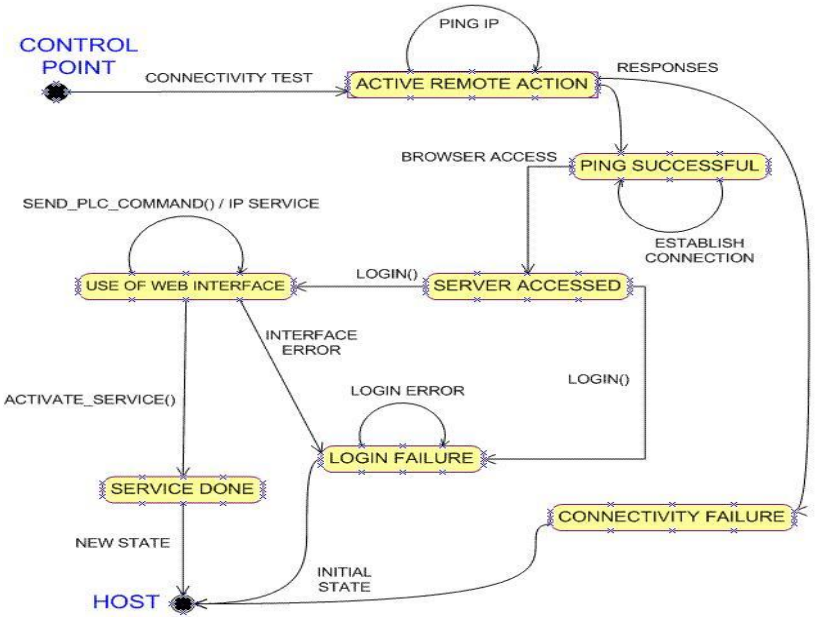

Figure 3. IP device remote control

The diagram represents the different states of the HAS since the web server is accessed until the service is processed r not by the host. Web server has to be login-session enabled.

4.2. Backup GSM Remote Control

The Global System for Mobile Communications (GSM) is a digital standard wireless technology GSM is the most widely used wireless technology in the world with one billion customers globally, which represents 72% of all wireless customers. GSM has a high presence among users (almost everybody has a mobile) raising the probability of the remote-controlled HAS to be accessible, furthermore by programming the GSM modem using AT/AT+ commands it provides another security layer (modem will respond only to specific mobiles) and certain robustness. At this backup level, the interaction with the user is very simple; the bilateral communication is reduced to the minimum, only representing emergency processes. Eventually, the remote-controlled HAS will send alerts to the user´s mobile informing about unusual state changes in the sensors within the building, afterwards user is able to activate/deactivate some automated devices required to solve the issue either by dials or messaging or, in the usual case, using a web interface, in any case the user will have always two possible accesses in case that one fails. Normally the probability of accessing the GSM network will be higher than accessing the Internet.

The schema of the system is as follows:

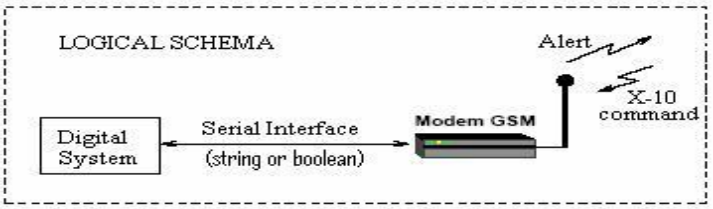

Figure 4. Logical schema for GSM control

The simplicity of the X-10 command "<X10 address>", "<RF command>", "<keydata>", "<timestamp>" (*All parameters are specified as string values)*, permits to encode the command as a string, and eventually some Booleans might be used to manage the state of the modem.

It is important to mention that the use of a friendly- user interface is extremely relevant in an emergency backup control, to achieve it, exists the possibility to use templates already defined in the mobile to send messages, and simple and visible ON/OFF selections to establish different dialling.

Backup control cycle is as follows:

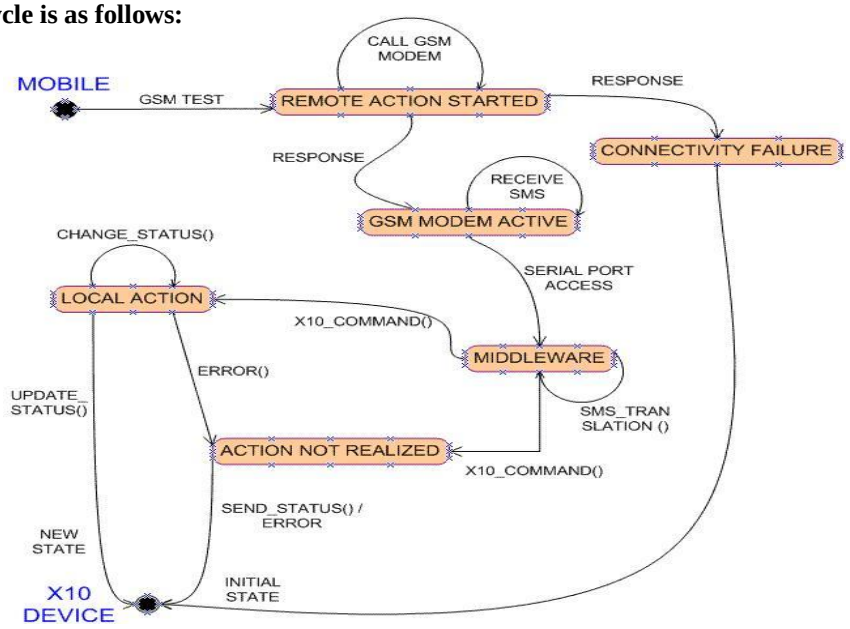

Figure 5. GSM Backup Control

4.3. User-friendly Interfaces

Nielsen, Jacob and Rolf Molich (1990) said that there are basically four ways to evaluate a user interface: Formally by some analysis technique, automatically by a computerized procedure, empirically by experiments with teat users, and heuristically by simply looking at the interface and passing judgement according to ones own opinion. In Domotics, the most suitable could be the empirical one, analyzing heuristically an interface can give an idea of the potential usability that it might have but since, in a home network, users may have any portfolio the best way of assuring the usability of the interface is experimenting with the user directly.

Some of the most extensive evaluation effort has been focused on determining exactly what users might want, using techniques such as surveys and interviews. Additionally, researchers investigating displays that combine ambient awareness with notification, or alarms, have conducted some formative analysis. In particular, Chewar and Mc-Crickard (2002) have discussed work in progress on modifying a formative in-use study methodology to apply to notification displays.

Undoubtedly the solution proposed by P. Rigole et al. (2005), seems to adjust closely to different specific user requirements by means of an indirect exposure of a component's
interfacing needs through Interaction Components (ICs). This way, interfacing needs can be described in an abstract way at the level of a component, and transformed into concrete interfacing widgets at runtime by the ICs. In addition, this approach also tackles the problem of runtime user interface mobility between devices offering heterogeneous interfacing capabilities. During a relocation of software components from one host to another, the concrete user interface is regenerated using the abstract interface representation and the limitations of the new host. The point is to build a modular interface flexible enough to adapt to all users in order to fit user's individual preferences or needs.

The user will be able to have larger buttons that are easier to press or fewer options to make the interface less cluttered. For disabled users, the HAS could generate an interface with suitable properties for that disability, such as a Braille interface for a blind person or an interface with only a few buttons for someone with a cognitive impairment.

To finalize, interfaces have to achieve another important feature: reusability; different devices in the home may operate similarly executing comparable processes that can be almost equally developed in the HAS, this saves a significant amount of time and makes the system more stable.

5. Conclusions and Future Work

The process of standardization in Domotics is becoming the most important factor to introduce an automated environment in all homes. There are already E- home standards settling up in Europe, the example is the European Installation Bus (EIB) that is the world's leading system for "intelligent" electrical installation networking. Not to forget That UPnP providing total compatibility with XML and IP. I agree with Simon Aurell (2005) that the most likely way of interfacing with devices in the future will be IP; it is more flexible, scalable and compatible. The biggest issue will be probably to make it usable and accessible to all kinds of users.

Since this is a new field of investigation, the results of the project are likely to be worthy of further analysis. The completion of a whole cycle of control between a remote device and the building will be critical for the success of the research; once control is achieved a meticulous study about how users and the system interact has to be done. It is important to clarify that this research does not exclude local control of HASs - it is simply focused on remote control as an important field for HASs in the future. To conclude, this research should help other researchers to achieve their goals with their future HAS projects and it will contribute positively to the E-Home community.

6. References

1) José Manuel Huidobro Moya and Ramón Millán Tejedor (2004) “Domótica. Edificios inteligentes”.
2) Cortes, Francisco Javier (2002) “Convergencia TCP/IP en Home Networking”. Tesis Doctoral en Electrónica y Comunicaciones. Instituto Tecnológico de Aragón (ITA) Advanced services department. December 2002.
3) Myers, Brad A. et al (2004) “Taking handheld devices to the next level”. IEEE Computer Society, December 2004. pp. 36-45.
4) D. Greaves. "Control Software for Home Automation, Design Aspects and Position Paper”. Icdcsw. Proceedings of the 22nd International Conference on Distributed Computing Systems Workshops (ICDCSW '02), 2002.
5) P.Rigole, Y. Berbers, T. Holvoet. “A UPnP software gateway towards EIB home automation”, May 2003, in proceedings of the IASTED International Conference on Computer Science and Technology - CST 2003 (Cancun, Mexico)
6) P. Rigole, C. Vandervelpen, K. Luyten, Y. Vandewoude, K. Coninx, and Y. Berbers, “A component-based infrastructure for pervasive user interaction” Proceedings of Software Techniques for Embedded and Pervasive Systems (Varea, M. and Cortes, L., eds.), pp. 1 -16, 2005 .
7) Simon Aurell “Remote Controlling devices using Instant Messaging”. Bachelor Thesis in Software Engineering, June 2005 (University of Gothenburg)
8) J. Nichols et al. (2002) “Generating Remote-Control interfaces for Complex Appliances”. Proceedings of the ACM Conference of User-Interface software and Technology (UIST02), ACM press, 161 -170.
9) Myers, Brad A. et al (2004) Taking handheld devices to the next level. IEEE Computer Society, December (2004) pp. 36-45.
10) Nielsen, J. & Molich, R. (1990), Heuristic evaluation of user interfaces, in Proceedings of the SIGCHI conference on Human factors in computing systems , ACM Press, pp. 249 --256.
11) Kalaoja, J. Analysis of vocabularies for Amigo home domain, to be presented as a poster and published in the proceeding of 8th International Conference on Enterprise Information Systems 23 - 27, May 2006
12) European Standard for Home and Building Electronic Systems, (Accessed 22 November 2005)
13) Roychowdhury, A. Moyer. "Instant Messaging and Presence for SIP Enabled Networked Appliances", (Publisher unknown), 2001 (Accessed 10 February 2005)
14) Moraes, Fernando; Amory, Alexandre M.; Petrini, Juracy Jr. Sistema Cliente-Servidor para Supervisão de Processos através da Web. trabalho de conclusão do curso de informática da PUCRS. dezembro de 2000. 167p.
15) Jennifer Mankoff, Anind Dey, Gary Hsieh, Julie Kientz, Scott Lederer, and Morgan Ames . Heuristic Evaluation of Ambient Displays. In Proceedings of the SIGCHI conference on Human factors in computing systems, 2003 pp. 169-176.
16) C. Chewar and D. S. McCrickard. Adapting uems for notification systems. Accepted to Design and evalua tion of notification interfaces for ubiquitous computing, Ubicomp 2002 workshop 9 , September 2002.
17) E. H. M. van Dantzich, D. Robbins and M. Czerwinski. Scope: Providing awareness of multiple notifications at a glance. In Proceedings of the 6th Intl Working Conf. on Advanced Visual Interfaces (AVI ’02), page To Appear. ACM Press, May 2002.

Rainwater Harvesting Structures - A Case Study

C.L.Jejurkar[1], N.S.Naik[2]

[1]*Asso .Professor, SRES College of Engineering, Kopargaon, Dist. Ahmed Nagar,* ***India***

[2]*Asst. Professor, SRES College of Engineering, Kopargaon, Dist. Ahmed Nagar,* ***India***

Abstract: Feasibility of harvesting water at Konkamthan Village in Ahmednagar District of Maharashtra State is studied using yearly rainfall data. It is said that "**water is life**" because, the water is required from birth to death for human being. In the global picture, India is identified as a country where water scarcity is expected to grow considerably in the coming decades. Further drought condition, climatic variability cause considerable human suffering in many parts of the country in the form of scarcity of water for both satisfaction of drinking needs and irrigation needs. The results of man made crisis be seen as global warming and change in climatic conditions. The rain has become irregular because of disturbance in natural cycle and therefore do not reach when one wants them. **"A Drop Harvested is a Crop Harvested"** dictates upon the importance of rain water harvesting.

The quantity of rainfall is erratic, reduced and uncertain. Hence, need for conservation has been felt much more than ever before. In this study, hydro-meteorological data is obtained from Indian Meteorological Station at Kumbhari, of Kopargaon taluka. To study the profile of ground, survey was carried out with Total Station. Contour sheet was plotted with scale 1" to 160' at 0.5 m contour interval. The infiltration rate of soil was studied by double ring infiltrometer. Depending upon design requirements different runoff harvesting structures, like contour bunding, compartment bunding, nalah bunding and farm pound has been suggested. The study shows that with the help of harvesting structures 60 to 70 % of rainfall can be harvested.

Key words: Yearly rainfall, Rain water harvesting structures, global warming, Total stations, Profile, Contour, Infiltration, Double ring infiltrometer.

Introduction

It is well known that, the land pressure is increasing day by day due to population growth, causing the more and more water is required for domestic, agriculture and industrial purposes. At every place there is ground water, but its exploration needs money, as a result it becomes a constraint, however there are other constraints such as rainfall pattern, availability of surface runoff and storage of water. Hence rain water harvesting structures are essential for effective utilization of excess rainfall.

Rainwater harvesting is the intentional collection of rainwater from a surface and its subsequent storage in order to supply water during the time of demand. Rain-water harvesting is essential in view of the fact that rainfall, which is a source of fresh water , occurs in every short spells and runs off as a waste unless arrangements are made for its storing (NIH,1993).

In the present study attempt has been made to study the topography of the area , based on survey work carried out using total stations. Also the rainfall pattern for six years and soil strata has been studied. The rain water harvesting structures were proposed based on topography, rainfall pattern, climatic conditions, and geological features of the study area.

Site Details

The location of site is at Kokamthan, 03 km away from Kopargaon, District Ahmednagar. The Latitude and Departure of Sanvatsar village are 19^0 54' N and 74^0 33' E respectively. The area under investigation is about 125 acres.

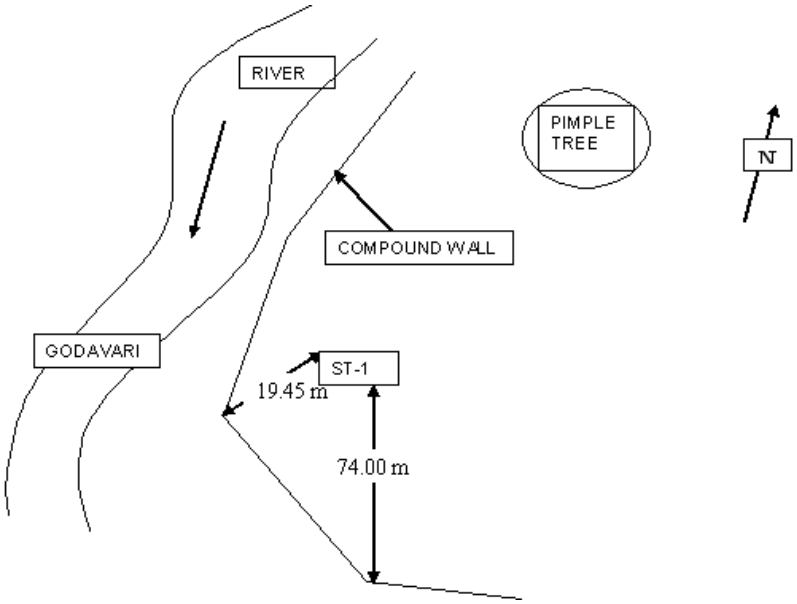

Fig 1 Site Details

Data Collection

The data collection part of the area under investigation has been broadly carried out in two parts,

1] Topographical studies

2] Hydrological studies

Survey Record

The survey for the proposed site has been carried out with the help of Total Station **DTM-352** and R.Ls of 405 stations are determined and listed in the table below.

Table 1 Sample Record of observations

Obs. No.	Northing	Easting	R.Ls	Description
1	0	0	100	ST1
2	-70.6743	-24.8749	98.5763	WC
3	-63.305	-35.5295	98.5771	RC1
4	-34.5137	-58.375	98.6694	RVC1
5	-27.3761	-34.3426	98.5275	RC2
6	-26.4177	-21.1967	98.363	WC2

Based on total station observations, the Contour map has been prepared with a contour interval of 0.5m., as shown in figure-3. It is observed that the elevational difference in the surveyed area in two ends is about 2m.

Rainfall Data - The rainfall data of last 20 years was obtained from the Irrigation Department and Indian Meteorological Department, Jeur Kumbhari. The data is tabulated as below and rainfall trend has been observed as shown in figure-2.

Table2 20 Year Rainfall Data

Year	Rainfall (mm)
1987-88	520.4
1988-89	610.8
1989-90	715.6
1990-91	680.5
1991-92	500.4
1992-93	560.1
1993-94	180.4
1994-95	270.2
1995-96	165.8
1996-97	650.9
1997-98	353.6
1998-99	501.3
1999-00	311.5
2000-01	504.8
2001-02	477.2
2002-03	531.3
2003-04	376.6
2004-05	455.2
2005-06	484.4
2006-07	761.9

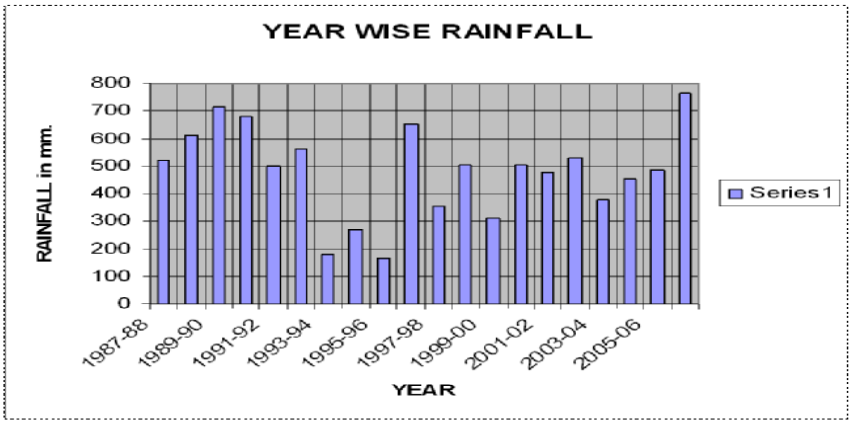

Fig 2 Rainfall Pattern

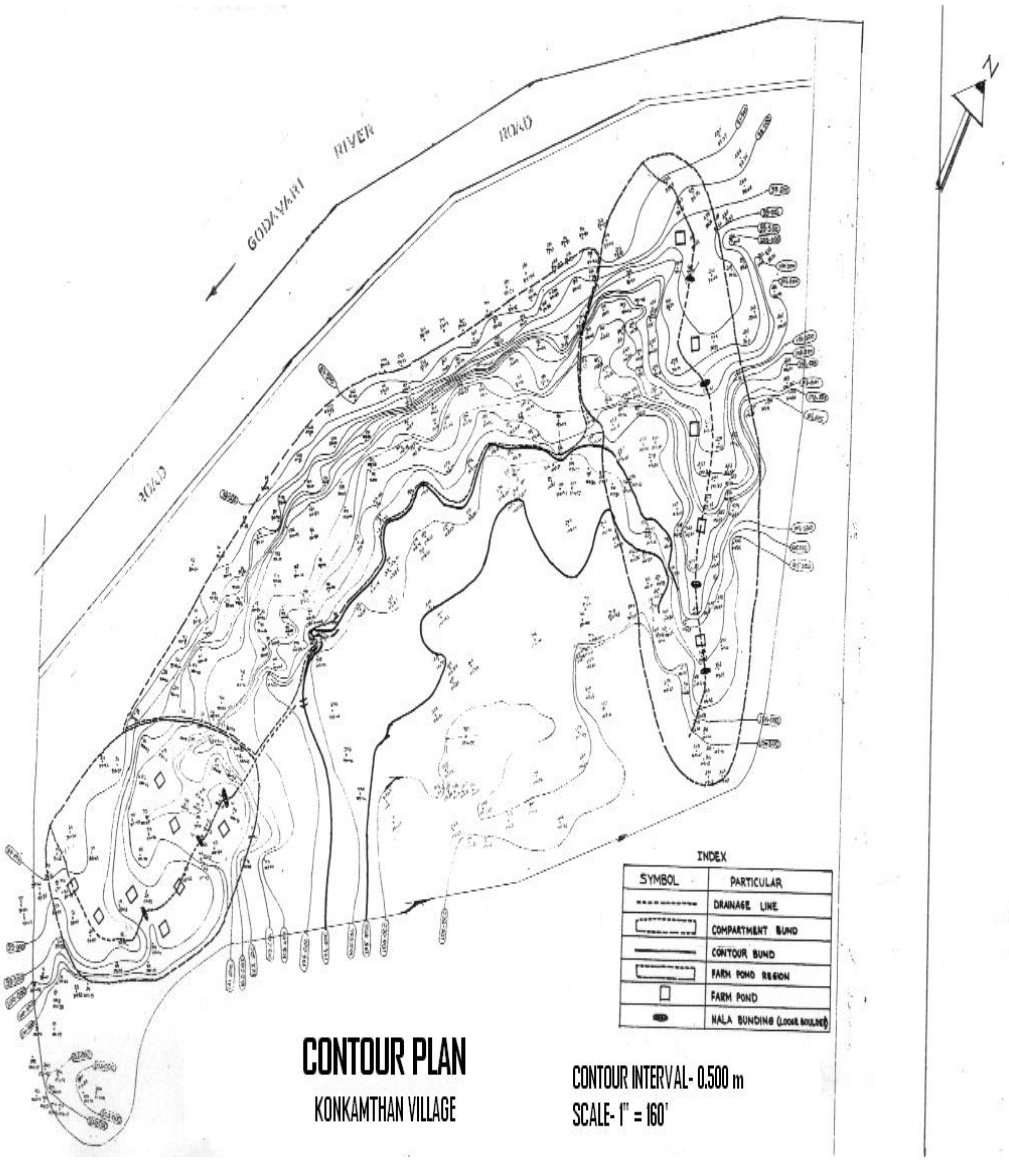

Fig 3 Contour Plan showing RWH Structures

Proposed Action Plan

To design the rain water harvesting structures, the rainfall, runoff, evaporation and seepage data are essentially required but these are generally not available for most of the sites, however if these are available, the cost of an extensive hydrologic investigation is seldom justified. However, based on few main factors affecting the design, a general guideline has been followed to design the contour bund, compartment bund and nalah bund.

Water harvesting and runoff recycling has four distinct components , viz., collection (harvesting) of excess rainfall, efficient storage of harvest water, water application (including lifting and conveyance) and optimum utilization of applied water for maximum benefits.

Based on the catchment area, rainfall, land slope and runoff volume, the suitability requirements of the farm pond has been proposed to construct on both right and left side of the investigation area.

Conclusion

The basic thinking behind rainwater harvesting is that the rainfall in India is highly seasonal, with most of the precipitation occurring within a few months of the year and within that period the intensity, being concentrated within a few weeks, that precipitation is also highly variable between different parts of the country and from year to year, that's why it is necessary to store rainwater with various structures suitable for that area.

The principal concern in undertaking this project is to recharge the ground water, meet the industrial demand, protecting agriculture from the vagaries of the monsoon, and fulfill the domestic need and to control the floods to a certain extent.

The detailed contour survey of area under investigation at Sanvatsar was carried out with the help of total Station and contour sheet was plotted. By studying the soil characteristics, metrological factors, infiltration rate and land slope of the area under investigation, we have suggested the contour bunding, compartment bunding, farm pond and nalah bunding as the rain water harvesting structures suitable for that area. Looking into the different losses and other factors it can also be concluded that about 70% of the rain falling in that area can be harvested.

Looking into the scarcity of water and high energy input for water supply scheme, it should be made mandatory to implement such rain water harvesting techniques so that the problem of water scarcity can be minimized.

References

1) B.G. Karale, 'Utilization of Runoff Water by Means of Artificial Recharge Scheme of Rainwater Harvesting With Special Reference to Ratnagiri District of Konkan Region', 408 - 410.
2) B.R. Chandurkar and A. B. Murkute, Role of Percolation Tank in Rainwater Harvesting a Case Study of Percolation Tank at Village Chinchgat Taluka , District -Yavatmal, 406 - 408.
3) M.M. Sardhukan, an Integrated Approach for Rainwater Harvesting and Water Conservation Technique by Suitable Structures within the Micro Watershed in Deccan Trap Terrain of Maharashtra, 461 - 468
4) P.N. Phadtare, Rainwater Harvesting – Integrated approach, 114 -120
5) S.K. Dutta, Soil Conservation and Land Management, 120 -124.

Infiltration studies for varying land cover conditions

C. L. Jejurkar
Research Scholar, S.G.G.S. I.E & T,
Nanded., India (M.S.)

Dr. M. P. Rajurkar
Professor, Department of Civil (WM) Engg.
S.G.G.S. I.E & T, Nanded., India (M.S.)

Abstract — Procedures adopted for infiltration calculations vary greatly in sophistication right from the application of reported average rates for specific soil types and vegetal land covers to the use of differential equations governing the flow of water in unsaturated porous media. In this work attempt is made to determine infiltration rates of soil under different land cover conditions and to compare validity of different infiltration equations viz. Kostiakov, modified Kostiakov, Horton and Philip. The various land covers such as Grapes, Gram, Bajra, Weeds and Cucumber were selected at a location Brahmangaon in Tq. Kopargaon, dist. Nagar (M.S.). Observations were taken by using double ring infiltrometer for two seasons' winter and summer. The field observations, analysis of data and graphical representations indicates that the infiltration rate in summer was around twice the infiltration rate in winter. Suitability of the infiltration model under different conditions has been indicated. Further, the Kostiakov equation was found to be the best for almost all cultivated land covers.

Keywords- infiltration, double ring infiltrometer, land cover, season, Horton, Kostiakov, Philip, modified Kostiakov

I. INTRODUCTION

The infiltration rate is of prime importance to the irrigation engineers as it influences the application rate of irrigation. [2], [6], [13] It is difficult to design an irrigation system without proper knowledge of infiltration characteristics of soil. [5], [11], [12]. In dry-land agricultural infiltration characteristics will also be required for proper water management. It is useful for determination of availability of water for plants, runoff rate and percolation. Accurate determination of infiltration rates is essential for reliable prediction of surface runoff. [1],[7],[9] This is useful for mitigation of hydrological risk. The infiltration capacity of soil influences the occurrence of overland flow. [3], [4] An evaluation of the risk of overland flow is needed in order to minimize the risk of transferring pollutants from soil to rivers and lakes. Further, the prediction of runoff has a crucial role in designing hydraulic structures as well as water resources planning and management. [2], [6], [11]

II. OBJECTIVES

The present infiltration study is undertaken with the following main objectives:

i) To evaluate the infiltration capacity of the soil and to evaluate the reliability of infiltration tests,
ii) To determine the infiltration rate for summer season and winter season and
iii) To study the suitability and validity of various commonly used infiltration equations

III. INFILTRATION PROCESS

Infiltration on pervious surface is controlled mainly by three mechanisms, namely initial entry of water through the soil surface followed by the movement of water through infiltration zones and finally.repenishment of soil water storage The Infiltration rate usually shows a sharp decline with time from the start of the application of water. The constant rate approached after a sufficiently large time is referred to as the steady Infiltration rate. The surface entry rate of water may be affected by the presence of a thin layer of silts and clay particles at the surface of the soil and vegetation.

The infiltration process is influenced by various factors such as: i) Soil texture and structure; ii) Sealing of surface or crust formation; iii) Initial moisture content; iv) Aggregation and Structure; v) Frozen Surface; vi) Organic Matter; vii) Pores; viii) Land cover and evaporation; and ix) Compaction due to rain. The initial moisture content has pronounced effect on the initial infiltration rate though the basic infiltration rate is not appreciably affected. A dry soil reaches the basic infiltration rate latter than the wet soil. This is an important aspect from the irrigation point of view.

IV. LITERATURE REVIEW

A number of Literatures and research papers have been studied, which deals with infiltration through different types of soils and related investigations. The findings of these papers have been presented here.

Vardhan Ravi, Ying Ouyang and Joseph R. Williams, [1]. 1998 carried out an investigation on Estimation of Infiltration Rate in the vadose zone. In this study a compilation of simple mathematical models has been presented for quantifying the rate of soil- water movement due to infiltration. This paper discusses the techniques for characterizing goals for their chemical, physical and hydraulic properties. It also provides a list of available field and laboratory measurement techniques and look-up methods for these parameters. In addition to the identification of parameters, a document provided a table of common unsaturated zone models and their parameter requirements. An extensive survey of unsaturated zone models was provided by Van Der Hiejde (1994). A related effort is the release of the Soil Screening Guidance (U.S.EPA, 1996). This Guidance provides the public with a tool for determining risk-based site-specific, soil screening levels (SSLs) for the evaluation of the need for further investigation at NPL (National Priority List) sites.

Robert Pitt Janice L. [3]. (1999), carried out an extensive experimental study on infiltration through Disturbed Urban Soils and Compost. This study examined a common, but poorly understood, problem associated with land development

and the modifications made to soil structure. The project was divided into two tasks namely, testing infiltration rates of impacted soils, and Enhancing soil by amending with compost to increase infiltration and prevent runoff. This project evaluated a widespread problem, decreased infiltration due to disturbed soils, and a potential solution, soil amendment with compost. A large number of infiltration tests were conducted to identify the factors significantly affecting infiltration parameters

John Diamond and Thomas Shanley, [4]. (2003), carried out infiltration rate assessment (spatial and temporal variability) of some extensive soils in Ireland at Castle Research Centre, Wexford. The objectives of investigations were to evaluate the infiltration capacity of the dominant component of major soil associations and to evaluate the reliability of infiltration tests. Infiltration capacity was measured by using double ring infiltrometers at one poorly drained, one imperfectly drained and eight freely drained sites for both winter and summer seasons. The study indicated a significant relationship between infiltration capacity and the antecedent soil water content, which contributed to the seasonal effect.

Jean-Claude and Mailhol, [5]. (2003), carried a study to validate a predictive form of Horton infiltration for simulating furrow irrigation. An operative modeling approach for predicting the advance- infiltration process under furrow irrigation through the irrigation season was proposed. The applicability of the model was then extended to heavy clay soils where the parameters λc (capillary length) and K_s (hydraulic conductivity) agreed with the values proposed in the study.

Sharma D.C., Dubey O. P., and Chhabra S. S., [9]. (2004), worked on determination of infiltration rate in Chitaurgarh dam command area (U.P.). In this study authors used radio-active tracer method and double-ring infiltrometer method for determination of average infiltration rate. For implementing the technique, tritiated water was injected into the ground at a certain depth between root zones. The tracer as a result of subsequent rainfall or irrigation moves downward. Infiltration tests were carried out at 12 sites in the canal system of dam. The study concluded that the results of radio-active tracer technique are comparable with double-ring infiltrometer and therefore can also be used for determination of infiltration rate.

Singh R.V. and Bhakar S.R. [8]. (2004), reported a study on comparison of infiltration equations for different land covers. A comparison of various infiltration equations e.g. Kostiakov equation, modified Kostiakov equation, Green Ampt and Horton equation were made. The various land covers in a sandy loam, soils e.g. cultivated land, fallow land, Pasture land and farm pond bed were considered.

Mohan S. and Kumari S., [10]. (2005), presented an experimental study on Recharge Estimation Using Infiltration Models. Different infiltration models were tested at 50 locations in a basin based on the soil type and land use variations at Neyveli. The Infiltration models namely Green Ampt Model, Modified Kostiakov model and Horton model were found to be statistically fit to the observed field data. The results were compared with that of the standard SWAT (Soil and Water Assessment Tool) Model developed by the USDA, agricultural research service (ARS). The study concluded that Horton Model is the most appropriate infiltration model for estimating recharge in Neyveli region.

Nestor L. Sy, [12]. (2006), carried out investigation for Modelling the in the Infiltration process with multi-layer perceptron artificial neural network in Netherlands. In this study, the ANN multilayer perceptron was used for the model the infiltration process. The data derived from plot scale simulator experiments conducted was used for analysis purpose. The networks were trained using physically measurable data from rainfall simulator experiments. The simulator produced 3.7mm average sized raindrops. At a height of 1.5m above the ground. The simulator produced an average velocity of 7.8m/s. Test plots of one square meter size were chosen. A vertical trench was dug at the downstream end of the test plot and a trough was positioned to catch the runoff water. The experiments usually lasted between one and three hours and runoff was recorded every 5 minutes. Total 80 experiments were conducted. The data was divided into two sets, 56 samples were used in the ANN training and 24 for testing.

The infiltration parameters of the Green–Ampt, Kostiakov, Horton and Philip infiltration models using field rainfall simulator data were determined by empirical filling using linear regression. The cumulative Infiltration by different infiltration model was compared with ANN model. The ANN model provided the highest accuracy. Therefore one can estimate Infiltration from easily available physical data using ANN.

V. LOCATION DETAILS

The location of sites is at Village Brahmangaon, 10 Km away from Kopargaon, Dist. Ahmednagar. The measurements were made in winter and summer at four land covers having different crops in it. The sites were chosen to represent the dominant component of major soil associates.

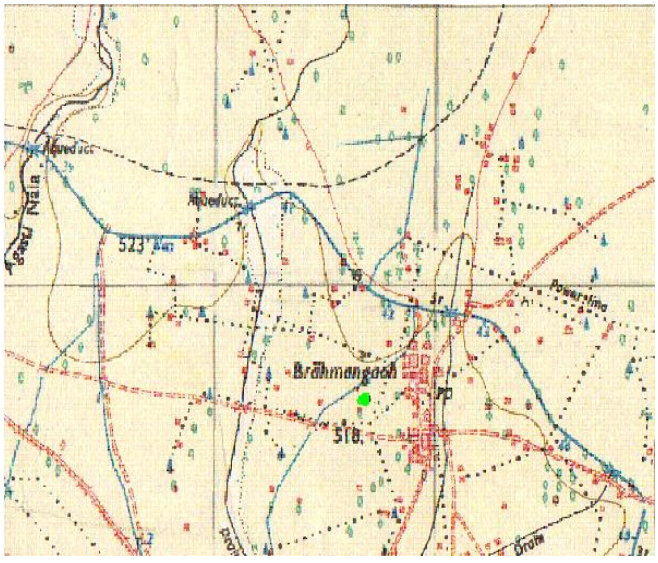

Figure 1. Map of the Study Area

VI. CLIMATIC CONDITIONS

Usually the temperature in Kopargaon and adjoining areas is quite high in months of March, April and May. The temperature variation was from 20°C to 40°C from morning to afternoon.

TABLE 1. Commonly Used Infiltration Equations

Sr. No.	Name of Equation	Expression	Method of Determination of Constants
1	Horton's Equation	$f = f_c + (f_o - f_c)\, e^{-kt}$	Graphical and Numerical
2	Kostiakov Equation	$Y_c = at^b$	Experimental
3	Modified Kostiakov Equation	$Y_c = at^b + c$	Method of average
4	Green Ampt Equation	$f_p = K_s(L+S)/L$	Field measurement
5	Philip's Two-Term Model	$q(t) = 1/2\ S\ t^{-1/2} + A$ $I(t) = S\ t^{1/2} + A\ t.$	Field measurement

VII. MEASUREMENT OF INFILTRATION

Infiltration rate was measured by double-ring infiltrometer, consisting of two concentric rings. The rate of fall of water level was measured in the inner ring while a pool of water was maintained at approximately the same level in the outer ring to reduce the amount of lateral flow from the inner ring. The diameter of the inner ring is 300mm ± 10mm and the outer ring diameter is 600mm ± 10mm. The slight variation in diameter allowed nesting of the rings during transport. Rings are 250 mm deep and were made from 6 mm thick steel plate with sharpened bottom edge. They were driven into the ground to 100 mm depth. Generally the water level was kept at 50 mm depth; the difference in height between the inner and outer rings was kept to a minimum. Other equipments used were water container, a measuring flask, wooden plank, hammer, plastic sheet, stop watch, hook gauge and scale. The rate of fall of the water level in the inner cylinder water was measured at 1, 2, 3, 5, 10, 15 and 30 minute intervals. The process was stopped once a steady infiltration rate had been found. The duration of each test was 4 to 7 hours.

VIII. RESULTS AND DISCUSSION

Cumulative infiltration is calculated for the observed time intervals with evaluated infiltration equation. Then comparison between measured cumulative infiltration and cumulative infiltration by evaluated infiltration equation is carried out. The same is tabulated and compared graphically. Table 2 indicates a sample comparison.

TABLE 2: GRAPES GARDEN- 01(WINTER SEASON)

Timmin	Kostiakov Eqn. (cm)	Modified Kostiakov Eqn. (cm)	Horton's equation		Measured Yc (cm)
			Rate (cm / hr)	Yc (cm)	
0	0	0	0	0	0
2	1.06	1.11	5.848	0.19	1.45
4	1.39	1.46	5.846	0.39	1.63
9	1.93	2.00	5.841	0.876	1.88
14	2.30	2.38	5.837	1.36	2.16
19	2.60	2.68	5.832	1.85	2.42
24	2.85	2.94	5.830	2.33	2.67
29	3.08	3.16	5.823	2.81	2.92
34	3.28	3.36	5.818	3.30	3.15
44	3.63	3.72	5.809	4.26	3.50
54	3.95	4.03	5.799	5.22	3.89
64	4.22	4.30	5.790	6.176	4.27
74	4.47	4.55	5.780	7.13	4.64
89	4.82	4.89	5.767	8.55	5.04
104	5.13	5.20	5.750	9.97	5.39
119	5.41	5.48	5.739	11.38	5.77
149	5.92	5.98	5.710	14.18	6.21
179	6.37	6.43	5.684	16.96	6.59
209	6.78	6.83	5.657	19.70	6.89
239	7.15	7.19	5.629	22.42	7.01
269	7.50	7.53	5.600	25.118	7.12
299	7.82	7.85	5.575	27.785	7.22
329	8.13	8.15	5.549	30.42	7.30
359	8.42	8.43	5.522	44.04	7.37

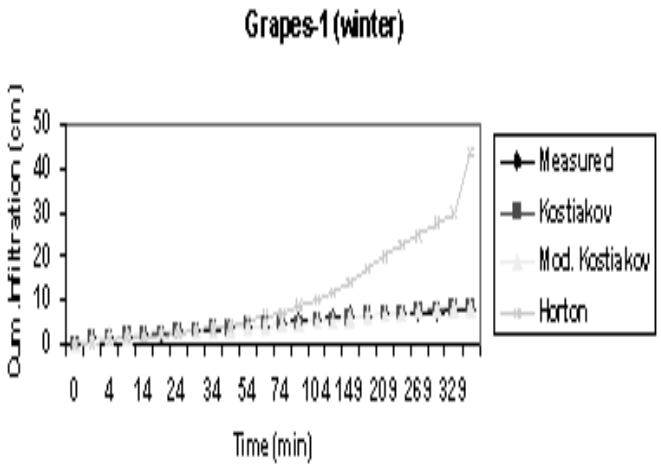

Figure 2. Measured Vs. Estimated Cumulative Infiltration for Grapes- I

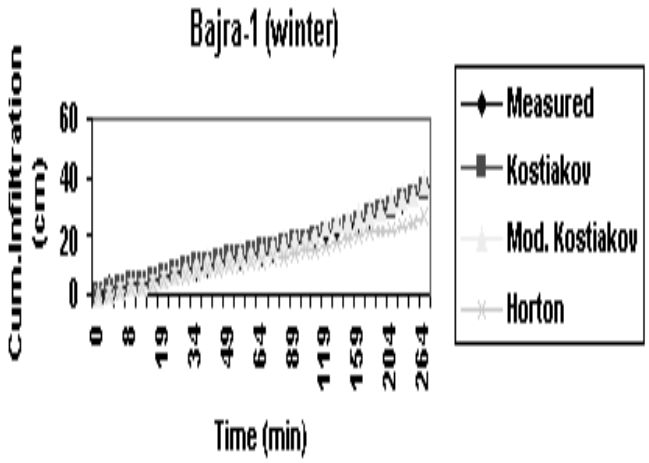

Figure 3. Measured Vs. Estimated Cumulative Infiltration for Bajra- I

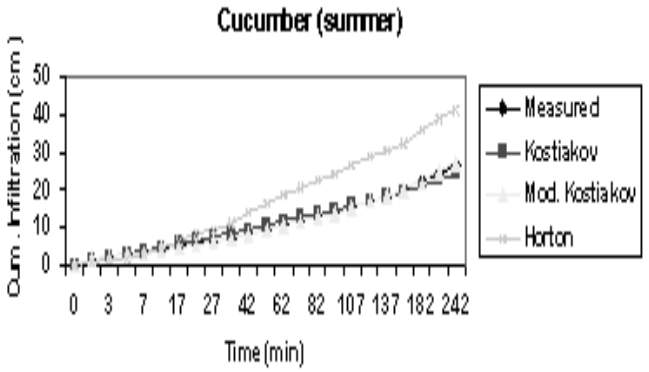

Figurer 4. Measured Vs. Estimated Cumulative Infiltration for Cucumber

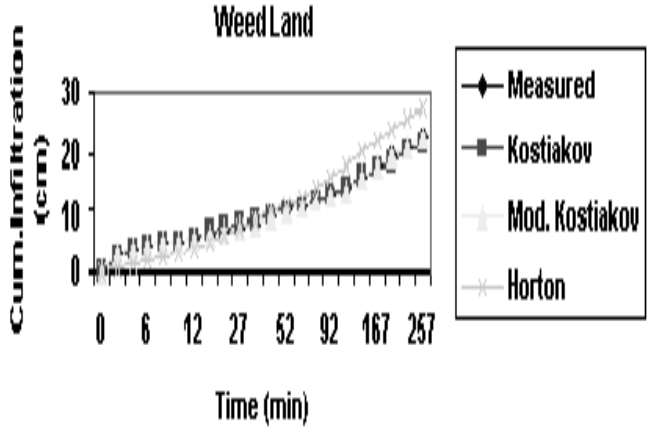

Figure 5. Measured Vs. Estimated Cumulative Infiltration for Weed Land (summer)

IX. ANALYSIS AND DISCUSSION

The study was undertaken for the determination of infiltration rate and evaluation of different infiltration equations stated earlier under different land covers, like Grapes garden, Bajra land, Gram land, Cucumber land and Weed's land in winter season and summer season.

The infiltration depth at the selected time intervals was measured in all the land covers based on double-ring infiltrometer field observations. Total fourteen experiments were conducted, six in winter season and eight in summer season. The infiltration curves were plotted for infiltration rate vs. time and cumulative infiltration vs. time separately for each land cover and for both seasons.

The infiltration observations indicated that for almost all land covers in winter season the infiltration rate was low and it requires more time to reach to constant infiltration rate. For almost all land covers in summer season the infiltration rate was more and it requires less time with compare to winter season to reach to constant infiltration rate. The total depth of cumulative infiltration in winter season and in summer season was near about same for grapes garden. The total depth of cumulative infiltration in summer season for Gram land was about 1.5 times the cumulative infiltration in winter season for Bajra crop on the same land.

Analysis was carried out for Kostiakov equation, modified Kostiakov equation, Horton equation and Philip equation for different land covers, in winter season and in summer season. In Kostiakov and modified Kostiakov for obtaining soil constant a, b and c by conventional approaches. Davis method was adopted to find out soil constants. In case of Horton's equation, analysis was carried out graphically for all the land covers in winter season and summer season. In Philip equation analysis was carried out by using Philip Two Term model, which is in the form of Taylor power series solution.

The relationship of measured cumulative infiltration and estimated cumulative infiltration with time under different land covers was determined and tabulated in table 1. The relationship of measured cumulative infiltration and estimated cumulative infiltration is also represented graphically. The infiltration rate shows much variation for the same land covers which may be due to the presence of pores below the crust or variations in soil texture and structure. Observations show that, the rate of infiltration for different land covers in summer season was about twice the infiltration rate in winter season. Based on the observations and analysis the following conclusion can be drawn.

X. CONCLUSIONS

In winter season-

- For Grapes land Horton equation shown much variation but Kostiakov equation and Modified Kostiakov equations were almost coinciding with measured cumulative infiltration.
- For Bajra land covers the Horton infiltration equation shown much variation, Kostiakov equation shown very little variation but modified Kostiakov equation was coinciding with measured cumulative infiltration.

- For weeds land Horton equation shown much variation and Kostiakov equation and modified Kostiakov equation shown little variation with measured cumulative infiltration curve.

In summer season

- For Grapes garden Horton equation shown much variation but Kostiakov equation and modified Kostiakov equation shown little variation with measured cumulative infiltration.
- For Cucumber land Horton equation shown too much variation but Kostiakov equation and modified Kostiakov equations were almost coinciding with measured cumulative infiltration curve.
- For Gram land Horton equation, Kostiakov equation and Modified Kostiakov equation all were suiting best with measured cumulative infiltration.
- For Weed land Horton equation shown variation but Kostiakov equation and Modified Kostiakov equation were coinciding with measured cumulative infiltration curve. Philip equation shown much variation for all the land covers.
- From the foregoing discussion it can be concluded that, Kostiakov equation was found to be the best for all the land covers In Brahmangaon area of Kopargaon Taluka.

REFERENCES

[1]. Joseph, R., Williams, Vardhan, R., Ying Ouyang, "Estimation of infiltration rate in the vadose *zone," Journal of EPA, U.S., vol.–II, pp 1-25, 1998.*

[2]. Chow, V.T., Maidment, D.R., Mays, L.W., Applied Hydrology, McGraw-Hill International Editions, McGraw-Hill Book Company, New York, 1988.

[3]. Robert, P., Janice, L., "Infiltration through disturbed urban soils," Vol. I, (EPA), pp 1-11, 1999.

[4]. John, D., Thomas, S., "Infiltration rate assessment of some major soils," Irish Geography, vol. 36 (1), pp 32 – 46, 2003.

[5]. Mailhol, Jean-Claude, "Validation of a predictive form of Horton infiltration for simulating furrow irrigation," Journal of Irrigation and Drainage Engineering, vol. 129, No. 6, pp 412 – 421, 2003.

[6]. Michael, A. M., Irrigation Theory and Practice, Vikas Publishers House Pvt. Ltd, New Delhi, 2003.

[7]. Rajurkar, M.P., Kothyari, U.C., Chaube, U.C., "Modeling of the daily rainfall runoff relationship with artificial neural network," Journal of Hydrology, vol. 285, pp 96- 113, 2004.

[8]. Singh, R. V., Bhakar, S.R., "Comparison of different infiltration equations on different land covers," Jl. of IWRS, Vol. 24, pp19 – 26, 2004.

[9]. Dubey, O. P., Sharma, D. C., Chhabra, S.S., "Determination of infiltration rate in Chitaurgarh dam command area, Hydrology journal, pp 17 – 24. 2005.

[10]. Mohan, S., Kumari, S., "Recharge estimation using Infiltration models," Journal of Hydraulic Engg., Vol. 11, pp 1- 10. 2005.

[11]. Jain, A., Kumar, A., "An Evaluation of artificial neural network technique for the determination of infiltration model parameters," Journal of Applied Soft Computing, vol. 6, pp 272-282, 2006.

[12]. Nesor, L., Sy, "Modelling the infiltration processes with a multi-layer perceptron artificial neural network," Hydrological Sciences Journal, vol. 51, pp 3-20, 2006.

[13]. Dr. P. Jaya Rami Reddy, A Text Book of Hydrology, 3rd Edition, Laxmi Publications Pvt. Ltd., New Delhi, 2011

Simulation of Turbulent Flow around an Airfoil by using κ-ε Model: Angle of Attack Effects

Morteza Bayareh[1], Kaveh Ardeshirzadeh[2]
[1]Department of Mechanical Engineering, Young researchers Club, Lamerd Branch, Islamic Azad University, Lamerd, Iran
[2] Department of Chemical Engineering, Lamerd Branch, Islamic Azad University, Lamerd, Iran

Abstract
In this paper, unsteady turbulent flow around an airfoil has been studied. Navier-stokes equations solved by Simple C algorithm exerted to specified structured and unstructured grids. Turbulent models used are two-equation *κ-ε* standard model. Equations solved by staggered method and discretization of those done by upwind method. Results show that lift and drag coefficients are increasing functions of the angle of attack.

Keywords: Turbulent flow, *κ-ε* model, airfoil, angle of attack, lift, drag.

1. INTRODUCTION

Simulation of the turbulent flow around airfoil is an up to date problem. This problem is complex and difficult to solve numerically, because many phenomena occur in this flow. Flows around aerodynamic shapes at low-to-moderate Reynolds numbers have a complex nature known as large separation bubble (LSB) [1] characterized by boundary layer separation, flow transition to turbulence, flow reattachment In many engineering applications involving a fully turbulent flow, turbulent quantities can be predicted using conventional turbulence models. While the simulation at high Reynolds numbers has been difficult, some groups have turned to simulate the flow for lower Reynolds numbers [2, 3].

Fundamentally, an airfoil generates lift by diverting the motion of fluid flowing over its surface in a downward direction, resulting in an upward reaction force by Newton's third low [4]. While this is an acceptable qualitative way of looking at airfoils, understanding the design of applicable systems such as airplanes, helicopters, and turbine blades requires a quantitative method of analyzing fluid flow and lift.

The present work aims to study the angle of attack effects on the turbulent flow around an airfoil using the commercial software FLUENT. The *κ-ε* model is derived from the Navier-Stokes equations and it is one of the simplest models of turbulence with two-equation models in which the solution of two separate transport equations allows the turbulent velocity and length scales to be independently determined.

2. GOVERNING EQUATIONS

The most important equations such as conservation of mass and momentum used by the software's solver are listed as follows:

Continuity equation:

$$\frac{\partial \rho}{\partial t} + \nabla . \rho v = 0$$

Conservation of momentum:

$$\frac{\partial u_i}{\partial t} + u_j \frac{\partial u_j}{\partial x_j} = -\frac{1}{\rho}\frac{\partial p}{\partial x_i} + \frac{\partial}{\partial x_j}\left(\nu \frac{\partial u_i}{\partial x_j}\right)$$

Transport equations for κ and ε:

$$\rho \frac{Dk}{Dt} = \frac{\partial}{\partial x_i}\left[\left(\mu + \frac{\mu_t}{\sigma_k}\right)\frac{\partial k}{\partial x_i}\right] + G_k + G_b - \rho\varepsilon - Y_m$$

$$\rho \frac{D\varepsilon}{Dt} = \frac{\partial}{\partial x_i}\left(\alpha_\varepsilon \mu_{eff} \frac{\partial \varepsilon}{\partial x_i}\right) + C_{1\varepsilon}\frac{\varepsilon}{k}(G_k + C_{3\varepsilon}G_b) - C_{2\varepsilon} p \frac{\varepsilon^2}{k} - R$$

where κ is the specific turbulence kinetic energy and it is defined as the variation in the velocity fluctuations. ε is the turbulence dissipation of small velocities (eddies), in other words, the rate at which the velocity fluctuations are dissipated. G_k represents the generation of turbulence kinetic energy due to the mean velocity gradients, G_b is the generation of turbulence kinetic energy due to buoyancy, Y_m represents the contribution of the fluctuating dilatation in compressible turbulence to the overall dissipation rate. σ_k and σ_ε are the inverse effective Prandtl numbers for κ and ε respectively.

3. RESULTS

An airfoil is the shape of a wing or blade or sail as seen in cross-section. In fluid dynamics, angle of attack (AOA, or α) is the angle between a reference line on a lifting body (known as the chord line of an airfoil) and the vector representing the relative motion between the lifting body and the fluid through which is moving (figure 1).

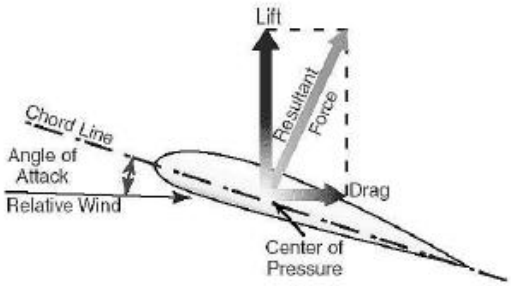

Figure 1. Resultant forces on an airfoil.

The leading edge is the part of the wing that first contacts the fluid. The trailing edge of an aerodynamic surface such as a wing is its rear edge, where the flow separated by the leading edge rejoins. Lift force is the component of the surface force that is perpendicular to the oncoming flow direction. This force can be determined using the following equation:

$$L = \frac{1}{2}\rho U_\infty^2 A C_L$$

where L is lift force, U_∞ is is the velocity of the uniform flow, C_L is the lift coefficient, and A is platform area.

Drag force refers to force which acts on a solid object in the direction of the relative flow velocity. This force can be determined using the following equation:

$$D = \frac{1}{2}\rho U_\infty^2 A C_d$$

where D is lift force, and C_d is the lift coefficient.

The airfoil was modeled in the software package GAMBIT. The geometry of the airfoil has been shown in figure 2. A fine mesh is needed in the closer regions of the airfoil. Figure 3 shows the mesh around the airfoil (MS (1)-0313).

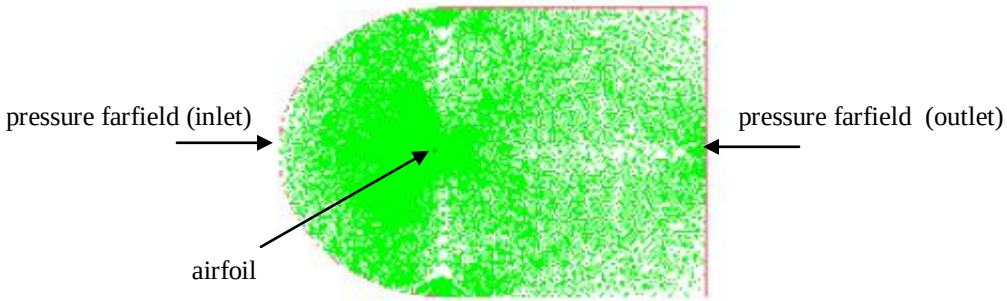

Figure 2. Geometry of the airfoil.

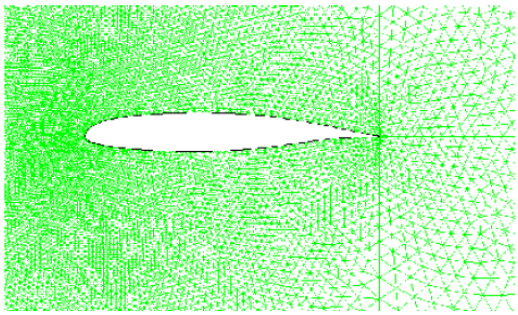

Figure 3. Mesh around the airfoil (MS(1)-0313).

The magnitude of the lift generated by an airfoil depends on the shape of the airfoil and how it moves through the fluid. For thin airfoils, the lift is directly proportional to the angle of attack for small angles (within +/- 10 degrees). As an airfoil moves through the fluid, fluid molecules stick to the surface. This creates a layer of fluid near the surface called boundary layer. Figure 4 shows the variation of lift coefficient with the angle of attack. One can see that the lift coefficient increases with increasing the angle of attack. Figure 5 shows the variation of drag coefficient with the angle of attack. The drag force increases with increasing the angle of attack. The increases in the angle of attack increases lift and drag forces. Depending on the angle of attack, there will be a force backward (induced drag) and a force upward (lift). If the angle of attack is small, the drag and the lift are comparatively small.

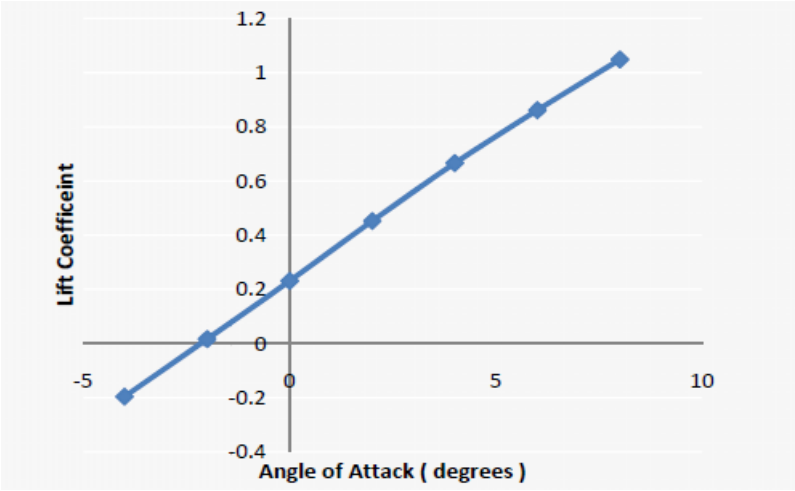

Figure 4. Lift coefficient versus angle of attack ($\mathrm{Re} = 4\times10^{6}$**).**

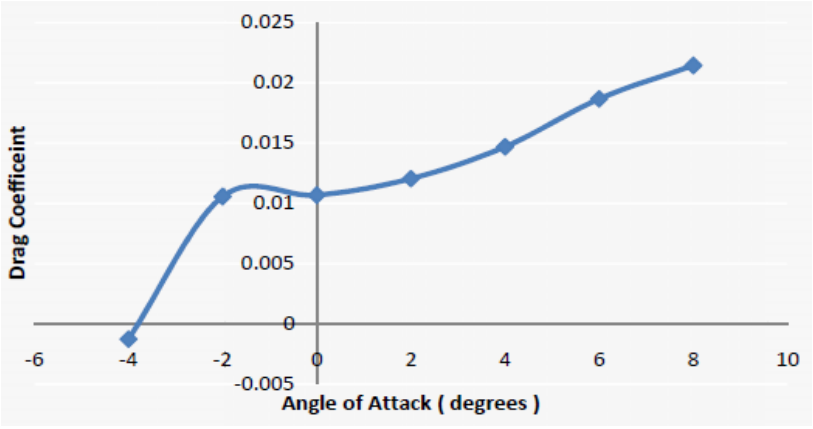

Figure 5. Drag coefficient versus angle of attack ($\mathrm{Re} = 4\times10^{6}$**)..**

4. CONCLUSIONS

In this paper, unsteady turbulent flow around an airfoil has been studied. Navier-stokes equations solved by Simple C algorithm exerted to specified structured and unstructured grids. The present work aims to study the angle of attack effects on the turbulent flow around an airfoil using the commercial software FLUENT. Turbulent models used are two-equation κ-ε standard model. Equations solved by staggered method and discretization of those done by upwind method. Results show that lift and drag coefficients are increasing functions of the angle of attack. Depending on the angle of attack, there will be a force backward (induced drag) and a force upward (lift). If the angle of attack is small, the drag and the lift are comparatively small.

REFERENCES

1. B. H. Carmichel, 1981, "Low Reynolds airfoil survey", volume 1, technical report, national aerodynamics and space administration.
2. F. Richez, V. Gleize, I. Mary and C. Basdevant, 2006, "Zonal RANS/LES coupling simulation of a transitional and separated flow around an airfoil near stall", conference of turbulence and interactions T12006, Porquerolles, France.
3. N. Jovicic, M. Breuer, J. Jovanovic, 2006, "Anisotropy-invariant mapping of turbulence in a flow past an upswept airfoil at high angle of attack", J. Fluids Engineering, 128(3), 559-567.
4. Anderson, David, and Scott Eberhardt, 1988, "Understanding flight", 2nd edition, Prentice Hall.

NUMERICAL SIMULATION OF THE MOTION OF A DROP IN PLANE POISEUILLE FLOW: DENSITY RATIO EFFECTS

Morteza Bayareh
Department of Mechanical Engineering, Young researchers Club, Lamerd Branch, Islamic Azad University, Lamerd, Iran

Abstract
The density ratio effects on the motion of a three-dimensional drop in Poiseuille flow are examined at finite Reynolds numbers using a finite difference front tracking method. The elliptic pressure equation is solved by a multi-grid method. For deformable drops, the wall repulsion increases and this effect moves the equilibrium position closer to the centerline of the channel. Results show that all drops with deferent density ratios migrate to an equilibrium position about halfway between the centerline and the wall. The drops move to an equilibrium position closer to the wall with increasing the density ratio. The axial velocities of the drops increase with decreasing the density ratio, because the drop with smaller density ratio moves to a lower final position. Also, the deformation of the drops is the same after an initial transient period. During the initial transient period, the deformation increases as the density ratio increases.

***Keywords*:** Poiseuille flow, finite difference method, front tracking method, density ratio, Reynolds number.

1. INTRODUCTION

Motion of drops through channels and tube has been always a matter of interest for many years. Segre and Silberberg (1962) [1] found that neutrally buoyant particles released off center in a pressure-driven flow, will not migrate to the pipe center-line, but instead will find an equilibrium position at about 0.6 radii off the center-line. Karnis et al. (1966) [2] showed that neutrally buoyant particles stabilized midway between the centerline and the wall. The equilibrium position was closer to the wall for larger flow rates and closer to the center for larger particles. The phenomenon of migration of liquid drops in Couette flow between concentric cylinder due to non-Newtonian fluid properties and shape deformation has been studied experimentally by Paul et al. (1981) [3]. Significant observations include the migration of a deformable Newtonian drop to an equilibrium position between the centerline and the inner rotor, and the competition between normal stresses and shape deformation effects for the case of a Newtonian drop in a non-Newtonian fluid. The stability of plane Poiseulle flow of two immiscible liquids of different viscoelastics and equal densities studied by Than et al. (1987) [4]. They found that regions of stability when there are three layers with one of the fluids centrally located. They showed the stability results depend on the viscosity and volume ratio in a fairly complicated way. Also, the flow with the high viscosity fluid centrally located is always stable. Feng, et al. (1994) [5] reported the results of a two-dimensional finite element simulation of the motion of a circular particle in a Couette & Poiseuille flow. They showed that a neutrally buoyant particle migrates to the centerline in a Couette flow and the stagnation pressure on the particle surface is particularly important in determining the direction of migration. Mortazavi & Tryggvasson (1999) [6] studied the motion of a drop in poiseuille flow. They simulated the motion of many drops at finite Reynolds numbers. Three-dimensional numerical simulation was presented on the motion of a deformable capsule undergoing large deformation in a plane Poiseulle flow in a channel by Doddi and Bagchi (2008) [7]. The numerical methodology was based on a mixed finite-difference/Fourier transform method for the flow solver and a front-tracking method for the deformable interface. Migration velocity and capsule deformation were observed to increase with increasing Capillary number. Bayareh and Mortazavi (2009, 2010) [8,9,10,11] studied the motion of a single drop and the interaction between two drops in simple shear flow at finite Reynolds numbers neglecting the gravity influence. They showed that the drops migrate to the centerline of the channel in shear flow. Also, they reported that the drop deformation depends strongly on the capillary number, so that; the proper non-dimensional number for the interfacial tension is the capillary number. Hudson (2010) [12] studied the drop circulation in microchannels. Two characteristic of transport of fluids in rectangular microchannels were addressed as a function of the cross-sectional aspect ratio.

2. FORMULATION

2.1 Governing Equations

The motion of a drop in Poiseuille flow at finite Reynolds numbers is governed by the Navier-Stokes equations. The Navier-Stokes equations are written in conservative form and variable physical properties. The surface tension is added to the equations by a delta function.

$$\frac{\partial \rho \mathbf{u}}{\partial t} + \nabla.\rho \mathbf{u}\mathbf{u} = -\nabla P + \nabla.\mu(\nabla \mathbf{u} + \nabla \mathbf{u}^T) + \sigma \int \kappa \mathbf{n} \delta^{\beta}(\mathbf{x} - \mathbf{X}) ds.$$

This equation is valid for the whole flow field, even if the density field, ρ, and the viscosity field, μ, change discontinuously. Here ***u*** is the fluid velocity, p is the pressure, and σ is the surface tension coefficient. δ^{β} is a two- or three-dimensional delta function (for $\beta = 2$ and $\beta = 3$) respectively. κ is the curvature for two-dimensional flows and twice the mean curvature for three-dimensional flows. ***n*** is a unit vector normal to the drop surface pointing outside of the drop. ***x*** is the position in Eulerian coordinate and ***X*** is the position of front in Lagrangian coordinate. The integral is over the interface between the two fluids.

The fluids are incompressible and immiscible with constant material properties. Therefore:

$$\nabla.\mathbf{u} = 0.$$

$$\frac{D\rho}{Dt} = 0.$$

$$\frac{D\mu}{Dt} = 0.$$

he governing non-dimensional numbers of the flow are: the geometric ratio $\xi = R/H$, the ratio of the radius of the drop R to the height of the channel H. The viscosity ratio $\lambda = \mu_d / \mu_f$, the density ratio $\eta = \rho_d / \rho_f$. The viscosity and the density of the drop are denoted by μ_d and ρ_d, respectively, and the ambient fluid has viscosity μ_f and the density ρ_f. The bulk Reynolds number is defined in terms of the undistributed channel centerline velocity U_c and the channel height H, as $\mathrm{Re}_b = \rho_f U_c H / \mu_f$. The Reynolds number based on the centerline velocity and the drop diameter d is defined by $\mathrm{Re}_d = \rho_f U_c d / \mu_f$. A particle Reynolds number is defined as $\mathrm{Re}_p = \rho_f U_c R^2 / \mu_f H$. The Capillary number $Ca = \mu_f U_c / \sigma$ describes the ratio of the viscous stress to the interfacial tension.

2.2 NUMERICAL METHOD

In front tracking methods a separate front marks the interface but a fixed grid, is used for the fluid within each phase. In addition to front tracking methods that are applicable to the full Navier Stokes equations, specialized boundary integral methods have been used for both potential and Stokes flows. In general, the interface representation can be explicit (moving mesh) or implicit (fixed mesh) or a combination of both. The front-tracking method is combination of fixed and moving mesh method. Although an interface grid tracks the interface, the flow is solved on a fixed grid. The interface conditions are satisfied by smoothing the interface discontinuities and interpolating interface forces from the interface grid to the fixed grid. In this method, the governing equations are solved for whole flow field. Front capturing has two difficulties. The first is a sharp boundary between the fluids and the second is accurate computation of surface tension. Different methods have been made in overcoming these problems.

The front is resolved by discrete computational points that are moved by interpolating their velocities from the grid. These points are connected by triangular elements to form a front that is used to keep the density and viscosity stratification sharp and to calculate surface tension. At each time step information must be passed between the front and the stationary grid. This is done by a method that discussed by Unverdi & Tryggvason (1992), where the density jump is distributed to the grid points next to the front and a smooth density field that changes from one density to the other over two to three grid spaces generated by the solution of a Poisson equation. While this replaces the sharp interface by a slightly smoother grid interface, numerical diffusion of the density and the viscosity fields is eliminated, since the grid field is reconstructed at each step. The spatial differentiation is calculated by second order finite difference on a staggered Eulerian grid. We use an explicit second-order time integration method. Combining the incompressibility condition and momentum equations results in a non-separable elliptic equation for the pressure.

3. RESULTS

The geometry of the flow is shown in figure 1. The channel is bounded by two no-slip walls in the z-direction. The domain is periodic in the x- and y-directions. Tangential stresses are continuous on the surface of the drop and normal stresses show the jump across the interface by surface tension.

Figure 2 shows the trajectories of a neutrally buoyant drop released at different initial positions ($\mathrm{Re}_b = 10$, Ca = 0.1, λ = η = 1, ξ = 0.125). The flow parameters in simulations of Feng et al. (1994) [4] are: $\mathrm{Re}_b = 10$, λ = η = 1, ξ = 0.125. One can see that all drops with different initial positions migrate to an equilibrium position about halfway between the centerline and the wall (Segre-Silberberg effect). Feng et al. (1994) [4] reported that the rigid particles move to an equilibrium position a little outside the midpoint between the wall and the centre at z = 0.252 H. for deformable drops, the wall repulsion increases and this effect moves the equilibrium position closer to the centerline of the channel.

The effect of the density ratio on the lateral migration of a drop in plane Poiseuille flow was examined by carrying out three simulations with η = 1, 2 and 5. The other flow parameters are the same as the last simulation (Figure 2). Figure 3 shows the trajectories of drops versus their axial locations. It is observed that the drops migrate to an equilibrium position closer to the wall with increasing the density ratio. The axial velocity increases with increasing density ratio. This matter can be observed in figure 4 that shows the axial velocities of the drops versus the axial location. Because of similar final position of drops, it is expected that the deformation of the drops is the same after an initial transient period. The deformation of the drop is examined by considering the Taylor deformation parameter define by D = (L-B) / (L+B), where L and B are, respectively, the major and minor axis of deformed drop (defined by the largest and smallest distance of the surface from the centre) (not shown).

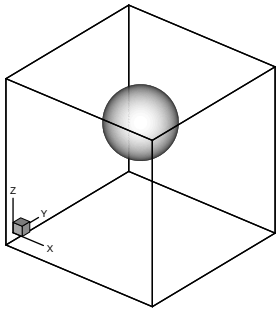

FIGURE 1. The geometry for the simulation of a drop in a channel.

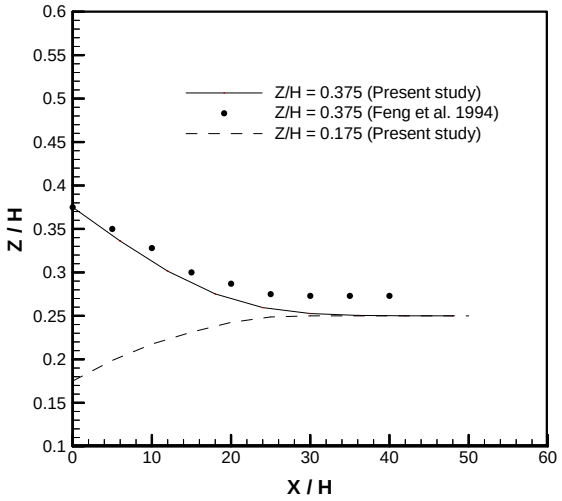

FIGURE 2. The Segre-Silberberg effect in a plane Poiseuille flow.

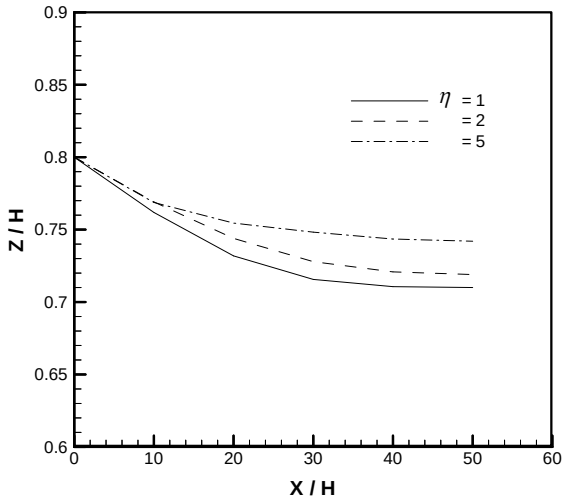

FIGURE 3. The lateral migration.

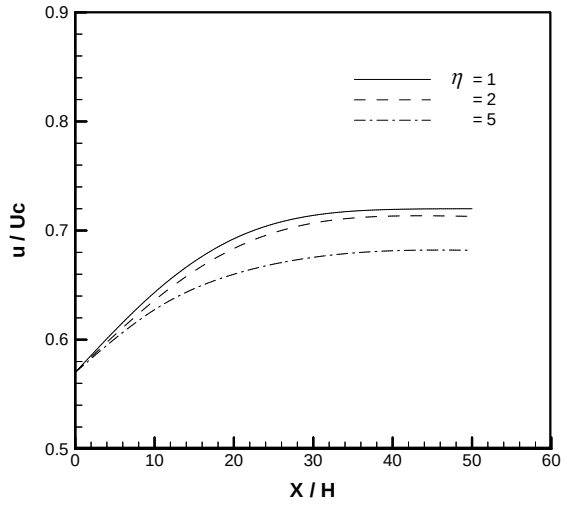

FIGURE 4. The axial velocity.

4. CONCLUSIONS

The density ratio effects on the motion of a three-dimensional drop in Poiseuille flow are examined at finite Reynolds numbers using a finite difference front tracking method. All drops with different initial positions migrate to an equilibrium position about halfway between the centerline and the wall (Segre-Silberberg effect). For deformable drops, the wall repulsion increases and this effect moves the equilibrium position closer to the centerline of the channel. The drops migrate to an equilibrium position closer to the wall with increasing the density ratio. The axial velocity increases with increasing density ratio. Results show that the deformation of the drops is the same after an initial transient period. During the initial transient period, the deformation increases as the density ratio increases.

REFERENCES

1. Segre, G. and Silberberg, A., 1962, "Behavior of macroscopic rigid spheres in Poiseuille flow. Part 1. Determination of local concentration by statistical analysis of particles passages through crossed light beams," *J. Fluid Mech.*, vol. 14, pp. 115-135.
2. Karnis, A., Goldsmith, H. L., and Mason, S. G., 1966, "The flow of suspensions through tubes, Inertial effects", *J. Chem. Engng*, 44, pp. 181-193.
3. Paul, C., Chan, H., and Leal, L. G., 1981, "An experimental study of drop migration in shear flow between concentric cylinders", *Int. J. Multiphase flow*, 7, pp. 83-99.
4. Than, P. T., Rosso, F., and Joseph, D. D., 1987, "Instability of Poiseulle flow of two immiscible liquids with different viscosity in a channel", *J. Chem. Engng*, 25, pp. 189-304.
5. Feng, J., Hu, H.H., and Joseph, D.D., 1994, "Direct simulation of initial value problems for the motion of solid bodies in a Newtonian fluid. Part2. Couette and Poiseuille flows", *J. Fluid Mech*, vol. 277, pp. 271-301.
6. Mortazavi S. and Tryggvason G., 2000, "A numerical study of the motion of drop in Poiseuille flow Part1: Lateral migration of one drop," *J. Fluid Mech*., vol. 411, pp. 325-350.
7. Doddi, S. K. and Bagchi, P**.,** 2008, **"**Lateral migration of a capsule in a plane Poiseuille in a channel,' *Int. J. Multiphase flow*, vol. 34, pp. 966- 986.
8. Bayareh M. and Mortazavi S., 2009, "Numerical simulation of the motion of a single drop in a shear flow at finite Reynolds numbers", *J. Iranian science and technology*, 33, 441-452.
9. Bayareh M. and Mortazavi S., 2009, "Numerical simulation of the interaction of two equal-size drops in a shear flow at finite Reynolds numbers", proceeding of ISME2009 (international conference), Tehran, Iran, 323-324.
10. Bayareh M. and Mortazavi S., 2009, "Geometry effects on the interaction of two equal-sized drops in simple shear flow at finite Reynolds numbers", 5th international conference: Computational methods in multiphase flow (WIT), **63**, 379-388.
11. Bayareh M. and Mortazavi S., 2010, "Migration of a drop in simple shear flow at finite Reynolds numbers: size and viscosity ratio effects", Proceeding of international conference on mechanical engineering, Cape Town, South Africa.
12. Hudson, D, 2010, "Poiseulle flow and drop circulation in microchannels", *J. Rheol. Acta.*, 49, pp. 237-243.
13. Unverdi, S.O. and Tryggvason, G., 1992, "A front tracking method for viscous incompressible flows," *J. Comput. Phys*, vol.100, pp. 25-37.

THERMODYNAMIC ANALYSIS OF R134A – DMAC VAPOR ABSORPTION REFRIGERATION (VAR) SYSTEM

[1]V. Mariappan ,[2] M. Udayakumar,[3] Pratisthit Lal Shrestha,[4]S. Suresh

[1]Assistant Professor, [2] Professor, [3] M.Tech. Scholar, [4]Assistant Professor
Department of Mechanical Engineering
National Institute of Technology, Tiruchirappalli – 620 015
Tamil Nadu, India

Abstract

This study primarily focuses on the thermodynamic analysis of single stage vapor absorption refrigeration system using R134a – DMAC solution as the working fluid. Variations in the performance parameters of the system are studied against various operating temperatures of generator and absorber. The result of this theoretical study show that coefficient of performance (COP) value can be improved by elevating generator temperature up to certain level and lowering absorber temperature. At such elevated generator temperature, value of circulation ratio (CR) is lowered. The scope of this study is limited to the system with 1kW evaporator capacity and effectiveness of solution heat exchanger (SHX) as 0.8. For the proposed condition of source and sink temperature 120˚C and 40˚C respectively the maximum value of COP was found to be 0.41 and corresponding CR value as 3.90.

Keywords: Thermodynamics analysis, absorption refrigeration, generator temperature, absorber temperature, R134a–DMAC

Nomenclature

Symbols	
COP	Coefficient of Performance
CR	Circulation Ratio
DMAC	Dimethyl Acetamide
h	Enthalpy (kJ/kg)
m	Mass flow rate (kg/s)
P	Pressure (bar)
Q	Heat duty (kW)
R	Universal Gas Constant (8.3145 J/molK)
T	Temperature (˚C)
v	Specific volume (m^3/kg)
V	Volume (m^3)
W	Work supplied (kW)
X	Mass fraction (kg/kg)

Subscripts	
a	Absorber
c	Condenser
d	DMAC
e	Evaporator
f	Fluid
g	Generator
p	Pump
ref	Refrigerant
s	Strong solution
sol	Solution
w	Weak solution
E	Excess
SHX	Solution heat exchanger

Greek letters

ε	Effectiveness of SHX
ρ	Density of solution (kg/m^3)

Introduction

Vapor compression refrigeration is the most commonly used commercial system for refrigeration wherein, a compressor is used to compress refrigerant. Compression utilizes high-grade energy as electricity. Alternatively, cooling may be achieved by means of an absorption refrigeration system, wherein the compressor of the compression system is replaced by a generator and pump combination. A low-grade heat source such as solar energy, industrial waste heat is supplied to generator and the system only needs less pumping power compared to a mechanical compression system. Most of the heat produced during industrial process to produce steam or heat is ejected to surrounding as waste after completion of process. This waste heat can be converted to useful refrigeration by using a heat operated refrigeration system, such as an absorption refrigeration cycle [1]. The thermal driven absorption system is noticed as the alternative to the vapor compression system which may cause environmental problems such as global warming and ozone layer depletion [2].

The most common binary fluid for absorption system is H_2O/LiBr and NH_3/H_2O. Lithium Bromide and water is mostly popular but the evaporator temperature is limited to minimum of 5˚C. Ammonia water combination can be used for evaporator

temperature below 0˚C but this system exhibits a relatively lower COP, and therefore efforts are being made to search for better refrigerant-absorbent pairs that can improve system performance. The search for new working fluids has centered on the halo hydrocarbon group of fluids commercially known as Freon [3]. A comparison of R134a, R22 and R124 fluorocarbon refrigerants with organic absorbents has been carried out in single- and double-stage absorption heat pumps [4]. These fluids meet most of the requirements for the desirable refrigerant. In a comparative experimental study of performance of R134a and R22 based vapor absorption refrigeration systems was performed by Songara et al. [5] who found that DMAC as a very promising solvent for R22 in VARS applications, and suggested further study on performance of R134a – DMAC solution in VARS. Some researchers have considered and reported data for R134a – DMAC as the refrigerant – absorbent pair for VARS and proved its feasibility in the absorption system. R-134a – DMAC working fluid pair is having zero ozone depletion potential and negligible global warming potential (0.25) with a comparatively lower heat source temperature [6].

Arivalagan et al. [7] performed a simulation studies on R134a – DMAC based half effect absorption refrigeration and found COP of the cycle to be 0.4, with an evaporator temperature of 5˚C, generator temperature of 70˚C and condenser temperature of 25˚C. This system is mostly applicable in industries, where low temperature waste heat (70˚C) is available. Muthu [8] performed experimental studies on performance of R134a – DMAC based absorption cooling system using low potential thermal sources. The study proved that R134a – DMAC based absorption cooling system yielded an optimum COP of 0.4, when the heat source temperature is 70˚C. Crepinsek et al. [9] performed a simulation studies on a half effect vapor absorption refrigeration cycle for solar energy based cold storage system using R134a – DMAC as working fluids showing that the COP of this cycle is about 0.35 - 0.46 for an evaporating temperature of -5 to 5˚C, heat input at 70˚C and a condensing temperature at 25˚C. COP improved up to 13% using a condensate pre-cooler. Muthu et al. [3] performed an experimental study on R134a – DMAC hot water based vapor absorption refrigeration systems of 1kw capacity. They found out the COP of the system to be 0.25 – 0.45 for sink and source temperatures of 30 and 80˚C respectively and a typical heat input of 4kW.

The heat-driven auto-cascade absorption refrigeration cycle has been analyzed by Yijian He and Guangming Chen [10] for low temperature applications. They used mixture of R23 + R32 +R134a/DMF as working pair and its characteristic study is carried out under different operational conditions.

Various studies in R134a – DMAC have been conducted in the past and COP has been identified around 0.2 to 0.4 for typical operating conditions with heat input at 70 to 80˚C, evaporating temperature at -5 to 5˚C and 25 to 30˚C for condenser as well as absorber. For absorption refrigeration system, COP, rich and poor solution concentrations are functions of generator temperature. [11] Further reducing the cooling water temperature from 30 ºC to 25 ºC, the absorber heat load and refrigerant mass absorption rate increases by 16.3% and 15 % respectively [12]. No literature is available on analysis of R134a – DMAC at high generator temperature and also theoretical prediction of maximum COP with respect various operating conditions are not dealt. Hence, this study is focused on the thermodynamic investigations on R134a – DMAC based absorption refrigeration systems for the typical operating conditions with source temperature from 90 to 140˚C, evaporator temperature of 5˚C, absorber temperature from 30˚C to 50˚C along with condenser temperature of 40˚C.

System description

Figure 1 shows the schematic of a simple vapor absorption refrigeration system. The liquid refrigerant from valve V1 (9) evaporates after absorbing Q_e amount of heat in evaporator. The vapor refrigerant from evaporator (10) travels to absorber where it is absorbed by the weak solution (solution containing lower concentration of refrigerant and higher concentration of absorbent) coming from generator after expanding through valve V2 (6) forming a strong solution in Absorber. During absorption process, Q_a amount of heat of mixing rejected from the system. Thus formed strong solution (1) is now pumped to generator (3) using a circulating pump. Before reaching generator, the strong solution (2) absorbs some amount of heat from the weak solution coming from generator in solution heat exchanger (SHX) which is supposed to improve performance of the system. Further, Q_g amount of heat is supplied to the strong solution in generator through external heat source so as to separate refrigerant from the refrigerant-absorbent solution. Vapor refrigerant (7) moves to condenser leaving weak solution in the generator. The weak solution (4) passes through SHX. After losing some heat in SHX the weak solution (5) is allowed to expand through valve V2. Further heat is removed from vapor refrigerant in condenser. The condensed refrigerant (8) then passes through valve V1 which liquefies the refrigerant and is supplied to evaporator for the next cycle.

Correlations

Thermodynamic and thermophysical properties such as bubble point, dew point, vapor pressure, liquid and vapor mass fractions, enthalpy and specific heat are obtained from the literature [6,14,15]. The heat transfer coefficient for R134a – DMAC is in the range of 100 – 400 W/m^2K [13].

The density of R134a – DMAC solution with respect to temperature and concentration at saturation condition is Given by : [6]

$$\rho = \sum_{j=0}^{3}\sum_{i=0}^{3} A_{i,j} X^{i} T^{j} \qquad (1)$$

where *A* is a constant.

Enthalpy of R134a – DMAC solution with respect to the enthalpies of individual component and excess enthalpy of solution is expressed as: [6]

Enthalpy of solution is given by

$$h_{sol} = h_{ref} + h_{d} + h_{\mathrm{E}} \qquad (2)$$

Enthalpy of R134a with respect to temperature at saturated condition is given by

$$h_{ref} = \left(0.0009T^{2} + 0.32T + 99.636\right) \times 4.187 \qquad (3)$$

The enthalpy of DMAC with respect to temperature at saturated condition is given by

$$h_{d} = \left(100 + AT + 0.5BT^{2}\right) \times 4.187 \qquad (4)$$

Excess Enthalpy of R134a – DMAC solution with respect to temperature and mole fraction of R134a at equilibrium condition is given by

$$h_{E} = \sum_{j=0}^{7}\sum_{i=0}^{7} C_{i,j} X^{i} T^{j} \qquad (5)$$

where *C* is a constant.

The vapor enthalpy of R134a leaving from the generator for a given pressure and temperature is given by following correlation: [14]

$$h_{g} = h_{f} + h_{fg} = h_{o} + h_{g} \text{ (Refrigerant vapor)} \qquad (6)$$

$$h_{f} + h_{fg} = h_{o} + \left[\int \sum_{i=1}^{N} C_{pi}^{\ o} x_{i} dT + \left(\frac{a}{b} - \frac{T}{b}\frac{da}{dT}\right)\ln\frac{V}{V+b} + RT\left(\frac{pV}{RT} + 1\right)\right] \qquad (7)$$

where h_o is an arbitrary constant, which is calculated at 273K and which is fixed even for varying the temperature and pressure of R134a vapor.

The pressure at vapor-liquid equilibrium with respect to the temperature and concentration of R134a in the solution is given by Borde [6]:

$$P = \sum_{j=0}^{7}\sum_{i=0}^{7} C_{i,j} X^{i} T^{j} \qquad (8)$$

where *C* is a constant.

Thermodynamic analysis

Thermodynamic analysis in this study is carried out for 1 kW refrigerating capacity. The temperatures of evaporator and condenser are kept constant at 5°C and 40°C respectively. The mass and energy balance equations for various parts of the system are as follows:

The mass flow rate of refrigerant, weak and strong solution based on steady flow analysis of evaporator is determined as follows:

$$m_{ref} = \frac{Q_e}{(h_{10} - h_9)} \quad (9)$$

$$m_w = m_{ref} \frac{(X_{ref} - X_s)}{(X_s - X_w)} \quad (10)$$

$$m_s = m_w + m_{ref} \quad (11)$$

The energy balance in absorber yields

$$Q_a = m_{ref} h_{10} + m_w h_6 - m_s h_1 \quad (12)$$

For solution heat exchanger, the energy balance is as follows

$$T_5 = T_4 - \varepsilon(T_4 - T_2) \quad (13)$$

$$h_3 = \frac{m_w}{m_s}(h_4 - h_5) + h_2 \quad (14)$$

$$T_3 = \varepsilon \frac{m_w}{m_s}(T_4 - T_2) + T_2 \quad (15)$$

In Generator, the energy balance provides

$$Q_g = m_{ref} h_7 + m_w h_4 - m_s h_3 \quad (16)$$

Circulation Ratio

$$CR = \frac{m_s}{m_r} \quad (17)$$

The pump power is deduced as

$$v_{sol} = \frac{1}{\rho} \quad (18)$$

$$w_p = CP \times m_s v_{sol}(P_c - P_e) \quad (19)$$

Energy balance in the condenser yields

$$Q_c = m_{ref}(h_7 - h_8) \quad (20)$$

Coefficient of performance is given by

$$COP = \frac{Q_e}{Q_g + w_p} \quad (21)$$

Results and Discussion

Figure 2 shows the variation of COP of system with the generator temperature (T_g) for three different absorber temperatures. It is found that for a fixed absorber temperature, as the generator temperature increases, a rapid increase in the value of COP is observed up to certain temperature followed by a gradual drop after the particular generator temperature is crossed. For 40˚C absorber temperature the maximum COP of 0.41 is obtained at 120˚C generator temperature. As the generator temperature exceeds 120˚C the COP curve starts declining. Similar effect can be seen for 30˚C and 50˚C absorber temperature. This effect on COP can be explained using figure 3 and figure 4.

As the heat load to evaporator is fixed in this study, the complete effect seen on COP is due to the generator heat load. In figure 3 starting from 100˚C up to 140˚C the energy for strong solution (H3) and weak solution (H4) are decreasing whereas energy of refrigerant is almost constant. Generator heat load is the sum of weak solution and refrigerant energy deducted by strong solution energy. Now, taking the case of 40˚C absorber temperature, from figure 3 as the generator temperature increases up to 120˚C the generator load decreases. Then further increasing the generator temperature beyond 120˚C, the generator heat load gradually increases. Since, COP is inverse of generator load (as Q_e is 1kW for this study and neglecting small pump work) this decreasing and increasing phenomenon of Q_g causes the COP of the system to form a hill type curve of first increasing and then decreasing with increasing generator temperature as shown in figure 4.

In the figure 2, the performance of the system is more significant in case of lower absorber temperature i.e. for a particular generator temperature the value of COP increases as the absorber temperature decreases. For example, when T_g is fixed to 140˚C, the COP is 5 % higher for 30˚C absorber temperature than for 40˚C and 15 % higher than that of 50˚C which clearly shows that performance of system is improved by maintaining lower the absorber temperature. Lowering the absorber temperature from 40˚C to 30˚C the maximum COP value shifts from 0.41 at 120˚C T_g to 0.46 at 100˚C T_g i.e. improving the maximum COP value by 12%.

Different minimum generator temperature exists for different absorber temperatures. This minimum point can be considered as a Minimum Critical Point i.e. below this minimum temperature inaccurate COP value is obtained. This is because below this minimum generator temperature, the concentration of the weak solution becomes higher than that of strong solution which is not a desirable condition for absorption system. This effect has been plotted in figure 5. For example; the minimum generator temperature is 87.81˚C when absorber temperature is 40˚C. Similarly, unique minimum generator temperature exists. This value of minimum generator temperature is lowered as absorber temperature is lowered.

Figure 5 shows the curve drawn between generator temperature and concentration of strong as well as weak solution. Strong solution concentration is unaffected by change in generator temperature. In other hand, weak solution concentration keeps on decreasing. This is because large volume of refrigerant gets evaporated from the strong solution when the heat Q_g is supplied to the generator. On the other side, there is no change in weak solution concentration with respect to T_a whereas; strong solution concentration is decreasing as T_a increases.

Critical Point (1, 2 & 3) can be seen in the figure 5 which can be considered as the minimum operating generator temperature for a particular absorber temperature. Critical Point is the point where the curves for strong and weak solution intersect each other (i.e. for a particular absorber temperature the concentration of weak as well as strong solution is equal). For a system to work effectively, the concentration of strong solution should always be greater than that of weak solution. But for generator temperature below the critical temperature, concentration of weak solution is greater than that of strong solution hence forming an undesirable effect on the absorbing process i.e. the absorbing capacity of the solution is reduced as the solution in the absorber is already saturated and cannot absorb further amount of vapor refrigerant coming from evaporator. For example, the minimum generator temperature is 87.81˚C when absorber temperature is 40˚C.

Figure 6 shows the effect of generator temperature on the Circulation Ratio (CR) which is the ratio of mass flow rate of strong solution to mass flow rate of refrigerant. Refrigerant mass flow rate is unaffected by any change in the generator temperature whereas flow rate of strong solution decreases with increase in generator temperature as shown in figure 7. Thus, this results a decline in the value of CR. Analogous to value of Q_g, for a fixed absorber temperature the value of circulation ratio falls continuously with rise in generator temperature. For 40˚C absorber temperature the value of CR is 3.9 at 120˚C generator temperature.

As seen from graphs between COP and CR as well as from the mathematical relation between two (i.e. Q_g is directly proportional to CR and Q_g is inversely proportional to COP), these two terms seem to have an inverse relation between each other i.e. lower values of CR will represent higher COP. Same can be observed in figure 8 i.e. the value of CR decreasing and COP is increasing up to 120˚C generator temperature (for T_a = 40˚C). Beyond it, value of both COP and CR declines.

A combined plot for COP ad CR is shown in the figure 8 for T_a = 40˚C. The inverse relation between COP and CR is clearly illustrated in the figure. For a fixed generator temperature of 120˚C as the absorber temperature reduces from 50˚C to 30˚C the value of CR drops from 4.8 to 2.2 which is around 54 % drop. For the same conditions of generator and absorber temperature from figure 2, COP is increased by 15 % when absorber temperature drops to 30˚C from 50˚C. Hence, this proves that lower value of absorber temperature is preferable for an absorption system.

In figure 9 various heat duties like generator, condenser, absorber and solution heat exchanger have been plotted against the generator temperature. As we have already discussed the behavior of Q_g against generator temperature for a particular absorber temperature similar effect is seen in SHX and absorber. But the Q_c varies linearly with change in generator temperature as Q_c is dependent on mass of refrigerant and enthalpy only. The change in mass flow of refrigerant is negligible with change in generator temperature. With increase in generator temperature Q_c also increases linearly whereas Q_a, Q_g and Q_{SHX} first decreases and then increases after certain generator temperature. This effect in absorber and SHX heat duty can be explained similar to that of generator heat duty.

Figure 10 is the other form of figure 2 where COP of the system has been plotted against the absorber temperature for different generator temperature. For all generator temperature, the COP seems to be better for lower absorber temperatures. Another

important point this graph reveals is that with increasing generator temperature the stability in COP of system is increased i.e. the drop in COP with increasing T_a for higher generator temperature is small relative to the lower generator temperature.

Conclusions

Vapor absorption refrigeration system with R134a – DMAC as the working fluid have been studied and analyzed theoretically. From the analysis following outcomes were obtained:

1. The value of COP is increased when generator temperature is elevated up to certain level and later declines slightly forming a hill shaped curve. For 40˚C absorber temperature, the value of maximum COP obtained is 0.41 at 120˚C generator temperature.

2. For all absorber temperatures, the shape of the COP curve is identical (i.e. hill shaped, first increasing and then decreasing). The performance of the system is improved as the absorber temperature is lowered. By lowering the absorber temperature to 30˚C from 40˚C, the maximum COP of the system is increased to 0.46 (at 100˚C generator temperature) which means 12% improvement of the maximum COP.

3. As the generator temperature is elevated or the absorber temperature is lowered, value of CR is lowered. For a fixed generator temperature of 120˚C as the absorber temperature reduces from 50˚C to 30˚C the value of CR drops from 4.8 to 2.4 which is around 54 % drop. For a fixed absorber temperature of 40˚C, the value of CR reduces from 34.66 at T_g = 90˚C to 7.56 at T_g = 100˚C and finally 3.05 at T_g = 140˚C.

References

[1] P. Srikhirin, S. Aphornratana, S. Chungpaibulpatana, 2001. A review of absorption refrigeration technologies, *Renewable and Sustainable Energy Reviews*, Vol 5, pp 343-372.

[2] Y. T. Kang, J.K. K. 2005. The effect of nano-particles on the bubble absorption performance in a binary nanofluid. *International Journal of Refrigeration*, pp 22-29.

[3] V. Muthu, R. Saravanan, 2007. Experimental studies on R134a – DMAC hot water based vapor absorption. *International Journal of Thermal Sciences*, pp 175-181.

[4] M. Jelinek , I. Borde, 1998. Single- and double-stage absorption cycles based on fluorocarbon refrigerants and organic absorbents, *Applied Thermal Engineering*, Vol18, pp 765-771

[5] A.K. Songara, M. Fatouch, S. Srinivasa Murthy, 1997. Comparative performance of R134a and R22 based vapor absorption refrigeration systems, *International Journal of Energy Research*, Vol 21, pp 374-381

[6] I. Borde, M. Jelinek, NC. Daltrophe, 1995. Absorption based on R-134a. *International Journal of Refrigeration*, Vol 18, pp 387–394.

[7] S. Arivazhagan, Murugesan,R. Saravanan, S. Renganarayanan, 2005. Simulation studies on R134a – DMAC based half effect absorption cold storage systems. *Energy Conversion and Management*, Vol 46, pp 1703–1713.

[8] V. Muthu V, 2003. Studies of vapor absorption refrigeration system for exploiting low potential thermal sources. *PhD Thesis*, Institute for Energy Studies, Anna University.

[9] Z. Crepinsek, D. G, 2009. Comparison of the performances of absorption refrigeration cycles. *Wseas Transactions on Heat and Mass Transfer*, Vol 4 (3), pp 65-76.

[10] Y. He, G. Chen, 2007. Experimental study on an absorption refrigeration system at low temperatures, International Journal of Thermal Sciences, Vol 46, pp 294–299

[11] A. Zohar, M. Jelinek, A. Levy, I. Borde, 2009. Performance of diffusion absorption refrigeration cycle with organic working fluids, *International Journal of Refrigeration*, Vol 32, pp 1241-1246.

[12] S.Tharves Mohideen,S.Renganarayanan, 2006. Heat and Mass Transfer Studies on 134 A-DMAC Based Falling Film Absorbers for Absorption Refrigeration System. *Fourth WSEAS Int. Conf. on Heat Transfer, Thermal Engineering and Environment*, Elounda, Greece, pp342-350.

[13] L. Harikrishnan, M. P. Maiya, S. Tiwari, A. Wohlfeil, F. Ziegler, 2009. Heat and mass transfer characteristics of absorption of R134a into DMAC in a horizontal tube absorber, *Heat Mass Transfer*, Vol 45, pp 1483–1491.

[14] Yokozeki, A, 2005. Theoretical performances of various refrigerant–absorbent pairs in a vapor-absorption refrigeration cycle by the use of equations of state. *Applied Energy*, Vol 80(4), pp 383 – 399.

[15] E. W. Lemmona, Richard T Jacobsen, 2004. Equations of State for Mixtures of R-32, R-125, R-134a, R-143a, and R-152a, *J. Phys. Chem. Ref. Data*, Vol. 33, No. 2.

Illustrations

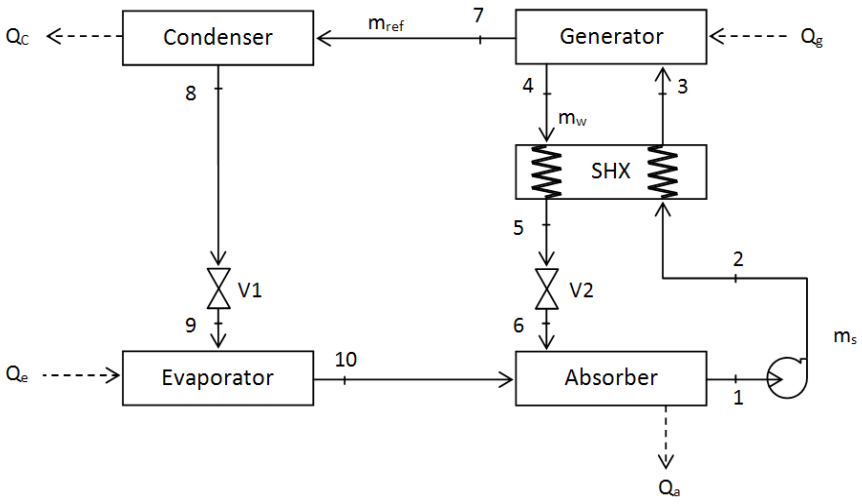

Figure 1: Simple Schematic for Vapour Absorption Refrigeration System

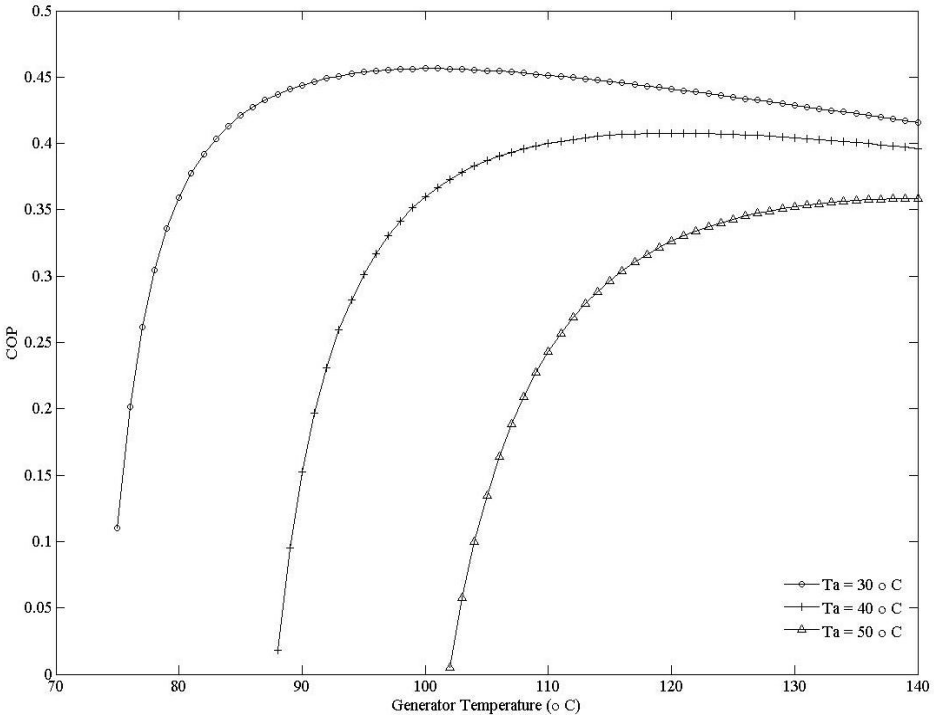

Figure 2: Variation of COP with generator temperature

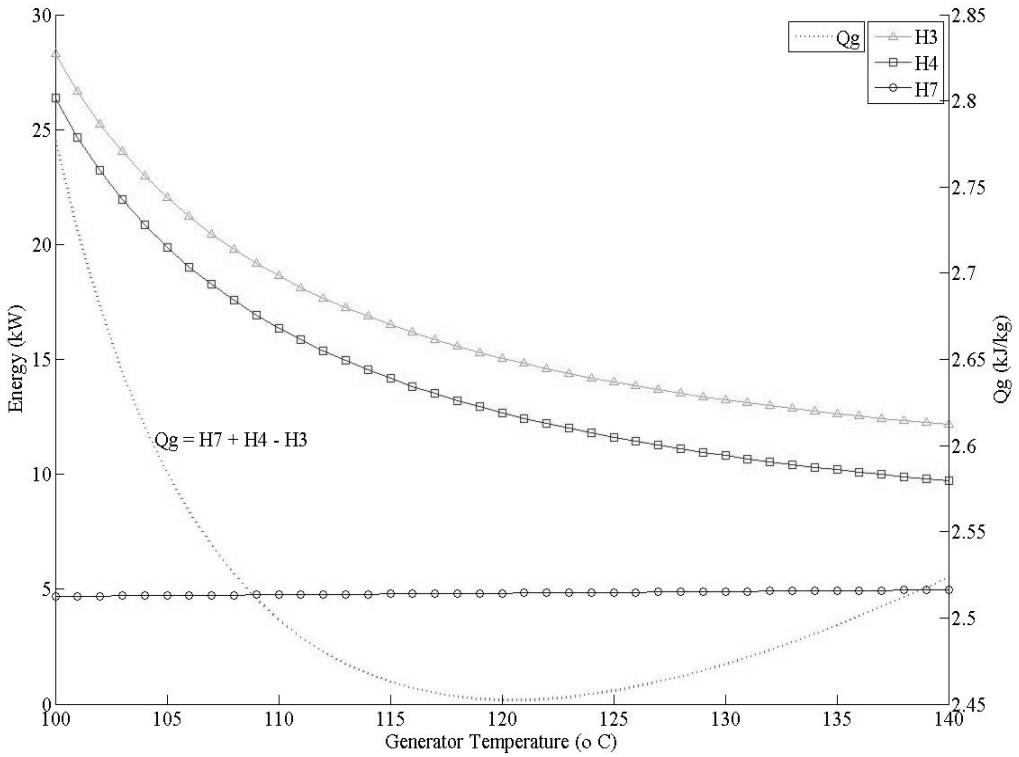

Figure 3: Variation of Energy & Qg with generator temperature for Ta = 40˚C

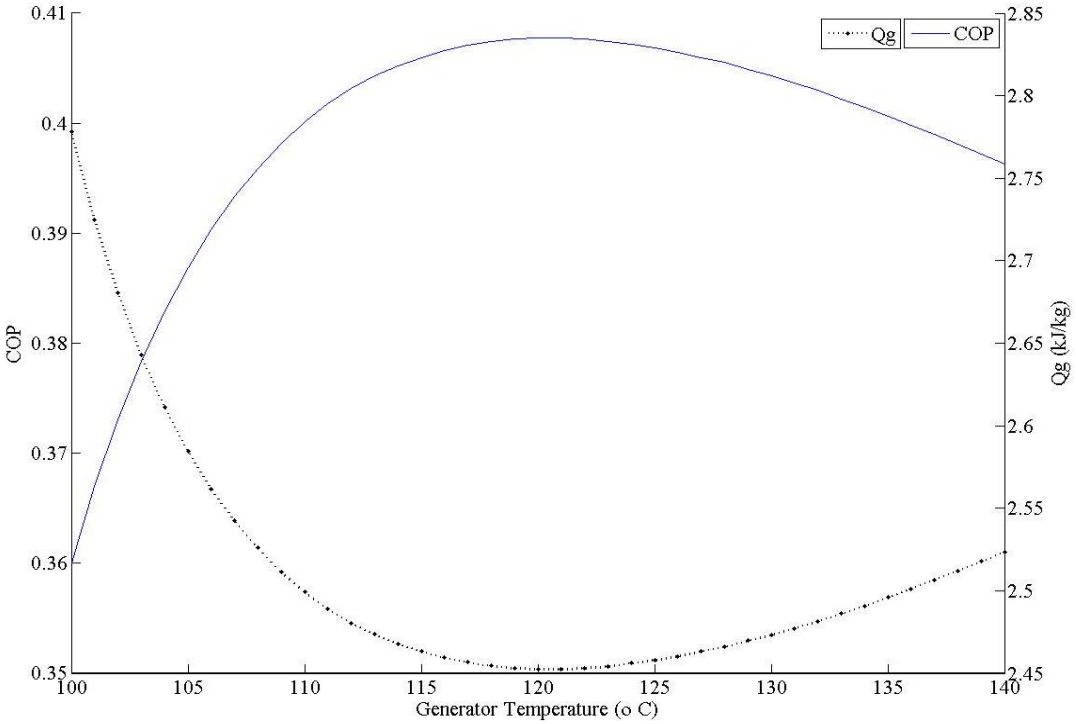

Figure 4: Variation of Qg & COP with generator temperature for Ta = 40˚C

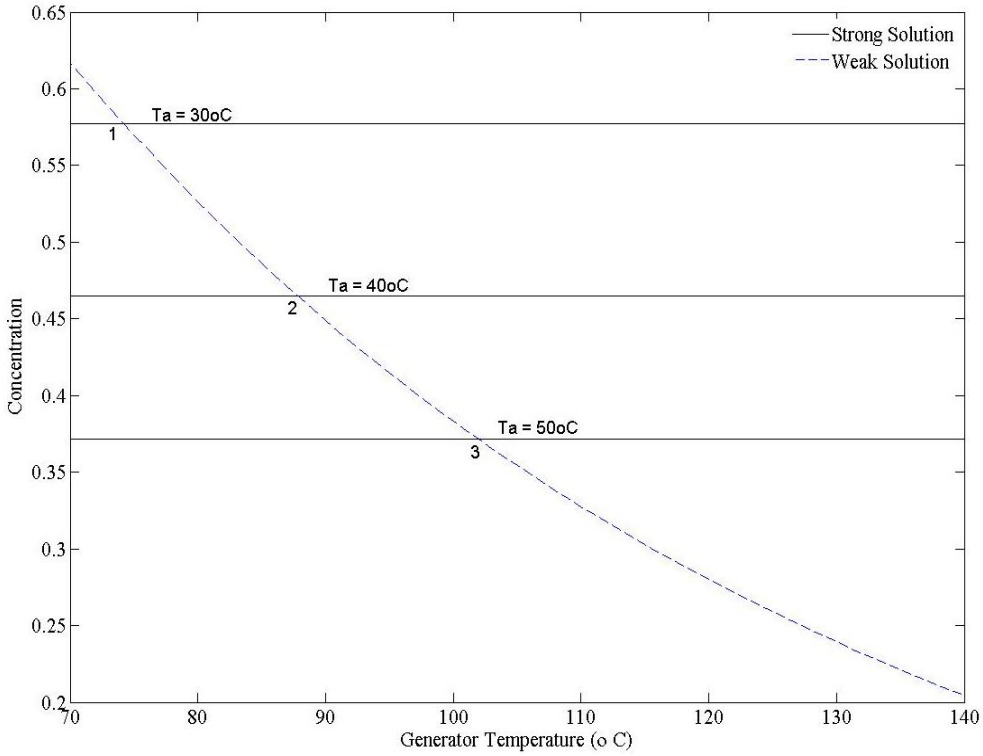

Figure 5: Variation of Solution Concentration with generator temperature for Ta = 40˚C, 50˚C & 60˚C

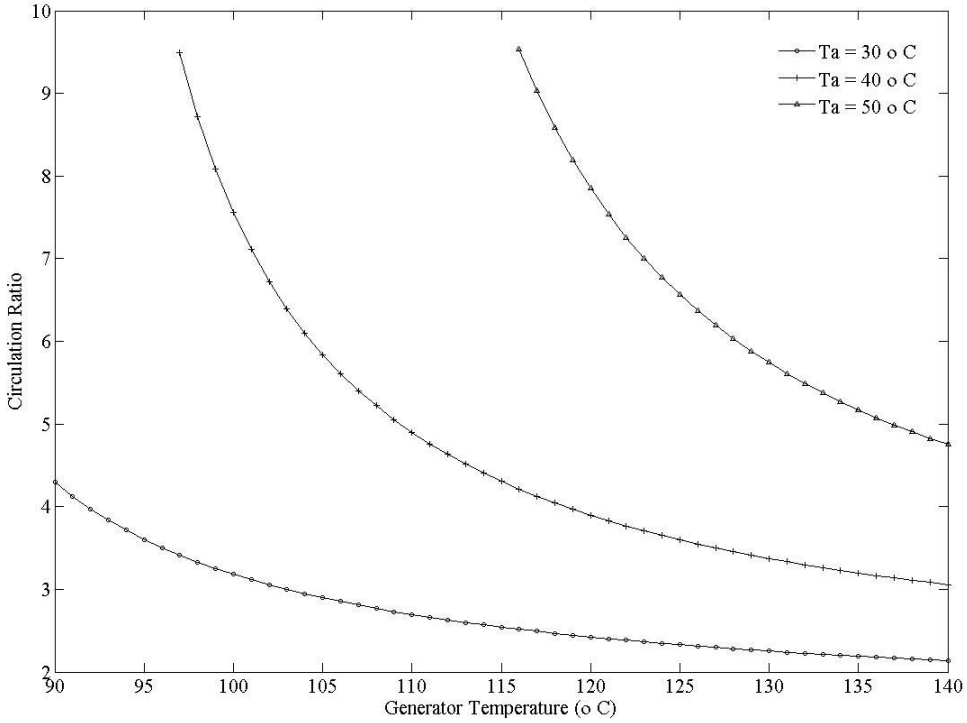

Figure 6: Variation of Circulation Ratio with generator temperature

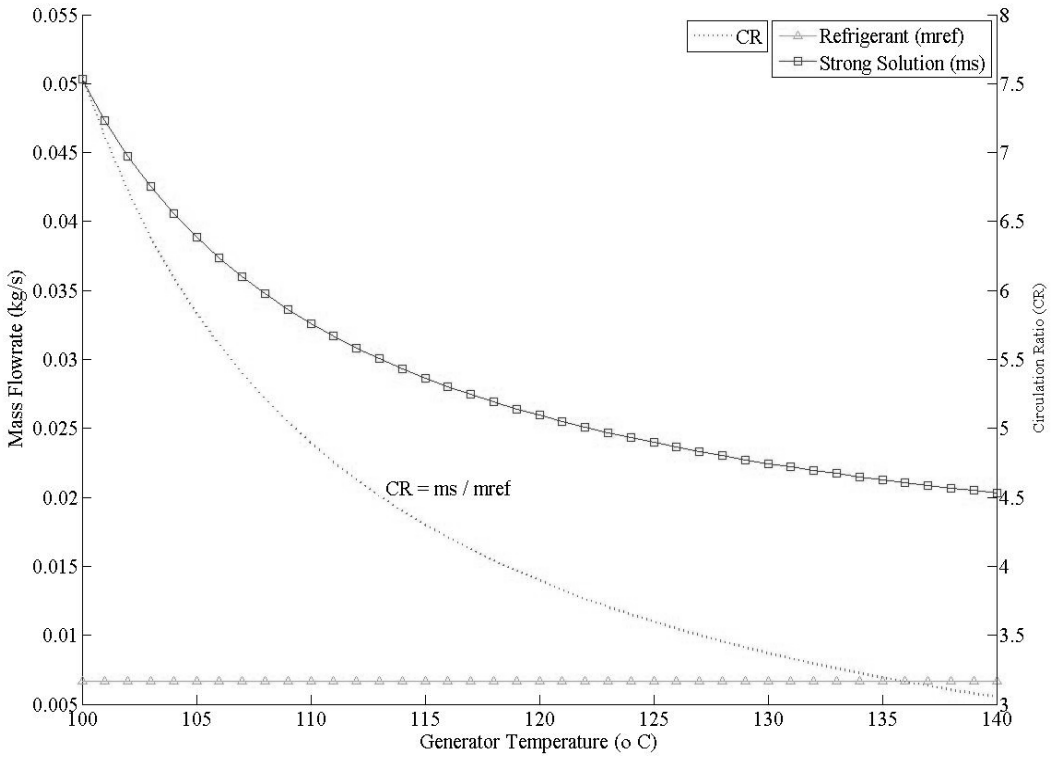

Figure 7: Variation of mass flow rate and CR with generator temperature for Ta = 40˚C

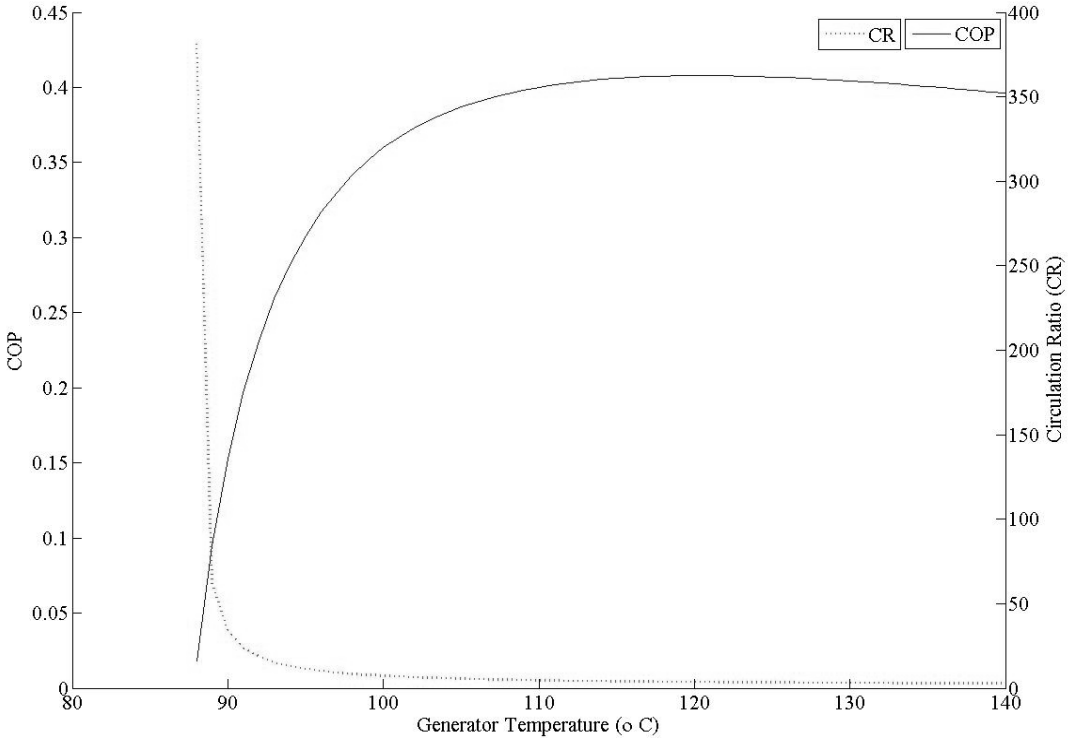

Figure 8: Variation of COP & CR with generator temperature for Ta = 40˚C

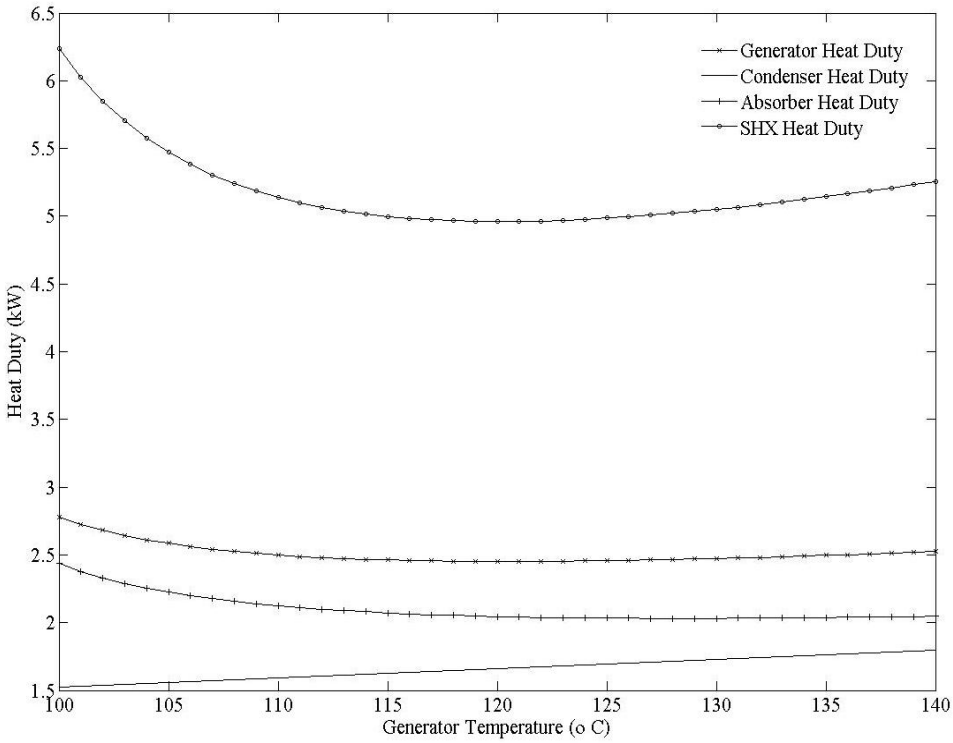

Figure 9: Variation of various heat duties with generator temperature at Ta = 40˚C

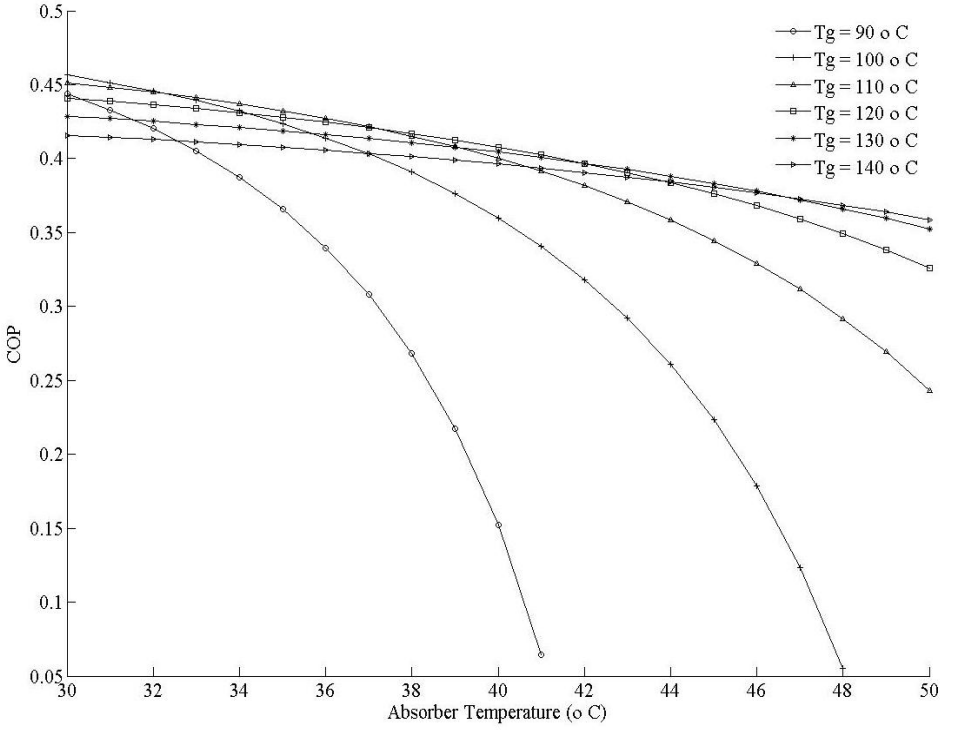

Figure 10: Variation of COP with Absorber Temperature for different generator temperature

A THEORETICAL SIMULATION OF A PEM FUEL CELL WITH 4-SERPENTINE FLOW CHANNEL

B.Sreenivasulu[a,*] , S.V.Naidu[b] , V.Dharma Rao[c], G.Vasu[d]

[a]Department of Chemical Engineering,G.V.P College of Engineering, Visakhapatnam 503048, India.
[b]Department of Chemical Engineering,Andhra University, Visakhapatnam 503048, India.
[c]Department of Mechanical Engineering,G.V.P College of Enginnering, Visakhapatnam 503048, India.
[d]Fuel cell and Renewable Energy,BHEL(R&D), Hyderabad,India.

Abstract
The effects of different operating parameters on the performance of proton exchange membrane (PEM) 4-Serpentine flow channel fuel cell have been studied theoretically by modeling the problem in FLUENT. Pure hydrogen is used on the anode side and oxygen on the cathode side. Computer simulation results are obtained for voltage as a function of current density at different cell temperatures, operating pressures ,different humidities, gas diffusion layer thickness and catalyst layer thickness . The simulation results are compared with the experimental data, and the agreement is found to be good.

Keywords : 4-Serpentine flow channels, Fuel cell , GDL, PEM

Introduction

Polymer electrolyte membrane fuel cell (PEMFC) is the most promising system among several kinds of fuel cells due to their various advantages such as easy start-up, operation at room temperature, no liquid electrolyte and high current density. To achieve high current density, the optimal operating conditions need to be identified for fuel cell systems in addition to design parameters such as membranes and their thickness, catalysts and alloys, particle size, catalyst quantity, catalyst layer thickness, nature of gas diffusion layers and the bi-polar plates.

Parthasarathy et al. (1992) studied temperature dependence of the electrode kinetics of oxygen reduction at the Platinum/Nafion Interface. Vladimir Gurau et al. (1998) studied two dimensional modal for PEM fuel cells. Shimpalee et al.(2000) presented numerical predictions for temperature distribution in PEM fuel cell. Berning et al. (2002) carried out three dimensional computational analysis to describe transport phenomena in a PEM fuel cell. Ling Wang et al. (2003) studied experimentally the performance of fuel cell at different operating temperatures, cathode and anode humidification temperatures, and pressures.

Berning and Djilali et al. (2003) developed a three-dimensional, non-isothermal model of a PEM fuel cell. Model was solved using commercial software package CFX-4.3. In this effect of various operational parameters such as temperature and pressure, and geometric and material parameters such as GDL thickness, porosity and channel width to land ratio were investigated.

Um and Wang (2004) used a three-dimensional model to study the effects an interdigitated flow field. The model accounted for mass transport, electrochemical kinetics, species profiles and current density distribution within the cell. Interdigitated flow fields result in forced convection of gases, which aids in liquid water removal at the cathode. This would help improve performance at high current densities when transport limitations due to excessive water production are expected.

Hamilton and Pollet (2010) described some recent developments in the area of flow field plates (FFPs) for proton exchange membrane fuel cells. The function, parameters and design of FFPs in PEM fuel cells are outlined and considered in light of their performance.

Wei-Mon Yan et al. (2008) investigated experimentally the cell performance and pressure drop for two commercial size 16 cm×16 cm serpentine flow field proton exchange membrane fuel cells with Core 5621 and Core 57 membrane electrode assemblies at various cell temperatures and humidification temperatures. At cell temperature lower than the humidification temperature, the cell performance improved as the cell temperature increased, while reversely at cell temperature higher than the humidification temperature. At a specified cell temperature, increasing the cathode and/or anode humidification temperature improved the cell performance and their effects weakened as cell temperature decreased. For the constant mass flow rate mode, both cathode and anode pressure drops increased as humidification temperature increased, while anode pressure drops decreased and cathode pressure drops increased as average current density increased. The optimal cell performance occurred at cell temperature of 65^{o}C and humidification temperature of 70^{o}C. The effects of these operating parameters on the cell performance and pressure drop were analyzed based on the catalytic activity, membrane hydration, and cathode flooding.

Xiao-Dong Wang et al. (2008) investigated the effects of the relative humidity (RH) of the reactants on the cell performance and local transport phenomena in proton exchange membrane fuel cells with parallel and interdigitated flow fields. A three-dimensional model was developed taking into account the effect of the liquid water formation on the reactant transport.

Antolini, (2004) investigated a significant lowering of the platinum loading of polymer electrolyte fuel cell electrodes from about 4–10 mg cm^{-2} (platinum black) to about 0.4 mg cm^{-2} or even less (carbon supported platinum), by the introduction of ionomer (liquid Nafion) impregnated gas diffusion electrodes, extending the three-dimensional reaction zone. The loss of performance during cell operation due both to the presence of liquid water causing flooding of the catalyst layer and mass transport limitations and to the poisoning of platinum by the use of reformed fuels.

The survey of literature reveals the necessity to understand the effects of various system parameters in a PEM fuel cell in order to improve its performance. Hence an attempt is made to carry out a parametric study by modeling the problem using FLUENT and by obtaining simulation results over wide ranges of parameters such as fuel cell temperature, pressure and relative humidity.

Formulation of the problem

The dimensions of the fuel cell are 9.6 cm, 0.8948 cm and 9.8 cm in the X, Y and Z directions respectively. The cross-sectional area of the membrane electrode assembly is 9.6 x 9.8 = 94 cm^2. The flow and diffusion of gases and production of electric power in the fuel cell are governed by the coupled transport processes in the membrane, catalyst layer, on gas diffusion electrodes. The reactants hydrogen and oxygen pass through 4-Serpentine flow channels. The schematic diagram of a 4-Serpentine flow channel is shown in Fig.1.

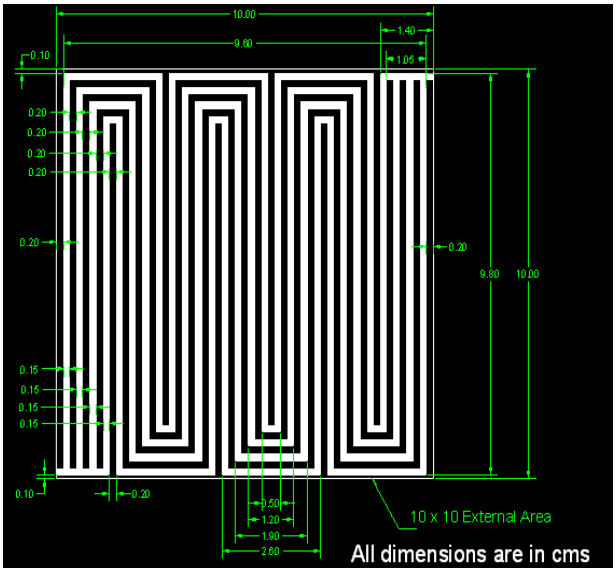

Fig.1 Schematic Diagram of 4-Serpentine flow channel.

A detailed description of the configuration of the PEM fuel cell considered in the theoretical model is presented below. The membrane electrode assembly (MEA) consists of the polymer electrolyte membrane (Nafion 1135, 88 µm), the anode and cathode catalyst layers and the anode and cathode gas diffusion layer (GDL). The electro-catalyst used is activated carbon supported platinum. The catalyst ink is prepared from platinum-carbon powder with ethyl alcohol. The catalyst ink is applied as a layer on the gas diffusion layer (which is a carbon paper).

The catalyst loading on the anode-side is 0.15 mg/cm^2 with a thickness of catalyst layer of 20 µm. A catalyst loading of 0.3mg/cm^2 is used on the cathode-side with a thickness of catalyst layer of 40 µm. Carbon papers having thickness of 400 µm are used as gas diffusion layers on both sides. The membrane electrode assembly (viz., membrane, GDLs and catalyst layers) is placed between two graphite plates and is pressed between gold-coated copper plates.

The flow of hydrogen and oxygen in a fuel cell takes place in the channel formed by a flow field plate and a carbon paper, which serves as gas diffusion layer. The flow channel contains a number of bends to facilitate diffusion of the gas through the gas diffusion layer (GDL) while the gas passes through the channel.

Dimensions of the channel:

Length=98 mm , width=1.5mm, height=0.8mm rib width is 2mm. The various inlet parameters and electrode material properties which are given as inputs to the fluent solver are as follows: cell temperature= 333K, pressure=1atm, humidity = 100%, flow rate of hydrogen= 3.65799 $x10^{-7}$kg/sec, flow rate of oxygen = 5.85278 $x10^{-6}$kg/sec. Permeabilities of membrane, GDL and CL are $1.8x10^{-18}$, 1.76 $x10^{-11}$and 1.76 $x10^{-11}$ m^2 respectively. Thermal conductivities of membrane, GDL and CL are 0.5, 1.7 and 0.27 W/m-K respectively. Electrical conductivities of membrane, GDL and CL are 11.6733, 50 and 50 S/m respectively. Porosities of the membrane, GDL and CL are maintained at 0.5. Reference current densities at anode and cathode are 1x 10^8 and 650 A/m^3 respectively. Reference concentrations of hydrogen and oxygen maintained at 0.04088 $kmol/m^3$.

The problem of the single fuel cell which contains the membrane electrode assembly with 4-Serpentine flow channel is modeled and solved using FLUENT software. A geometric model is created in GAMBIT module. This model is solved in FLUENT module with appropriate boundary conditions. The three dimensional CFD model of PEM fuel cell in parallel flow arrangement of the gases is shown in Fig.2.

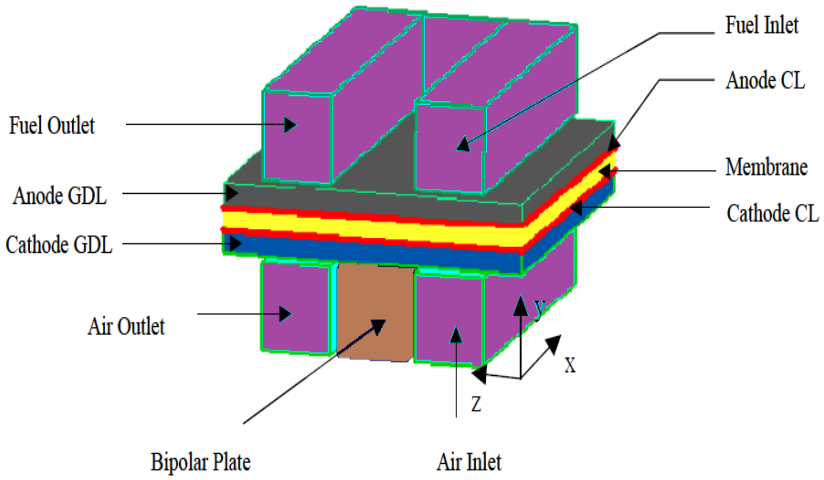

Fig.2 Three-dimensional computational domain (Components are not to scale).

Boundary conditions:

There are several zones which must be specified in the boundary conditions panel are shown in Fig.3.
Anode inlet: Mass flow rate = $3.65774x10^{-7}$ kg/s, Temperature =333K, Species (mass fractions): H_2=0.3126, H_20= 0.6874. *Cathode inlet:* Mass flow rate = $5.85238x10^{-6}$ Kg/s, Temperature =333K, Species (mass fractions): O_2=0.8792, H_20= 0.1208. *Anode outlet:* Temperature =333K, Pressure outlet =0 P(gauge pressure).
Cathode outlet: Temperature =333K, Pressure outlet =0 P(gauge pressure). *Anode voltage terminal:* Electric potential=0, Protonic potential=0, Temperature=333K. *Cathode voltage terminal:* Electric potential= Value (say 0.4), Protonic potential=0, Temperature=333K.

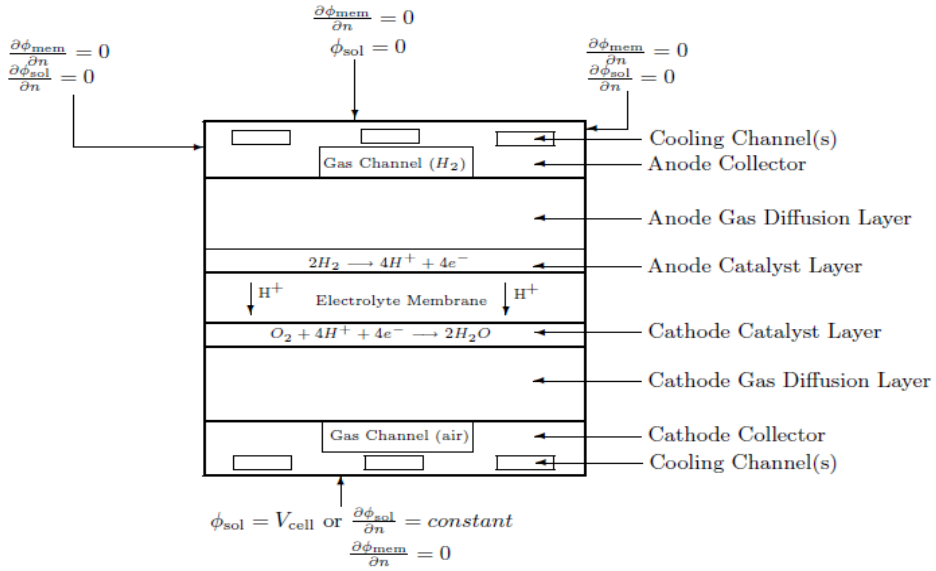

Fig. 3 Boundary conditions

Results and Discussion

Results are obtained using FLUENT for the following set of operating conditions: temperature=333K, pressure=1atm, humidity=100%, GDL thickness=400 µm, catalyst layer thickness at anode is 20 µm and at cathode 40 µm. These simulation results are compared with the experimental data of Sreenivasulu (2011), and the comparison is shown in Fig.4. The agreement between the simulation results and experimental data is found to be good.

The validated model is now ready for studying the effects of several operating parameters on fuel cell performance. The performance of the fuel cell based on a certain parameter can be obtained by varying that parameter while keeping all other parameters constant. Results obtained from these parametric studies will allow in identifying the critical parameters on the fuel cell performance. The fuel cell performance at various operating conditions is analyzed using the polarization curves and power curves.

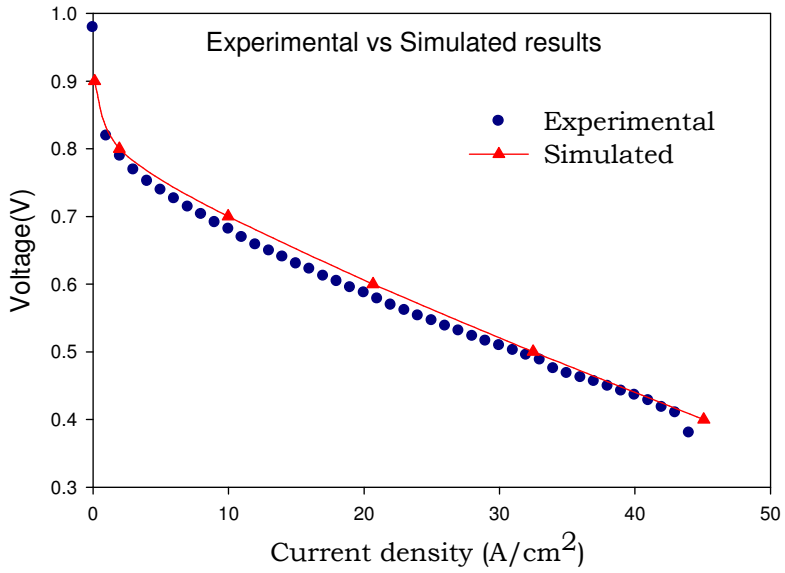

Fig. 4 Comparison of simulation results with the experimental data.

FLUENT results are obtained for voltage as a function of current density at four different cell temperatures (40, 50, 60 and 70°C), five operating pressures (1, 2, 3, 4 and 5 atm) , four different humidities (10, 25, 50, and 65%), three different GDL thicknesses (200 , 300 and 400 µm), and three different cathode catalyst layer thicknesses (20 , 30 and 40 µm) . These results are presented and discussed below.

Effect of Temperature

The pressure and electrode porosity are kept constant at 1atm. and 0.5 respectively, while the temperatures are varied from 40 to 70°C. The polarization curves of the cell at different operating temperatures are shown in Fig. 5. It is observed that the voltage across the fuel cell increases with an increase in temperature. The performance is better in all regions along the polarization curve. This is because the gas diffusivity, exchange current density and membrane conductivity are high at higher temperatures. The P-I curves are also shown in Fig. 6 for the same conditions as mentioned above.

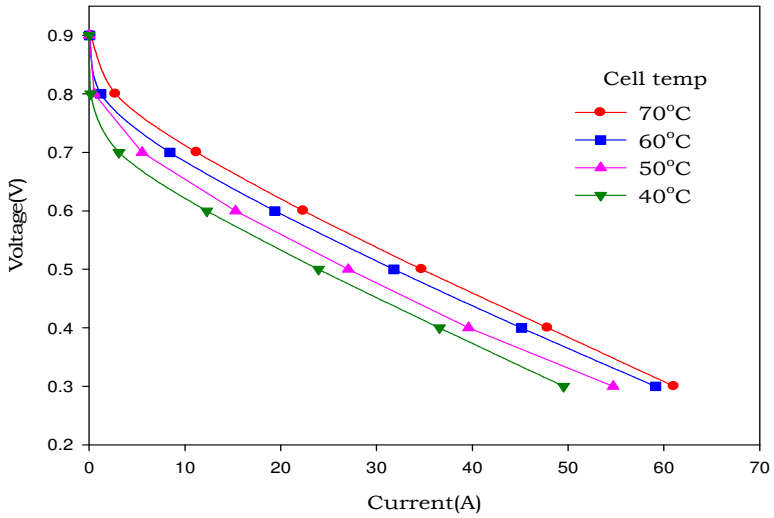

Fig.5 Effect of temperature on cell performance (V-I curve).

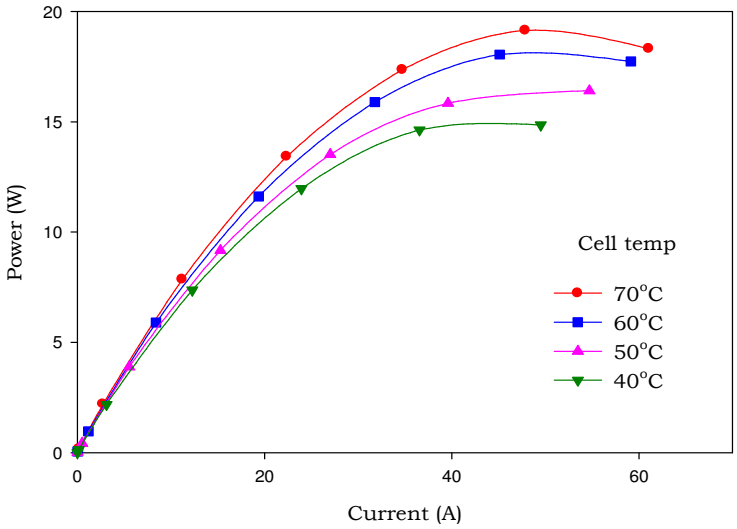

Fig.6 Effect of temperature on cell performance (P-I curve).

Effect of Pressure

Pressure is another operating parameter that has a large effect on fuel cell performance. The polarization curves at different cell operating pressures are shown in Fig. 7. The cell temperature and electrode porosity are maintained at 343 K and 0.5 respectively. It is observed from Fig.7 that as the operating pressure is increased from 1 to 5 atm. the fuel cell performance increases. This is due to an increase in gas diffusivity with an increase in pressure. However additional energy is required to compress the gases to raise the pressure, which may outweigh the gain in efficiency. For the same conditions the P-I curve also shown in Fig. 8.

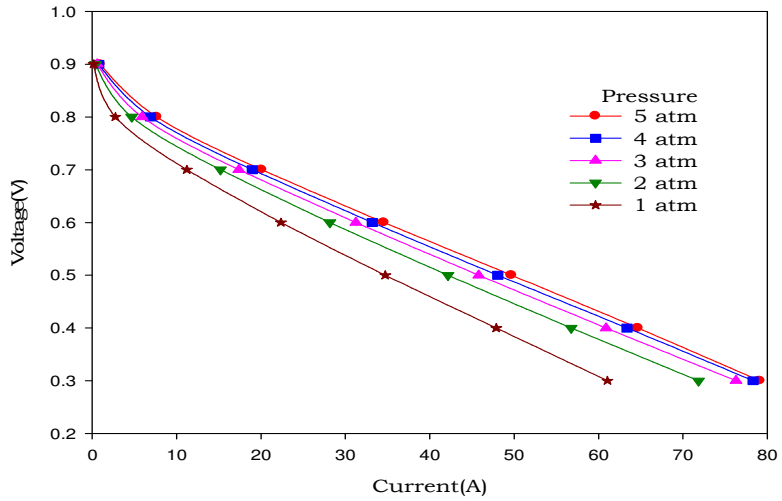

Fig.7 Effect of pressure on cell performance (V-I curve).

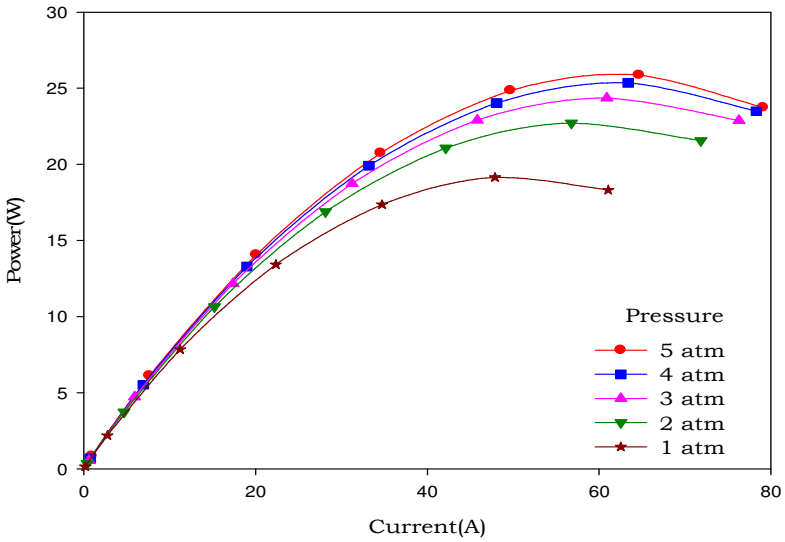

Fig.8 Effect of pressure on cell performance (P-I curve).

Effect of Gas Humidity

The effect of gas humidity on cell performance is shown in Figs.9 and 10. It is observed that the performance of fuel cell increases with humidity up to 65%, and there is no further improvement in the performance with an increase in humidity above 65%. Below 65% of reactant stream humidity the voltage drop occurs due to insufficient amount of water at the electrolyte membranes of the fuel cell. These membranes must maintain a minimum level of moisture in order to properly conduct ions.

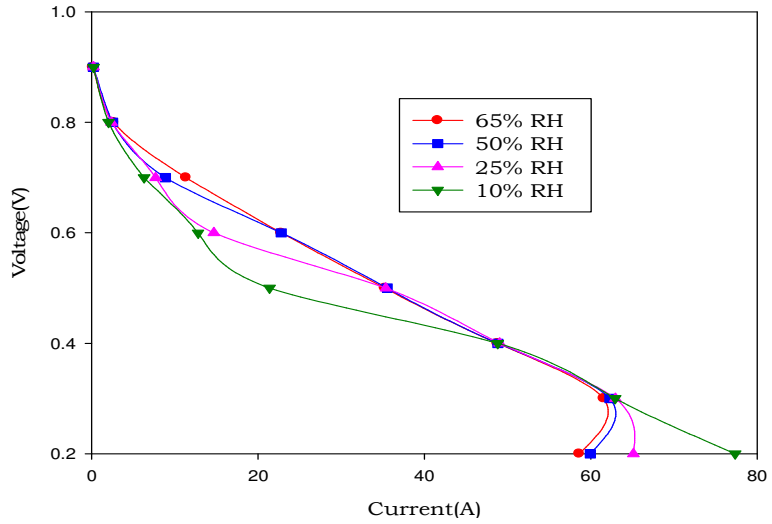

Fig.9 Effect of humidity on cell performance (V-I curve).

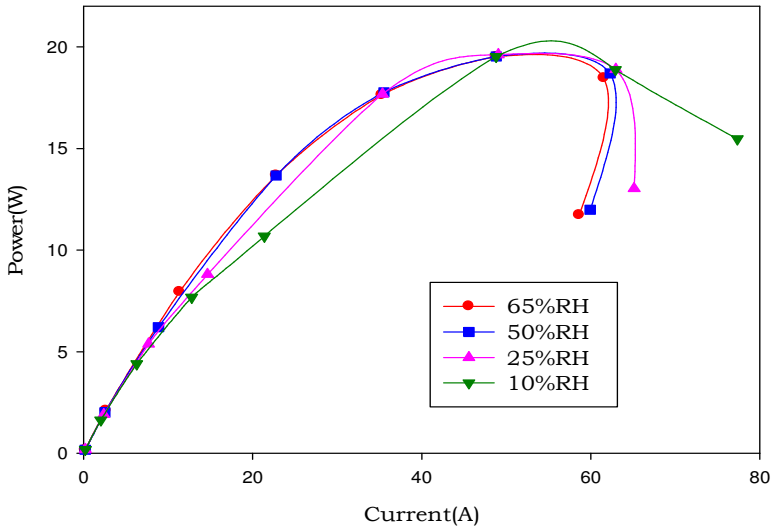

Fig.10 Effect of humidity on cell performance (P-I curve).

Effect of GDL Thickness.

The effect of GDL thickness is shown in Figs. 11 and 12. When the GDL thickness is 200 μm, the average potential is higher than the case of 300 μm and 400μm. A thinner GDL results in a larger oxygen transfer from the gas channel to the catalyst layer, and thus a larger potential is generated. The effect of the GDL thickness on the fuel cell performance is again mostly on the mass transport, as the Ohmic losses of the electrons inside the GDL can be neglected due to the high conductivity of the carbon fiber paper.

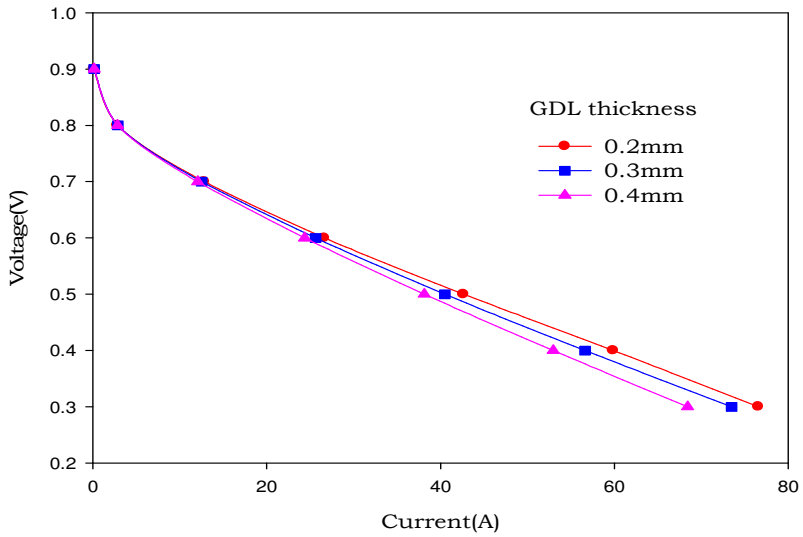

Fig.11 Effect of GDL thickness on cell performance (V-I curve).

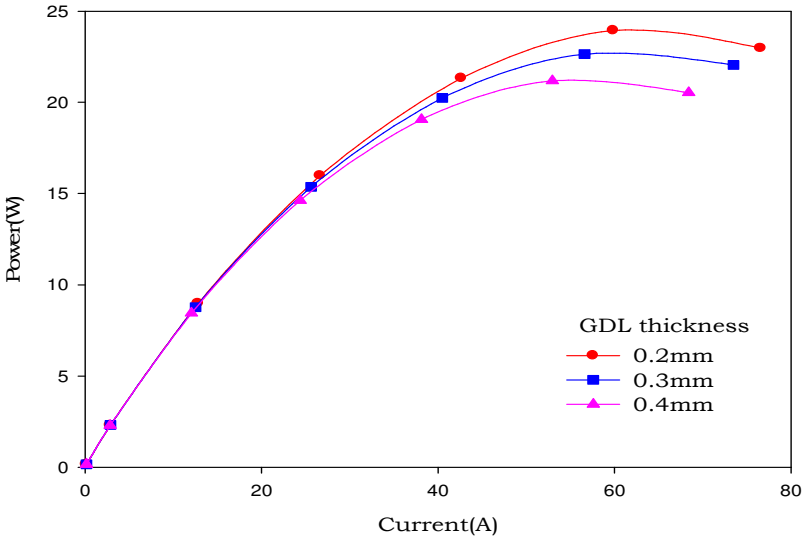

Fig.12 Effect of GDL thickness on cell performance (P-I curve).

Effect of cathode catalyst layer thickness

Figure 13 and 14 shows the effect of cathode catalyst layer thickness on performance of the fuel cell. The theoretical results for different catalyst layer thickness (20, 30 and 40µm) and at a 20µm constant anode catalyst layer are shown in Figs.13 and 14. It is observed from Figs. 13 and 14 the performance is increases by an increase with catalyst layer thickness. It is also observed that the performance is superior for 40µm compared to the 20µm and 30µm. This is due to the fact that the reactant gases do not have as many reaction sites in the later case as in the former case. However the performance is decreases beyond certain thickness due to in catalyst layer's electric and ionic resistance and to the increase in mass transport limitation. Due to increased mass transport resistance in higher catalyst thickness, at higher current densities, the reactant gases are unable to reach all the reaction sites and the catalyst at the inner half of the catalyst layer (i.e., adjacent to the membrane) largely remain underutilized.

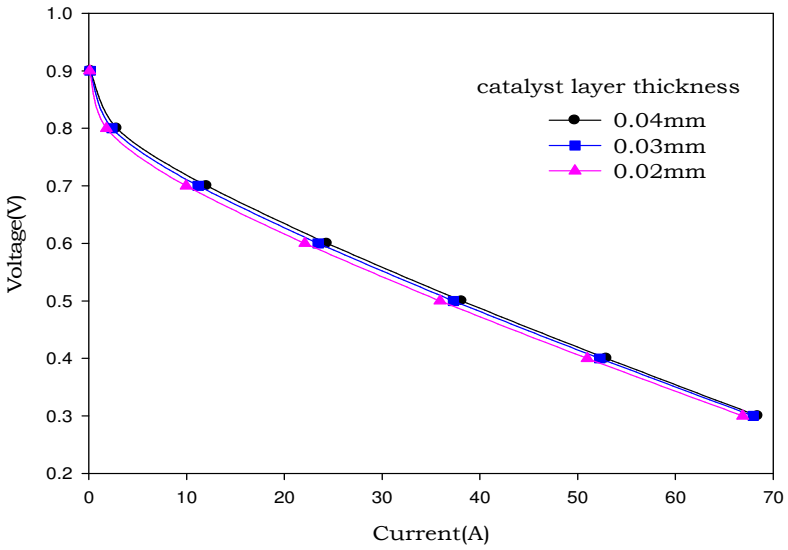

Fig.13 Effect of catalyst layer thickness on cell performance (V-I curve).

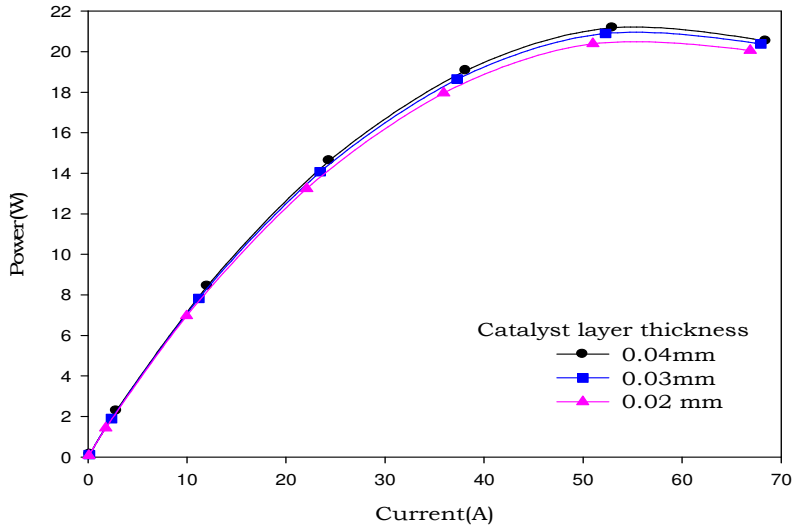

Fig.14 Effect of catalyst layer thickness on cell performance (P-I curve).

CONCLUSIONS:

The following conclusions can be drawn from the results.

1. The theoretical model developed for single PEM fuel cell simulates effectively the various conditions that exist in a real fuel cell, which is evident from the comparison of the theoretical results with experimental data.
2. The fuel cell performance is improved with an increase in temperature from 40^{o}C to 70^{o}C. This is due to increase of gas diffusivity, exchange current density and membrane conductivity at higher temperature.
3. As the operating pressure is increased from 1 to 5 atm, the fuel cell performance also increases due to increase in inlet concentration of oxygen.
4. A thinner GDL results in a larger oxygen transfer from the gas channel to the catalyst layer, and thus a larger potential is generated.
5. As the catalyst layer thickness increases there is an improvement in the performance was observed. However the performance is decreases beyond certain thickness due to in catalyst layer's electric and ionic resistance and to the increase in mass transport limitation.

References:

1. Berning T D. M. Lu, N. Djilali (2002), "Three-dimensional computational analysis of transport phenomena in a PEM fuel cell", Journal of Power Sources, Vol.106, pp.284-294.
2. Lin Wang, Attila Husar, Tianhong Zhou, Hongtan Liu (2003), "A Parametric study of PEM fuel cells performances", International Journal of Hydrogen Energy, Vol. 28, pp. 1263-1272.
3. Parthasarathy, A., S. Srinivasan, J. A. Appleby, C. R. Martin (1992), "Temperature Dependence of the Electrode Kinetics of Oxygen Reduction at the Platinum/Nafion Interface - A Microelectrode Investigation", J Electrochem. Soc., 139(9), pp. 2530-2537.
4. Shimpalee S, Dutta S (2000), "Numerical prediction of temperature distribution in PEM fuel cells", Numerical heat transfer, part A, Vol.38, pp.111-128.
5 B.Sreenivasulu, S.V. Naidu, V. Dharma Rao, P.S.V. Kurma Rao, P.V.J. Mohana Rao(2011) , A Parametric Study to improve the performance of a PEM Fuel Cell – A Theoretical Study", Proceedings of the 21st National and 10th ISHMT-ASME Heat and Mass Transfer Conference, Dec 2011,IIT Madras, India
6. Um S, Wang C.Y (2004), "Three-dimensional analysis of transport and electrochemical reactions in polymer electrolyte fuel cells", J Power Sources, 125(1), pp.40-51.
7. Vladimir Gurau, Hongtan Liu, Sadik kakac (1998), "Two Dimensional Modal for Proton Exchange Membrane Fuel Cells", AIChE Journal, Vol.44(11), pp.2410-2422.
8. P.J. Hamilton and B.G. Pollet (2010), "Polymer Electrolyte Membrane Fuel Cell (PEMFC) Flow Field Plate: Design, Materials and Characterisation", Fuel Cells, 10(4), pp.489-509.
9. Berning T., Djilali N.(2003), "Three-dimensional computational analysis of transport phenomena in a PEM fuel cells-a parametric study", Journal of Power Sources, Vol. 124, pp. 440-452.
10. Wei-Mon Yan,Hung-Yi Li,Po-Chiao Chiu, Xiao-Dong Wang (2008), "Effects of serpentine flow field with outlet channel contraction on cell performance of proton exchange membrane fuel cells", *Journal of Power Sources,* Vol.178,pp.174–180.
11. Xiao-Dong Wang, Yuan-Yuan Duan, Wei-Mon Yan, Xiao-Feng Peng(2008), "Local transport phenomena and cell performance of PEM fuel cells with various serpentine flow field designs", *Journal of Power Sources*, Vol.175, pp. 397-407.
12. Antolini (2004), "Recent developments in polymer electrolyte fuel cell electrodes", *Journal of Applied Electrochemistry,* Vol.34, pp.563-576.

EXPERIMENTAL STUDIES ON EMISSION AND PERFORMANCE OF C.I. ENGINE WITH BIODIESEL AND ITS BLENDS

[1] Mr. Jaysukh Ghetiya, [2] Mr. Amitesh Paul, [3] Dr. G.R. Selokar

[1]M.Tech. [Thermal Engineering] Student, Department of Mechanical Engg, Shri Satya Sai Institute of Science and Technology, Sehore, Madhya Pradesh[1]

[2] Head of Department, Department of Mechanical Engg. , Shri Satya Sai Institute of Science and Technology, Sehore, Madhya Pradesh

[3] Principal, Shri Satya Sai Institute of Science and Technology, Sehore, Madhya Pradesh

ABSTRACT:

Many researchers have done a lot of experimental studies in the field of biodiesel to find an alternative to mineral diesel. It has shown that Jatropha biodiesel can be used as an alternative fuel in Diesel engine without modification. An experimental study was carried out to find out the effect of Jatropha bio-diesel on engine performance and emissions. For this experimental setup a 7 kW single cylinder, air-cooled, constant speed direct injection diesel engine with alternator was used for the experimental work. Emissions like NO_X, CO, HC and smoke opacity were measured. Engine performance parameters such as brake thermal efficiency (BTE), brake specific energy consumption (BSEC) and exhaust gas temperature were also calculated. Results indicated that B20 have closer performance to diesel. The brake thermal efficiency for bio-diesel fuelled engine was slightly higher than diesel fuelled engine. There was increase in specific energy consumption and exhaust gas temperature with increase in bio diesel proportion in biodiesel blends. The rate of NO_X emissions from biodiesel was gradually increased by 15, 18, 16 and 11 per cent higher than that of the diesel at 2.58, 3.83, 4.99 and 5.88 BMEP (2.9, 4.3, 5.6 and 6.6 kW) load conditions respectively. The carbon monoxide reduction by biodiesel was 11, 10, 15 and 19 per cent at 2.58, 3.83, 4.99 and 5.88 BMEP (2.9, 4.3, 5.6 and 6.6 kW) load conditions. Hydrocarbon (HC) and smoke opacity from the biodiesel and its blends was found lower than diesel fuel during the whole experimental range. Exhaust gas temperature increased with increase in load and amount of biodiesel. The highest exhaust gas temperature was observed as 455ºC for biodiesel among the four load conditions. The diesel mode exhaust gas temperature was observed as 368ºC.

Keywords— diesel, biodiesel, bio-diesel blends, performance, emissions**.**

I: INTRODUCTION

The diesel engine is typically more efficient than the gasoline engine due to higher compression ratio. Diesel engines also do not suffer from size and power limitations, which the SI engine is prone to. Hence, keeping these factors into account, they are the invariable choice for industrial, heavy duty and truck/trailer engines. Buses and certain locomotives also use diesel engines. Diesel engines also find use as small captive power plant engines, tractor engines and irrigation pump sets. India, which is at a developing stage in its history, has a huge demand for diesel driven machines and unlike countries like USA, is a diesel driven economy. India is an agriculture based economy and agriculture is an energy transformation process as energy is produced and consumed in it. The production of energy is carried through process of photosynthesis in which solar energy is converted into biomass. Agriculture in India is heavily based upon petroleum and its derived products such as fertilizers and pesticides. Energy sources used in agriculture are oil and electricity whereas indirect energy sources are chemical fertilizers and pesticides. Thus, keeping the above discussion in mind it is imperative for the Indian economy to find a substitute to fuel variety of diesel engines that it is so much dependent upon so as to fulfill its journey to becoming a developed nation.

The consumption of diesel is 4-5 times higher than petrol in India. Due to the shortage of petroleum products and its increasing cost, efforts are on to develop alternative fuels especially, to the diesel oil for full or partial replacement. It has been found that the vegetable oils are promising fuels because their properties are similar to that of diesel and are produced easily and renewably from the crops. Vegetable oils have comparable energy density, cetane number, heat of vaporization and stoichiometric air–fuel ratio with that of the diesel fuel. None other than Rudolph Diesel, the father of diesel engine, demonstrated the first use of vegetable oil in compression ignition engine in 1910. He used peanut oil as fuel for his experimental engine [1]. So the use of vegetable oils as alternative fuels has been around for one hundred years when the inventor of the diesel engine Rudolph Diesel first tested peanut oil, in his compression-ignition engine. In the 1930s and 1940s vegetable oils were used as diesel fuels from time to time, but usually only in emergency situations. In 1940 first trials with vegetable oil methyl and ethyl esters were carried out in France and, at the same time, scientists in Belgium were using palm oil ethyl ester as a fuel for buses. Not much was done until the late 1970s and early 1980s,

when concerns about high petroleum prices motivated extensive experimentation with fats and oils as alternative fuels. Bio-diesel (mono alkyl esters) started to be widely produced in the early 1990s and since then production has been increasing steadily. In the European Union (EU), bio-diesel began to be promoted in the 1980s as a means to prevent the decline of rural areas while responding to increasing levels of energy demand. However, it only began to be widely developed in the second half of the 1990s [2].

Vegetable oils have almost similar energy density, cetane number, heat of vaporization, and stoichiometric air/fuel ratio compared to mineral diesel fuel. However, straight vegetable oils cannot be used directly in engines. Straight vegetable oils or their blends with diesel pose various long-term operational and durability problems in compression ignition engines, e.g. poor fuel atomization, piston ring-sticking, fuel injector coking and deposits, fuel pump failure, and lubricating oil dilution etc. The properties of vegetable oils responsible for these problems are high viscosity, low volatility, and polyunsaturated character. Several techniques are proposed to reduce the viscosity of vegetable oils such as blending, pyrolysis, micro-emulsion and transesterification etc. Heating and blending of vegetable oils reduce the viscosity but its molecular structure remains unchanged hence polyunsaturated character and low volatility problems exist. It has been reported that transesterification is an effective process to overcome all these problems associated with vegetable oils [3].

Vegetable oil can be directly mixed with diesel fuel and may be used for running an engine. The blending of vegetable oil with diesel fuel in different proportion were experimented successfully by various researchers. Blend of 20% oil and 80% diesel have shown same results as diesel and also properties of the blend is almost close to diesel. The blend with more than 40% has shown appreciable reduction in flash point due to increase in viscosity. Some researchers suggested for heating of the fuel lines to reduce the viscosity. Although short term tests using neat vegetable oil showed promising results, longer tests led to injector coking, more engine deposits, ring sticking and thickening of the engine lubricant [4]. Micro-emulsification, pyrolysis and transesterification are the remedies used to solve the problems encountered due to high fuel viscosity. Although there are many ways and procedures to convert vegetable oil into a Diesel like fuel, the transesterification process was found to be the most viable oil modification process [3].

The use of vegetable oils, such as palm, soya bean, sunflower, peanut, and olive oil, as alternative fuels for diesel is being promoted in many countries [5].

China is rich in cottonseed and research on using cottonseed oil as diesel engine fuel has been intensively and widely studied there. From a technological point of view, the fuel property of cottonseed oil seems to meet the fundamental requirements of diesel engine. Y.He et al. [6] conducted tests with blend of 30% cottonseed oil and 70% diesel on diesel engine. The experimental results obtained showed that a mixing ratio of 30% cottonseed oil and 70% diesel oil was practically optimal in ensuring relatively high thermal efficiency of engine, as well as homogeneity and stability of the oil mixture. For this purpose, a modification of diesel engine structure is unnecessary, as has been confirmed by the literature. High viscosity of cottonseed oil is one of the key problems preventing its widespread application.

Deshpande [7] used blends of linseed oil and diesel to run the CI engine. Minimum smoke and maximum brake thermal efficiency were reported in this study. Barsic et al. [8] conducted experiments using 100% sunflower oil, 100% peanut oil, 50% of sunflower oil with diesel and 50% of peanut oil with diesel. A comparison of the engine performance was presented. The results showed that there was an increase in power and emissions. In another study, Rosa et al. [9] used sunflower oil to run the engine and it was reported that it performed well. Blends of sunflower oil with diesel and safflower oil with diesel were used by Zeiejerdki et al. [10] for his experimentation. He demonstrated the least square regression procedure to analyze the long-term effect of alternative fuel and I.C. engine performance.

II: EXPERIMENTAL SETUP AND METHODOLOGY

A Kirloskar make, single cylinder, air cooled, direct injection, DAF 10 model diesel engine was selected for the present research work, which is primarily used for agricultural activities and household electricity generations.

It is a single cylinder, naturally aspirated, four stroke, vertical, air-cooled engine. It has a provision of loading electrically since it is coupled with single phase alternator through flexible coupling. The engine can be hand started using decompression lever and is provided with centrifugal speed governor. The cylinder is made of cast iron and fitted with a hardened high-phosphorus cast iron liner. The lubrication system used in this engine is of wet sump type, and oil is delivered to the crankshaft and the big end by means of a pump mounted on the front cover of the engine and driven from the crankshaft. The inlet and exhaust valves are operated by an overhead camshaft driven from the crankshaft through two pairs of bevel gears. The fuel pump is driven from the end of camshaft. The detailed technical specifications of the engine are given in Table 1.

Make and Model	Kirloskar DAF 10
TYPE	single cylinder, naturally aspirated, 4 stroke, vertical, air-cooled
Rated Brake Power (kW)	7
Rated Speed (rpm)	1500
Number of Cylinder	One
Bore x Stroke (mm)	102 x 110
Compression Ratio	17.5:1
Lubrication System	Forced Feed

Table 1:- Specifications of the Diesel Engine

For conducting the desired set of experiments and required data together from the engine, it is essential to get the various instruments mounted at the appropriate location on the experimental setup. A two fuel tank system is used to easy switch from diesel to biodiesel or vice versa.

After finalizing the procedures for data collection and procurement of the desired instruments, they were put on a panel. A MS Control panel was fabricated and Instruments such as voltmeter, ammeter, watt meter, speed counter, six channels digital temperature display was mounted on the front side of the control panel. Electrical load bank (12 bulbs each of 500 watts and 2 bulbs each of 300 watts) mounted on the rear side of the control panel and their switches provided on the front side of the control panel.

One 50ml burette with stop cocks was also mounted on the front side of the panel for fuel flow measurements of either diesel or biodiesel fuel. The two fuel tanks were mounted on the rear side of the panel at highest position with stop cocks.

A voltmeter, ammeter and wattmeter were connected between alternator and load bank. A nut was welded on the flywheel and the photo reflective sensor was mounted on a bracket attached to engine body. The thermocouples were mounted in the exhaust manifold to measure the exhaust temperature. The AVL 437 smoke meter and AVL 4000 Di Gas Analyzer were also kept in proximity for the measurements of various exhaust gas parameters.

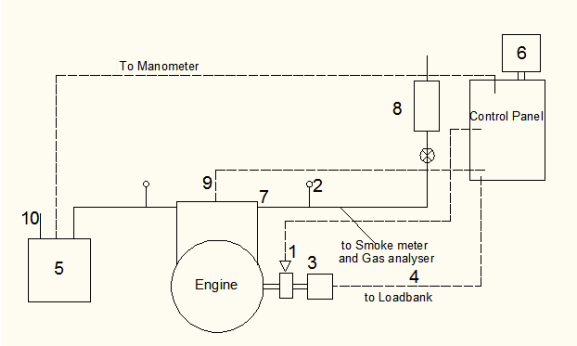

1. Engine Speed, 2.Exhaust Manifold Temperature,

3. Alternator , 4.Electical loading arrangement, 5. Inlet Air box, 6.Fuel Tank, 7.Engine Exhaust, 8. Muffler,

9. Fuel to Engine and 10. Fresh Air

Figure 1: Experimental set up

(1) The fuel properties

The fuel properties of the jatropha biodiesel and its blends are furnished in the table 1.

Sr. No	Properties	Diesel	Jatropha biodiesel				
			B20	B40	B60	B80	B100
1	Calorific value, MJ/kg	44.42	43.25	42.07	41.14	40.17	39.17
2	Flash point, ºC	50	58	79	104	119	194
3	Specific gravity	0.841	0.844	0.848	0.853	0.858	0.862
4	Kinematic viscosity at 40ºC, cSt	4.86	4.96	5.03	5.14	5.26	5.37
5	Carbon residue, %	0.21	0.21	0.22	0.22	0.24	0.24

Table 1: Fuel Properties of Jatropha Biodiesel and Its Blends.

III: PERFORMANCE CHARACTERISTICS

1) Specific Fuel Consumption and Specific Energy Consumption

The fuel consumption of engine was increased with increase in amount of biodiesel blends is shown in Figure. 2. In the case of jatropha biodiesel alone, the fuel consumption was about 14 per cent higher than that of diesel. This may be due to higher specific gravity and lower calorific value of the biodiesel fuel as compared with diesel fuel. The calorific value of the jatropha biodiesel was about 13 per cent lower than that of diesel fuel. The percent increase in fuel consumption of biodiesel blends (B20 to B80) ranged from 2 to 12 per cent than diesel fuel due to decrease in calorific value of these fuels.

The specific fuel consumption was calculated by fuel consumption divided by the rated power output of the engine. The percent increase in specific fuel consumption ranged from 2 to 13 for B20 to B100 fuels. The range of increase in fuel consumption was found to be similar under all load conditions. The percent increase in specific fuel consumption was increased with decreased amount of diesel fuel in the blended fuels. This may due to lower heating value of the fuels and higher mass of fuel flow to meet the engine loads.

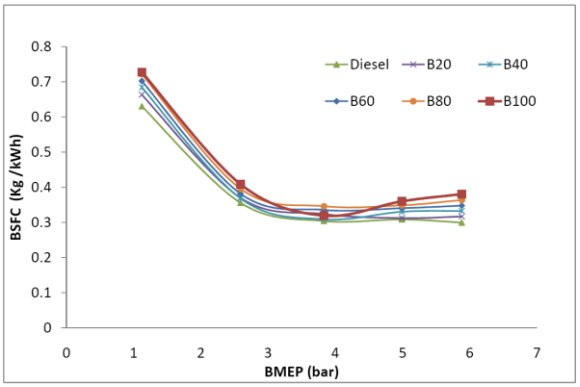

Figure 2: BSFC v/s BMEP with different biodiesel blends

Since Brake Specific Fuel Consumption is not a very reliable parameters to compare the performance of two different fuels since density and calorific value of both the fuel are significantly different. Therefore, brake specific energy was taken as a parameter to compare the energy requirement for producing unit power in case of different test fuels. It can be observed from figure 3 that the BSEC is higher at medium load for biodiesel and it is lower at high load. This means biodiesel performance for BSEC of biodiesel gives nearer results to diesel fuelled engine.

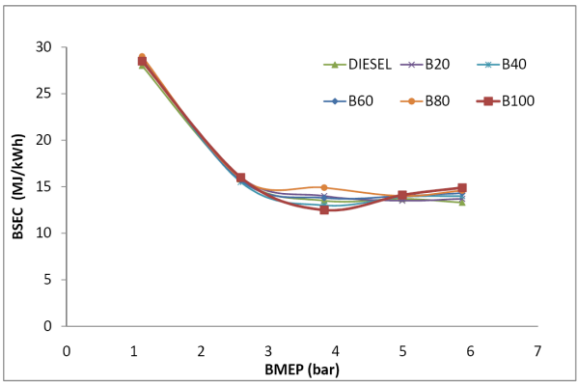

Figure 3: BMEP v/s BSEC with different biodiesel blends

2) Brake Thermal Efficiency

The brake thermal efficiency with biodiesel and its blends was found to be slightly higher than that of diesel fuel at tested load conditions. It varied from 23 to 26.0 per cent for diesel fuel alone. There was no difference between the biodiesel and its blended fuels on efficiencies. The brake thermal efficiencies of engine, operating with biodiesel mode were 22.5, 28, 26, and 23.5 per cent at 2.9, 4.3, 5.6 and 6.6 kW (2.58, 3.83, 4.99, and 5.88 BMEP) load conditions respectively (Figure 4).

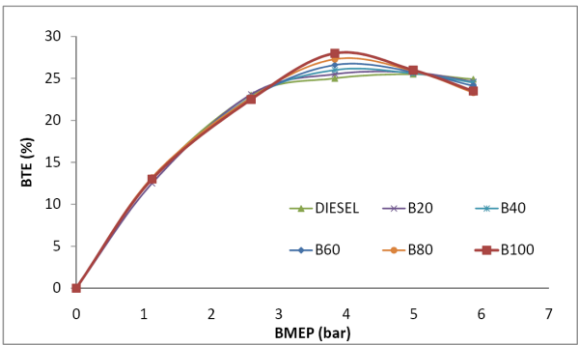

Figure 4: BTE Vs BMEP with different biodiesel blends

3) Exhaust Gas Temperature

The exhaust gas temperature gives an indication the amount of waste heat going with exhaust gases. The exhaust gas temperature of the different biodiesel blends is shown in Figure 5. The exhaust gas temperature of B100 varies from 10 to 14 per cent higher than that of diesel at all load conditions. The highest exhaust gas temperature was observed as 455ºC for biodiesel among four load conditions. The diesel fuel mode exhaust gas temperature was observed as 368ºC (Figure 5).

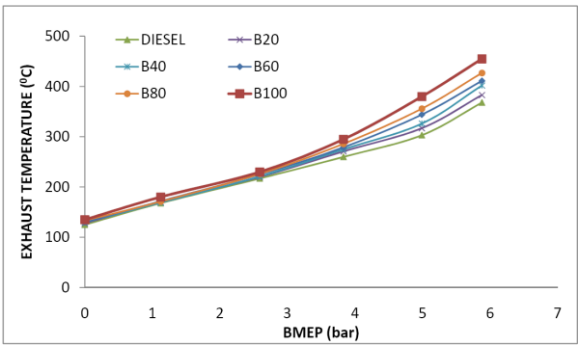

Figure 5: Exhaust Temperature v/s BMEP with different biodiesel blends

IV: EMISSION CHARACTERISTICS

1) NO_X Emission

The variations of NO_X emissions for all the test fuels are shown in Figure 6. The NO_X emissions increased with the increasing engine load, due to higher combustion temperature. This proves that the most important factor for the emissions of NO_X is the combustion temperature in the engine cylinder.

The NO_X emission from engine with different jatropha biodiesel blended fuels and biodiesel is shown in Figure. 6. The NO_X emission increased for biodiesel by 15, 18, 16 and 11 per cent higher than diesel fuel at 2.9, 4.3, 5.6 and 6.6 kW

(2.58, 3.83, 4.99, and 5.88 BMEP) load conditions. The percentage of increase in NO_X concentration for blended biodiesel fuels were observed as 1 to 18 per cent when compared with diesel fuel. The NO_X emission increased with increase in biodiesel amount in the blended fuels and also found that NO_X emission from the biodiesel fuel was higher than that of diesel. An important observation is that Biodiesel blend B20 has lower NO_X emissions than the baseline data for diesel. However, the increase in NO_X concentration is the main problem in biodiesel and it can be reduced by making suitable change in the engine parameters.

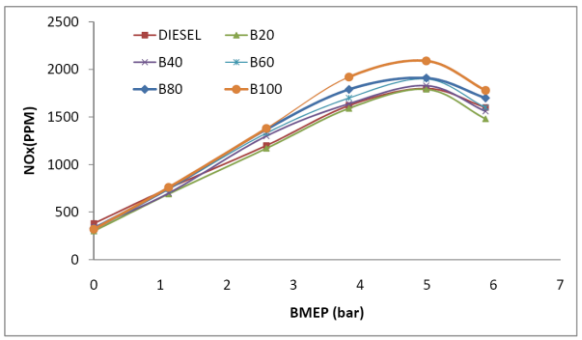

Figure 6: NO_X v/s BMEP with different biodiesel blends

2) Carbon Monoxide (CO) Emission

The CO emission from the diesel fuel with biodiesel blended fuels and biodiesel is shown in Figure 7. The CO reduction by biodiesel was 11, 10, 15 and 19 per cent at 2.9, 4.3, 5.6 and 6.6 kW load conditions. With diesel fuel mode the lowest CO was recorded as 360 ppm at 2.9 kW load and as load increased to 4.3 kW, CO also increased to 904 ppm. Similar results were obtained for biodiesel blended fuels and biodiesel with lower emission than diesel fuel. The amount of CO emission was lower in case of biodiesel blended fuels and biodiesel than diesel.

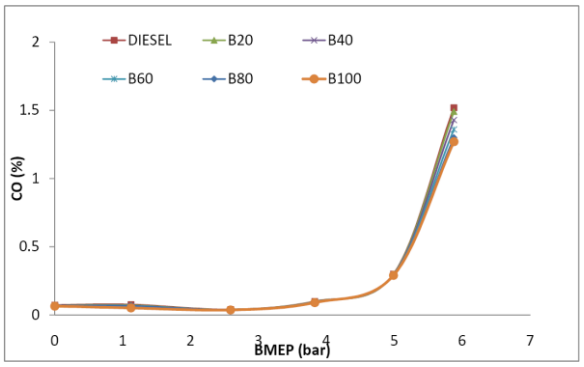

Figure 7: CO v/s BMEP with different biodiesel blends

3) Un-burnt Hydro Carbon Emissions

The un-burnt hydro carbon emission from the diesel engine with different blends is shown in Figure. 4. The HC emissions increased with increase in load conditions for diesel and for biodiesel blended fuels. The jatropha biodiesel followed the same trend of HC emission, which was lower than in case of diesel. The HC in the exhaust gas was decreased gradually with increased biodiesel proportion.

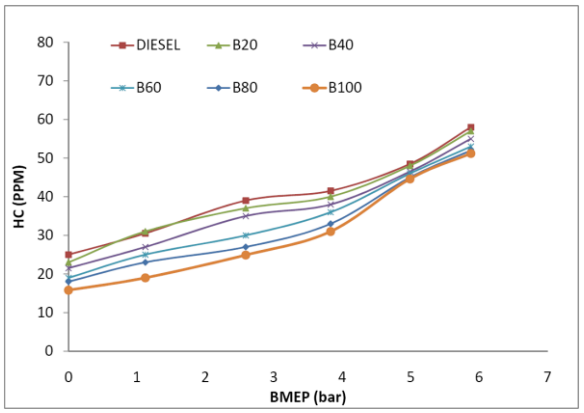

Figure 8: HC v/s BMEP with different biodiesel blends

4) Smoke Opacity

The smoke opacity from the diesel fuel with biodiesel blended fuels and biodiesel is shown in Figure 9. The smoke opacity reduction by biodiesel was 14, 15, 18 and 21 per cent at 2.9, 4.3, 5.6 and 6.6 kW load conditions. The Smoke opacity found to be decrease with increased biodiesel rate in fuel and it is seen that at full biodiesel fuel there was lowest smoke opacity.

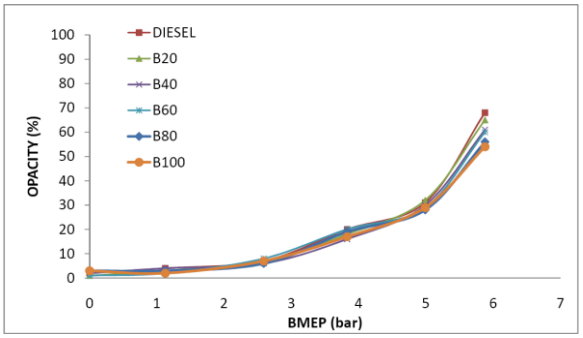

Figure 9: Opacity v/s BMEP with different biodiesel blends

V: CONCLUSIONS

In this experimental work Emissions like NO_X, CO, HC and smoke opacity were measured. Engine performance parameters such as brake thermal efficiency (BTE), brake specific energy consumption (BSEC) and exhaust gas temperature were also calculated. Results indicated that B20 have closer performance to diesel. The brake thermal efficiency for bio-diesel fuelled engine was slightly higher than diesel fuelled engine. There was increase in specific energy consumption and exhaust gas temperature with increase in bio diesel proportion in biodiesel blends. The rate of NO_X emissions from biodiesel was gradually increased by 15, 18, 16 and 11 per cent higher than that of the diesel at 2.58, 3.83, 4.99 and 5.88 BMEP (2.9, 4.3, 5.6 and 6.6 kW) conditions respectively. The carbon monoxide reduction by biodiesel was 11, 10, 15 and 19 per cent at 2.58, 3.83, 4.99 and 5.88 BMEP (2.9, 4.3, 5.6 and 6.6 kW) load conditions. Hydrocarbon (HC) and smoke opacity from the biodiesel and its blends was found lower than diesel fuel during the whole experimental range. Exhaust gas temperature increased with increase in load and amount of biodiesel. The highest exhaust gas temperature was observed as 455ºC for biodiesel among the four load conditions. The diesel mode exhaust gas temperature was observed as 368ºC.

VI: REFERENCES

1. A.S. Ramadhas, C. Muraleedharan, S. Jayaraj, “Performance and emission evaluation of a diesel engine fueled with methyl esters of rubber seed oil” Renewable Energy 30 pp1789–1800, 2005.
2. Mustafa Balat, Havva Balat, “A critical review of bio-diesel as a vehicular fuel” Energy Conversion and Management 49 pp 2727–2741, 2008.
3. Ayhan Demirbas. Biodiesel fuels from vegetable oils via catalytic and non-catalytic supercritical alcohol transesterifications and other methods: a survey elsvier, Energy Conversion and Management 44 (2003) 2093–2109
4. Nwafor. Emission characteristics of diesel engine running on vegetable oil with elevated fuel inlet temperature, Biomass and Bio energy journal, 27 (2004) 507 – 511
5. B.K. Barnwal, M.P. Sharma. Prospects of biodiesel production from vegetable oils in India, elsvier, Renewable and Sustainable Energy Reviews, 9 (2005) 363–378
6. Y. He, Y.D. Bao. Study on cottonseed oil as a partial substitute for diesel oil in fuel for single-cylinder diesel engine, Renewable Energy, 30 (2005) 805–813
7. Deshpande NV. Bio-diesel: An alternative fuel for compression ignition engines, Proceedings on Recent trends in alternative fuels, Nagpur, India, 2002.
8. Barsic NJ, Humke H. Performance and emission characteristics of a naturally aspirated diesel engine with vegetable oil, SAE 810262, 1981.
9. Rosa Radu. The use of sunflower oil in diesel engines, SAE 972979, 1997.Tavel, P. 2007 Modeling and Simulation Design. AK Peters Ltd.
10. Zeiejerdki K, Pratt K. Comparative analysis of the long term performance of a diesel engine on vegetable oil, SAE 860301, 1986.

Author's Addresses:

MR.JAYSUKH GHETIYA
"Laxmi Nivas", Sitaram Park-1, Near Railway Crossing, Morbi Road, Rajkot Gujarat-360003,

MR. AMITESH PAUL
Shri Satya Sai Institute of Science and Technology, SH-18, Indore-Bhopal Road, Pachama, District: Sehore, M.P-466002

DR. G.R. SELOKAR
Shri Satya Sai Institute of Science and Technology, SH-18, Indore-Bhopal Road, Pachama, District: Sehore, M.P-466002

Wired Network Security – Challenges for Researcher

Aiyeshabi S. Mulla
Dept. of Computer Applications,
Bharati Vidyapeeth Deemed University,
I.M.R.D.A., Sangli.

Riyajuddin Y. Mujawar
Dept. of Computer Applications,
Bharati Vidyapeeth Deemed University,
I.M.R.D.A., Sangli.

Abstract –
Network security has become more important to personal computer users, organizations, and the military. Thus Security is crucial to networks and applications. Although, network security is a critical requirement in emerging networks, there is a significant lack of security methods that can be easily implemented. Securing the network is just as important as securing the computers and encrypting the message. This paper focuses on the fuzzy based approach for various parameters of network security that will adjust the security measure and improve the security performance.
Keywords - Fuzzy logic, Network security, Security Measure, Security Performance.

1 INTRODUCTION

A Network security is a threat, intrusion, denial of service or other attack on a network infrastructure that analyzes and gain information to eventually cause network to crash or to become corrupted. The entire field of network security is vast and in an evolutionary stage. It consists of the provisions and policies adopted by the network administrator to prevent and monitor unauthorized access, misuse, modification, or denial of the computer network and network-accessible resources. It covers public and private computer networks used in everyday jobs i.e. businesses, government agencies and individuals.

There exists a "communication gap" between the developers of security technology and developers of networks. Network design is a well-developed process that is based on the Open Systems Interconnections (OSI) model. The OSI model has several advantages when designing networks. It offers modularity, flexibility, ease-of-use, and standardization of protocols. The protocols of different layers can be easily combined to create stacks which allow modular development. The implementation of individual layers can be changed later without making other adjustments, allowing flexibility in development. In contrast to network design, secure network design is not a well-developed process. There isn't a methodology to manage the complexity of security requirements. Secure network design does not contain the same advantages as network design. Hence protecting network parameters is an important task to improve network security.

An essential factors which are termed as important keys for network security are:

- Identification
- Authentication
- Authorization
- Access Control
- Data Integrity
- Confidentiality
- Non-repudiation.

Identification means identifying authorized user, Authentication is for finding identity or origin of user or user name and password, Authorization gives access for using resources by authorized user, Access Control gives restricted to access data, Data Integrity ensures whether existing information complete and accurate & protect it from unauthorized modification, Confidentiality means protecting information from unauthorized disclosure.

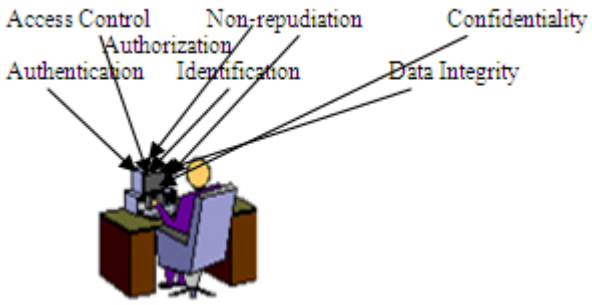

Fig.1 Secure User-Machine Interaction Hurdle Chain

While Communicating user has to go through specified hurdles for secure communication as shown in Fig.1.Mentioned parameters are important keys of network security otherwise system will suffer from its disadvantages like

- Intrusion
- Leak of information like hijack, access password, document etc.
- Unauthorized access
- Modification in data etc.[5]

Hence developing an effective network security plan understanding security issues, potential attackers, needed level of security and factors that make a network vulnerable to attack must be implemented.

I. NEED OF NETWORK SECURITY

Network Security includes two basic securities

- Information Security
- Computer Security.

Information Security protects data from unauthorized access and loss. Whereas Computer Security protects system from unwanted damages caused due to network like viruses, spywares, Trojan horse. The people who intentionally put such software on the network are called Hackers. Hence System needs

- Data link layer security
- Network layer security
- Transport layer security

Data link layer security includes link control. Network layer security includes routing of packets, packet scheduling. Transport layer security includes flow control. Hence Buffer management, Queue management, Routing, Load management are playing an important role in network security.

II. POLICIES AND OPERATIONS IN NETWORK SECURITY

Network Security Policy and Services should includes understanding of at which level of Network security to be established and maintained, what assets need to protect, what threats to what degree, identifying appropriate security policy elements for networks and meet the needs of network. Security Mechanisms includes security at various levels of layered architecture.

Network security operates in layers. It starts with firewall which controls network traffic. The
Next layers of security are antivirus programs on desktops and servers. Layers beyond that include password policies, data access permissions.

Following table shows seven layers of OSI model, their importance in security and which security mechanism should be applied for each layer for secure communication is mentioned.

TABLE I
OSI MODEL LAYERS & THEIR ROLE IN SECURITY MECHANISM

Layer No.	*OSI Layers*	*Security mechanism*
7	Application Layer	Identification, Authentication, QoS
6	Presentation Layer	Encryption Standards
5	Session Layer	Secure Password Policy
4	Transport Layer	Flow Control
3	Network Layer	Secure Routing, Congestion Control Policies, packet sequencing
2	Data Link Layer	Flow & Error Control
1	Physical Layer	Password management, topology

Network security is mostly contained within the physical layer. Cryptography occurs at Application layer. Authentication is performed on a layer above the physical layer.

For authentication, one may use one actor authentication, two-factor authentication or three-factor authentication. In one actor authentication, user uses username and password for authentication. In two-factor authentication, user uses something like security token or 'dongle' or an ATM card or a mobile phone. Where as in three-factor authentication, the user 'is' is also used like fingerprint or retinal scan. Network security in the physical layer requires failure detection, attack detection mechanisms, and intelligent countermeasure strategies.

III. TYPES OF ATTACKS AND SECURITY POLICIES IN WIRED NETWORK

A. Local Area Network

Wired LAN uses Ethernet cables and network adapters. Although two computers can be directly wired to each other using an Ethernet crossover cable, wired LANs generally require central devices like hubs, switches, or routers to accommodate more computers. Wired LANs offer superior performance. Wired LANs utilizing hubs can suffer performance slowdown if computers heavily utilize the network simultaneously.

Threats to a LAN environment [1] are-

- Unauthorized LAN
- Inappropriate access to LAN resources
- Disclosure of data
- Spoofing of LAN traffic
- Disruption of LAN functions

Unauthorized LAN includes poor password management for authentication, identification, known system holes. Inappropriate access to LAN resources is due to improper use of privilege mechanism for users, providing no access control for PC's on a file level basis. Disclosure of data is due to use of system default permission settings that are too permissive to users. Unauthorized Modification to data and software includes lack of a cryptographic checksum on sensitive data, lack of virus protection and detection tools. Disclosure of LAN traffic is due to lack of a cryptographic checksum on sensitive data. Spoofing of LAN traffic includes lack of a date/time stamp, lack of message authentication code mechanism or digital signature. Disruption of LAN functions includes inability to detect unusual traffic patterns (i.e. intentional flooding), inability to reroute traffic, handle hardware failures, unauthorized changes made to hardware components, improper physical security of LAN hardware.

1) Security policies for LAN

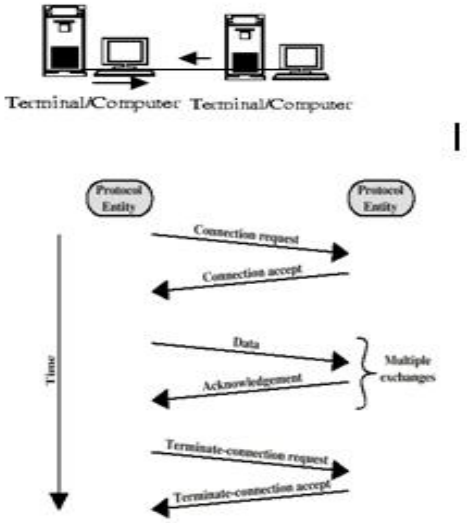

Fig. 2. Communication Methodology for Wired LAN

As shown in Fig.2 for communication, two ends must connect with each other with *handshaking* which is important to start communication. And then further communication will be proceeded. After finishing transmission established link must be disconnected.
To keep communication secure, polling, link control protocols plays an important role. Those protocols will work for buffering, routing, flow control mechanism etc.

Most factors affecting on LAN network performance are topology, load balancing, transmission media used for data transmission etc.

Hence for secure communication generally following mentioned precautions can be taken –

i. For identification and authentication, strong userid/password scheme, smartcards/smart tokens, biometrics based mechanism can be used.
ii. Restricted access to resources using grants or privileges.
iii. For data integrity various encryption technologies can be used.
iv. For logging and monitoring various LAN traffic management tools, auditing tools can be used.

2) Designing a Secure Local Area Network

To design and build a well-secured network topology, placement of hosts within the network, selection of hardware and software technologies, careful configuration of each component should be considered. Its flow is shown in Fig.3.

Here geographical arrangement, interconnection of hosts; used hardware and software, each components configuration matters largely in communication.

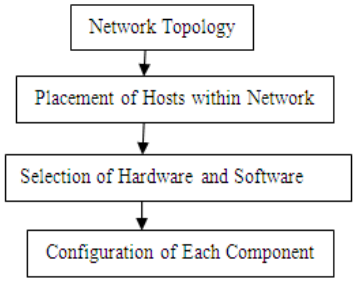

Fig.3.Secure Flow diagram for LAN

B. Telephone Network

Threats to the Public Switched Telephone Network are Service denial or disruption , unauthorized disclosure of sensitive information, Fraud, Masquerade, traffic analysis as shown in Fig.4. Due to such threats crosstalk communication, echo or other types of problems may arises.

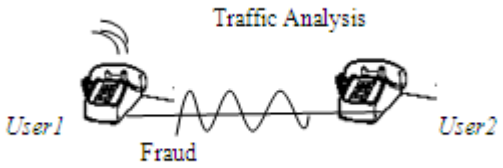

Fig.4. Threats in Telephone Network

1) Security policy in telephone network

Security policy in telephone network is achieved by using network monitoring tools. Internet Usage Monitor is used for monitoring telephone charges incurred during dial-up connections through dial-up modems.

IV. WHY FUZZY FOR NETWORK SECURITY?

Use of fuzzy logic in telecommunication systems and networks is recent and limited. Fundamentally, Zadeh's fuzzy set theory provides a robust mathematical framework for "real-world" imprecision and non-statistical uncertainty. Fuzzy logic-based approaches in network security can be used for -

Queuing : Queue stores IP packets with priority level inside routers or switches. Queue management algorithm[4] provide methods to determine order of sending data packets, control network transmission, solve congestion problem. Also it provides buffer management and packet scheduling.

Buffer Management[3] *:* It is at front of queue determining whether to drop packets or not. Its control scheme analyzed at 2 levels – data flow and data packet.

Distributed Access Control : Centralized approach has high security risk. Whereas decentralized approach provides authorization, flexibility, efficiency(n/w traffic minimized), enhanced security, resource sharing, better performance and reliability.

Load Management : Load balancing[9] is a technique to spread work between two or more computers, n/w links, CPU's, hard drives or other resources to get optimal resource utilization, throughput or response time. Using multiple components with load balancing instead of a single component increases reliability through redundancy.

Routing : Routing occurs at level 3 of OSI model. Routing determines optimal routing path through network. Routing algorithm stored in routers memory which affects on n/w performance.

Policing : Centralized policy management strategies regulate network and control traffic load for performance, efficiency and security. Various characteristics of effective policy based traffic and n/w management includes classification of n/w traffic (voice, data, audio, video) , degrees of control (rate, congestion level, bandwidth), stateful traffic inspection, user identification (IP address, hostname, login account), application identification (well known service), policy enforcement. Access control policy optimize use of shared resources.

Congestion Mitigation[6] **:** Due to inefficiency of buffer, packets may lost or overflowed. Hence implementation of connection-oriented protocols, such as TCP protocol watch for packet errors, losses, or delays in order to adjust the transmit speed.

Bandwidth Allocation : Bandwidth is the average rate of successful data transfer through a communication path. Bandwidth Allocation Protocol, along with its control protocol used to add and remove links in a multilink bundle over PPP, specifying which peer is responsible for making decisions regarding bandwidth management.

All above mentioned factors & their role for network are more important. Therefore, as present day complex networks are dynamic, hence there is great uncertainty associated with the input traffic and other environmental parameters, which subject to unexpected overloads, failures and also disobey accurate analytical modeling, hence fuzzy logic appears to be a promising approach to address many important aspects of networks.

V. CONCLUSION

According to the Fuzzy Logic Theory, everything is a matter of degree. Present day complex networks are dynamic, hence there is great uncertainty associated with the input traffic and other environmental parameters, which subject to unexpected overloads, failures and also disobey accurate analytical modeling. As Network security development system is a nonlinear task. Various parameters affecting on network security will slows down the performance of security. Hence use of fuzzy for this non linearity aspect will improves the performance of real time traffic and avoids the fragmentation problem.

VI. REFERENCES

[1] A. S. Sodiya, S. A. Onashoga, and B. A. Oladunjoye, "*Threat Modeling Using Fuzzy Logic Paradigm Issues*", in Informing Science and Information Technology Volume 4, 2007.

[2] Abbas Karimi, Faraneh Zarafshan, Adznan b. Jantan, A.R.
Ramli, M. Iqbal b.Saripan, "*A New Fuzzy Approach for Dynamic Load Balancing Algorithm*", *(IJCSIS)*

International Journal of Computer Science and Information Security, Vol. 6, No. 1, 2009

[3] *Amit Uppal, Yul Chu "An Efficient Buffer Management in a Network Interface Card*" IJCSNS International Journal of Computer Science and Network Security, VOL.6 No.7A, July 2006 .

[4] Bor-Sen Chen, Senior Member, IEEE, Sen-Chueh Peng, Member, IEEE, and Ku-Chen Wang, "*Traffic Modeling,Prediction, and Congestion Control for High-Speed Networks: A Fuzzy AR Approach*", IEEE TRANSACTIONS ON FUZZY SYSTEMS, VOL. 8, NO. 5, OCTOBER 2000.

[5] Chao-Hsien, "*Hacking Techniques in Wired Networks*".

[6] C. CHRYSOSTOMO, "*Congestion Control in Computer Networks using Fuzzy Logic*"

[7] Hua Jiang, "*Fuzzy Evaluation on Network Security Based on the New Algorithm of Membership Degree Transformation— M(1,2,3)*", JOURNAL OF NETWORKS, VOL. 4, NO. 5, JULY 2009.

[8] KEVIN BUTLER TONI FARLEY PATRICK MCDANIEL, "*A Survey of BGP Security* ".

[9] Ming-Chang Huang, S. Hossein Hosseini1 and K. Vairavan "*Load Balancing in Computer Networks"*

[10] Seyed Rasool Moosavi, "*Fuzzy based Design and tuning of distributed systems load balancing controller*"

[11] Tom Chothia, Dominic Duggan, Jan Vitek "*Type-Based Distributed Access Control*".

[12] Yuping Li, Jingyuan Yin, Guoqiang Wu, "*An Approach to Evaluating the Computer Network Security with Intuitionistic Fuzzy Information*", Advances in Information Sciences and Service Sciences, Volume3, Number7, August 2011.

[13] Zhang Lijuan Wang Qingxian, "*A Network Security Evaluation Method based on FUZZY and RST*", 2nd International Conference on Education Technology and Computer (ICETC), 2010.

Color Image Segmentation Based on a Modified Fuzzy C-means Technique and Statistical Features

R. Harrabi and E. Ben Braiek
CEREP, ESSTT, 5 Av. Taha Hussein, 1008, Tunis, Tunisia

Abstract:
In this paper, a novel method of color image segmentation based on the Fuzzy C-means algorithm and statistical features is presented. The role of including first order statistical feature vector in the Fuzzy C-means technique is studied in this paper to obtain the optimally segmented image. Instead of using the simple pixel value, feature vectors are extracted from sliding window centered on the pixels. The Fuzzy C-means (FCM) algorithm is used to cluster the obtained feature vectors into several classes corresponding to the different regions of the image. Classification accuracies of the proposed technique are compared with those of the recent techniques in literature for the same image data. The experimental results on medical and textures color images demonstrate the superiority of combining statistical features and the standard Fuzzy C-Means algorithm for image segmentation.

Keywords— Texture segmentation, Medical color image, Fuzzy Logic, Fuzzy C-means, Statistical features.

I. INTRODUCTION

The image segmentation is an essential component which determines the quality of the final results and analysis [1]. It consists in partition of an image into homogeneous regions, according to a choice criterion. In the case of color images segmentation, the used characteristic is the colorimetric components of the pixel.
Several approaches of different complexity already exist to color images segmentation [1] [2]. Until now there is no general technique that can solve all the different image segmentation types. Generally, the image segmentation approaches can be divided into four categories, thresholding, clustering, edge detection, and region extraction.
Monochrome image segmentation techniques can be extended to color image, such as histogram thresholding, clustering, region growing, edge detection, fuzzy logic and neural networks, by using RGB or their transformations (linear/non-linear) as shown in Fig. 1. Monochrome segmentation methods can be directly applied to each component of a color space, then the results can be combined in some way to obtain the final segmentation results.

Color Segmentation Approaches	=	**Monochrome Segmentation Approaches**	+	**Color Spaces**
		Histogram Thresholding, Region Based Approaches, Edge Detection Approaches, Fuzzy Approaches, Neural Networks,		RGB, YIQ, YUV, HSI, YC_bC_r CIEL*u*v*

Fig. 1. Commonly used color image segmentation approaches**.**

The acquisition of color image consists in getting three primitive colors representing the components red (R), green (G) and blue (B). The superposition of the three components gives the color original image. Different spaces colors have been developed by several authors [3] [4] [5]. These spaces are obtained by using the linear and non-linear transformations of the RGB color space. Each color representation has its advantages and disadvantages. There is still no color representation that can dominate the others for all kinds of color images yet. Nonlinear color transformations such as HSI have essential singularities which are non-removable, and there are spurious modes in the distribution of values resulting from non linear transformations. RGB is suitable for color display, but not good for color scene segmentation and analysis because of the high correlation among the R, G, and B components [6] [7]. By high correlation, we mean that if the intensity changes, all the three components will change accordingly. Hence, linear spaces are very difficult to discriminate highlights, shadows and shading in color images.
Using HSI can solve this problem to some extent except that hue is unstable at low saturation [8]. Hence, the main problem of the color image segmentation is the choice of the adapted color model for a specific application.

Several methods [9] [10], are proposed for color images segmentation including fuzzy homogeneity and fuzzy logic [3] [11] [12] [13].

In this context, S. B. Chaabane et al. [3] have proposed a method of color image segmentation based on fuzzy homogeneity and data fusion techniques. The fuzzy homogeneity vector is used to determine the fuzzy region in each primitive color, whereas, the evidence theory is employed to merge different data sources in order to increase the quality of the information and to obtain an optimal segmented image.

In the same objective, Cheng et al. [11] have provided a segmentation approach using homogeneity. In the first segmentation, uniform regions are identified via multilevel thresholding on homogeneity histogram (MTHH). An efficient peak-finding algorithm is employed to identify the most peaks histogram. In the second phase, a histogram analysis is performed for each uniform region obtained in the first phase.

Also, Cheng et al. [12], have presented a color images segmentation approach based on homogram thresholding and region merging. Fuzzy entropy is utilized as a tool to perform homogram analysis for finding all major homogeneous regions at the first stage. Then region merging process is carried out based on color similarity among these regions to avoid oversegmentation.

The key point of this approach is that homogram analysis is used to extract all major homogeneous regions at the first stage and the region merging process is performed iteratively based on color similarity among these regions to solve the problem of oversegmentation.

In another study, S. B. Chaabane et al. [13] have proposed a method of color images segmentation based on fuzzy c-means and data fusion techniques (FCMDS). The fuzzy algorithm is used to determine the membership degrees of each pixel covering the three components images (R, G and B), whereas, the evidence theory is employed to merge different data sources in order to increase the quality of the information and to obtain an optimal segmented image.

Furthermore, a combination of different segmentation approaches is often utilized for color image segmentation. In this context, Y. Lim et al. [14] have proposed a color image segmentation method based on the thresholding and the fuzzy c-means (FCM) techniques. The methodology uses a coarse-fine concept to reduce the computational technique burden required for the FCM.

The coarse segmentation attempts to segment coarsely using the thresholding technique wile the fine segmentation assigns the pixels, which remain unclassified after the coarse segmentation, to the closest class using the FCM. In this context, S. B. Chaabane et al. [15] have presented a color image segmentation approach based on automatic thresholding and the Fuzzy C-Means Techniques (ATFCM). The FCM algorithm is used to extract homogeneous region in each primitive color, and the fuzzy combination rule is applied to obtain the final segmentation results.

The most widely used clustering method is the Fuzzy C-Means (FCM) algorithm, which is a "fuzzy relative" to the simple C-means technique [16]. There has been considerable interest, recentlys, in the use of fuzzy segmentation methods, which retains more information from the original image than hard segmentation methods. The Fuzzy C-means algorithm (FCM), in particular, can be used to obtain a segmentation via fuzzy pixel classification. Unlike hard classification methods which force pixels to belong exclusively to one class, FCM allows pixels to belong to multiple classes with varying degrees of membership. A major disadvantage of its use in imaging applications, however, is that FCM does not incorporate information about spatial context, causing it to be sensitive to noise and other imaging artifacts.

Recently, some approaches [17] [18] have been proposed for increasing the robustness of FCM to noise by directly modifying the objective function. In this context, Raghu et al. [19] reformulate the fuzzy clustering problem so that the clustering method can be used to generate memberships with typical interpretation. They argue that the existing fuzzy clustering methods do not provide appropriate membership values for applications in which memberships are to be interpreted as degrees of compatibility or possibility. For that, the authors formulate a new algorithm by modifying the objective function in the fuzzy C-means algorithm to obtain a good possibilistic partition of the data.

Also, Liew et al. [17] have provided a new dissimilarity index that considers the influence of the neighboring pixels on the center pixel, this in the goal to replace the conventional normed distance in the FCM algorithm. However, this method can handle only a small amount of noise [20]. With the same objective, Ahmed et al. [21] have introduced a regularization term into the standard FCM to impose neighborhood effect. Later, Li et al. [18] incorporated this regularization term into the adaptive FCM (AFCM) algorithm [22] to overcome the noise sensitivity of AFCM algorithm. Although this method is promising, it is computationally expensive that means more consuming time is needed during the computation.

In this paper an investigation of how the user can choose the best statistical features for segmenting the color images using the fuzzy C-means algorithm is described. This work may be seen to be straightforwardly complementary to that in the paper proposed by M. Sayadi et al. [23]. In their paper, the authors have proposed a clustering method for grey level texture segmentation based on a modified fuzzy C-means algorithm. Hence, this paper is devoted to this task, applied to colour image segmentation that contains more than two classes. The idea is based on the fuzzy C-means algorithm and the statistical features.

Instead of using the simple pixel value in the FCM method, we propose in this paper to extract a feature vector from a sliding window centred on the pixels. The Fuzzy C-means algorithm is modified and used to cluster the obtained feature vectors into

several classes corresponding to the different regions of the image. This technique allows obtaining excellent color image segmentation results, superior to the classical version of the FCM algorithm [24].
The rest of the paper is organized as follow: Section 2 briefly describes the Fuzzy C-means algorithm. Section 3 gives a detailed description of the proposed MFCM method. The experimental results and discussions are in section 4. Finally, conclusions are in section 5.

Ii. Ecall of the fuzzy c-means clustering

The Fuzzy C-means (FCM) [25], an unsupervised clustering algorithm, has been applied successfully to a number of clustering problems. The algorithm minimizes the objective function for the partition of data set, $X = \{x_1, x_2, ..., x_n\} \subset R^s$, given by:

$$J_m(u,v) = \sum_{k=1}^{n}\sum_{i=1}^{c} u_{ik}^m d^2(x_k, v_i) \qquad (1)$$

with

$$\sum_{i=1}^{c} u_{ij} = 1, \quad 1 \le j \le n \qquad (1a)$$

$$u_{ij} \ge 0, \quad 1 \le i \le c, 1 \le j \le n \qquad (1b)$$

$$\sum_{j=1}^{n} u_{ij} > 0, \quad 1 \le i \le c \qquad (1c)$$

where $X = \{x_1, x_2, ..., x_n\} \subset R^s$, s is the dimension of space, n is the number of samples, c is the number of clusters $(1 \le c \le n)$, m is the fuzzy factor $(m > 1)$, $d_{ij} = \|x_j - v_i\|$ is the distance between the sample x_j and clustering center v_i, $v_i \subset R^s$ with $(1 \le i \le c)$. u_{ij} is the membership of the j[th] sample to the i[th] clustering center, $U = \{u_{ij}\}$ is a matrix of size (c×n). $V = [v_1, v_2, ... v_c]$ is a matrix of size (c×s).

The FCM algorithm minimizes the objective function $J_m(u,v)$ with respect to the membership functions u_{jk} and the centroids v_k. The FCM clustering technique can be summarized by the following steps:

- Input an $N \times M$ image with gray levels *zero* to *255*.

Step 1: Initialization (iteration 0)
Scan the image line by line to construct the vector X containing all the gray level of the image.
Randomly initialize the centers of the classes vectors V(0)
From the iteration t=1 to the end of the algorithm:

Step 2: Calculate the membership matrix U(t) of element u_{ik} using (2a):

$$u_{ik} = \frac{1}{\sum_{j=1}^{c} \left(\frac{d_{ik}}{d_{jk}}\right)^{\frac{2}{m-1}}} \qquad (2a)$$

u_{ik} is a matrix of size (c×n)

Step 3: Calculate the vector V(t) =[v_1, v_2,…,v_c] using:

$$v_i = \frac{\sum_{k=1}^{n} u_{ik}^{m} x_k}{\sum_{k=1}^{n} u_{ik}^{m}}$$

(2b)

Step 4: Convergence test:

If $\left\| V^{(t)} - V^{(t-1)} \right\| > \varepsilon$, then increment the iteration t, and return to the step 2, otherwise, stop the algorithm. ε is a chosen positive threshold.

The algorithm above can also start from membership matrix $U^{(0)}$.

III. The proposed method

Recently, most analytic fuzzy approaches have been derived from Bezdek's Fuzzy C-means (FCM) [26]. The FCM algorithm is an iterative clustering method that produces a C partition by minimizing the weighted within group sum of squared error objective J_m. Like the Hard C-means algorithm, the Fuzzy C-means aims to minimize an objective function.

On the other hand, this algorithm has a considerable drawback in noisy environments, and the memberships degree resulting from FCM do not correspond to the intuitive concept of belonging or compatibility. Also, the Hard C-means (HCM) [27] is one of the oldest clustering methods. This method is used to learn the prototype of clusters or classes, and the cluster centers are used as prototypes. But, HCM memberships are hard (i. e, 1 or 0).

However, the Fuzzy C-means algorithm is better than the Hard C-means (HCM) algorithm, since in HCM algorithm feature vectors of the data's set can be partitioned into hard clusters, and the feature vector can exactly be a member of one cluster only.

Instead, the FCM relaxes the condition, and allows the feature vector to have multiple membership grades to multiple clusters, Suppose the data set with known clusters and a data point which is close to both clusters but also equidistant to them. Fuzzy clustering gracefully copes with such dilemmas by assigning this data point equal but partial memberships to both clusters, that is the point may belong to both clusters with some degree of membership grades varies from 0 to 1.

However, in an image processing system an image or its derivatives can be represented in various feature spaces. An image can be represented in terms of pixels, which are associated with a location and a gray level value. It can also be represented by its derivatives, e.g., regions with features like average greyscale value, standard deviation, variance, entropy, third order moment, gradient, etc. Features for clustering can be extracted from regions masked by a window $(n \times n)$. By applying FCM, a partition of the feature vectors into new regions can

be found. Combination of statistical features characterization and fuzzy clustering has some advantages for both techniques.

A. Modified FCM method (MFCM method)

The purpose of segmentation is to partition the image into homogeneous regions. In this paper, we employ the MFCM algorithm to cluster the feature vectors into several classes with every class corresponding to one region in the segmented image. The MFCM algorithm is applied to the Hue component of the original image represented in HSI color space. The idea is to replace the vector *X* used in the image segmentation method based on the pixel value and the FCM algorithm by a matrix *F* containing the same number of lines, i.e. *n*, but with 4 columns. These columns contain 4 statistical features extracted from the sliding window centered around every pixel. Hence, this algorithm scans the image using a (n×n) sliding window, as shown in Fig. 2, from left to right and top to bottom. A feature vector is extracted from each block.

However, the selection of the best attributes is based on the characterization degree (≠) [28]. This criterion is based on the report/ratio of the between classes (inter-class) variance by the intraclass variance.

Assume $y_{k,n}$ is the n^{th} feature vector estimated for the k^{th} image class $(1 \le k \le 12,\ 1 \le n \le 100)$, k is the number of images and n is the imagettes number of each image.

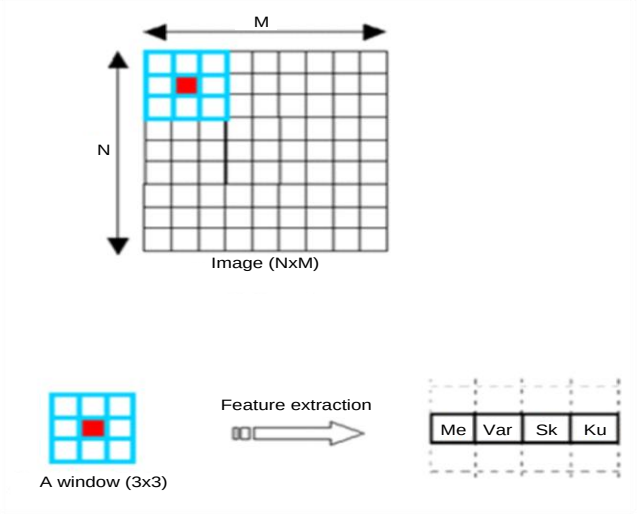

Fig. 2. Features extraction using a sliding window

The mean of the feature m_k vectors is calculated for the k^{th} image class as follow:

$$m_k = \frac{1}{100}\sum_{k=1}^{100} y_{k,n} \quad (3)$$

and the total mean of the features vectors m_c is determined as follow:

$$m_c = \frac{1}{12}\sum_{k=1}^{12} m_k \quad (4)$$

The mean of the intraclass dispersion matrices which represents the maximum likelihood estimation of the covariance matrix of the class, is given by the matrix:

$$S_{intra} = \frac{1}{1200}\sum_{k=1}^{12}\sum_{n=1}^{100}(y_{k,n} - m_k)(y_{k,n} - m_k)^t \quad (5)$$

whereas, the mean of the between (inter-class) dispersion matrices which describes the scattering of the class sample means is computed using:

$$S_{inter} = \frac{1}{12}\sum_{k=1}^{12}(m_k - m_c)(m_k - m_c)^t \quad (6)$$

Consequently, the characterization degree (Ψ) is given by:

$$\Psi = \text{trace}\,(S_{intra}^{-1}.S_{inter}) \quad (7)$$

In the present study, the best features are the mean *Me*, the variance *Var*, the third order moment *Sk* and the forth order moment *Ku* of the window.

Assume $g(i,j)$ is the intensity of a pixel $p(i,j)$ at the location (i,j) in an $(N \times M)$ image, w_{ij} is a size $(t \times t)$ window centred at pixel $p(i,j)$.

A feature vector for a pixel is then extracted from the windowed block. The 4 features extracted from the window centered at pixel (i,j) are given by the following equations:

$$Me = \frac{1}{t \times t}\sum_{k=-\frac{t-1}{2}}^{\frac{t-1}{2}}\sum_{l=-\frac{t-1}{2}}^{\frac{t-1}{2}} g(k+i, l+j) \quad (8)$$

$$Var = \frac{1}{t \times t} \sum_{k=-\frac{t-1}{2}}^{\frac{t-1}{2}} \sum_{l=-\frac{t-1}{2}}^{\frac{t-1}{2}} (g(k+i, l+j) - Me)^2 \qquad (9)$$

$$Sk = \frac{1}{t \times t} \sum_{k=-\frac{t-1}{2}}^{\frac{t-1}{2}} \sum_{l=-\frac{t-1}{2}}^{\frac{t-1}{2}} (g(k+i, l+j) - Me)^3 \qquad (10)$$

$$Ku = \frac{1}{t \times t} \sum_{k=-\frac{t-1}{2}}^{\frac{t-1}{2}} \sum_{l=-\frac{t-1}{2}}^{\frac{t-1}{2}} (g(k+i, l+j) - Me)^4 \qquad (11)$$

where $(t \times t)$ and $g(i, j)$ are respectively the size of sliding window and the gray scale value of pixel $p(i, j)$, $\frac{t+1}{2} \leq i \leq N - \frac{t-1}{2}$ and $\frac{t+1}{2} \leq j \leq M - \frac{t-1}{2}$.

Notes that t must have an odd value to obtain a centered window around each pixel. So, the fuzzy C-means algorithm is used to cluster the obtained feature matrix *F* into *c* different classes. Every class corresponds to one region in the segmented image. The spatial scanning order of an image is performed, as shown in Fig. 3, pixel by pixel from left to right and top to bottom.

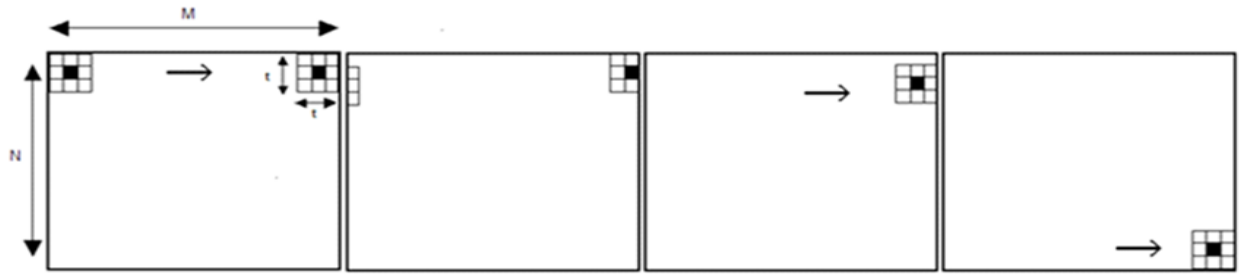

Fig. 3. The adaptive sliding window from left to right and top to bottom

However, the size of the window has an influence on the calculation of the feature vectors. The window should be big enough to allow enough information to be involved in the computation of the feature vectors. As shown in Fig.9, the regions are identified by MFCM method using a (3x3) window for computing the feature vector (see Fig. 9(b)), but are not signified using a (5x5) and (7x7) window (see Fig 9(c) and Fig. 9(d), respectively). Experimentally, a (3×3) window for computing the feature vector is chosen.

The proposed image segmentation technique using the FCM algorithm combined with the statistical features can be summarized by the following steps:

- Input an $N \times M$ image

Step 1: Initialization (iteration 0)

Randomly initialize the centers of the classes vectors V(0) of size $(c \times 4)$ containing the centers of the classes.

Step 2: Compute the matrix F of size $(n \times 4)$ containing the statistical features extracted from the image.

From the iteration t=1 to the end of the algorithm:

Step 3: Calculate the membership matrix U(t) of element u_{ik} using (12):

$$u_{ik} = \frac{1}{\sum_{j=1}^{c} \left(\frac{\|F_k - v_i\|}{\|F_k - v_j\|} \right)^{\frac{2}{m-1}}} \quad (12)$$

In the modified method, F_k and v_i are vectors of size (1×4).

Step 4: Calculate the matrix V(t) composed of 4 columns v_i using:

$$v_i = \frac{\sum_{k=1}^{n} u_{ik}^m F_k}{\sum_{k=1}^{n} u_{ik}^m} \quad (13)$$

Step 5: Convergence test:

If $\|V^{(t)} - V^{(t-1)}\| > \varepsilon$, then increment the iteration t, and return to the step 3, otherwise, stop the algorithm. ε is a chosen positive threshold.

B. Fuzzy segmentation using color feature hue

Color is perceived by human as a combination of tristimuli R (red), G (green) and B (blue) which are usually called three primary colors.

From RGB, we can calculate different kinds of color representations by using linear or nonlinear transformations. Several color representations (spaces) such as RGB, HSI, CIEL*u*v*, etc., are employed for color segmentation, but none of them can dominate the others of all kinds of colors images.

Each color representation has its advantages and disadvantages. Nonlinear color transformations such as HSI and normalized color space have essential singularities which are non-removable, and there are spurious modes in the distribution of values resulting from nonlinear transformations. The major problem of linear color spaces is the high correlation of the three components, which makes them dependent upon each other and associates strongly with intensity. Using HSI can solve this problem to some extent except that hue is unstable at low saturation [29].

The HSI system separates color information of an image from its intensity information. Color information is represented by hue and saturation values, while intensity, which describes the brightness of an image, is determined by the amount of the light. Hue is the most useful attribute in color segmentation since it is less influenced by the nonuniform illumination such as hade, shadow, or reflect lights [30].

Hue can be obtained by a nonlinear transformation from R, G and Blue color features [31]:

$$Hue = \arctan\left(\frac{\sqrt{3}(G - B)}{(R - G) + (R - B)} \right) \quad (14)$$

Hue represents basic colors, and is determined by the dominant wavelength in the spectral distribution of light wavelengths. It reflects the predominant color of an object and has a great capability in subjective color perception [32].

In our application, instead of using the segmentation method based on the pixel gray-level value and the standard FCM algorithm, we propose in this paper to extract a feature vector from a sliding window centered on the pixel of the color feature hue. The fuzzy c-means clustering technique is then used to cluster the obtained feature vectors into several classes with every class corresponding to one region in the segmented image. Therefore, the pixels are divided into several groups with each group having similar colors. The proposed method can be described by a flowchart given in Fig. 4.

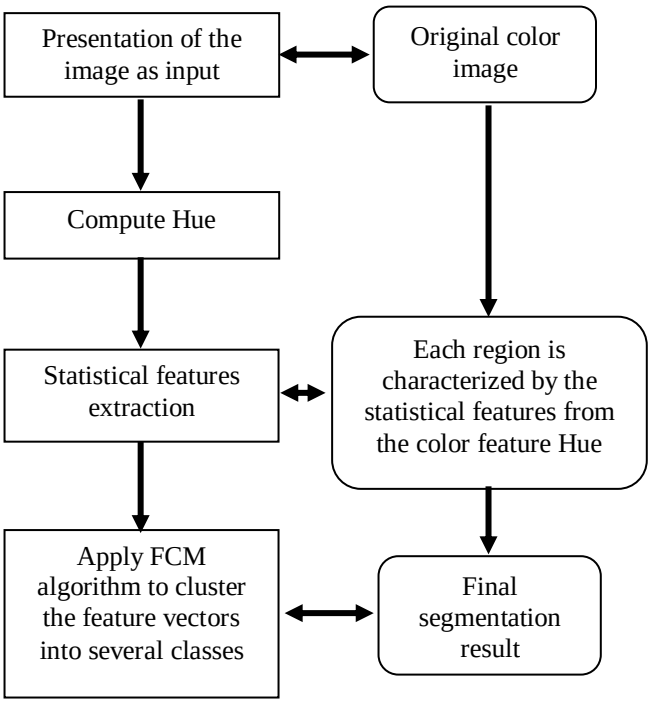

Fig. 4. Flowchart of the proposed method

IV. Experimental results

In order to illustrate the method presented in the previous section, a large variety of medical and synthetic colour images (Fig. 5) are employed in our experiments. Also, several simulation results of color image segmentation illustrating the ideas presented in the previous section are performed.

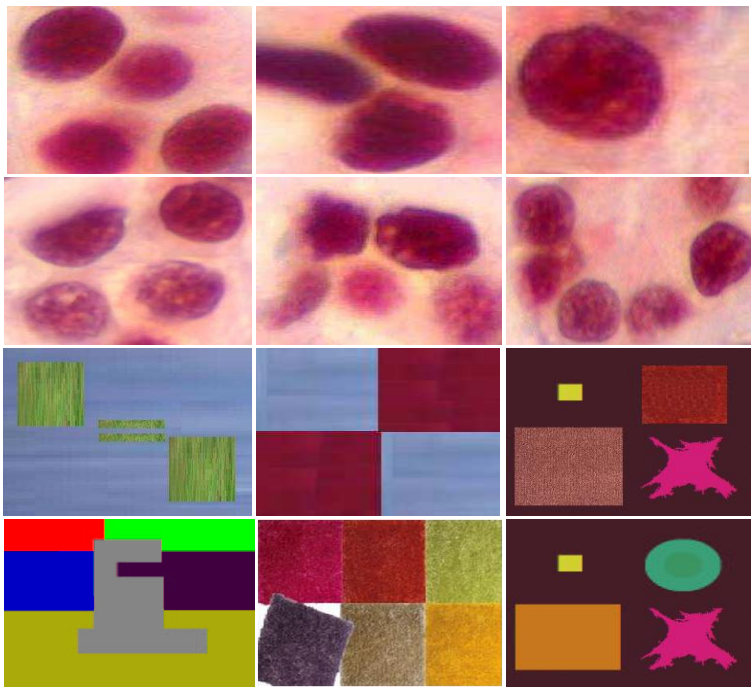

Fig. 5. Data set used in the experiment. Twelve images were selected for a comparison study. The patterns are numbered from 1 to 12, starting at the upper left-hand corner.

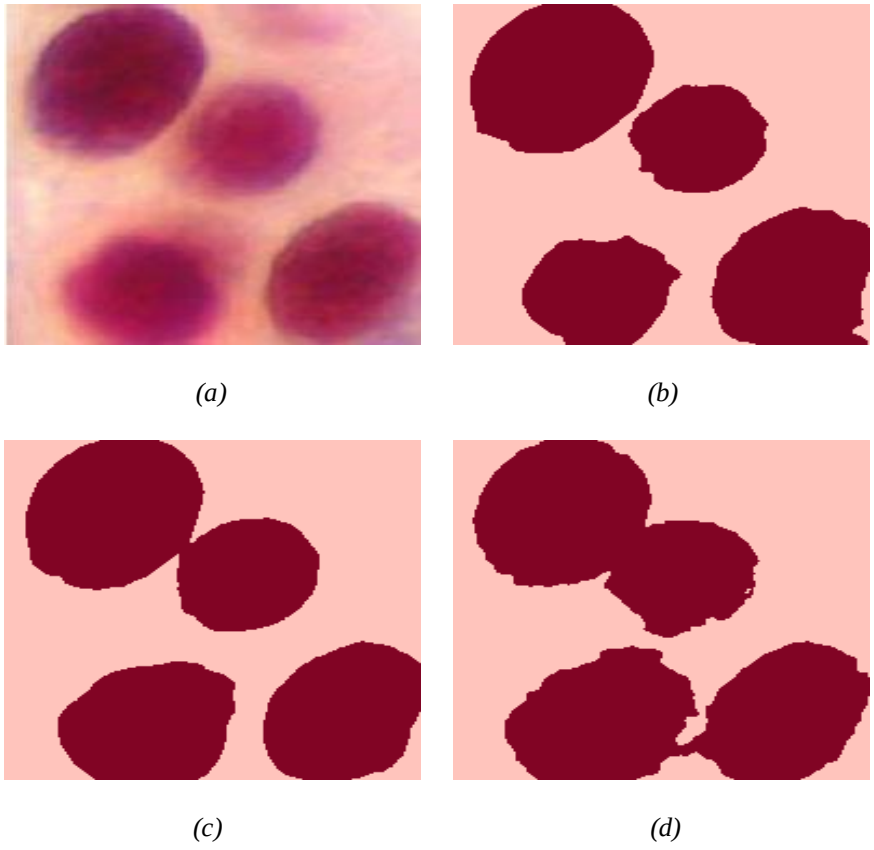

(a) *(b)*

(c) *(d)*

Fig. 6. Segmentation results on a colour image, (a) Original image (256x256x3) with gray level spread on the range [0,255]. (b) Red resulting image by MFCM method. (c) Green resulting image by MFCM method. (d) Blue resulting image by MFCM method.

Some experimental results are shown in Figs. 6-12. The images are originally stored in RGB format. Each of the primitive colors (red, green and blue) is represented by 8 bits and has an intensity ranging from 0 to 255.
In order to evaluate the performance of the proposed method based segmentation algorithm on color cells images segmentation, the segmentation results of the datasets are described in this section. Consequently, a synthetic image dataset is developed and used for numerical evaluation purpose.
Figs. 6-12 demonstrate the results of the proposed approach. Fig. 6 presents the segmentation results in the RGB color space by applying the MFCM algorithm to the red, green and blue color features, respectively.
In this case, a region is recognized in red component but is not identified by green and blue components. This shows that the RGB space has a strong correlation of its three components, and hence, the use of a single information source leads to bad results.
Comparing the results, we can find that the cells are much better segmented in (b) than those in (c) and (d). Also, the first resulting images contain some missing features in one of the cells, which do not exist in the other resulting images.

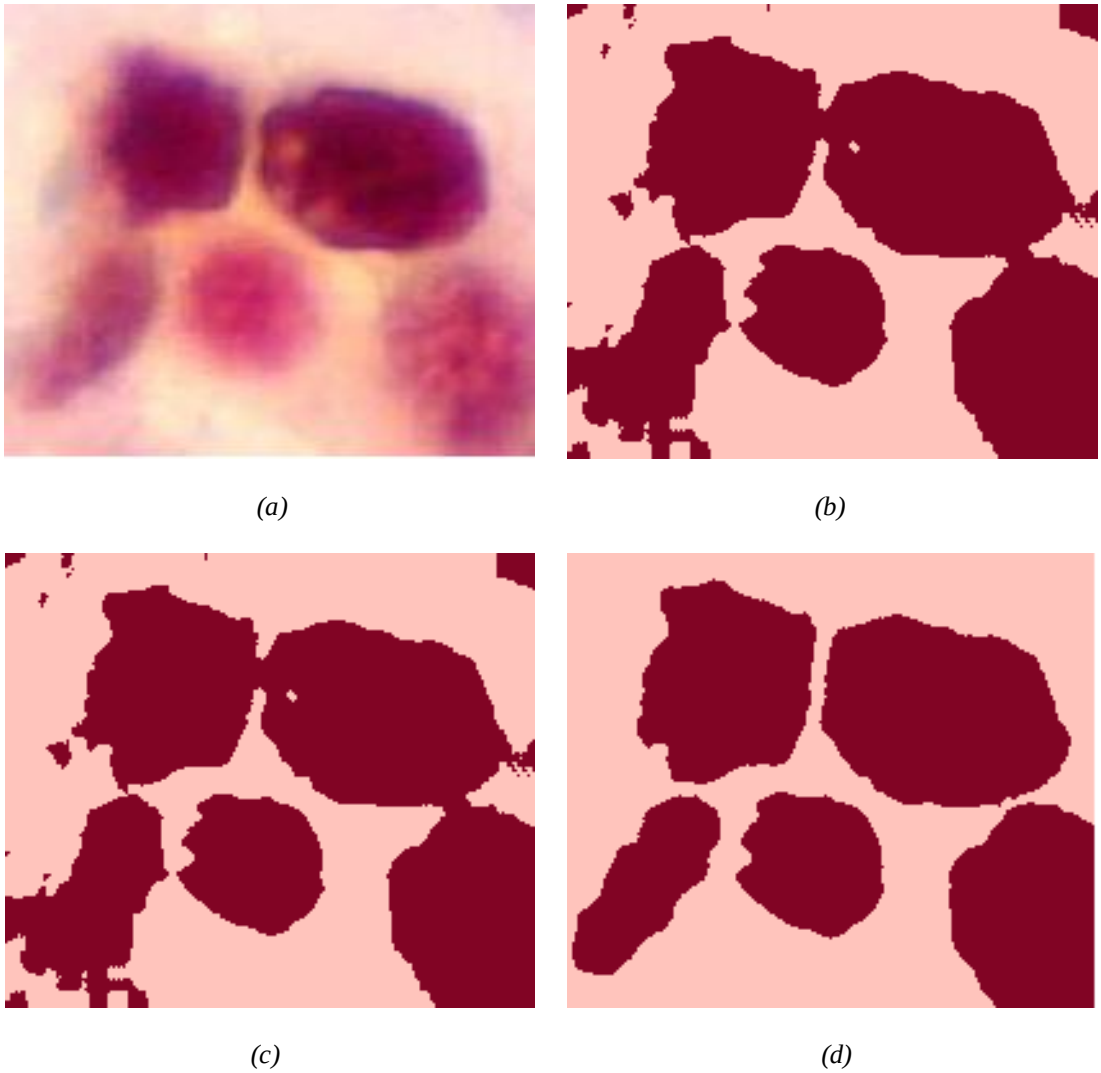

(a) *(b)*

(c) *(d)*

Fig. 7. Comparison of the proposed segmentation method with other existing methods on a medical image (2 classes, 1 cell), (a) Original image with RGB representation (256x256x3), (b) Hue resulting image by HCM method (c) Hue resulting image by FCM method, (d) Hue resulting image by MFCM method (our method).

The experimental results indicate that the proposed approach, which combines statistical features and the standard Fuzzy C-Means clustering algorithm, is better than the traditional methods (HCM and FCM). As shown in Fig. 7, the cells are better recognized by the proposed approach. The difference of the segmentation result lies in the combination of statistical features and the fuzzy classification.

The pixels of the cells are grouped into the same region in the color segmentation based on FCM algorithm due to the similarity of the statistical features from each block on the color feature hue.

In fig. 7, the red color of the cells is identified by the proposed approach (see fig. 7(d)), but is not signified by the traditional approaches (see fig. 7(b) and fig. 7(c)).

In fact, the experimental results indicate that the proposed method, which combines the statistical features and the fuzzy classification, is more accurate than the traditional methods (HCM and FCM) in terms of segmentation quality as denoted by the segmentation sensitivity, see Table 1.

TABLE I
Segmentation sensitivity from HCM algorithm, FCM algorithm and MFCM method for the Data set Shown in Fig. 5

	HCM	FCM	MFCM
	Segmentation sensitivity (%)		
Image 1	80.41	90.21	94.54
Image 2	64.74	85.12	88.88
Image 3	72.10	80.25	91.10
Image 4	82.14	86.52	97.64
Image 5	74.89	89.25	95.12
Image 6	75.45	85.74	90.80
Image 7	69.95	77.84	96.92
Image 8	72.12	84.74	90.50
Image 9	87.32	92.21	98.04
Image 10	78.74	84.01	95.80
Image 11	86.41	91.78	97.55
Image 12	83.73	93.47	98.21

For purpose of comparison, we apply the proposed approach and some existing approaches to the same color image segmentation. The latter methods include those of Cheng and Sun (*THH*) [11], Ben Chaabane et al. (*DSFCM*) [13], Lim and Lee (*TFCM*) [14], J. C. Bezdek (*FCM*) [26] and R. Duda et al. (*HCM*) [27]. The segmentation results are shown in Figs. 8, 9, 10, 11 and 12.
Figure 8 shows a comparison of the results between the traditional methods HCM [27], FCM [26], and the proposed method. They correspond, respectively, to Fig. 8(c), Fig. 8(d) and Fig. 8(e).
In fact, obviously a better result is obtained by the proposed method due to the combination of statistical features and the fuzzy classification, as shown in Fig. 8(e).

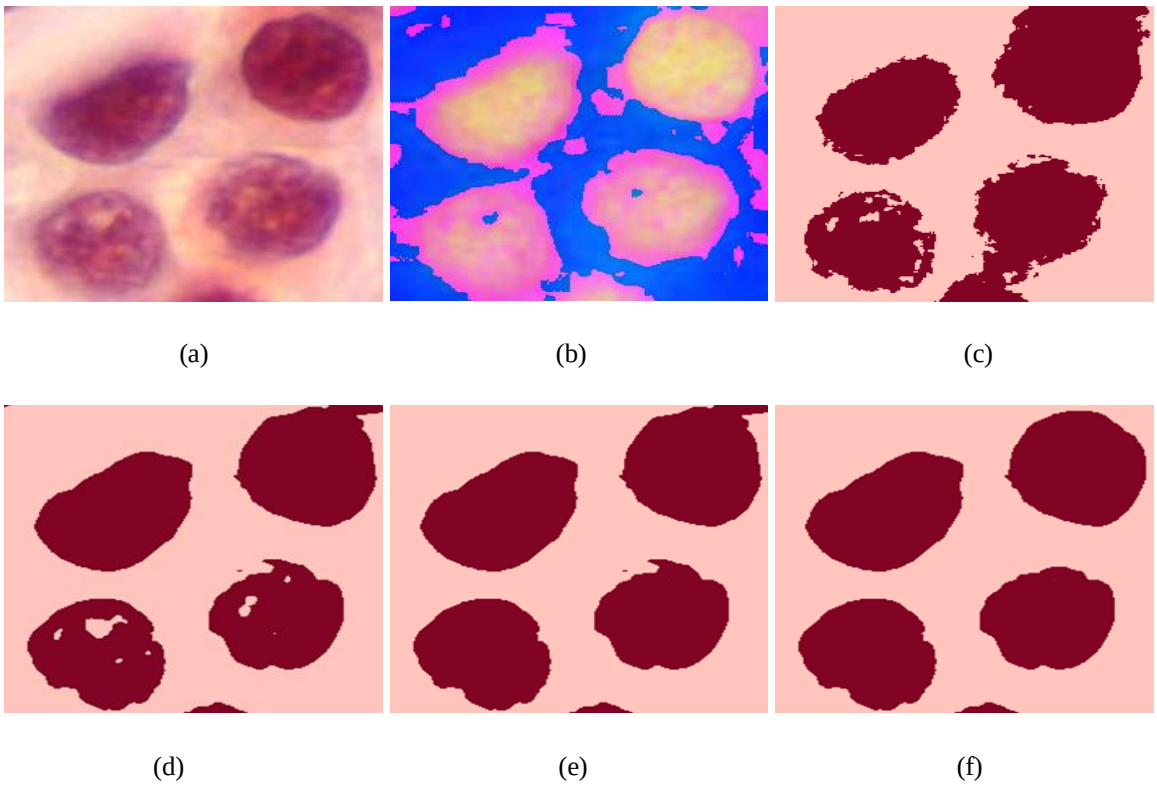

(a) (b) (c)

(d) (e) (f)

Fig. 8. Comparison of the proposed segmentation method with other existing methods on a medical image (2 classes), (a) Original image with RGB representation (256x256x3), (b) Original image with HSI representation (256x256x3), (c) Hue

resulting image by HCM method (d) Hue resulting image by FCM method, (e) Hue resulting image by MFCM method, (f) reference segmented image. (The various medical images used in this paper are provided with permission fromCancer Service, Salah Azaiez Hospital, Bab Saadoun, Tunis, Tunisia).

Comparing Figs 8(c), 8(d), and 8(e), we observe that the two regions are correctly segmented in Fig 8(e), showing that the quality of the segmentation result is much improved by combining statistical features and the Fuzzy C-means algorithm.
It can be seen from Table 1 that 17.86% and 13.48% of the pixels were incorrectly segmented by HCM and FCM based methods, respectively, but only 02.36% are incorrectly segmented pixels by our proposed method.
Comparing Fig. 8(c) and 8(d) with 8(e), we can see that the image resulting from the proposed method is clearer than the one resulting from the HCM and FCM based methods.
To evaluate the performance of the proposed segmentation algorithm, its accuracy was recorded.
Regarding the accuracy, Tables 1 and 2 list the segmentation sensitivity of the different methods for the data set used in the experiment.
The segmentation sensitivity [33] [34] (Sens %) is computed using:

$$Sens = \frac{Np_{cc}}{N \times M} \times 100 \qquad (15)$$

where: Sens, Npcc and N×M correspond to the segmentation sensitivity (%), number of correctly classified pixels and the image sizes, respectively.

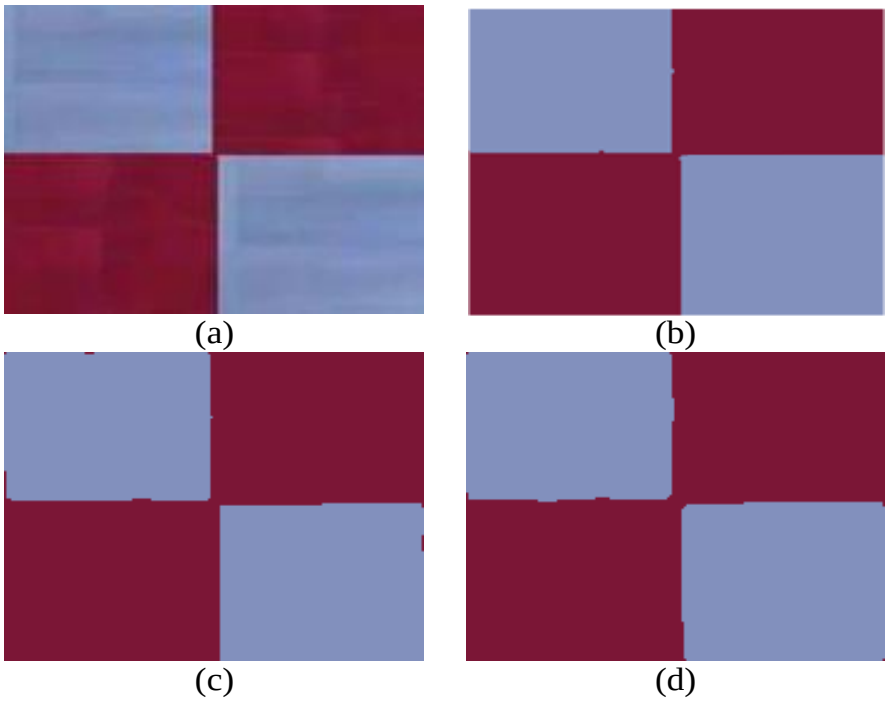

Fig. 9. Segmentation results on a colour image, (a) Original image (256x256x3) with gray level spread on the range [0,255]. (b) Resulting image by MFCM method using a (3x3) window for computing the feature vector. (c) Resulting image by MFCM method using a (5x5) window for computing the feature vector.. (d) Resulting image by MFCM method using a (7x7) window for computing the feature vector.

The correctly classified pixel denotes a pixel with a label equals to its corresponding pixel in the reference image as shown in Fig. 8 (f). The labeling of the original image is generated by the user based on the image used for segmentation. Consequently, the image segmentation ground truths is generated manually by the doctor (specialist) using the original image. Fig. 8(f) shows the ideal segmented image.
To provide insights into the proposed method, we have compared the performance of the proposed method with those of the corresponding Hard and Fuzzy C-Means algorithms. The method was also tested on synthetic images and compared with other existing methods based on fuzzy homogeneity (*THH*) [11], data fusion techniques (*DSFCM*) [13] and a modified FCM algorithm (*TFCM*) [14].

The comparison of the proposed approach will be presented through the next experiment. Fig. 10(c), (d), (e) and (f) show the final segmentation results obtained from the *THH* method, the *DSFCM* method, the *TFCM* method and the *MFCM* method, respectively, when a ‘’salt and pepper” noise of *D* density is added to the original image *I*, shown in Fig. 10(a). This affects approximately ($D \times (N \times M)$) pixels. The value of *D* is 0.02.

As shown in fig. 10(c), the fuzzy homogeneity approach (*THH*) is applied to Hue component to partition the color space into several clusters.

However, the cells and the background are not correctly segmented in Fig. 10(c). This indicates that the segmentation results depend on the optimal threshold selection.

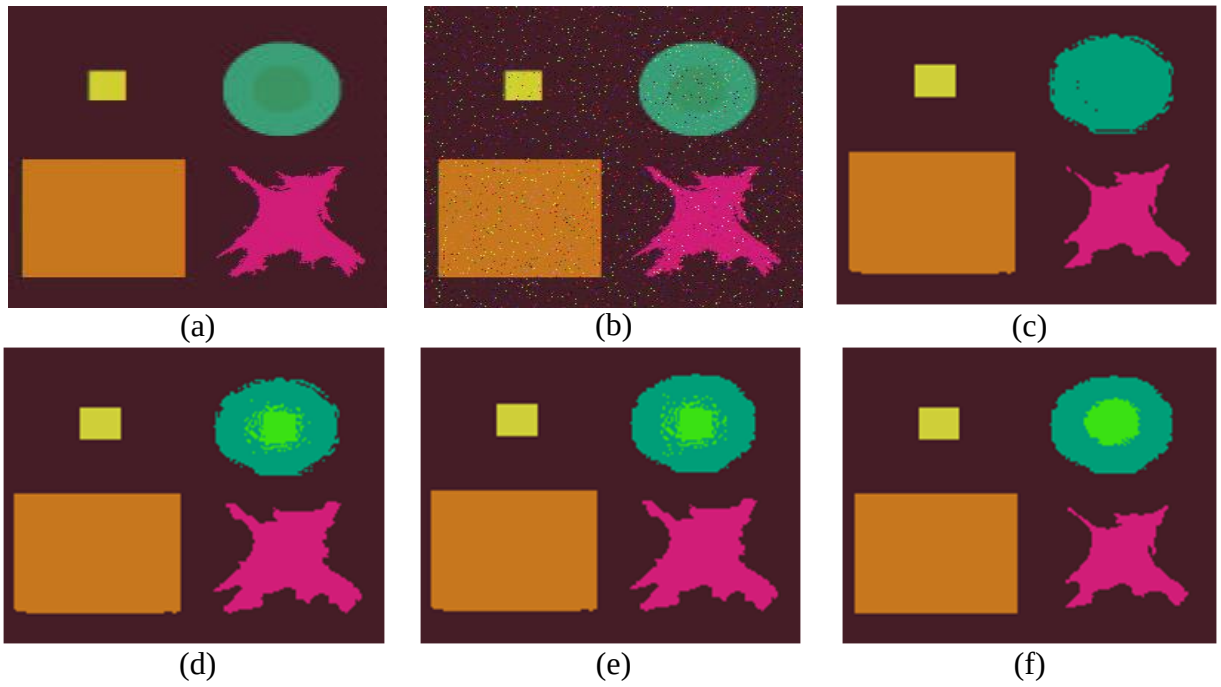

Fig. 10. Comparison of the proposed segmentation method with other existing methods on a synthetic image (6 classes), (a) Original image with RGB representation (256x256x3), (b) Original image (256x256x3) disturbed with a “salt and pepper” noise and with grey level zero to 255 of each primitive colors, (c) Hue resulting image by THH method (d) Hue resulting image by DSFCM method, (e) Hue resulting image by TFCM method, (f) Hue resulting image by MFCM method (our method).

TABLE II

SEGMENTATION SENSITIVITY FROM THH METHOD, DSFCM METHOD, TFCM METHOD AND MFCM METHOD FOR THE DATA SET SHOWN IN FIG. 5

	THH	DSFCM	TFCM	MFCM
	Segmentation sensitivity (%)			
Image 1	92.45	93.88	90.80	94.54
Image 2	87.09	87.89	86.42	88.88
Image 3	84.55	88.54	82.11	91.10
Image 4	91.29	95.16	89.20	97.64
Image 5	92.37	93.97	90.89	95.12
Image 6	88.09	90.20	87.45	90.80
Image 7	93.41	95.01	79.65	96.92
Image 8	82.77	86.44	87.08	90.50
Image 9	95.97	97.15	94.78	98.04
Image 10	95.09	96.52	94.92	95.80
Image 11	94.64	95.03	93.10	97.55
Image 12	96.18	97.01	94.09	98.21

Also, the segmentation method based on the thresholding and the fuzzy c-means techniques (*TFCM*), do not consider the spatial dependencies among the pixels, there are some isolated pixels that are remaining (see fig. 10(d)).
Furthermore, the methods based on data fusion techniques (*DSFCM*) require a lot of computation time, due to the large number of iterations and the number of operations (multiplications, addition and exponent) that are necessary for the computation of the mass functions for the simple and composite classes, and the performance of such a segmentation scheme is largely conditioned by the appropriate estimation of mass functions in the DS evidence theory (see fig. 10(e)).
Comparing Figs 10(c), 10(d), 10(e) and 10(f), we observe that the two regions are correctly segmented in Fig 10(f), showing that the new method is very efficient for color images segmentation.
It can be seen from Table 2 that 03.82%, 02.99% and 0.5.91% of the pixels were incorrectly segmented by *THH*, *DSFCM* and *TFCM* based methods, respectively, but only 01.79% are incorrectly segmented pixels by our proposed method. Comparing Fig. 10(c), 10(d) and 10(e) with 10(f), we can see that the image resulting from the proposed method is much more clearer than the one resulting from the *THH*, *DSFCM* and *TFCM* based methods.
The segmentation sensitivity values reported in Table I and 2 are plotted in Figures 11 and 12, respectively.
Figure 11 shows three segmentation sensitivity plots using traditional methods such as HCM and FCM compared with the proposed method plot.
Figure 12 shows three other segmentation sensitivity plots using traditional methods such as THH, DSCM and TFCM compared with the proposed method plot.
As seen on both Figures 11 and 12, the proposed method plot is clearly located on the top of the other methods plots.

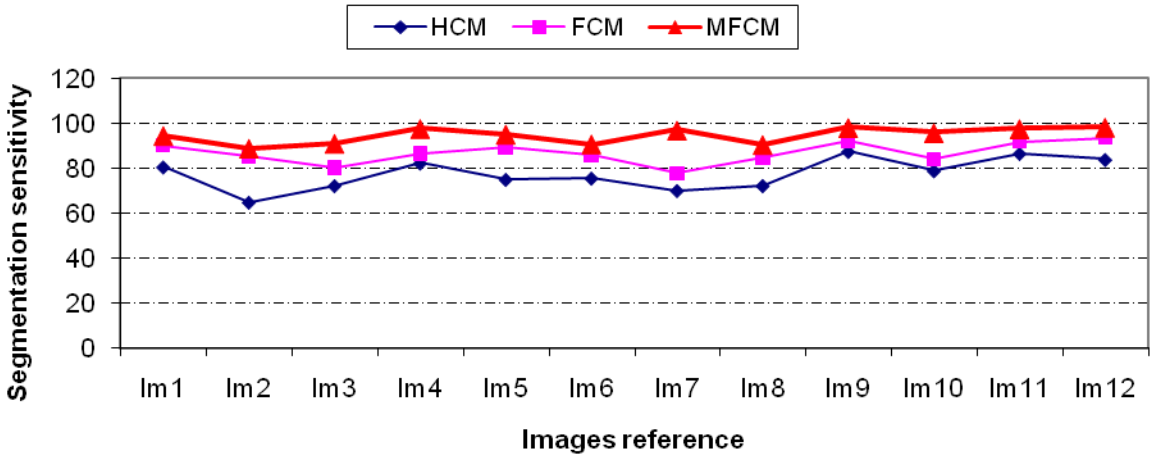

Fig. 11. Segmentation sensitivity plots using HCM algorithm, FCM algorithm and MFCM method for the Data set Shown in Fig. 5.

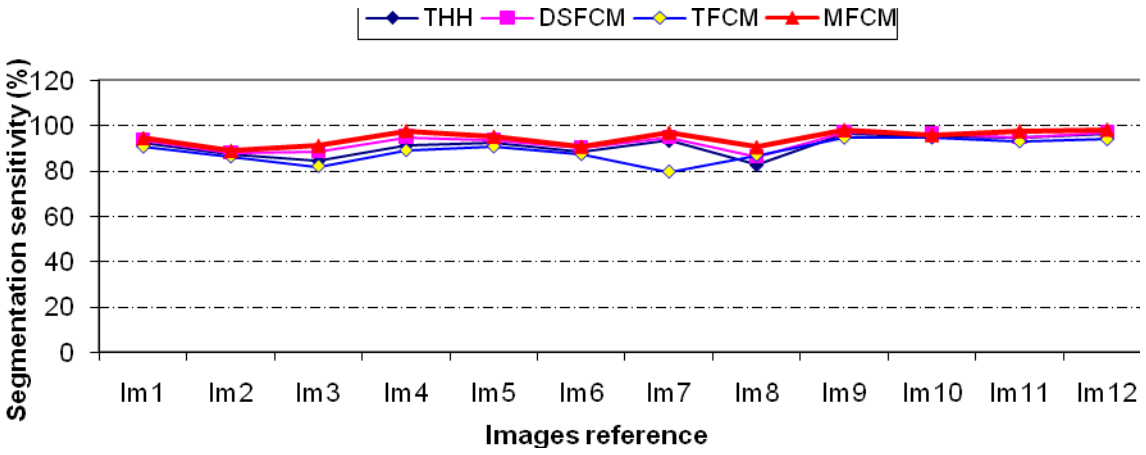

Fig. 12. Segmentation sensitivity plots using THH method, DSFCM method, TFCM method and MFCM method (our method) for the Data set Shown in Fig. 5.

Referring to segmentation sensitivity plots given in Fig. 11, one observes that 25.11% and 10.75% of pixels were incorrectly segmented in Figs. 7(b) and 7(c), respectively, but only 04.88% are incorrectly segmented pixels by our proposed method. Comparing Fig. 7(b) and 7(c) with 7(d), the resulting image by the proposed method is much more clearer than the one given by the HCM and *FCM* based methods.
Hence, the experimental result presented in Fig. 7(d) is quite consistent with the visualized color distribution in the objects, which makes it possible to take an accurate measurement of the cells volumes [35].

V. Conclusion

In this paper, we propose a new fuzzy classification method to color image segmentation. In the first phase, the feature vector containing the statistical features is identified in each block on the color feature hue. While the feature vector is calculated in each block, the Fuzzy C-means algorithm is used to cluster the feature vectors into several classes with every class corresponding to one region in the segmented image. The color feature hue is proved to be more efficient than RGB color features by this research. The experimental results show that the MFCM method tends to be more effective to find homogeneous regions. The proposed method can be useful for color image segmentation.

REFERENCES

1. D. Keren and A. Gotlib, “Denoising Color Images Using Regularization and Correlation Terms”, Journal of Visual Communication and Image Representation, 2002, Vol. 9, no. 4.
2. M. B. Meenavathi and K. Rajesh, “Volterra Filter for Color Image Segmentation”, International Journal of Computer Science and Engineering, 2008, Vol. 2, no.1.
3. S. Ben Chaabane, M. Sayadi, F. Fnaiech and E. Brassart, “Colour Image Segmentation using Homogeneity method and Data Fusion Techniques,” Eurasip journal on advances in signal processing, 2009.
4. N. Ohta, “Correspondance between ceilab and cieluv color differences”, 1977, Vol. 2, no. 4, pp. 178-182.
5. G. Wyszecki and W. S. Stiles, “Color Science: Concepts and Methods, Quantitative Data and formulae”, John Wiley and Sons, second edition, 1982.
6. X. Gao, K. Hong, P. Passmore, L. Podladchikova, and D. Shaposhnikov, “Colour Vision Model-Based Method for Segmentation of Traffic Signs”, EURASIP Journal on Image and Video Processing, October 2008.
7. E. Littmann and H. Ritter, “Adaptive colour segmentation – a comparison of neural and statistical methods”, IEEE Trans. Neural Network, 1997, Vol. 8, no. 1, pp. 175–185.
8. P. W. M. Tsang and W. H. Tsang, “Edge detection on object color”, IEEE Intern. Conf. On Image Processing-C, 1996, pp. 1049-1052.
9. E. Navon, O. Miller and A. Averbuch, “Colour image segmentation based on adaptive local thresholds”, Image and Vision Computing, 2005, Vol. 23, no. 1, pp. 69-85.
10. R. E. Cummings, P. Pouliquen, and M. A. Lewis, “A Vision Chip for Colour Segmentation and Pattern Matching”, EURASIP Journal on Applied Signal Processing, 2003, no. 7, pp. 703-712.
11. H. D. Cheng and Y. Sun, “A hierarchical approach to color image segmentation using homogeneity”, IEEE Transaction on Image Processing, 2000, Vol. 9, no. 12, pp. 2071-2082.
12. H. D. Cheng, X. H. Jiang and J. Wang, “ Color image segmentation based on homogram thresholding and region merging”, Pattern Recognition, 2002, pp. 373-393.
13. S. Ben Chaabane, M. Sayadi, F. Fnaiech and E. Brassart, “Dempster-Shafer Evidence Theory for Image Segmentation: Application in Cells Images”, International Journal of Signal processing, IJSP, 2009, Vol. 5, no. 2, pp. 126-132.
14. Y. W. Lim and S. U. Lee, “On the color image segmentation algorithm based on the thresholding and the fuzzy c-means techniques”, Pattern Recognition, 1990, Vol. 23, no. 9, pp. 935-952.
15. S. Ben. Chaabane, M. Sayadi and F. Fnaiech, “Color Image Segmentation using Automatic Thresholding and the Fuzzy C-Means Techniques”, IEEE MELECON, 2008, pp. 857-861.
16. Y. Yang, Ch. Zheng and P. Lin, “Fuzzy C-means clustering algorithm with a novel penalty term for image segmentation”, Opto-Electronics Rev, 2005, Vol. 13, no. 4.
17. A. W. C. Liew, S. H. Leung and W. H. Lau, “Fuzzy image clustering incorporating spatial continuity”, IEE Proc. Visual Image Signal Process, 2000, no. 147, pp. 185-192.
18. X. Li, L. Li, H. Lu, D. Chen and Z. Liang, “Inhomogeneity correction for magnetic resonance images with fuzzy C-mean algorithm”, Proc. SPIE 5032, , 2003, pp. 995-1005.
19. K. Raghu and J. M. Keller, “A possibilistic approach to clustering ”, IEEE Transactions on Fuzzy Systems, 1993, Vol. 1, no. 2.
20. M. J. Kwon, Y. J. Han, I. H. Shin and H. W. Park, “Hierarchical fuzzy segmentation of brain MR images”, Int. J. Imaging Systems and Technology, 2003, no. 13, pp. 115-125.
21. M. N. Ahmed, S. M. Yamany, N. Mohamed, A. A. Farag and T. Moriarty, “A modified fuzzy c-means algorithm for bias field estimation and segmentation of MRI data”, IEEE Trans. On Medical imaging, 2002, no. 21, pp. 193-199.

22. D. L. Pham and J. L. Prince, "Adaptive fuzzy segmentation of magnetic resonance images", IEEE Trans. Medical Imaging, 1999, no. 18, pp. 737-752.
23. M. Sayadi, L. Tlig and F. Fnaiech, "Texture Segmentation Based on a Modified Fuzzy C-Mean Algorithm and Statistical Features", Applied Mathematical Sciences, 2007, Vol. 1, no. 60, pp. 2999–3007.
24. Y. A. Tolias and S. M. Panas, "On applying spatial constraints in fuzzy image clustering using a fuzzy rule-based system", IEEE Signal Processing Letters, 1998, Vol. 5, no. 10, pp. 245-247.
25. M. N. Ahmed, S. M. Yamany, N. Mohamed, A. A. Farag, and T. Moriary, "A modified fuzzy c-means algorithm for bias field estimation and segmentation of MRI data", IEEE Trans. On Medical Imaging, 2002, vol. 21, pp. 193-199.
26. J. C. Bezdek, "Pattern recognition with fuzzy objective function algorithms", Plenum Press, New York, 1981.
27. R. Duda and P. Hart, "Pattern Classification and Scene Analysis", New York, Wiley, 1973.
28. G. Van de Wouwer, P. Scheunders, and D. VanDyck, "Statistical texture characterisation from discrete wavelet representation", IEEE Transactions on Image Processing, 1999, vol. 8, no. 4, pp. 592-598.
29. P. W. M. Tsang and W. H. Tsang, "edge detection on object color", IEEE International Conference on Image Processing-C, 1996, pp. 1049-1052.
30. D. C. Tseng and C. H. Chang, "Color segmentation using perceptual attributes," in IEEE Int. Conf. Image Processing, 1992, pp. 228–231.
31. D. Hoy, "On the use of color imaging in experimental applications", Exper. Tech., July/Aug. 1997.
32. W. Kim and R. Park, "Color image palette construction based on the HSI color system for minimizing the reconstruction error", in IEEE Int. Conf. Image Processing, 1996, pp. 1041–1044.
33. V. Grau, A. U. J. Mewes, M. Alcaniz, R. Kikinis, and S. K. Warfield, "Improved watershed transform for medical image segmentation using prior information", IEEE Transactions on Medical Imaging, 2004, Vol. 23, no. 4, pp. 447–458.
34. R. O. Duda, P. E. Hart, and D. G. Sork, "Pattern Classification", Wiley-Interscience, New York, NY, USA, 2000.
35. O. Colot et al., "A Colour Image Processing Method for Melanoma Detection", Lecture Notes in Computer Science, Springer, Berlin, 1998.

BIOGRAPHIES

Rafika Harrabi born in 1981 in Kairouan (Tunisia), she received the BSc degree in Electrical Engineering and the DEA degree in Automatic and Signal Processing from the High school of sciences and techniques of Tunis, respectively in 2007 and 2009. Currently, she is in the last preparation year of its PhD. Its research interests are focused on signal Processing, image processing, classification, segmentation and data fusion.

Ezzedine Ben Braiek obtained his HDR on 2008 in Electrical engineering from ENSET Tunisia. He is, presently, professor in the department of electrical engineering at the technical university ESSTT and manager of the research group on vision and image processing at the CEREP. His fields of interest include automatics, electronics, control, computer vision, image processing and its application in handwritten data recognition.

A Fast and Efficient Non-Blocking Coordinated Movement-Based Check pointing Approach for Distributed Systems

Jayanta Datta[1]
Department of Computer Application
RCC Institute of Information technology
Kolkata-700015, West Bengal, India
***Harinandan Tunga**[2]
Department of Computer Sc. & Engineering
RCC Institute of Information technology
Kolkata-700015, West Bengal, India
Rudranath Mitra[3]
Department of Information Technology
Heritage Institute of Technology
Anandapur, Kolkata-700107, West Bengal, India

Abstract
In this paper, we have presented an efficient non-blocking coordinated check pointing algorithm for distributed systems. It produces a consistent set of checkpoints, without the overhead of taking temporary checkpoints; the algorithm also makes sure that only few processes are required to take checkpoints in its any execution; it uses very few control messages and the participating processes are interrupted fewer number of times when compared to some noted related works. The two most important criteria are non-blocking and minimum number of checkpoints. Cao-Singhal showed in their algorithm that it is impossible to design minimum process non-blocking algorithm but it is not desirable in mobile environment that underlying computation will be blocked whenever a check pointing algorithm invoked. If the check pointing scheme is blocking then the performance of the system will be highly affected by the frequent initiation of check pointing algorithm. We must try to minimize the blocking time while keeping the number of checkpoints minimum. So, the proposed scheme concentrate to minimize this overhead by combining coordinated check pointing with minimum blocking time.

Keywords: Check-pointing, Dependency Vector (DV), distributed algorithm, Mobile Support Stations (MSS), Message Handling System (MHS), and Received Pronunciation (RP).

Introduction

Distributed system consists of only static hosts. But nowadays, the needs of mobile devices have been increased greatly which in turn, gave rise of a new technology, called mobile computing. We can consider mobile computing is a special case of distributed computing system. The term ‘mobile’ implies able to move while retaining its network connection and a host which can move is called mobile host (MH). The infrastructure machines that can communicate directly with mobile hosts are called mobile support stations (MSS). Due to mobility and portability of devices mobile computing is characterized by some constraints [3]:

- Mobile elements are resource-poor relative to static - For a given cost and level of technology, considerations of weight, power, and size ergonomics will exact a penalty in computational resources such as processor speed, memory size, and disk capacity. While mobile elements will improve in absolute ability, they will always be resource- poor relative to static elements.
- Mobility is inherently hazardous- A Wall Street stockbroker is more likely to be mugged on the streets of Manhattan and have his laptop stolen than to have his workstation in a locked office be physically subverted. In addition to security concerns, portable computers are more vulnerable to loss or damage.
- Mobile connectivity is highly variable in performance and reliability - Some buildings may offer reliable, high-bandwidth wireless connectivity while others may only offer low-bandwidth connectivity. Outdoors, a mobile client may have to rely on a low-bandwidth wireless network with gaps in coverage.
- Mobile elements rely on a finite energy source - While battery technology will undoubtedly improve over time, the need to be sensitive to power consumption will not diminish. Concern for power consumption must span many levels of hardware and software to be fully effective.

Fault-tolerance [4] or graceful degradation is the property that enables a system to continue operating properly in the event of the failure of some of its components. An incremental check-pointing approach introduced by Elnozahy et.al [2]. In [1] first gives the idea, how a process in a distributed system can determine a global state of the system using special marker

message during computation. There are three most important parameter of coordinated check-pointing are synchronization message overhead, number of checkpoints and blocking time. The following algorithms [1][2][5][6][7][8][9] introduce the idea to minimize the overhead. Koo–Toueg[15] propose the two phase protocol that forces only a minimal number of additional processes to take checkpoints. Prakash - Singhal[5] first introduces the algorithm which makes it possible that only a minimum number of processes take checkpoint without blocking the underlying computation during check-pointing. In[8] Weigang-Susan introduce a strategy called proxy coordinator. In [13], a hybrid check-pointing protocol has been introduced that has been combined with selective sender based message logging. The idea proposed in [14] alleviates the problem of combining pessimistic message logging with uncoordinated check-pointing protocol.

Proposed Scheme

Consider a set of n processes, $\{P_1, P_2, \ldots, P_n\}$ involved in the execution of a distributed algorithm. Each process P_i maintains a dependency vector DV_i of size n which is initially empty and an entry $DV_i[j]$ is set to 1 when P_i receives since its last checkpoint at least one message from P_j. It is reset to 0 again when process P_i takes a checkpoint. Each process Pi maintains a checkpoint sequence number csni. This csni actually represents the current check pointing interval of process P_i. The check-pointing interval of a process denotes all the i^{th} and (i+l) Computation performed between its I checkpoint but not the checkpoint, including the i^{th} checkpoint. The csn_i is initially set to 1 and (i+l) incremented when process P_i takes a checkpoint. In this approach we assume that only one process can initiate the check pointing algorithm. This process is known as the initiator process. We define that a process P_k is dependent on another process P_r, if process P_r since its last checkpoint has received at least one application message from process P_k. In our proposed algorithm we assume primary and secondary checkpoint request exchanges between the initiator process and the rest n-1 processes. A primary checkpoint request is denoted by R_i (i = csnj) where i is the current checkpoint sequence number of process P_j that initiates the check pointing algorithm. It is sent by the initiator process P_j to all its dependent processes asking them to take their respective checkpoints. A secondary checkpoint request denoted by R_{si} is sent from a process P_m to a process Pn which is dependent on P_m to take a checkpoint. R_{si} means to its receiver process that i is the current checkpoint sequence number of the sender process. The control message exchange is explained with an illustration shown in Figure 1. Consider a distributed system with three processes P1, P2, and P3. We assume that P1 initiates the check pointing algorithm. To start with, P1 takes a checkpoint and sends a primary checkpoint request to P2, asking it to take a checkpoint as it is directly dependent on P1. P2 takes a checkpoint after it receives the primary checkpoint request. After taking its checkpoint P2 sends a secondary checkpoint request to P3 as P3 is dependent on P2, Process P3 then takes its checkpoint. In this work, an application message is represented by $M_{i,x}$, which means that it is the x^{th} message sent by process P_i. The checkpoint $C_{i,j}$ represents the j^{th} checkpoint taken by P_i. We have assumed that the events of taking a checkpoint and sending a checkpoint request are done atomically. Also, each process P_i piggybacks its current checkpoint sequence number with only every first outgoing application message to another process after taking We now state the situations in general when a process P_i needs to take a checkpoint. In our approach a process P_i takes a checkpoint if any of the following events occurs - if P_i is the initiator then if it receives a primary checkpoint request from the initiator. The first time it receives a secondary checkpoint request and prior to that it has not received any primary checkpoint request or any piggybacked application message. The first time it receives an application message piggybacked with the checkpoint sequence number, and prior to that it has not received any primary or secondary checkpoint request message.

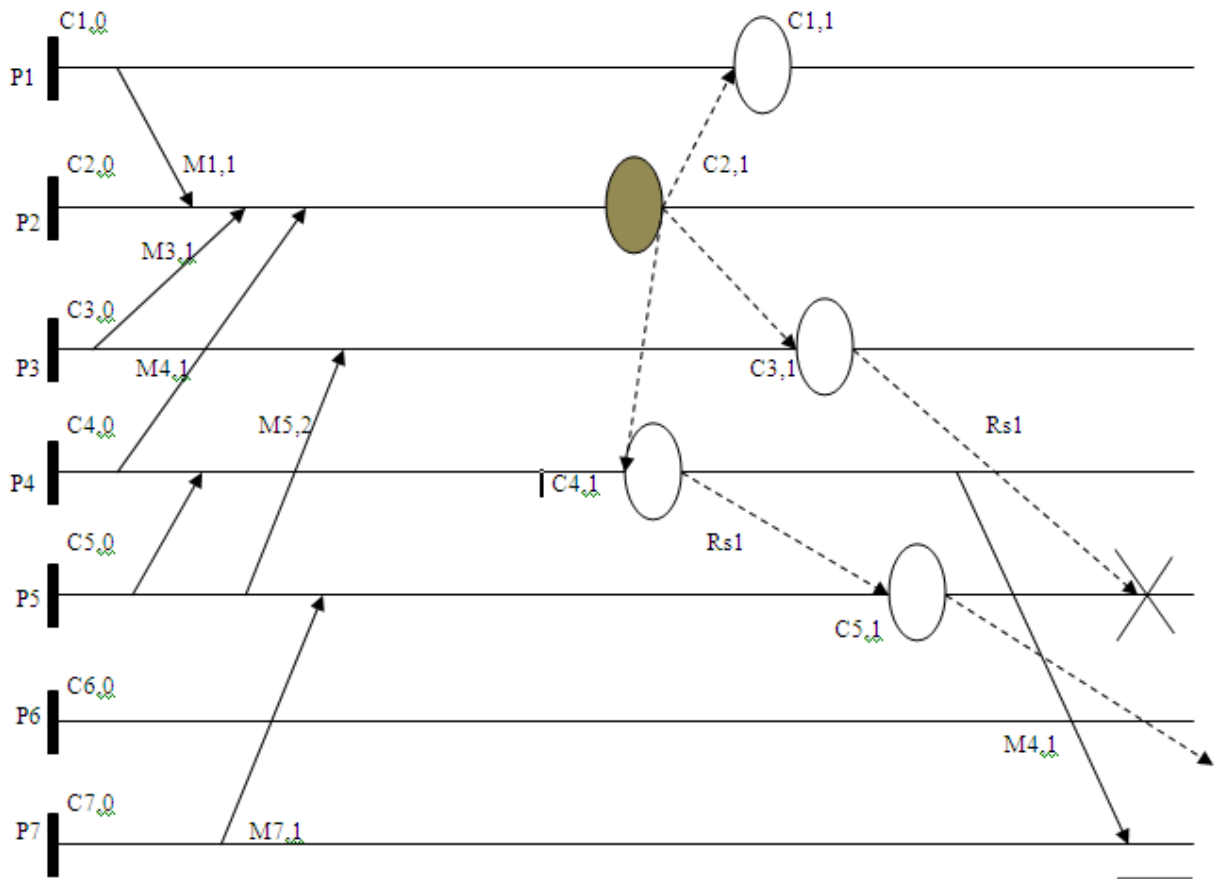

Figure 1: Process of taking Non-Blocking Coordinated checkpoint

Illustration

The behavior of each process in our approach is explained with the help of the following example. Unless otherwise mentioned a checkpoint request represents either a primary request or a secondary request. Note that an application message with piggybacked checkpoint sequence number, which may force a checkpoint to be taken at the receiving process may also be viewed as a checkpoint request. In our work a checkpoint means a permanent checkpoint. Consider the distributed system as shown in the Fig. 2. Assume that process P_2 initiates the check pointing algorithm. First process P_2 takes its permanent checkpoint $C_{2,1}$. It then checks its dependency vector $DV_2[]$ which is {1, 0,1,1,0,0,0}. This means that process P_2 has received at least one message from processes P_1, P_3, and P_4, and since P_2 has already taken its checkpoint $C_{2,1}$ these messages will become orphan if P_1, P_3, and P_4 do not take checkpoints. Therefore P_2 sends primary checkpoint request R_1 ($csn_2 = 1$) to P_1, P_3, and P_4. After sending the primary checkpoint request process P_2 increments its checkpoint sequence number csn_2 to 2 and finishes its participation associated with the current execution of the algorithm and continues with its normal computation. It shows the non-blocking nature of our approach. On receiving the primary checkpoint request R_1 from P_2, process P_3 first takes a checkpoint $C_{3,1}$ and then it checks its own dependency vector $DV_3[]$ which is {0,0,0,0,1,0,0}. Therefore process P_3 sends a secondary checkpoint request Rs_1 to process P_5. Then its checkpoint sequence number csn_3 is incremented to 2. Similarly processes P_1 and P_4 first take checkpoints $C_{1,1}$ and $C_{4,1}$ respectively, then each process checks its dependency vector to find the dependent processes. Process P_1 finds that its dependency vector DV_1 [] is null. Hence it increments its checkpoint sequence number to 2, and continues normal execution. Process P_4 finds that it has received a message from process P_5. Hence P_4 sends a secondary checkpoint request R_{s1} to process P_5. It then increments its checkpoint sequence number csn_4 to 2, and continues normal execution. At process P_5 let us assume that the secondary checkpoint request R_{s1} sent by process P_4 reaches before the secondary checkpoint request sent by process P_3. On receiving the secondary checkpoint request R_{s1} from process P_4, P_5 checks its own checkpoint sequence number csn_5 with that of the received checkpoint sequence number. P_5 finds that its current checkpoint sequence number ($csn_5 = 1$) is not greater than the received checkpoint sequence number which is also equal to 1. Hence it decides to take a checkpoint and takes checkpoint $C_{5,1}$.

After taking the checkpoint it checks its dependency vector DV_5 and finds that process P_7 has sent a message to it. Hence it sends a secondary checkpoint request Rs_1 to P_7. After sending the request it increments its checkpoint sequence number csn_5 from 1 to 2. Assume that later process P_5 receives the secondary checkpoint request sent by process P_3. As soon as process P_5 receives the checkpoint request it compares its current checkpoint sequence number csn_5 with the received checkpoint sequence number. It finds that its current checkpoint sequence number ($csn_5 = 2$) is greater than the received checkpoint sequence number which is 1. Hence it discards the checkpoint request. The above discussion takes care of the first three situations about when a process takes a checkpoint. Below, we consider the fourth situation. Suppose that process P_4 after taking the checkpoint continues normal execution and sends an application message $M_{4,1}$ to process P_7. Since the application message is the first application message to process P_7 from P_4 after taking the checkpoint, it is piggybacked with the current checkpoint sequence number (csn_4) of process P_4 which is 2. Process P_7 on receiving the application message piggybacked with the checkpoint sequence number compares its current checkpoint sequence number csn_7 with the received checkpoint sequence number. It finds that the received checkpoint sequence number is equal to 2 and is greater than its current checkpoint sequence number (csn_7) which is equal to 1. Therefore process P_7 decides to take a checkpoint before processing the application message $M_{4,1}$. P_7 then takes its checkpoint $C_{7,1}$ and increments its checkpoint sequence number to 2 and then processes the application message $M_{4,1}$. Eventually process P_7 also receives the secondary checkpoint request sent by process P_5. P_7 first compares its current checkpoint sequence number with the received checkpoint sequence number which is 1. It finds that its current checkpoint sequence number is greater than the received checkpoint request. Hence P_7 discards the secondary checkpoint request as it has already taken its checkpoint for the current execution of the algorithm. In the above example we observe that P_7 sent a message $M_{7,1}$ to P_5. So even if there was no such piggybacked message as $M_{4,1}$, process P_7 would eventually receive the secondary check-pointing request $R_{s,1}$ from P_5 and take its checkpoint $C_{7,1}$. Observe that because of the non-blocking nature of the algorithm the following situation may arise as well. Consider that there was no such message as $M_{7,1}$; that is, assume that P_7 has not sent any application message to any process at all. However, assume that it receives the piggybacked message $M_{4,1}$ from P_4. In our approach P_7 will take its checkpoint and then process the message and then would behave like any other process involved in the check pointing approach.

Data Structures

- Status: A Boolean variable maintained at each process P_i. If $Status_i = 1$, then P_i is in a check-pointing phase. When P_i receives a checkpoint request it sets $Status_i = 1$ and after receiving the checkpoint commit message it resets $Status_i = 0$.
- DP: A Boolean array of size n, maintained by MSS on behalf of its local MHs. $DP_i[j]=1$ means process P_i receives some computation messages from P_j. All elements of this array are initialized to 0 except $DP_i[i]=1$.
- RP: A Boolean array of size n, maintained by MSS on behalf of its local MHs. It is used to save dependency relation during the check-pointing interval. It is same as DP. After that interval n-bitwise OR operation is performed between the elements of DP and RP and the result is stored to DP. Then RP is refreshed.
- Count: It is an integer variable stored at process P_i. It is initialized to 0. Each time the check-pointing algorithm invoked by P_i, $count_i$ is incremented by 1.
- Mark: It is a Boolean variable which is used to indicate the blocking period at the receiver side MSS. If mark = 1, that means the MSS is waiting for the final dependency list and that time all incoming messages will be buffered at MSS.

Assumption

1. Processes communicate only through messages. They do not share any common memory or common clock
2. All communication channels between MHs and MSSs are FIFO. The channels between MSS and MSS are also FIFO.
3. No process fails during the check pointing phase.
4. Channels are lossless. Messages arrive with an arbitrary but finite delay.
5. A process will not receive any checkpoint request from another initiator before the current executing one is completed.

First Phase

1. When process P_i running on MH_i wants to save its state, it takes a tentative checkpoint and informs its current MSS, MSS_p so that MSS_p starts the checkpointing algorithm as a proxy coordinator on behalf of Pi. MSSp sets $mark_p = 1$.

2. MSSp sends request to all other MSSs in the system to collect the dependency vectors of other MHs in the system.

3. All other MSSs in the system respond to the request by sending the dependency vectors of their local MHs and starts waiting for final dependent set. After sending the dependency sets of their MHs, MSS_q (q!=p) sets *markq* = 1

3.1 MSS_q receives a computation message for a process P_j which is currently under it, if $mark_q$ = 1, then MSS_q buffers the message and update the dependency information in RP_j[].

3.2 MSS_q receives an outgoing computation message from an MH currently under it. It doesn't block the message. It forwards the message to the MSS of the receiver process.

3.3 If MSS_p receives a message, it checks the value of *mark* and if *mark* is set to 1, then it checks whether the receiver is the initiator i.e. MH_i. If receiver = MH_i then it forwards the message, otherwise buffers it.

4. MSS_p, the proxy coordinator receives the dependency vectors from other MSSs. After that MSS_p constructs an NxN dependency matrix with one row per process, represented by the dependency vectors of the process. Based on this NxN matrix, MSS_p can locally calculates both (direct and transitive) dependents of P_i.

5. MSS_p broadcasts the final dependent list to all other MSSs.

6. On receipt of the dependent list, MSS_q checks the buffered messages.

6.1 If receiver process (i.e. the process belongs to MSS_q) of the buffered message is in the dependent list, then MSS_q attaches a flag=1 with that message and sends to the intended process.

6.2 If sender process of the buffered message is in the dependent list, then MSS_q keeps the payload of the message in stable log on behalf of the receiving process and sends the message to the intended process.

6.3 If both the sender and the receiver is in the dependent list, then MSS_q checks the *status* of the sender.

6.3.1 If *status* of sender = 1, then set flag = 1.

6.3.2 If *status* of sender = 0, just delivers the message as it is.

7. MSS at the receiver side keeps the copy of the message in its volatile log. When MSS_q receives the final dependency list, it which MHs within its area are not in the dependency list. Then MSS_q checks the dependency list of process P_k, which is not in the final set. If MSS_q finds $DP_k[j] = 1$ and P_j belongs to final dependent set. Then MSS_q finds all the messages with sender P_j from the temporary log of P_k and flushed them to the stable storage.

8. When all buffered messages have been delivered MSS_q resets $mark_q$ = 0. sends checkpoint request to all its local processes which are in the dependent list.

9. Process P_j receives a computation message and it checks the value of the flag bit attached to the message

   9.1 If flag =1, then P_j takes a tentative checkpoint and sets its *status* to 1. Then it processes the message.
   9.2 If flag =0, then P_j simply processes the message.

10. Process P_j receives a checkpoint request message. It checks the value of $Status_j$. If $Status_j$ =1, it discards the checkpoint request and if $Status_j$ =0, it takes a tentative checkpoint, sets its *status* to 1 and sends back a reply to its MSS_q.

11. MSS_q has received reply messages from all the processes to which it sent checkpoint request messages, it sends a reply message to the initiator, MSS_p.

Second Phase

1. If MSS_p receives reply from all the dependent processes, then it broadcast a commit message to all the MSSs in the system. Otherwise abort the check-pointing algorithm.

2. On receipt of the commit message, the tentative checkpoint becomes permanent. The elements of dependency vectors DP of the processes, which have taken checkpoint, are refreshed and elements of RP are copied to DP.

Optimization

The performance of a check-pointing algorithm is determined by three parameters - blocking time, synchronization message overhead and number of checkpoints required. N= Number of MHs and M= Number of MSSs and N >> M. Let us assume, all processes running on the MHs and there is only one process running on each MH.

Experimental Results

Algorithm	Blocking Time	Messages
Koo-Toueg[8]	$N^* (4^* T_{mh} + T_{chkpt} + T_{search})$	$N^*(6^* C_{mh} + C_{search})$
Cao-Singhal[11]	$2^* T_{mss}$	$3N^* C_{mh}$
Proposed Scheme	T_{mss}	$3N^* C_{mh}$

Table 1: Comparative Study of Proposed Scheme

Meaning of Notations

- C_{mss} = cost of sending message between any two MSSs.
- C_{mh} = cost of sending a message from an MH to its local MSS.
- C_{broad} = cost of broadcasting a message in the static network.
- C_{search} = cost incurred to locate an MH and forward amessage to its current local MSS, from a source MSS.
- T_{mss} = average message delay in the static network.
- T_{mh} = average message delay in the wireless network.
- T_{search} = average delay incurred to locate an MH and forward a message to that MH.
- T_{chkpt} = Average delay to save a checkpointon the stable storage

In order to measure buffering time - after an MSS has sent all its local dependent vectors to the proxy MSS; it can't forward any computation message to its local MH until it receives the final set of dependent processes. An MSS buffers the messages during this time. Total blocking time of Cao-Singhal Algorithm was $2T_{mss.}$ When an MSS of a sending process receives a computation message immediate after sending the dependency vector to the proxy MSS, it forwards the message to the MSS of receiving process and the message will be buffered their. So, in worst case, the maximum time of buffering will be $T_{buffer} = 2T_{mss} - T_{search}$.

So, $T_{buffer} <= T_{mss.}$ Since $T_{search} >= T_{mss}$

Therefore, the computation will not be blocked for $2T_{mss}$ time.

Handling Lost Message- In this scheme, both the send and receive event is recorded in the dependency vector. So, here the lost messages have been handled properly. In figure 4.1, messages m_5 and m_1 will be lost though they have reached and processed successfully by process P_2 and $P_{6,}$ if only receive events are stored in the dependency vector. Because sending event of messages m_5 and m_1 are recorded since process $P_{3,}$ $P_{4,}$ P_5 will take checkpoints in case of storing only receive events. But here, both send and receive have been recorded in global checkpoint. No broadcast message - in this scheme, there is a broadcast message at the MH level. So, it will not interrupt that process that is in doze mode and hence, fulfilling the limited battery power constraint of mobile hosts. Search Cost-The mobility of hosts in mobile computing environment incurs a large amount of search delay and hence search cost. In this scheme, there is no search cost for checkpoint request messages since initiator broadcasts the final set of dependents to every MSS in the system. The MSSs forward the request message only to their local MHs.

Conclusion

The proposed scheme is developed to reduce the blocking time of the coordinated check pointing algorithm. The above scheme might be more optimized in terms of blocking time. The recovery issue has not been discussed here. Further developments are being carried out to handle recovery issues.

Acknowledgements

We express our sincere gratitude to seiner faculties, Department of Computer Science, Information Technology and Engineering and Computer Application, RCC Institute of Information Technology and Heritage Institute of Technology for extending his valuable time for us to take up this problem as a paper and also financial support our institutes. This paper deals with a system that to the best of our belief does not exist as yet.

Reference

[1] M. Chandy and L. Lamport. "Distributed snapshots: Determining global states of distributed systems." In ACM Transactions on Computing Systems, 3(1):63— 75, Aug. 1985.

[2] E.N. Elnozahy, D.B. Johnson, and W. Zwaenepoel. "The performance of consistent checkpointing." In Proceedings of the Eleventh Symposium on Reliable Distributed Systems, pp. 39— 47, Oct. 1992.

[3] B. Randell. "System structure for software fault-tolerance." IEEE Transactions on Software Engineering, SE-1(2):220—232, Jun. 1975.

[4] A Clematis. "Fault-tolerant programming for network based parallel computing." In Microprocessing and Microprogramming, vol. 40, pp. 765— 768, 1994.

[5] Prakash, R. and M. Singhal, "Low-Cost Checkpointing and Failure Recovery in Mobile Computing Systems," IEEE Trans. Parallel and Distributed Systems, pp.1035-1048, Oct. 1996.

[6] Cao, G. and M. Singhal, "On Coordinated Checkpointing in Distributed Systems," IEEE Trans. Parallel and Distributed Systems, pp. 1213-1225, Dec. 1998.

[7] Guohong Cao and Mukesh Singhal "On the Impossibility of Min-Process Non-Blocking Checkpointing and An Efficient Checkpointing Algorithm for Mobile Computing Systems" Department of Computer and Information Science The Ohio State University Columbus, OH 43210

[8] Weigang Ni, Susan V. Vrbsky and Sibabrata Ray "Low-cost Coordinated Nonblocking Checkpointing in Mobile Computing Systems", Department of Computer Science University of Alabama Tuscaloosa, AL 35487-0290, Proceedings of the Eighth IEEE International.

[9] Robert H. B. Netzer and Jian Xu "Necessary and Sufficient Conditions for Consistent Global Snapshots"IEEE transactions on parallel and distributed systems, vol. 6, no. 2, february 1995

[10] Guohui Li and LihChyun Shu "A Low-Latency Checkpointing Scheme for Mobile Computing Systems" Processing of the IEEE 29th Annual International Computer Software and Application Conference (COMPSAC'05), 2005.

[11] Y. M. Wang. "Space reclamation for uncoordinated checkpointing in message-passing systems." Ph.D. Thesis, University of Illinois Urbana-Champaign, Aug. 1993.

[12] Y. M. Wang. "Consistent global checkpoints that contain a set of local checkpoints." IEEE Transactions on Computers, 46(4):456— 468, Apr. 1997.

[13] Kwang-Sik Chung, Ki-Bom Kim, Chong-Sun Hwang, Jin Gon Shon and Heon-Chang Yu "Hybrid Checkpointing Protocol Based on Selective Sender-based Message Logging". IEEE , 1997.

[14] Mehdi Aminian, Mohammad k. Akbari and Bahman Javadi "Combining Coordinated and Uncoordinated Checkpointing with Pessimistic Message Logging". IJCSNS International Journal of Computer Science and Network Security, Vol. 6 NO. 4, 2006.

[15] Koo R. and Toueg S., "Checkpointing and Roll-Back Recovery for Distributed Systems," IEEE Trans. on Software Engineering, vol. 13, no. 1, pp. 23-31, January 1987.

STUDIES ON EFFECT OF SALT STRESS ON SOME MEDICINAL PLANTS

S.P Kiran kumari [1], V. Sridevi* [2], M.V.V. Chandana Lakshmi [3]

[1,2,3] Centre for Biotechnology, Department of Chemical Engineering, A.U College Of Engineering(A) Andhra University, Visakhapatnam 530003, Andhra Pradesh, India

Abstract:
Climatic change has become increasingly recognized as one of the greatest challenges to humankind and all other life on earth. The productivity of plants is greatly affected by various environmental stresses. Plant stress is a condition where excessive salts in soil solution cause inhibition of plant growth or plant death. Salinity stress negatively impacts agricultural yield throughout the world affecting production whether it is for subsistence or economic gain. The medicinal properties of plant species have made an outstanding contribution in the origin and evolution of many traditional therapies. In India, many government and non-government organizations have had focused attention on improving the medicinal plants sector. So the study is related to effect of salt stress on our selected medicinal plants which may help upto some extent for their cultivation. *Azadirachta indica* , *Cassia fistula*, *Catharanthus roseus*, *Aloe barbadensis*, and *Ocimum sanctum* were selected for our study and there biochemical parameters like total chlorophyll content and total carbohydrate content were estimated to know the salt tolerance among those plants. Through our field experiment *Azadirachta indica* showed the highest tolerance towards salinity both by morphological parameters and by biochemical parameters and remaining all four get wilted and the quality reduced gradually.

Keywords: Biochemical parameters , Chlorophyll content ,Medicinal plants, Salt stress.

1 Introduction

India is well known for the usage of medicinal plants in curing various diseases from ancient times .It has been estimated that in developed countries such as united states , plant drugs constitute as much as 25% of the total drugs, while in fast developing countries such as china and India it is as much as 80%. As medicinal plants play a vital role in Indian medicine so there is a need to know about the factors effecting their growth for the large scale cultivation. Plant growth and productivity are greatly affected by environmental stresses such as dehydration, high salinity, low temperature and biotic pathogen infection[1]. Salinity stress is one among the various environmental stresses .Salinity stress negatively impacts agricultural yield throughout the world affecting production whether it is for subsistence or economic gain. Salt stress negatively presents an increase threat to plant agriculture. This impact has been studied upon some selected medicinal plants to know the serious impact of salt stress among those plants which has a lot of significance in the Indian system of medicine[2-3].

Medicinal plants

FIG:1 *Azadirachta indica*

Azadirachta indica (**Neem**) is a tree in the mahogany family Meliaceae. It is one of two species in the genus ***Azadirachta***, and is native to India growing in tropical and semi-tropical regions. Its fruits and seeds are the source of neem oil. In East Africa it is also known as *Muarubaini* (Swahili), which means *the tree of the 40*, as it is said to treat 40 different diseases, and in Somalia it is known as "Geed Hindi" which means "the Indian tree".Neem is a fast-growing tree that can reach a height of 15–20 metres (49–66 ft), rarely to 35–40 metres (115–130 ft). It is evergreen, but in severe drought it may shed most or nearly all of its leaves. The branches are wide spread. The fairly dense crown is roundish or oval and may reach the diameter of 15–20 metres (49–66 ft) in old, free-standing specimens[5]. All parts of the tree are said to have medicinal properties (seeds, leaves, flowers and bark) and are used for preparing many different medical preparations. The chemical constituents nimbidin and nimbin have some spermicidal activity . Neem oil is used for preparing cosmetics (soap, neem shampoo, balms and creams such as Margo soap) and many oral health products. Besides its

use in traditional Indian medicine, the neem tree is of great importance for its anti-desertification properties and possibly as a good carbon dioxide sink[7-8].

FIG:2 *Cassia fistula*

Cassia ***fistula***, known as the **golden shower tree** and other names, is a flowering plant in the family Fabaceae, native to southern Asia, from southern Pakistan east through India to Myanmar and south to Sri Lanka. It is associated with the Mullai region of Sangam landscape. It is the national tree of Thailand, and its flower is Thailand's national flower. It is also state flower of Kerala in India and of immense importance amongst Malayali population. It is a popular ornamental plant and is an herbal medicine. In Ayurvedic medicine, golden shower tree is known as *aragvadha*, meaning "disease killer". The root is considered a very strong purgative, and self-medication or any use without medical supervision is strongly advised against in Ayurvedic texts[9-10].

FIG:3 *Aloe barbadensis*

Aloe barbadensis **,**common name ***Aloe vera*** , pronounced, also known as the **true aloe** or **medicinal aloe**, is a species of succulent plant in the genus *Aloe* that is believed to have originated in the Sudan. *Aloe vera* grows in arid climates and is widely distributed in Africa, India, Nepal and other arid areas. The species is frequently cited as being used in herbal medicine. Many scientific studies on the use of extracts of *Aloe vera* have been undertaken, some of them conflicting. There is some preliminary evidence that

Aloe vera extracts may be useful in the treatment of wound and burn healing, minor skin infections, sebaceous cysts, diabetes, and elevated blood lipids in humans[11-15]. These positive effects are thought to be due to the presence of compounds such as polysaccharides, mannans, anthraquinones, and lectins.

FIG:4 *Catharanthus roseus*

Catharanthus roseus (**Madagascar Periwinkle**) is a species of *Catharanthus* native and endemic to Madagascar. Synonyms include *Vinca rosea* (the basionym), *Ammocallis rosea*, and *Lochnera rosea*; other English names occasionally used include Cape Periwinkle, Rose Periwinkle, Rosy Periwinkle, and "Old-maid". In the wild, it is an endangered plant; the main cause of decline is habitat destruction by slash and burn agriculture. It is also however widely cultivated and is naturalised in subtropical and tropical areas of the world. The species has long been cultivated for herbal medicine and as an ornamental plant. In traditional Chinese medicine, extracts from it have been used to treat numerous diseases, including diabetes, malaria, and Hodgkin's disease. The substances vinblastine and vincristine extracted from the plant are used in the treatment of leukemia[16].

These are the plants which are subjected to salt stress to know the salinity withstanding capability and also verifying the biochemical changes in these plants due to the presence of excess salt in the soil.

2 Materials and methods

The selected medicinal plants were daily subjected to 1000mg of Nacl salt for 20 days after sown. Their respective control plants without the subjection to salt stress were sown in separate place so that it will be helpful for the comparision of salt stress on these subjected plants.

2.1 Soil chemical analysis

2.1.1 Determination of soil pH: Significance of pH lies in its influence on availability of soil nutrients, solubility of toxic nutrients elements in the soil , physical breakdown of root cells, cation exchange capacity in soils whose colloids(clay/humus) are pH-dependent, and on biological activity. At high pH values, availability of phosphorus(p) and most micronutrients, except boron(B) and molybdenum (MO),tends to decrease. Thus , soil pH is one of the most common measurements in soil laboratories[17]. It reflects whether a soil is acid , neutral, basic or alkaline. Procedure for determining soil pH in a 1:1 (soil: water) suspension is McKeague, 1978 and McLean,1982 methodolgy.

2.1.2 Determination of soil Electrical conductivity: The methodology of EC measurement followed by Richards and et al., 1954 was used by us.

2.2 Plant Morphological parameters:

2.2.1 Determination of plant height: Plant height was measured from the cotyledonary node to the growing tip and expressed in centimeters.

2.2.2 Determination of leaf area : The leaves from five randomly selected branches were used for the estimation of leaf area. Leaf area was computed by using disc method and expressed as $cm^2 plant^{-1}$.

2.3 Plant biochemical parameters:

2.3.1 Estimation of total carbohydrates content in plant leaves:

Plant sample preparation:

i) Plant leaves should be collected. Oven dried at 70 °C for 72 hrs.
ii) Grinded to fine powder.
iii) 5gms of plant powder was weighed and crushed in 25ml of sterile water.
iv) Boiled at 50-60 °C for 30 minutes on water bath.
v) It was used filtered through Whattman No.1 filter paper.
vi) The filterate was centrifuged at 2500 rpm for 15 minutes and filterate was stored in sterile bottles at 5°C for further use.

Reagent preparation: 0.2 gms of anthrone was dissolved in 100ml of concentrated Sulphuric acid. Fresh solution was prepared just before the use.

Procedure:

i) 1ml of the aliquot was taken in a test tube.
ii) The volume was made upto 2.5 ml with distilled water.
iii) All the test tubes were kept in the ice bath and to which 5ml of anthrone reagent was added slowly.
iv) Contents were stirred gently with a glass rod and heated on boiling water bath exactly for 7.5 mins and cooled immediately on ice bath.
v) After cooling, the absorbance of the solution were measured at 630nm against the blank in a spectrophotometer (Elico SL-177) and the sugar content was calculated through the standard curve.

Standard curve:

i) 100 mg of glucose was dissolved in little quality of water and make up to 100 ml to get a stock solution.
ii) From this, different concentration were made from 10-100mg/ml by diluting and used for standard curve.

2.3.2 Estimation of total chlorophyll content in plant leaves:

To the estimate the amount of chlorophyll in plant leaves Arnon methodology (1949) was used[18].

i) 0.25 gms of fresh leaves was weighed and homogenized with pure 80% acetone.
ii) Extract was filtered using whatman No.1filter paper.
iii) Wash 2-3 times using 80% acetone.
iv) Finally made the volume to 25 ml
v) Read the absorbance at 645 and 663 nm

Calculate the total chlorophyll content by using the Formulae:

Total chlorophyll content present in A/g tissue = $20.2(A_{645}) + 8.02(A_{663})$ *V/1000*W

A= absorbance at specific wavelength

V= final volume of chlorophyll extract in 80% acetone

W= Fresh weight of tissue extracted

3. Results and Discussion:

3.1 Soil chemical analysis:

Soil sampl	pH	E.C
Before salt stress	6	1.23dsm^{-1}
After salt stress	7.9	0.93dsm^{-1}

Table 1. Compares the pH and electrical conductivity of the soil before and the after the experimental work

3.2 Plant Morphological parameters:

3.2.1 Determination of plant height:

PLANTS	5th day	10th day	15th day	20th day
Azadirachta indica	C-46 S -47	C-46 S -48	C-47 S -49	C-48 S -**51**
Cassia fistula	C-45 S -45	C-46 S -45	C-47 S -45.5	C-48 S -46
Aloe barbadensis	C-20 S -20	C-21 S -20	C-22.5 S -21	C-24 S -21
Catharanthus roseus	C-13 S -12	C-14 S -13	C-14 S -13	C-16 S -14

Plant height was estimated for 21 days and the height in centimeters was estimated with a gap period of 5 days(Table.2)

Table 2.The observed plant height for 20 days in an interval of 5 days where C- indicates control and S- indicates salt stress on their respective plants.

Table 2, shows the parameter in terms of growth where we can see clearly the inhibitory effect of salt in all plants , but astonishingly *Azadirachta indica* shows the growth effect when compared with another plants while all other plants height were less when compared to their respective control plants.

3.2.2 Determination of leaf area:

Leaf area was determined in as cm^2plant^{-1}[19]**.** Here the control plants 20^{th} day area is tabulated so that direct identification can be done , at the same time the 5^{th} -15^{th} day leaves area is also tabulated so that the increase rate of area can be easily noticed(Table.3).

PLANTS	Control value on 20^{th} day	5^{th} day	10^{th} day	15^{th} day	20^{th} day
Azadirachta indica	**7**	7	7.85	7.99	**8.5**
Cassia fistula	4.5	4.5	4.22	4.55	4.44
Aloe barbadensis	15	15	14	13	14
Catharanthus roseus	12	12	13	13	14

Table 3.It shows the leaf area of the plant leaves which is a morphological parameter which helps to indicate the plant survival.

3.3 Plant biochemical parameters:

3.3.1 Total carbohydrates content in plant leaves:

Plants	Control on 20^{th} day	5^{th} day	10^{th} day	15^{th} day	20^{th} day
Azadirachta indica	**1.98**	1.888	1.87	1.47	**1.57**
Cassia fistula	1.45	1.23	1.22	1.20	0.878
Aloe barbadensis	1.23	1.01	0.67	0.64	0.56
Catharanthus roseus	1.23	1.21	1.023	0.98	0.77

Table 4 .Total carbohydrate content of the selected medicinal plants were tabulated with respect to five days of interval

Total carbohydrates content was estimated by Anthrone method, and the total carbohydrate content of all the plants with respect to their days of interval is tabulated here(Table 4).We found that more amount of carbohydrate was found in *Azadirachta indica* control plant and also the salt stress effected *Azadirachta indica* has nearby amount of carbohydrates in it [20,21].It resembles that *Azadirachta indica* has some internal tolerance towards salt stress.

3.2.2 Total chlorophyll content in plant leaves:

Plants	Control on 20th day	5th day	10th day	15th day	20th day
Azadirachta indica	**1.98**	1.78	1.88	1.91	**2.012**
Cassia fistula	1.33	1.23	1.12	1.01	0.98
Aloe barbadensis	1.23	0.98	0.96	0.88	0.77
Catharanthus roseus	1.42	1.09	1.02	0.98	0.92

Table 5.Chlorophyll content of the selected medicinal plants in an interval of five days are tabulated here.

In the chlorophyll content estimation of the selected plants for 20 days, in the interval of five days , we found high amount of chlorophyll in *Azadirachta indica*, which is amazing phenomenon when compared to other plants. Whereas total chlorophyll content is an indicative of photosynthetic and metabolic activity and it was found high in *Azadirachta indica* ,and the other plants like *Cassia fistula ,Aloe barbadensis, Catharanthus roseus* lack the ability to withstand the salinity condition.

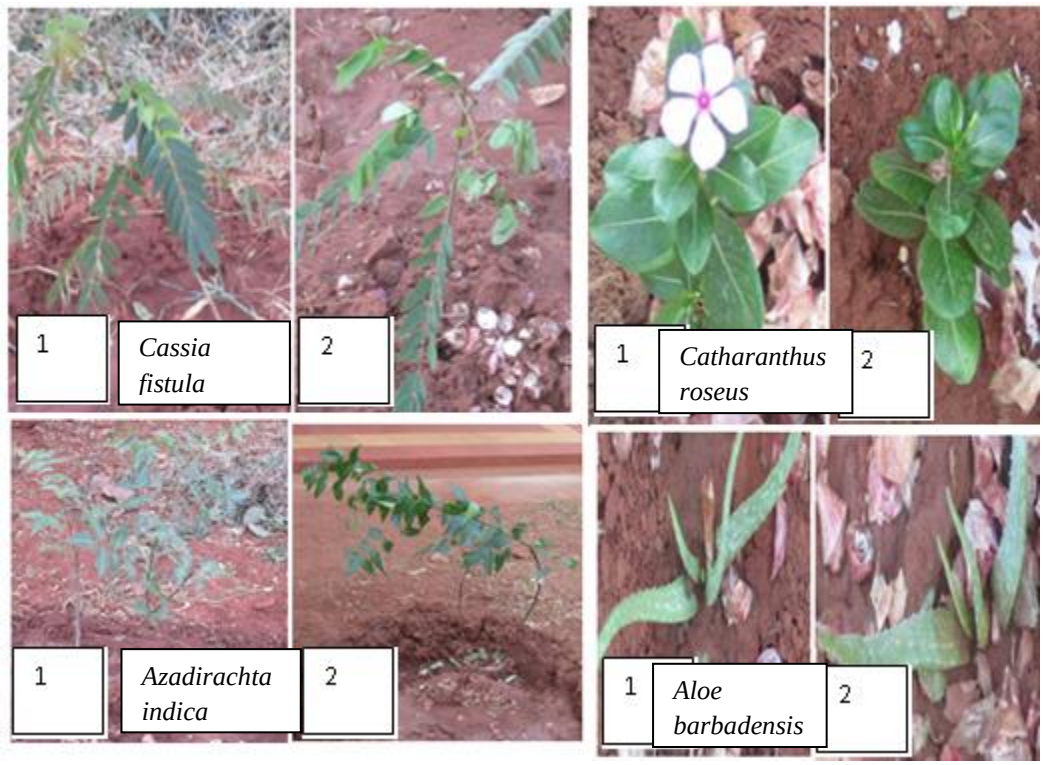

Figure 5. 1- indicates the control plant,2- indicates salt stress effected plant. The figure consist of *Cassia fistula and Catharanthus roseus in the first row, and Azadirachta indica and ,Aloe barbadensis* in the second row

From the above experimental work it was determined that *Azadirachta indica* which a most commonly used plant in medicinal works has the capability to survive in salinity conditions too. Its large scale cultivation is also easy in saline conditions as it has saline conditions withstanding property, while other plants have showed the suppressed growth conditions.

4.CONCLUSION:

Azadirachta indica has an ability to withstand salinity, was determined by some morphological and biochemical parameters. Whereas the salts stress varies from one plant to another which can be clearly observed from the experimental work which has been done. Good agricultural practice is specific for each country because of some differences in geoclimate, length of vegetative, time, precipitation, temperature and quality of soil[23-25]. Therefore there is a necessity for verification and adaptation of each plant in natural conditions of each region. By having advance research on these plants by gathering the genetic work and molecular work on these plants in addition to the morphological and biochemical parameters , new genetically manipulated traits can generated. This approach is promising, considering the novel approaches in combining genetic, physiological , biochemical and molecular techniques which results a excellent future of plants. One day soon, crops will be altered to survive and produce maximum yield grown under minimal conditions. The problem of salt stress will be alleviated and farmers will be satisfied[26].

5.REFERENCES

[1] J.P. Thornber, R.S. Alberte, F.A. Hunter, J.A. Shiozawa and K.S. Kan. *Brookhaven Symp. Biol.*, 1977, pp132–148.
[2] J. Argyroudi-Akoyunoglou and H. Thomou. *FEBS Lett.*, 1981, Vol 135, pp177–181.
[3] F.A. Wollman and P. Bennoun. *Biochim. Biophys. Acta*, 1982, Vol 680 , pp352–360.
[4] D. Ish-Shalom and I. Ohad. *Biochim. Biophys. Acta*,1983,Vol 722 , pp 498–507.
[5] J.M. Anderson, J.S. Brown, E. Lam and R. Malkin. *Photochem. Photobiol*, 1983,Vol 38 , pp205–210.
[6] P. Haworth, J.L. Watson and C.J. Arntzen. *Biochim. Biophys. Acta.*, 1983,Vol 724 , pp 151–158.
[7] N.H. Chua. *Methods Enzymol*,1980,Vol 69 , pp434–446
[8] D.I. Arnon. *Plant Physiol.*,1949, Vol 24 , pp1–15.
[9] E. Lam, W. Ortiz, S. Mayfield and R. Malkin, *Plant Physiol*,1984.
[10] J.E. Mullet, J.J. Burke and C.J. Arntzen. *Plant Physiol.*, 1980,Vol 65, pp823–827.
[11] G.W. Schmidt, S.G. Bartlett, A.R. Grossman, A.R. Cashmore and N.H. Chua. *J. Cell Biol*, 1981, Vol 91 , pp. 468–478.
[12] Ahuja AK: In *Himalayan Medicinal Plants: Potential and Prospects*. Edited by Samant SS, Dhar U, Palni LMS. Nainital: *Gyanodaya Prakashan*, 2001,pp1-21.
[13] Anonymous: *National Health Policy.* New Delhi: Ministry of Health and Family Welfare, Government of India; 1983.
[14] Kala CP: *International Journal of Sustainable Development and World Ecology* 2004, **11**(2)**:**205-210.
[15] Tolia RS.,*Patwari, Gharat and Chai*. Dehradun: Bishen Singh Mahendra Pal Singh; 2004
[16] Rawat RBS, Uniyal RC: Status of medicinal and aromatic plants sector in Uttaranchal: initiatives taken by the Government of India. *Financing Agriculture* 2004, Vol 36, pp7-13.
[17] Jain AP, Kumar H in: R and D funding in Himalayan region in India: A comparison. *Hima-Paryavaran* 1994, Vol 6, pp10-11.
[18] Kumar R., Medicinal, aromatic and herbal crops. *Financing Agriculture* 2004,Vol 36, pp3-5.
[19] Prahalathan S , Export potential of Indian medicinal plants and products. *FinancingAgriculture* 2004, Vol 36, pp33-36.
[20] Kaushik P, Dhiman AK in: *Medicinal Plants and Raw Drugs of India.* Dehradun: Bishen Singh Mahendra Pal Singh, 1999.
[21] Olsen CS, Larsen HO in: Alpine medicinal plant trade and Himalayan mountain livelihood strategies. *The Geographical Journal* 2003, pp169-243
[22] Joshi P, Dhawan V., in : *Swertia chirayita* – an overview, *Current Science* 2005, Vol 89, pp 635-640.
[23] Kumar S, *The Economic Plants of North East India.* Jodhpur: Scientific Publisher, 2000.
[24] Anonymous: *Herbals in India: Opportunities, Challenges and Initiatives by NABARD.* National Bank for Agriculture and Rural Development, India, 2004.
[25] Jain SK., Dictionary of Indian Folk Medicine and Ethnobotnay. New Delhi: Deep Publications, 1991.
[26] R. K. Sairam, and Aruna Tyagi, *Curent Science*, 2004,Vol 86, No. 3.

The Growing Phenomenon of Wireless Crime Forensic a Tracing and Tracing

Mr. Kapil Vyas, Mr. Ashish Sharma, Mr. Dalpat Songara.

Assistant Professors

* JECRC/F E & T, JODHPUR, INDIA

Abstract-

The wireless technology use is so widely spread illustrates that its benefits of the technology for now compensate the risks. Now the major bandwidth of the internet is being accessed more by the wireless links without concerning the security. The paper discusses the various aspects of wireless cyber crime with perspective of the venerability, detection and preventions of the malefic intentional use of the technology.

Key Words – Wireless forensic, Hitech Crime ,Wireless security. Wi-Fi threat.

I. Introduction

Currently, it is estimated that 75 percent of the wireless computer networks are vulnerable to attack. However, in spite of this statistic, the fact that wireless use is so widely prevalent illustrates that the benefits of the technology, for now, outweigh the risks.

These risks may become more problematic as the nation's critical IT infrastructure, namely, corporate sector, emergency services, and Government agencies, are becoming more and more tied to the Internet. This leads to an even bigger concern: the Internet is being accessed more and more frequently by wireless links connected to networks with inadequate security, which makes auditing and forensics all the more difficult. To counter or prevent the effects of these types of computer attacks, it is always best for organizations to ensure they are complying with basic network security guidelines. Although convenient and easy to deploy, wireless local area networks (WLANs) require proper planning, training, and an ongoing awareness of the security risks introduced by using wireless devices and networks. In this chapter we're going to cover threats, vulnerabilities, and security solutions related to Wi-Fi, PDAs, and cell

.

Ii Wireless Network Security Threats

The security risks in WLANs extend beyond those in a wired network to include the additional risks introduced by weaknesses in wireless protocols. The security threats posed by WLANs are considered in the following subsections.

Eavesdropping

Intercepting information that is transmitted over the WLAN is generally easier, as it can be done from a considerable distance outside of the building perimeter without any physical network connection. The information intercepted can be read if transmitted in the clear, or easily deciphered if only WEP encryption is used.

Traffic Analysis

The attacker gains information by monitoring wireless transmissions for patterns of communication and data flow between parties, and deciphers encrypted traffic that has been captured. Traffic analysis can result in the compromise of sensitive information.

Data Tampering

The information transmitted over the WLAN can be deleted, replayed, or modified by the attacker via man-in-the-middle attack. This can result in a loss of data integrity and availability.

Masquerading

The attacker gains unauthorized access to the information and network resources within the WLAN or other interconnected network by impersonating an authorized user. The attacker can cause further problems by launching attacks or introducing malicious code that can disrupt operations.

DENIAL -OF-SERVICE (Dos)

The attacker can jam the entire frequency channel that is used for wireless data transmission using a powerful signal generator, microwave, or a massive amount of broadcasted network traffic from a rogue wireless device. With high-gain antennas and WLAN attack tools, the perpetrator can cause denial-of-service without being close to the targeted WLAN, and although it is not impossible to direction-find (DF) the perpetrator, it is difficult and requires tools that are only now becoming available.

Wireless Client Attacks

The attacker can potentially gain access to the information shared or stored in the wireless client when it is connected to an unprotected ad hoc WLAN or an untrustworthy third-party WLAN. Additionally, the compromised wireless

client can potentially serve as a bridge to the internal network, thus allowing a perpetrator to gain access to or launch attacks against the internal corporate network and its resources.

OTHER ISSUES

Spread Spectrum Isn't Very Secure

Several of the 802.11 wireless LAN standards use spread spectrum, which is a modulation technique developed to prevent radio jamming. Spread spectrum, in general, is capable of changing the "spreading codes" in a way that makes decipherment impossible without knowing the correct codes. Wireless LAN vendors today still advertise the security that spread spectrum provides. This would be fine except that the 802.11 standard describes the spreading codes publicly so that companies can design interoperable 802.11 components. This means that a hacker or intruder would only need an 802.11-compliant radio NIC as the basis for connectivity, which nullifies the security benefits of spread spectrum

.Ssids ARE NOT DESINED AS PASSWORDS

The Service Set Identifier (SSID) is the name of a WLAN. All wireless devices on a particular WLAN must use the same SSID to communicate with each other. SSIDs were first introduced as a way to prevent people from connecting to the access point (AP) without foreknowledge of the SSID, which has now been incorporated into every AP as "Disabling broadcast SSID." So SSIDs serve a very useful function — identification of the AP or network; however, it should not be relied upon as a password.

WEP IS WEAK

The Wired Equivalent Privacy (WEP) protocol was designed to add security to WLANs. WEP was intended to give wireless networks the equivalent level of privacy of a comparable wired network. However, WEP occasionally produces typologically weak ciphers that are easily broken with modern tools. A step-by-step description of how the WEP protocol is cracked follows, to give you a better idea of the weakness of WEP and the speed with which it can be compromised:

1.A hacker runs Kismet, a wireless LAN discovery tool, to determine what wireless LANs are in the area. When the hacker discovers the SSID, the channel number it is operating on, and its BSSID (Basic Service Set Identifier—its Ethernet address), he has all the information needed to mount an attack to recover the WEP key.

2. If the SSID is unknown because the WLAN's owner has enabled mode that hides it (known as SSID Cloaking or SSID Broadcast Disable), the hacker can discover the SSID by waiting for a client to connect, in which case both the client as well as the AP disclose the SSID. Or the hacker can obtain the SSID by forcing an already connected client to disconnect and reconnect. This is done by sending a specially crafted packet pretending to be from the AP that tells the receiving client that it is no longer authenticated. The client has no way to tell that this is not actually coming from the AP, and so it attempts to rectify the problem by disconnecting from the AP and reconnecting, yielding the SSID in the process.

3. The hacker puts his wireless card into a monitor mode" in which the WLAN card eavesdrops on a WLAN without having to connect to it. He commands the WLAN card to monitor the channel on which the target AP is located, and begins capturing and saving all of the traffic monitored from that AP to disk in a file called a capture file.

4. The software used to capture the data notes the reception of packets encrypted with a weak Initialization Vector (IV), which in cryptography is a value used to initialize a cryptographic process. WEP misuses these IVs in an exploitable way, and when a certain number of weak IVs have been captured, the WEP key can be determined. Roughly 125,000 packets are required to crack most 40-bit WEP keys, and 200,000–250,000 packets for a 128-bit WEP key.

5. On a slow WLAN, capturing the requisite number of weak IVs can take some time. To accelerate the attack, the hacker will next inject a captured WEP frame back into the network to generate more traffic. This takes advantage of the fact that WEP has no "replay protection" mechanism to prevent this. An injection rate of 512 packets per second generally results in the required number of IVs being captured between 10 min for 40-bit and 30 min for 128-bit WEP. If no client is present on the WLAN to generate traffic that can be captured and reinjected, in most cases the attacker's own system can be made to do so.

6. After a sufficient number of IVs is captured, the hacker runs the AirCrack tool, which will attempt to crack and disclose the WEPkey.

7. Once the WEP key is known, the hacker can connect to the AP just as a legitimate client would — and the WLAN owner would be none be wiser.

WAR-DRIVING

War-driving is derived from the war-dialing exploits of the teenage hacker character in the 1983 movie War Games, who has his computer randomly dial hundreds of numbers. He eventually winds up tapping into a nuclear command and control system! With the growth of the Internet, scanning was the next version of this type of exploit. People often scan through large numbers of IP addresses looking for computers that are running certain types of servers.

The wireless age has introduced a new type of attack called war-driving.

Originally, war-driving was when crackers drove around in a car equipped with wireless gear looking for unsecured wireless networks to gain illicit access to. Over time, the term has evolved to include harmless types like us simply checking on the radio frequency (RF) environment.

- THE BASIC WAR-DRIVING KIT
- The basic kit consists of the following:
- Laptop computer

- Wireless NIC
- Antenna (optional)
- Software
- GPS unit (optional)

Why Are People War-Driving?
There is no clear answer to this question, because the act of war-driving can have so many different motivations. Technology is not bound to ethics. It is the application and use of that technology that brings ethics into it.
If someone is simply driving around a city searching for the existence of wireless networks, with no ulterior motive, it cannot be deemed illegal. However, if you are searching for a place to steal Internet access, or commit computer crimes, then war-driving is considered malicious and could be treated as such in court. Also remember that in the United States, simply receiving radio transmissions on the cellular telephone frequencies (895–925 MHz) is illegal.

A key differentiator here is that cellular interception takes place with equipment exclusive to the normal process of service, i.e., you don't use a cell phone to intercept someone else's call, you use a scanner. War driving (and wireless sniffing) uses the same equipment that you'd use to participate in a WLAN as a normal user. Further, because you have the right to monitor your own network, making monitoring tools illegal would certainly be questionable, especially in light of the current thinking that perhaps companies ought to be held liable for malicious activity occurring through their inadequately secured WLANs.

War-Chalking
War-chalking actually started out as something else. It was a secret sign language once used by hobos to alert fellow travelers of dangers or opportunities for food and work on the open road. Today, war-chalking is an extension of war-driving, in which people use chalk to place a special symbol on a sidewalk or other surface that indicates a nearby wireless network, especially one that offers Internet access.

War Flying
In yet another flavor of war-driving that has emerged in recent years, hobbyists are now taking their skills to the air. The term is appropriately named war flying and those using this technique are detecting hundreds of wireless LAN APs during short trips in private planes cruising at altitudes between 1500 and 2500 ft. On one war-flying tour over an area of San Diego County, a private plane detected 437 APs. Detection of so many APs is due to the increased range that wireless networks can broadcast upward because of lack of obstructions. However, the limit is currently around 2500 ft because most WLANs are vertically, not horizontally, polarized, and so most of the RF energy goes out parallel to the Earth's surface.

War-Driving And War-Chalking Ethics
In the previous subsections we have covered war-driving, war flying, and war-chalking; however, when we look beyond the definitions and techniques, we get into the ethical issues of these activities. Three questions come to mind:
1. Is it theft?
2. Is it harmful?
3. Is it stoppable?

Is It Theft?
According to the standard definition, theft is defined as "the felonious taking and removing of personal property with intent to deprive the rightful owner of it" Although war-chalking and war-driving activities identify and mark wireless networks, they do not remove or deprive the owner of his or her wireless connectivity. However, if common sense prevails here, this would be considered theft.

Wireless Crime Prevention Technique

In this new century we are entering a new age of policing, an age in which wireless technology will play a key role. Traditionally, police work has involved interviewing the public, searching the houses of suspects, and putting them under surveillance to discover whom the suspect was in touch with, where they traveled, etc. Today, in many cases, these techniques would reveal very little. In the future it will be far more useful to look at surveillance videos, review the suspect's e-mail and computer hard drive, and most importantly, gain access to cellular records as they will show where the suspect was and whom they were in contact with.

Is It Harmful?
War-chalking is only a process of identifying networks. It would be similar to going around a neighborhood and somehow making marks on public property identifying houses with weak security.

Is It Stoppable?
Not really, unless you are planning on installing lead walls. Owners of wireless networks can modify or shield their equipment, but it is by no means fool proof.

Proactive Measures
Now that we've seen an example of what's possible, let's look at some steps that can be taken to help protect a wireless network. In this section and the one that follows, we will cover some tools and best practices that will allow you to be proactive with our security. By using the same tools that hackers use to penetrate your network, you can to find and plug security holes beforehand. This combined

with using established security practices and policies, can help deter or prevent intrusions.
Tools for wireless networks:

Wlan Discovery Tools
- Netstumbler — Versions for Windows and Linux
- Kismet — Linux
- MacStumbler — Mac OS
- MiniStumbler — Pocket PC
- Mognet — Java

Wireless Network Sniffers
- AiroPeek — Windows
- AirTraf — Linux
- Ethereal — All OSs
- Sniffer Wireless — Windows and Pocket PC
- BSD AirTools — BSD

Wep Cracking Tools
- WEPCrack — Linux
- AirSnort — Linux
- BSD-Tools dweputils — BSD
- AirCrack — Linux and Windows
-

IV COMMON WI-FI SECURITY RECOMMENDATIONS: ACTIONS VERSUS REALITY

In the previous section we looked at some tools that will help you find out more about your wireless network and the information traveling across it. In this section we will take a closer look at what is commonly recommended
when securing wireless, and how effective those recommendations really are.

Recommended action: Turn SSID broadcasting off.Reality: Several software tools (such as Kismet) exist that will discover the SSID when a client connects — and common hacker tools can force a user to reconnect to the AP at will — thus giving up the SSID. In reality, this measure stops only two commonly used WLAN discovery tools from finding a WLAN, namely, Netstumbler and Windows XP.

Recommended action: Utilize static IP addresses.
Reality: Static IP address pools can be found quickly through simple traffic analysis, much quicker than you can eliminate DHCP from your network.

Recommended action: Turn 128-bit WEP encryption on.
Reality: WEP can be cracked in tens of minutes in essentially every case.

Recommended action: Change WEP keys periodically.
Reality: New WEP keys can be cracked just as quickly as old ones.

Recommended action: Enable MAC address filtering.
Reality: Simple traffic analysis will yield the authorized MAC addresses (which, after all, are the only ones passing traffic over the network). Because MAC addresses can be specified by a hacker for his WLAN card, this has no real security benefit. In fact, this "security tip" offers essentially zero security while requiring great effort to implement.

Recommended action: Utilize shared key authentication.
Reality: Again, WEP can be cracked quite rapidly.

Recommended action: Use personal firewalls.
Reality: A good idea to prevent anyone who does manage to connect with the AP from communicating with your mobile device and potentially obtaining data or doing harm. However, because attacks exist that fool the mobile device into believing that a hacker's system is a trusted one, this is not a panacea.

Recommended action: Administer wireless devices using secure protocols like SSH or HTTPS, instead of telnet or http. With the tunnel in place, anyone who tries to monitor the conversation between your laptop and the mail server will get something resembling line noise.
Reality: Unless the hacker is able to perpetrate a man-in-the-middle attack. SSH and HTTPS have been found vulnerable in the past to man-in-the-middle attacks in certain circumstances; wireless connections are easier to exploit in this regard than wired ones.

V. Personal Digital Assistants
Pda Threats And Vulnerabilities

Mobile Device Attacks
Although attacks on mobile devices are not as widely published or as prolific as the viruses and worms that infiltrate network security defenses, they do exist and can be equally dangerous. The open handheld operating systems are often left insecure, making the device highly susceptible to a variety of attacks. Some common attacks include: copying or stealing information from the device, loading malicious code onto the device, or destroying key files or applications on the device.

How A Pda Connects To Other Computers
A PDA connects to other computers by one or more of the following methods:

- Desktop synchronization
- Hardwired network interface card
- Wireless network interface card
- Bluetooth
- Wi-Fi

Viruses, Trojans, And Worms
As with desktop and laptop computers, PDAs and the programs they run can be vulnerable to malicious code, which include:

- Trojans: A program disguised as another program.
- Worms: Stand-alone programs that make full, running duplicationsof themselves, stealing system resources.

- Logic bombs: Programs within programs that perform destructive acts based on a trigger event.

One of the first reported wireless viruses was called Phage and was aimed at the Palm OS, back in 2000. Viruses depend on the type of PDA OS you are running. PDAs are also more likely to be a carrier of a virus than the actual target of an attack; however, this is probably of little comfort after a PDA has been synced with a workstation or worse, an enterprise.

Theft Of The Pda Device
PDAs and BlackBerrys are clearly more at risk for theft because of their size and weight. It's much easier to lift a device designed to go into your pocket as opposed to one that's not. The devices are often the main interest of the thief as they are typically worth a higher price tag despite their small size. However, this will not always be the case because as the data capacity and battery life increase, the data that resides on the device will interest the average thief.

Data Theft
Again, thanks to the portability of these devices and their ability to hold, in some cases, a variety of memory expansion cards, it often doesn't take much time for someone to quietly download all of your information to a removable flash card.

Mobile Code Exploits
Mobile code is software that is transmitted across a network from a server or other remote source to a local system and is then executed on that local system. Often, this is done without direct action by the user. This code may have flaws that can allow an attacker to compromise a PDA.

Authentication Theft
The theft of the device can also result in the theft of authentication information, which can allow access into additional resources or a larger network.

Dos Attacks
A DoS attack is an incident in which a user or organization is deprived of the services of a resource they would normally expect to have. In the instance of a PDA, everything from a mobile code exploit to the theft of the actual device constitutes a DoS.

Session Hijacking
Session hijacking is when someone takes over a TCP session between two machines, or in this case, a PDA and another PDA or network. Most authentications only occur at the start of a TCP session, allowing the hacker to gain access to the PDA or its host network.

Vi Pda Security

Anti-Virus Software
As with workstations and servers, running an anti-virus program on your PDA will help reduce the risks of data loss or corruption, and help prevent your PDA from being a target of attack when it syncs to a computer or network. Norton, Symantec, F-Secure, and Kaspersky all produce PDA anti-virus products.

Other Pda Security Measures
The following are important PDA security measures:

- Database security and authentication
- Faraday bag (which blocks all wireless signals to the device)
- Encryption — Ccrypt, PDA Secure (TrustDigital)
- Firewalls — Mobile Firewall Plus
- Password enforcement — HotSync security, PDA Defense
- VPN — VPN 3000 (Cisco), MovianVPN

Combating Handheld Attacks
As we've seen, mobile device platforms have their own set of threats and vulnerabilities. These pose unique challenges to security administrators. Every mobile user and mobile enterprise needs to carefully evaluate its own device-side security needs.

The following best practices, from Bluefire Security Technologies, Baltimore, Maryland, provide a basic guide to begin the process:

1. Define handheld security policy
2. Centrally enforce and monitor handheld security
3. Enforce use of power-on passwords
4. Block unauthorized handheld network activity
5. Detect handheld intrusions
6. Protect handheld integrity
7. Encrypt sensitive data stored on handhelds
8. Protect traffic sent/received by handhelds
9. Maintain up-to-date anti-virus protection
10. Back up frequently

Vi. Wireless Network Security Threats
The security risks in WLANs extend beyond those in a wired network to include the additional risks introduced by weaknesses in wireless protocols.
The security threats posed by WLANs are considered in the following subsections. Eavesdropping Intercepting

information that is transmitted over the WLAN is generally easier, as it can be done from a considerable distance outside of the building perimeter without any physical network connection. The information intercepted can be read if transmitted in the clear, or easily deciphered if only WEP encryption is used. Traffic Analysis The attacker gains information by monitoring wireless transmissions for patterns of communication and data flow between parties, and deciphers encrypted traffic that has been captured. Traffic analysis can result in the compromise of sensitive information.

E911
E911 is a location technology promoted by the FCC that will enable mobile, or cellular, phones to process 911 emergency calls and enable emergency services to locate the geographic position of the caller.

When a person makes a 911 call using a land line, the call is routed to the nearest public safety answering point (PSAP), which sends the emergency call to the proper service, such as the police, the fire department, etc. The PSAP receives the caller's phone number and the exact location of the phone call. This is how things would work if you were calling from a landline.
But what about mobile phones?

Before 1996, all 911 calls made using a mobile phone would have toaccess their carriers first. The carrier would then have to verify subscription
of service. Once verified, the call would be routed to a PSAP. The FCC refined this process, and ruled that all 911 calls must go directly to the PSAP without receiving subscription verification from the cellular carrier.
Intrado of Longmont, Colorado, is a company that provides 911 solutions for wireless cellular carriers. Intrado has so far deployed Phase 1 of the E911 directive, which identifies the cell site from which a cellular call originates. More than 190 million 911 calls are placed annually, and almost 50 million of those are made from wireless phones.

Police Use Of Wireless Devices
The police and law enforcement forces have used the radio for decades. The maxim "You can't outrun a radio" when referring to a car chase with the police is just one small example. Today, police and law enforcement officials are using some newer programs that surpass the traditional radio.

Packetcluster
PacketCluster Patrol software allows patrol cars direct access to crime fighting information from a car-based laptop. This technology is in practical use in Salinas and Monterey County in California. Using a wireless network, more than 400 patrol officers can access records from county, state, and federal databases.

Totalroam
TotalRoam is another in-vehicle platform that is designed to manage data routing for wireless network communications. TotalRoam allows highway patrol officers to use the wireless system to instantly and directly access critical information from databases covering vehicle registration, outstanding warrants, and much more. TotalRoam will also enable the wireless transmission of information gathered by other onboard equipment, such as breathalyzers and GPS. Another significant quality of TotalRoam is its redundancy. Its multiple networking design guarantees continual communication, ensuring that during emergency situations officers will always have backup.

Hi-Tech Patrol Cars
In the Sacramento Police Department, all 190 police cars are being fitted with wireless IP networking equipment and onboard computers, allowing each officer to access any database the department would normally have access to. SACPD cars will also be fitted with equipment to allow them to view live video feed from police helicopters. This will help officers make much better decisions during a chase, as well as aid superior officers in making more informed decisions in, for example, hostage situations.
SACPD is also working toward moving to a paperless, or paper reduced, system by giving officers wireless PDAs to streamline the paperwork
process. Additionally, these systems will eventually be integrated with the electronic tagging systems used by the judicial and prison services.

Wireless Honeypots
To quote Lance Spitzner, the leader of the Honeynet Project, the definition of a honeypot is:
A honeypot is an information system resource whose value lies in unauthorized or illicit use of that resource.

A wireless honeypot, used properly, could reveal pertinent and accurate statistics about attacks on your infrastructure, including:

- The frequency of attacks
- The attacker's skill level
- Goals and methods

Wireless honeypots, similar to their wired counterparts, can help protect your networks by diverting the attacker's time and resources on fake targets. In the black hat community, hackers enjoy penetrating wireless networks for the following reasons:

- They are somewhat safe, because the attacker isn't directly connected to the network.
- They are easy to hack, because there are a huge number of open or unsecured access points (APs) around.
- They are fun to attack, because the wireless network is still considered relatively new.
- They allow for a great deal of anonymity.

Vii Wireless Crime Prevention Techniques

In this new century we are entering a new age of policing. An age in which wireless technology will play a key role. Traditionally, police work has involved interviewing the public, searching the houses of suspects, and putting them under surveillance to discover whom the suspect was in touch with, where they traveled, etc. Today, in many cases, these techniques would reveal very little.

In the future it will be far more useful to look at surveillance videos, review the suspect's e-mail and computer hard drive, and most importantly, gain access to cellular records as they will show where the suspect was and whom they were in contact with.

Viii Conclusion

Crime is also evolving in many ways and adapting to newer technologies. Criminals are among the early adopters of new technologies and emerging platforms. Crime is here to stay in the wire-free world. The extortionist, criminal or murderer who in the past sent a threat message by sticking letters cut out from newspapers on a sheet, now prefers sending a text message while spoofing the mobile number to avoid identification and tracing.

References

[1]. Wireless Crime and Forensic Investigation (Auerbach, 2007).
[2]. Cyber Crime Investigations - A. Reyes (Syngress, 2007).
[3]. Investigating Computer-Related Crime - a Handbook for Corporate Investigators (CRC, 2000)
[4]. Farely, T., Basic Wireless Principles, Privateline.com, January 3, 2006.
[5]. Galeev, M., Home networking with Zigbee, Embedded.com, April 2004.
[6]. Reed T., War Chalking, Airshare.org, November 2003.
[7]. Tyrrell, K., An Overview of Wireless Security Issues, SANS Institute, 2003.

Towards the Artificial Vision – the retina implanting and visual Perception

Mr. Ashish Sharma, Mr. Kapil Vyas, Mr. Dalpat Songara.

* JECRC/F E & T, JODHPUR, INDIA

Abstract— Artificial vision for the blind was once the stuff of science fiction. But now, a limited form of artificial vision is a reality .Now we are at the beginning of the end of blindness with this type of technology. In an effort to illuminate the perpetually dark world of the blind, researchers are turning to technology. They are investigating several electronic-based strategies designed to bypass various defects or missing links along the brain's image processing pathway and provide some form of artificial sight.

I. INTRODUCTION

Bionic eye,' also called a Bio Electronic eye, is the electronic device that replaces functionality of a part or whole of the eye. It is still at a very early stage in its development, but if successful, it could restore vision to people who have lost sight during their lifetime. A bionic eye work by stimulating nerves, which are activated by electrical impulses. In this case the patient has a small device implanted into the body that can receive radio signals and transmit those signals to nerves.

II. HOW RETINA WORKS

The eye is one of the most amazing organs in the body. To understand how artificial vision is created, it's important to know about the important role that the retina plays in how you see Here is a simple explanation of what happens when you look at an object:

- Scattered light from the object enters through the cornea.
- The light is projected onto the retina.
- The retina sends messages to the brain through the optic nerve.
- The brain interprets what the object is.

In a healthy eye, the rods and cones on the retina convert light into tiny electrochemical impulses that are sent through the optic nerve and into the brain, where they're decoded into images.

The retina is complex in itself. This thin membrane at the back of the eye is a vital part of your ability to see. Its main function is to receive and transmit images to the brain. These are the three main types of cells in the eye that help perform this function:

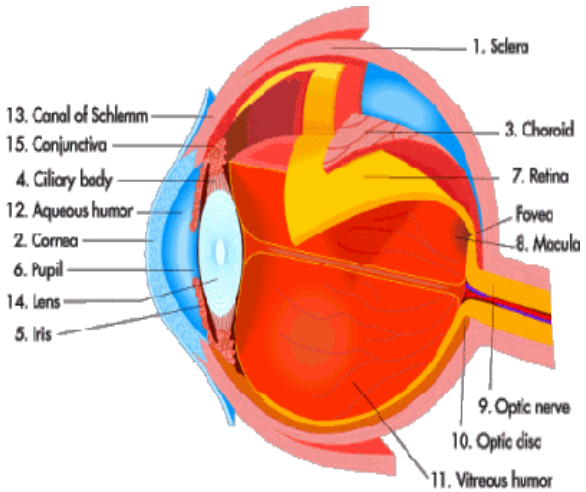

Fig 1. the anatomy of the eye

- Rods
- Cones
- Ganglion Cells

There are about 125 million rods and cones within the retina that act as the eye's photoreceptors. Rods are the most numerous of the two photoreceptors, outnumbering cones 18 to 1. Rods are able to function in low light (they can detect a single photon) and can create black and white images without much light. Once enough light is available (for example, daylight or artificial light in a room), cones give us the ability to see color and detail of objects. Cones are responsible for allowing you to read this report, because they allow us to see at a high resolution.

The information received by the rods and cones are then transmitted to the nearly 1 million ganglion cells in the retina. These ganglion cells interpret the messages from the rods and cones and send the information on to the brain by way of the optic nerve.

III. BLINDNESS

Blindness is more feared by the public than any ailment with the exception of cancer and AIDS.

Blindness is the condition of lacking visual perception due to physiological or neurological factors.

Various scales have been developed to describe the extent of vision loss and define blindness. Total blindness is the complete lack of form and visual light perception and is clinically recorded as NLP, an abbreviation for "no light perception." Blindness is frequently used to describe severe visual impairment with residual vision. Those described as having only light perception have no more sight than the ability to tell light from dark and the general direction of a light source.

A. Causes Of Blindness

There are a number of retinal diseases that attack these cells, which can lead to blindness.

The most notable of these diseases are

- Retinitis Pigmentosa
- Macular Degeneration

Retinitis Pigmentosa

Retinitis Pigmentosa (RP) is the name given to a group of hereditary diseases of the retina of the eye. RP may be caused by a breakdown in the function of the rods or the cones in some part of the retina. The retina is so complex that breakdowns may occur in a variety of ways and so RP is not a single disorder but a great number of disorders. The breakdown of cone function may be called Macular Degeneration.

Macular Degeneration

Macular is a sensitive area in the centre of the retina which provides us with sight in the centre of our field of vision. It allows us to see the fine details when we look directly at something. In macular degeneration, a layer beneath the retina, called the retinal pigment epithelium (RPE), gradually wears out from its lifelong duties of disposing of retinal waste products. A large proportion of macular degeneration cases are age- related.

B. Engineering Of The Bionic Eye

First, for visually impaired people to derive the greatest benefit from an enhanced-vision system, the image must be adapted to their particular blind areas and areas of poor acuity or contrast sensitivity.

The thrust of all prosthetic vision devices is to use an electrode array to give the user perceptions of points of light (phosphenes) that are correlated with the outside world.

Thus, to achieve the expected shift of the image across the stimulating electrode array, the camera capturing the image must follow the wearer's eye or pupil movements by monitoring the front of the eye under infrared (IR) illumination.

The eye-position monitor controls the image camera's orientation. If the main imageacquisition camera is not mounted on the head, compensation for head movement will be needed, as well.

Finally, if a retinal prosthesis is to receive power and signal input from outside the eye via an IR beam entering the pupil, the transmitter must be aligned with the intraocular chip. The beam has two roles: it sends power, and it is pulse-or amplitude modulated to transmit image data. Under the control of eye movement.

C. Bionic Eye Implants

There are two approaches by which we can implant a bionic eye:

- Artificial Silicon Retina – ASR
- Multi-unit Artificial Retina Chipset - MARC

Artificial Silicon Retina(Asr)

The ASR is a silicon chip 2 mm in diameter and 1/1000 inch in thickness. It contains approximately 3,500 microscopic solar cells called "micro photodiodes," each having its own stimulating electrode.

These micro photodiodes are designed to convert the light energy from images into thousands of tiny electrical impulses to stimulate the remaining functional cells of the retina in patients suffering with AMD and RP types of conditions.

Multiple Unit Artificial Retinachipset (Marc)

The other revolutionary bio electronic eye is the MARC; this uses a ccd camera input and a laser beam or rf to transmit the image into the chip present in the retina. Using this, a resolution of 100 pixels is achieved by using a 10x10 array. It consists of a platinum or rubber silicon electrode array placed inside the eye to stimulate the cells.

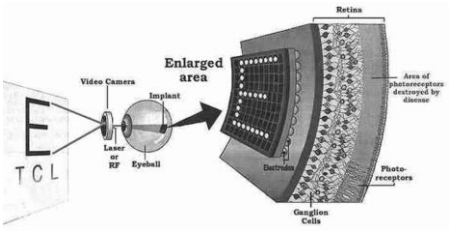

Fig 2 Multi-unit Artificial Retina Chipset

The schematic of the components of the MARC to be implanted consists of a secondary receiving coil mounted in close proximity to the cornea, a power and signal transceiver and processing chip, a stimulation-current driver, and a proposed electrode array fabricated on a material such as silicone rubber thin silicon or polyimide with ribbon cables connecting the devices.

The stimulating electrode array, an example of which is given in the figure below, is mounted on the retina while the power and signal transceiver is mounted in close proximity to the cornea.

An external miniature low-power CMOS camera worn in an eyeglass frame will capture an image and transfer the visual information and power to the intraocular components via RF telemetry.

The intraocular prosthesis will decode the signal and electrically stimulate the retinal neurons through the electrodes in a manner that corresponds to the image acquired by the CMOS Camera.

D. Working Of Bionic Eye

It uses a small video camera-equipped device to capture images, encode them and send them into the eye implant (a silicon chip inserted into the eyeball) via a laser beam that also powers the chip's solar cell.

Photo sensors convert the light and images into electrical impulses,which charge a plate that stimulates the nerves and transmits visual information to the brain. The laser and camera can easily be mounted on eyeglasses without having to wear bulky headgear.

The patient would wear goggles mounted with a small video camera. Light enters the camera, which then sends the image to a wireless wallet-sized computer for processing. The computer transmits this information to an infrared LED screen on the goggles.

The goggles reflect an infrared image into the eye and on to the retinal chip, stimulating photodiodes on the chip. The photodiodes mimic the retinal cells by

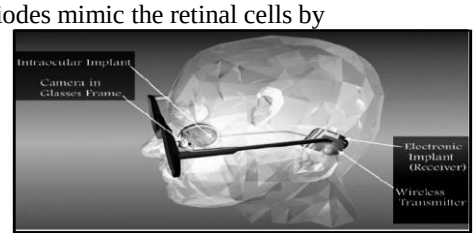

Fig 3. Working of Bionic Eye

converting light into electrical signals, which are then transmitted by cells in the inner retina via nerve pulses to the brain.

The goggles are transparent so if the user still has some vision, they can match that with the new information - the device would cover about 10° of the wearer's field of vision. The device involves a miniature video camera fitted to a pair of glasses.

The camera sends compressed digital images to a bionic implant on the back of the eye. Thousands of tiny electrodes in the bionic chip then stimulate the optic nerve, sending a signal to the visual centre at the back of the brain, where it is translated into an image.

Normal vision begins when light enters and moves through the eye to strike specialized photoreceptor (light-receiving)cells in the retina called rods and cones. These cells convert light signals to electric impulses that are sent to the optic nerve and the brain.

Retinal diseases like age-related macular degeneration and retinitis pigmentosa destroy vision by annihilating these cells. With the artificial retina device, a miniature camera mounted in eyeglasses captures images and wirelessly sends the information to a microprocessor (worn on a belt) that converts the data to an electronic signal and transmits it to a receiver on the eye. The receiver sends the signals through a tiny, thin cable to the microelectrode array, stimulating it to emit pulses.

The artificial retina device thus bypasses defunct photoreceptor cells and transmits electrical signals directly to the retina's remaining viable cells. The pulses travel to the optic nerve and, ultimately, to the brain, which perceives patterns of light and dark spots corresponding to the electrodes stimulated. Patients learn to interpret these visual patterns.

It takes some training for subjects to actually see a tree. At first, they see mostly light and dark spots. But after a while, they learn to interpret what the brain is showing them, and they eventually perceive that pattern of light and dark as a tree. Researchers are already planning a third version that has 1000 electrodes on the retinal implant, which they believe could allow for reading, facial recognition capabilities etc.

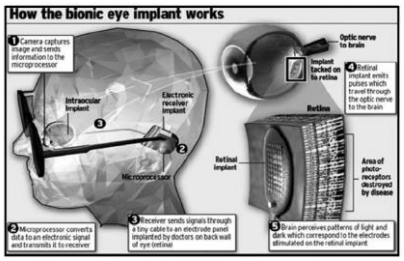

Fig. 4. Implantation of Bionic Eye

E. References

[1] Dowling, J. "Current and Future Prospects for Optoelectronic Retinal Prostheses." Eye 23.10 (2008): 1999-2005. Academic Search Premier.

[2] "Breakthrough Eye Implant Helps 3 Blind Patients See." The Vancouver Providence [British Columbia] 3 Nov. 2010, Final ed. LexisNexis Academic. Web. 27 Jan. 2011

[3] Park, Robert I. "The Bionic Eye: Retinal Prostheses." International Ophthalmology Clinics 44.4 (2004): 139-54. Wolters Kluwer Health. OvidSP, Fall 2004. Web. 26 Jan. 2011. <http://ovidsp.tx.ovid.com>.

[4] Victor Shnayder, Bor-rong Chen, Konrad Lorincz, Thaddeus R. F. Fulford-Jones, and Matt Welsh. "Sensor Networks for Medical Care", Harvard University Technical Report TR-08-05, April 2005.

[5] Anthony's textbook of Anatomy and Physiology -Gary A Thibodeau, Kevin T Patton
Image processing for a high-resolution optoelectronic retinal prosthesis. Asher, A; Segal, WA; Baccus, SA; Yaroslavsky, LP; Palanker, DV; IEEE Transactions on Biomedical Engineering, 54(6): 993-1004 (2007).

[6] Optoelectronic retinal prosthesis: system design and performance. J.D. Loudin, D.M. Simanovskii, K. Vijayraghavan, C.K. Sramek, A.F. Butterwick, P. Huie, G.Y. McLean, and D.V. Palanker. Journal of Neural Engineering, 4: S72–S84 (2007).

[7] High-Resolution Electronic Retinal Prosthesis: Physical Limitations and Design. D. Palanker, A. Vankov, P. Huie, A. Butterwick, I. Chan, M.F. Marmor and M.S. Blumenkranz; Chapter 14 in ARTIFICIAL SIGHT: BASIC RESEARCH,BIOMEDICAL ENGINEERING, AND CLINICAL ADVANCES; M.S. Humayun, J.D. Weiland, G. Chader, E. Greenbaum (Eds.), Springer Series: Biological and Medical Physics, Biomedical Engineering, New York, 2007.

[8] Effect of shape and coating of a subretinal prosthesis on its integration with the retina. A. Butterwick, P. Huie, B.W. Jones, R.E. Marc, M. Marmor, D. Palanker. Experimental Eye Research

Distribution Simulation Package for Low Voltage Distribution Network

R. Chitra[1], R. Neelaveni[2]

[1.] DGM / TNEB, Research Scholar/Department of Electrical and Electronics Engineering, PSG College of Technology, Coimbatore, India

[2] Assistant Professor, Department of Electrical and Electronics Engineering, PSG College of Technology, Coimbatore, India

Abstract

Distribution loads vary in response to temperature, time of the day, day of the week and other factors such as humidity precipitation and season. The effects of daily load patterns of a typical low voltage network (LV network) need to be studied in depth for optimization. This requires a detailed collection of distribution transformer load recordings of all electrical parameters such as voltage, current, power and power factor for all three phases. Load analysis is the detailed systematic study of all load recordings to derive significant conclusions. Hence there arises a need for the development of distribution simulation package (DSP) for LV network load analysis and optimization.

In the design of simulation package, LabVIEW is used as software simulation tool. There are four modules developed in the DSP namely, Load Survey Module, Power measurement Module, Display Module and Unbalance Prediction Module. In the existing system of distribution network, the distribution transformers (DT) are fixed with energy meters in the secondary of the DT and energy meter readings are downloaded with common meter reading instrument (CMRI). The energy meter reading includes voltage current profile (vi – profile) with power factor and serves as input to the DSP. Outputs of DSP are Power and Energy Measurement, Voltage Graph, Load Graph, Power Graph and Prediction of unbalance in the LV distribution Network.

DSP can be termed as effective Management and Monitoring Module (**MMM**) for LV networks. With the DSP, LV networks are studied, analyzed results obtained; Hypotheses derived and significant conclusions are drawn.

Keywords: distribution simulation package, load analysis, lv network, optimization, reconfiguration and unbalance prediction.

1. Introduction

Electrical utility has three functional areas namely generation, transmission and distribution. In the distribution network there are two main distribution network lines namely, primary distribution lines (33kV/22kV/11kV) and secondary distribution lines (415 volts line voltage). Primary distribution lines feed the HT consumers and distribution transformers. The distribution transformers feed the low voltage distribution networks which are the secondary distribution lines. Hence low voltage distribution network (LV network) is the last link connecting the consumers. Each of the primary distribution line leaves the sub-station as a three-phase circuit and supplies a number of distribution transformers. On the secondary side of the distribution transformer, the Secondary distribution lines are connected. The distribution transformers and secondary distribution lines are rated to maintain the voltage received by consumers within a prescribed tolerance over the full range of loading conditions. The Figure 1 shows the distribution system prevalent in India.

The main part of distribution system includes:-

1. Receiving Substation.
2. Sub-transmission lines.
3. Distribution substation located closer to the load centre.
4. Secondary circuits on the LV side of the distribution transformer.
5. Service mains with metering arrangement.

The existing system in the distribution network is manually controlled. The distribution transformers are located at convenient places in the load area. At the distribution transformer, the voltage is stepped down to 415V and power is fed into the secondary distribution systems. The secondary distribution system consists of distributors (Pillar Boxes) which are laid along the road sides. The service connections to consumers are tapped off from the distributors.The main feeders, distributors may consist of overhead lines or cables or both. The distributors are 3- phase, 4 wire circuits, the neutral wire being necessary to supply the single phase loads. There are single phase and three phase services given by the electrical utility depending on the requirement of consumers. The service connections of consumer are known as service mains. A ground connection is normally provided, connected to conductive cases and other safety equipment, to keep current away from equipment and people. For single phase services the phase and neutral conductors from distribution transformer is connected

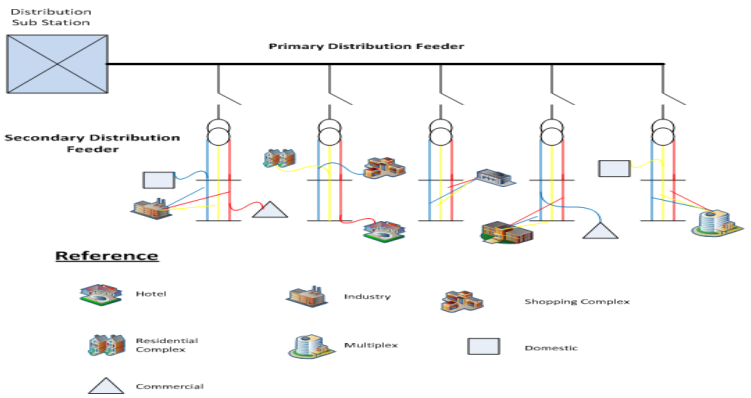

Figure 1 Distribution System

2. Performance of distribution system

The distribution system requires more attention as it is very difficult to standardize due to its complexity. As it involves consumers, power quality becomes paramount consideration in feeding the power supply. With a quality power there is need for uninterrupted supply of power. To avoid shortage of power one important consideration is reduction of transmission and distribution losses. Transmission and distribution losses (t & d losses) in india have been consistently on the higher side between the ranges of 21–25%. Out of these losses, 19% is at the distribution level in which 14% is contributed by technical losses. This is due to inadequate investments for system improvement work. The detailed analysis of distribution transformers with different types of loading patterns have to be studied for solving power quality issues. Such data are not available in scientific way for analysis across the country, India. Therefore, DSP has been developed .Utmost care has been taken to collect the data of LV network from different places like metro, urban and rural populated regions to be analysed using DSP. There are at least data from 100 transformers analyzed before presenting the inferences. Out of 100 transformers, a sample transformer have been presented in this work. The relevant work in the literature for the presented work is summarized below.

Valentina Cecchi and et al (2007) have designed instrumentation and measurement configuration for network configuration and meter placement. The work is in primary distribution network and it is not extended up to secondary distribution network. Aderiano Galindo Leal and et al (2009) describes artificial neural network approach for loss evaluation of distribution transformer. The authors have recorded seven-day load profiles of distribution transformers of Brazilian distribution utility which proves uniformity in stochastic nature of the loads. That is, load profiles of different categories of consumers can be grouped under clusters as residential, commercial and industrial. But it requires daily load profiles of consumers whereas daily load profiles of distribution transformer are only available in developed country's scenario. Hence development of DSP for developing countries' is significant contribution for distribution sector.

3. Development of distribution simulation package

In the existing system of distribution network, energy meters are provided for energy accounting. There is no means of sensing unbalance currents, voltage unbalance and power factor correction requirement for continuous 24 hours in three phases of LT Feeder. In other words, load curves, voltage curves, energy curves and power factor curves for individual three phases for full day are not available for monitoring, analyzing and controlling the LV network. To solve this, the modules developed in the DSP are listed below along with their associated function.

- ***Load Survey Module***: Collection of 30 minute readings on the daily load pattern of distribution transformer.
- ***Power measurement Module***: The measurement of power (Real, Reactive and Apparent) and display of voltage –current (vi-profile), power factor and power in the front panel for each phase R, Y and B.
- ***Display Module***: The display of voltage graph showing all three phases, current graph with all three phases, power graph showing all three phases and total power for any selected day for the low voltage distribution network. These graphs are effectively utilized for load analysis and to study the power quality performance of low voltage distribution network.
- ***Unbalance Prediction Module***: Prediction of unbalance in the network for the day selected and display them with LED indicators.

3.1 Design of Simulation Package

In the existing system of distribution network, the distribution transformers are fixed with energy meters in the secondary of the distribution transformer and energy meter readings are downloaded with CMRI. The energy meter reading includes voltage current profile (vi – profile) and power factor. It can be used for power measurement. With additional functionalities developed in this work like plotting of all electrical parameters on graph, prediction of unbalance current, LabVIEW based system can be termed as effective management and monitoring Module (**MMM**) for low voltage distribution networks.

3.1.1 Load Survey Module

The phase voltages, line currents and power factor of all three phases are monitored every half an hour in the meter fixed in the secondary of the distribution transformer. The voltage curve and load curve are obtained from these values. The active, the reactive and the apparent power are computed from these quantities after determining the phase angle. "VI-sub modules" are developed and the parameters listed below are plotted.

- Individual phase voltage.
- Individual phase current.
- Individual phase active power.
- Individual phase reactive power.
- Individual phase apparent power.
- Individual phase power factor.

With the above concepts, the front panel and block diagram are developed for three phase loads by downloading the vi-profile (voltage current profile) from energy meter installed in the distribution transformer and simulating the setup using practical values. From the actual values obtained load unbalance is predicted.

3.1.2 Power Measurement Module Design

The energy meter reading which includes vi-profile with power factor serves as one of the inputs to LabVIEW system. It consists of 30 minute readings and hence 48 samples per day. The other input for power calculation and display of voltage graph, current graph, power graph and energy graph is the 'day' input. For particular transformer and particular day of the month selected, all graphs of electrical parameters and power measurement has been designed in the block diagram of LabVIEW and displayed in the Front panel. Figure 2 shows the subVI for displaying the vi-profile on a particular date. The subVI for the measurement of power is shown in Figure 3. The block diagram for design of measurement of power is displayed in Figure 4.

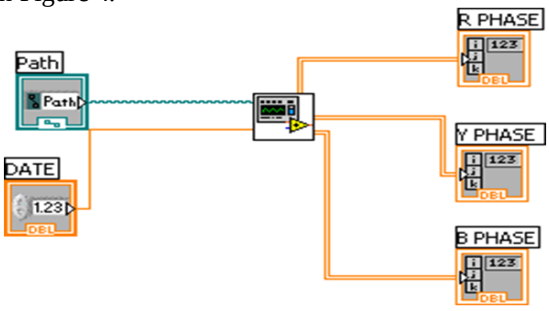

Figure 2 SubVI for vi-Profile

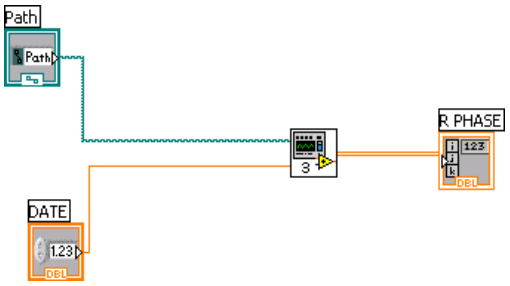

Figure 3 SubVI for Measurement of Power

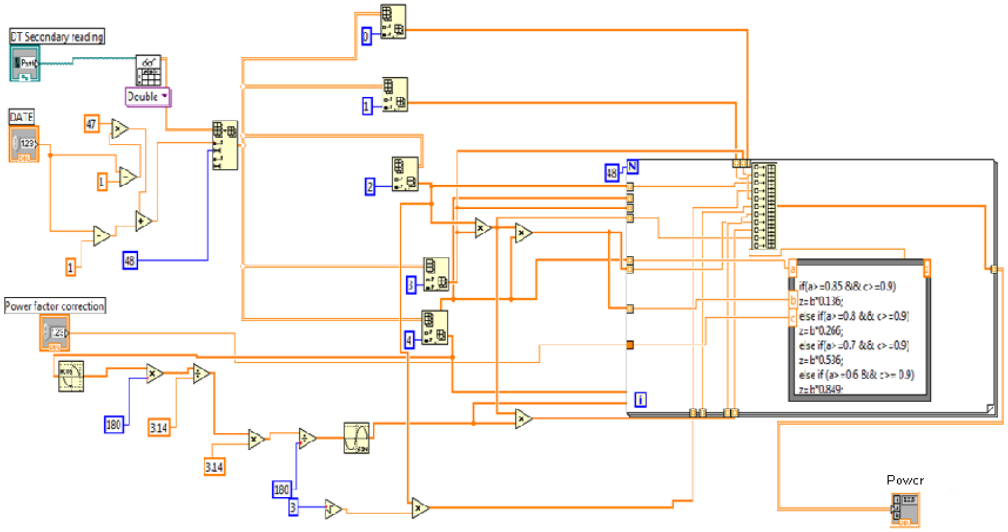

Figure 4 Block Diagram for Measurement of Power

3.1.3 Unbalance Prediction Module

Load analysis of transformer has to be done for full month to check for the consistency and stochastic nature of the loads. To balance the current in the secondary distribution network, only the peak load period is considered since the loads are predominant at peak load. The unbalance effect is more during peak loads. By attempting load balance during peak hours gives better performance throughout the day. SubVI for finding the maximum current in a particular day and particular phase is shown in Figure 5 and subVI for prediction of current unbalance is shown in Figure 6.

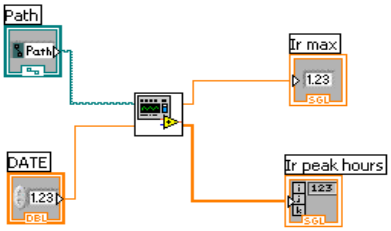

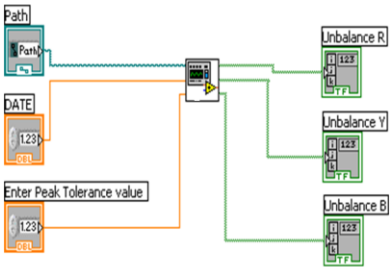

Figure 5 SubVI for Maximum Current **Figure 6 SubVI for Prediction of Current Unbalance**

The subVI displays the maximum current in a particular phase and it also displays current consumption in the peak load hours. In similar way, the LabVIEW is designed for all three phases.

The maximum current consumption in each phase is $I_{Rmax,}$ $I_{Ymax,}$ and $I_{Bmax.}$ The optimum current (I_{opt}) is given by equation 1

$$I_{opt}= (I_{Rmax} +I_{Ymax} + I_{Bmax})/3 \qquad (1)$$

The difference between I_{opt} and I_{Rmax} is then determined. Similarly the difference between I_{opt} and I_{Ymax} , I_{opt} and I_{Bmax} is computed. If the difference is positive then that phase is considered as overloaded and if the difference is negative then that phase is considered to be under loaded. If the difference is within the tolerance value, then that load is perfectly balanced. If there is unbalance, then it is displayed by the LED indicators as in Figure 7. Unbalance in particular phase is indicated by "RED" indication and balanced condition of particular phase is indicated by "GREEN" indication

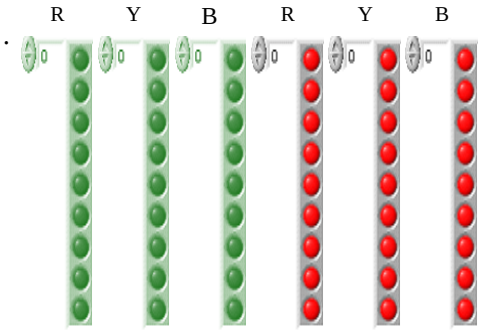

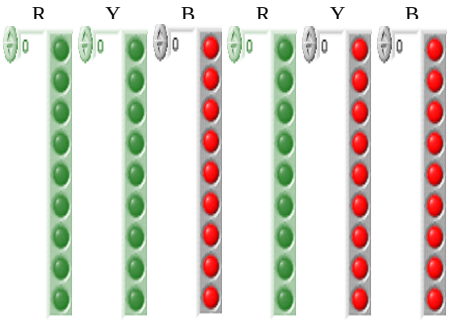

Balanced Condition Unbalanced condition Balanced Condition in two phases Unbalanced Condition in two phases

Figure 7 Display of Balanced/Unbalanced condition in LV Network

For the peak period, four hours is selected. There are 9 sets of reading for every half-an-hour. For example, if the peak period is 18 hrs to 22 hrs there will be nine set of half–an-hour reading starting with 18hrs reading and ending with 22hrs reading. LED display indicates the time of unbalance during peak hours and extent of unbalance studied from load graph display.

3.2 Load analysis

Load analysis of distribution transformers with different loading patterns deduces significant inferences for the work presented in this paper. For performing load analysis, distribution simulation package developed as discussed in Section 3.1 is effectively utilized. One number sample transformer has been presented in this paper as case study. Typical loads on low voltage networks are stochastic by nature. However it has to be ensured that there is similarity in stochastic nature throughout the day. For arriving at practical and effective conclusion for formulating this pragmatic methodology and to solve the power quality issues, the study has been undertaken using DSP.

Input to the DSP

- Low voltage distribution album of distribution transformer.
- Meter readings of distribution transformer (30minute readings).

Output from the DSP

- Power measurement
- Voltage graph
- Load (Current Graph)
- Power graph and Total power

3.2.1 Load Analysis of Sample Distribution Transformer

The schematic diagram with low voltage distribution album is shown in Figure 8. Energy Measurement for one day is shown in Figure 9 and load graphs for 2 different days taken at random are shown in Figure 10 and Figure 11.

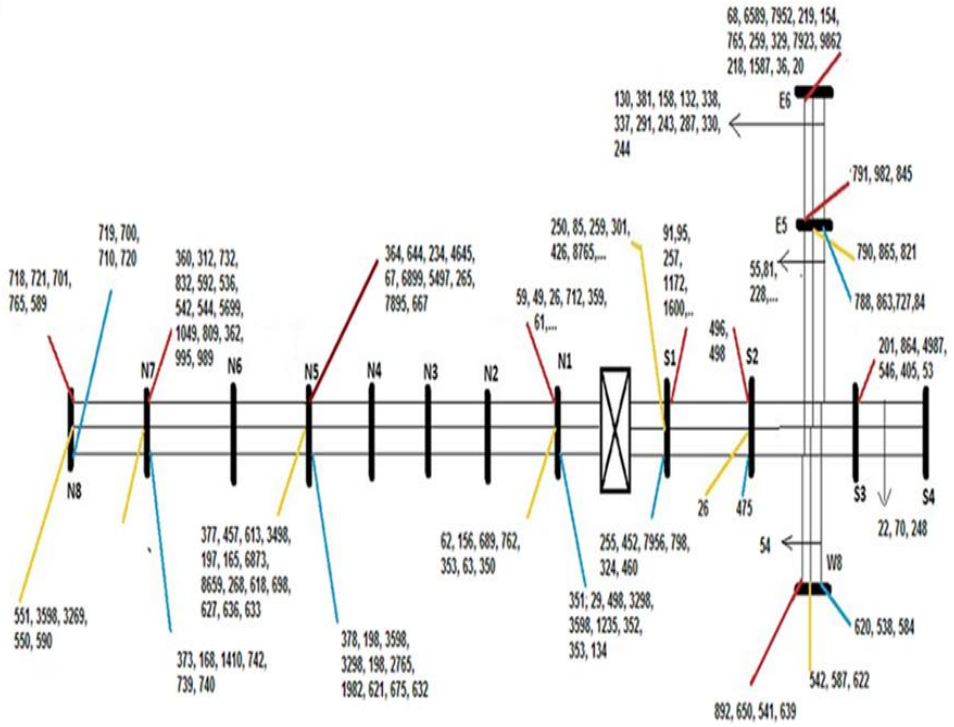

Figure 8 LT Album of Sample Distribution Transformer

Measurement of power and energy in low voltage distribution network

Date	Time	Voltage			Current			Active Power			Power Factor			Total Power	kWh
		R	Y	B	R	Y	B	R	Y	B	R	Y	B		
5/8/2009	0:00:00	255.29	254.12	256.47	275.4412	182.27	109.2227	63.29	41.69	25.21	0.9	0.9	0.9	130.18	65.09
5/8/2009	0:30:00	256.47	254.12	256.47	275.1129	175.8329	110.9525	63.5	40.21	25.61	0.9	0.9	0.9	129.33	64.66
5/8/2009	1:00:00	256.47	254.12	257.65	271.1734	171.0899	106.5045	62.59	39.13	24.7	0.9	0.9	0.9	126.42	63.21
5/8/2009	1:30:00	257.65	255.29	258.82	271.1734	176.8493	106.5045	62.88	40.63	24.81	0.9	0.9	0.9	128.32	64.16
5/8/2009	2:00:00	258.82	255.29	258.82	273.4715	171.7674	106.0103	63.7	39.47	24.69	0.9	0.9	0.9	127.86	63.93
5/8/2009	2:30:00	258.82	256.47	258.82	268.547	173.4614	98.8441	62.55	40.04	23.02	0.9	0.9	0.9	125.62	62.81
5/8/2009	3:00:00	257.65	255.29	258.82	263.2942	182.27	101.8094	61.05	41.88	23.72	0.9	0.9	0.9	126.65	63.32
5/8/2009	3:30:00	257.65	255.29	258.82	281.3606	190.7398	104.5276	65.24	43.82	24.35	0.9	0.9	0.9	133.41	66.71
5/8/2009	4:00:00	256.47	254.12	257.65	287.9165	182.27	107.7401	66.46	41.69	24.98	0.9	0.9	0.9	133.13	66.56
5/8/2009	4:30:00	256.47	254.12	256.47	293.1693	208.6957	125.7791	67.67	47.73	29.03	0.9	0.9	0.9	144.43	72.22
5/8/2009	5:00:00	255.29	254.12	254.12	335.5196	226.6517	115.6476	77.09	51.84	26.45	0.9	0.9	0.9	155.38	77.69
5/8/2009	5:30:00	252.94	250.59	251.76	401.8356	323.5462	118.3658	91.48	72.97	26.82	0.9	0.9	0.9	191.27	95.63
5/8/2009	6:00:00	249.41	248.24	249.41	488.8343	309.3169	102.5508	109.73	69.11	23.02	0.9	0.9	0.9	201.85	100.93
5/8/2009	6:30:00	242.35	243.53	243.53	540.377	375.0425	111.6938	117.86	82.2	24.48	0.9	0.9	0.9	224.55	112.27
5/8/2009	7:00:00	236.47	237.65	237.65	634.9265	421.457	154.9381	135.13	90.14	33.14	0.9	0.9	0.9	258.41	129.2
5/8/2009	7:30:00	241.18	243.53	243.53	640.5076	403.1622	141.8413	139.03	88.36	31.09	0.9	0.9	0.9	258.48	129.24
5/8/2009	8:00:00	241.18	242.35	243.53	528.5583	343.8737	167.0465	114.73	75	36.61	0.9	0.9	0.9	226.35	113.17
5/8/2009	8:30:00	241.18	242.35	244.71	540.7053	458.7241	206.0899	117.37	100.05	45.39	0.9	0.9	0.9	262.81	131.41
5/8/2009	9:00:00	241.18	241.18	243.53	509.517	501.7506	207.8197	110.6	108.91	45.55	0.9	0.9	0.9	265.06	132.53
5/8/2009	9:30:00	245.88	245.88	248.24	406.1035	425.1837	190.2749	89.87	94.09	42.51	0.9	0.9	0.9	226.47	113.23
5/8/2009	10:00:00	249.41	249.41	251.76	464.5404	382.4959	154.1968	104.27	85.86	34.94	0.9	0.9	0.9	225.07	112.54
5/8/2009	10:30:00	249.41	249.41	251.76	428.4277	374.0261	152.7141	96.17	83.96	34.6	0.9	0.9	0.9	214.73	107.36
5/8/2009	11:00:00	250.59	249.41	252.94	383.1227	359.7969	149.2546	86.41	80.76	33.98	0.9	0.9	0.9	201.15	100.57
5/8/2009	11:30:00	250.59	250.59	252.94	427.4428	379.4468	143.3239	96.4	85.58	32.63	0.9	0.9	0.9	214.61	107.3
5/8/2009	12:00:00	252.94	251.76	254.12	357.1872	328.9668	145.795	81.31	74.54	33.34	0.9	0.9	0.9	189.2	94.6
5/8/2009	12:30:00	0	0	0	0	0	0	0	0	0	0	0	0	0	0
5/8/2009	13:00:00	0	0	0	0	0	0	0	0	0	0	0	0	0	0
5/8/2009	13:30:00	0	0	0	0	0	0	0	0	0	0	0	0	0	0
5/8/2009	14:19:00	256.47	256.47	257.65	428.0994	344.2125	160.3746	98.82	79.45	37.19	0.9	0.9	0.9	215.46	107.73
5/8/2009	14:30:00	256.47	256.47	258.82	384.4359	326.2565	151.7257	88.74	75.31	35.34	0.9	0.9	0.9	199.39	99.69
5/8/2009	15:00:00	255.29	255.29	257.65	369.3342	280.5196	117.3774	84.86	64.45	27.22	0.9	0.9	0.9	176.53	88.26
5/8/2009	15:30:00	256.47	255.29	257.65	236.3739	202.5975	73.39174	54.56	46.55	17.02	0.9	0.9	0.9	118.13	59.06
5/8/2009	16:00:00	255.29	255.29	257.65	256.7283	229.7008	76.10996	58.99	52.78	17.65	0.9	0.9	0.9	129.41	64.71
5/8/2009	16:30:00	255.29	255.29	257.65	301.705	282.8911	75.61574	69.32	65	17.53	0.9	0.9	0.9	151.85	75.93
5/8/2009	17:03:00	255.29	255.29	257.65	323.3726	227.6681	95.63167	74.3	52.31	22.18	0.9	0.9	0.9	148.78	74.39
5/8/2009	17:30:00	251.76	251.76	254.12	427.7711	333.7099	139.6173	96.93	75.61	31.93	0.9	0.9	0.9	204.47	102.24
5/8/2009	18:00:00	248.24	249.41	251.76	514.4415	449.2379	220.4223	114.93	100.84	49.94	0.9	0.9	0.9	265.72	132.86
5/8/2009	18:30:00	248.24	249.41	251.76	559.4182	470.5818	234.7547	124.98	105.63	53.19	0.9	0.9	0.9	283.81	141.9
5/8/2009	19:00:00	249.41	250.59	251.76	615.2287	495.9912	236.4845	138.1	111.86	53.58	0.9	0.9	0.9	303.54	151.77
5/8/2009	19:30:00	251.76	252.94	255.29	639.1944	504.461	272.3155	144.83	114.84	62.57	0.9	0.9	0.9	322.24	161.12
5/8/2009	20:00:00	254.12	255.29	256.47	615.557	479.3904	233.025	140.78	110.15	53.79	0.9	0.9	0.9	304.72	152.36
5/8/2009	20:30:00	254.12	255.29	257.65	584.6971	442.8009	210.5379	133.72	101.74	48.82	0.9	0.9	0.9	284.28	142.14
5/8/2009	21:00:00	251.76	252.94	254.12	541.0336	401.4683	202.3833	122.59	91.39	46.29	0.9	0.9	0.9	260.27	130.13
5/8/2009	21:30:00	255.29	255.29	257.65	465.8535	352.0047	169.7647	107.03	80.88	39.37	0.9	0.9	0.9	227.28	113.64
5/8/2009	22:00:00	254.12	252.94	255.29	406.4318	313.0436	149.7488	92.95	71.26	34.41	0.9	0.9	0.9	198.62	99.31
5/8/2009	22:30:00	255.29	254.12	256.47	323.3726	281.8748	133.6866	74.3	64.47	30.86	0.9	0.9	0.9	169.62	84.81
5/8/2009	23:00:00	255.29	254.12	256.47	294.1542	209.0345	116.8831	67.59	47.81	26.98	0.9	0.9	0.9	142.37	71.19
5/8/2009	23:30:00	257.65	255.29	257.65	275.4412	197.5156	112.6823	63.87	45.38	26.13	0.9	0.9	0.9	135.38	67.69
Distribution transformer cumulative kilo watt hour in kWh															4431.29

Figure 9 Energy Measurement of sample Distribution Transformer

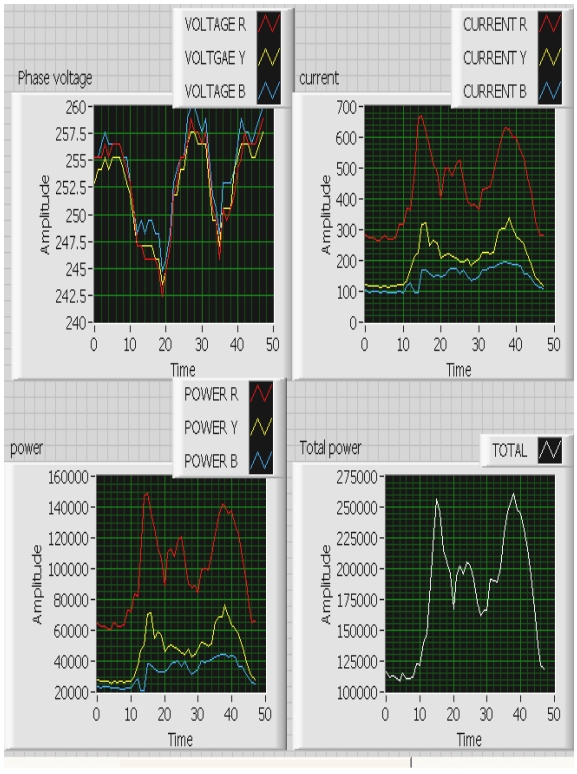

05-08-2009

Figure 10 Load Graphs

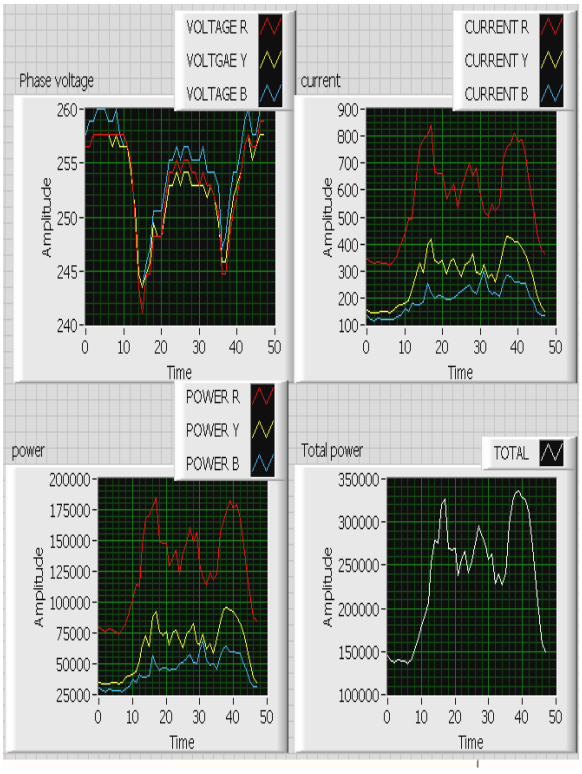

09-08-2009

Figure 11 Load Graphs

3.3 Results and Discussions

The detailed analysis of distribution transformers with different types of loading patterns leads to very interesting findings as summarized below.

- Though the load utilization of individual consumers is a variable factor, there is uniformity found in stochastic nature.
- The per-capita consumption of electricity is high in urban compared to rural areas.
- The peaks and valleys in load graphs tend to follow similarity though not identical in all types of distribution network.
- The high peak occurs in approximately same band of one hour every day, the major variation may be two hours which is also very rare.
- The peak load of the transformer occurs when majority of the consumers connected to distribution network utilizes most of the loads. It occurs in the same time band of peak load of the distribution transformer due to prevailing culture and habit of the people.
- The percentage of unbalance between phases is observed to be proportionate and hence value of unbalance will be maximum during peak loads.

3.4. Conclusion

All the inferences made out of low voltage distribution network load analysis prove that optimization of low voltage distribution network can be achieved by proper planning and successful reconfiguration of consumers to avoid unbalance of loads in distribution LV network. This distribution package serves as a backbone for the load analysis. With this method of load analysis and load reconfiguration there is a possibility of energy saving in terms of millions of rupees to the nation.

References

1) Adriano Galindo Leal, Antonio Jardini, Luiz Carlos Magrini and Se Un Ahn, “Distribution Transformer losses Evalution: A New Analytical Methodology and Artificial Neural Network Approach”, IEEE Transactions on Power Systems, Vol.24, No.May 2009.

2) Ajay Kumar Saxena, S.D. Bhatnakar, P.K.Saxena, “Decision Priorities and Seenarios for minimizing Electrical Power Loss in an Indian Power System Network”, Electric Power components and systems, pp.717-727 2003.

3) Balda J.C., A.R.Oliva, D.W.McNabb and R.D.Richardson, “Measurements of Neutral Currents and Voltages on a Distribution Feeder”, IEEE Transactions on Power Delivery Vol.12 No.4, October 1997.

4) Banaei.M.R., S.H.Hosseini, S.Khanmohamadi and G.B.Gharehpetian, ”Loss reduction of distribution system using APLC”, Elsevier: Simulation Modelling practice and Theroy, vol.12 (2005) pp.169-178.

5) Valentina Cecchi, Xiaoguang Yang, Karen Miu and Chipka Nwankpa, “Instrumentation and Measurement of a Power Distribution System laboratory for Meter Placement and Network reconfiguration Studies”, IEEE Instrumentation & Measurement Magazine, October 2007.

Survey on Content Based Image & Information Retrieval

S.Singaravelan[1]
Assistant Professor, Department of CSE
P.S.R. Engineering College
Sivakasi, Tamil Nadu

Dr.D.Murugan[2]
Assistant Professor (SG), Department of CSE
Manonmaniam Sundaranar University
Tirunelveli, Tamil Nadu

Abstract— In this paper, we present an complete survey about information and image retrieval process .users are not satisfied with the traditional information retrieval techniques. so nowadays the content based image retrieval are becoming a source of exact and fast retrieval. In this paper the techniques of content based image retrieval are discussed, analyzed and compared. It also introduced the feature like visual descriptor and ontology methods. The suggestion for feature methodology's to over come the difficulties and improve the result performance.

Keywords: Content based image retrieval, Visual descriptor, ontology, Relevance Feedback.

I. INTRODUCTION

In the early years Information retrieval is an area in which the computer user is not—or, at least, should not be —required to be a programmer . the system easy to use is its query language. Called DATAPLUS, the name derives from the system's ability to access data, plus the ability to process data. The systems was implemented early in 1967 [1].Content Based Image Retrieval (CBIR) is any technology that inprinciple helps to organize digital image archives by their visual content. By this definition, anything ranging from an image similarity function to a robust image annotation engine falls under the purview of CBIR The most common form of CBIR is an image search based on visual ,another one is query -by-pictorial example is a relational query language introduced for manipulating queries regarding pictorial relations as well as conventional relations. Queries can also be expressed in terms of pictorial examples through a display terminal.[3]-Content Based Image Retrieval (CBIR) is a technique which uses visual contents, normally called as features, to search images from large scale image databases according to users' requests in the form of a query image. - In the early 2003 some of the rule based approach is introduced for retrieving images under conditions. This approach allows the user to query in a more natural language. Some annotation methodologies are used to store and retrieve the images manually / automatically. The another methodology is ontology – based instructed information organization and retrieval are proposed when applying ontology to it. Based on the ontologies DB , the annotation of unstructured information is obtained.

II. SURVEY ON IR

In the early 1990s, as a result of advances in the Internet and new digital image sensor technologies, the volume of digital images produced by scientific, educational, medical, industrial, and other applications available to users increased dramatically. The difficulties faced by text based retrieval became more and more severe. The efficient management of the rapidly expanding visual information became an urgent problem.- In 1996, Greg Pass Ramin Zabih [2] described for comparing images called histogram refinement, which imposes additional constraints on histogram based matching. Histogram refinement splits the pixels in a given bucket into several classes, based upon some local property. Within a given bucket, only pixels in the same class are compared. Here describe a split histogram called a color coherence vector (CCV), which partitions each histogram bucket based on spatial coherence. - The texture features we use for the segmentation arise from a new approach to texture description and scale selection. Then Yong Rui,Thomas S. Huang and Sharad Mehrotra [2] in 1998 research many visual feature representations have been explored and many system built.

While these research efforts establish the basis of CBIR, the usefulness of the proposed approaches is limited. Specifically, these efforts have relatively ignored two distinct characteristics of CBIR systems: (1) the gap between high level concepts and low level features; (2) subjectivity of human perception of visual content. This research proposes a relevance feedback based interactive retrieval approach, which effectively takes into account the above two characteristics in CBIR. During the retrieval process, the user's high level query and perception subjectivity are captured by dynamically updated weights based on the user's relevant feedback. This approach greatly reduces the user's effort of composing a query and captures the user's information need more precisely CBIR involves the following four parts in system realization: data collection, build up feature database, search in the database, arrange the order and deal with the results of the retrieval

1) Data collection : Using the Internet programs that can collect webs automatically to interview Internet and do the collection of the images on the web site, then it will go over all the other webs through the URL, repeating this process and collecting all the images it has reviewed into the server.

2) Build up feature database : Using index system program do analysis for the collected images and extract the feature information. Currently, the features that use widely involve lowlevel features such as color, texture and so on, the middle level features such as shape etc.

3) Search the Database : The system extract the feature of image that waits for search when user input the image sample that need search, then the search engine will search the suited feature from the database and calculate the similar distance, then find several related webs and images with the minimum similar distance.

4) Process and index the results : After researching Index the image obtained from searching due to the similarity of features, then return the retrieval images to the user and let the user select. If the user is not satisfied with the searching result, he can re-retrieval the image again, and searches database again.

III. APPROACHES ON IR

A. Color-based retrieval

Color feature is the most intuitive and obvious feature of the image, and generally adopt histograms to describe it. Color histograms method has the advantages of speediness, low demand of memory space and not sensitive with the images' changes of the size and rotation, it wins extensive attention consequently.

B. The retrieval based on texture feature

When it refers to the description of the image's texture, we usually adopt texture's statistic feature and structure feature as well as the features that based on special domain are changed into frequency domain.

C. The retrieval based on shape feature

There is three problems need to be solved during the image retrieval that based on shape feature. Firstly, shape usually related to the specifically object in the image, so shape's semantic feature is stronger than texture. [15]

D. The retrieval based on annotation

In the year 2005 papers both keywords annotations and visual features is proposed. Set of statical models are built based on visual features, manually labeled images to represent to used to propagate keywords to other unlabeled images.

E. The retrieval based on Ontology (visual descriptor)

It is combination of using some special ontology visual descriptors to classify the images and find the query views and object views to compare the databases. Search to classify the resultant images is divided in to relevant group and irrelevant group of images.

F. The retrieval based on Rule-Based

A rule based system consists of a set of IF-THEN rules, a set of facts, and an interpreter controlling the application of the rules, given the facts. The rules and facts are used to convert the high-level query given by the user to a low-level query that can directly use the extracted features.

Block Diagram of CBIR

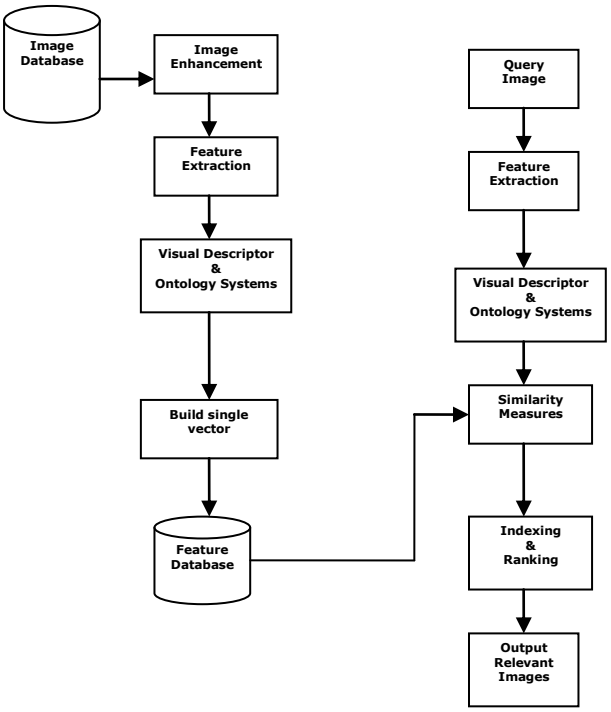

IV. RECENT WORK ON IR

Support vector machines (SVM) are extensively used to learn from relevance feedback due to their capability of effectively tackling the above difficulties. However, the performances of SVM depend on the tuning of a number of parameters. It is a different approach based on the nearest neighbor paradigm. Each image is ranked according to a relevance score depending on nearest neighbor distances. This approach allows recalling a higher percentage of images with respect to SVM-based techniques [22] there after quotient space granularity computing theory into image retrieval field, clarify the granularity thinking in image retrieval, and a novel image retrieval method is imported. Firstly, aiming at the Different behaviors under different granularities, obtain color features under different granularities, achieve different quotient spaces; secondly, do the attribute combination to the obtained quotient spaces according to the quotient space granularity combination principle; and then realize image retrieval using the combined attribute function.[23] Then a combination of three feature extraction methods namely color, texture, and edge histogram descriptor is reviewed. There is a provision to add new features in future for better retrieval efficiency. Any combination of these methods, which is more appropriate for the application, can be used for retrieval. This is provided through User Interface (UI) in the

form of relevance feedback. The image properties analyzed in this work are by using computer vision and image processing algorithms.

1. Evaluating an emotional response to color images. Its mainly used for the case – base reasoning methodology , emotional evolution of color images values , and also find out fuzzy similarity relational & inter and intra similarities and used for MPEG -7 visual descriptors. [27]
2. 3D Object: The 3D object make their efficient retrieval technology highly desired. Intelligent query methodology , multiple view and representative query view.[28]
3. Relevance Feedback Another methodology is classify the query in text or images to relevance / irrelevance set of images to select the positive images. Reference to retrieve the relevance images from databases.[3]

V. OPEN AREA ON IR

There are various areas to work with for the improvement of the content based image retrieval system. It is already been discussed that the existing techniques may be used to improve the quality of image retrieval and the understanding of user intentions. An approach that combines two different approaches to image retrieval, together with active use of context information and interaction has been proposed. The problem of bridging the semantic gap between high level query which is normally in terms of an example image and low level features of an image such as color, texture, shape and object forced to apply techniques to reduce the semantic gap.

VI. CONCLUSION

In this work, most of systems use color and texture features, few systems use shape feature, and still less use layout features. Ontological Visual descriptor used extensively in various areas to improve the performance of the system and to achieve better results in different applications. Its integrates various features perfectly in content based image retrieval system and reflects the user's subjective requirements, the experiments achieve good performance and demonstrate the efficiency and robustness of system.. This survey also highlighting the significant contributions of content based image & information's Retrieval field.

VII. REFERENCE

[1] Norman R.Sinowitz " DATAPLUS – A language for real time information retrieval from hierarchical databases." spring joint computer conference,1968.

[2] Greg Pass, Ramin Zabih, "Histogram refinement for content based image retrieval" WACV '96.

[3] Yong Rui,Thomas S. Huang and Sharad Mehrotra "Relevance Feedback Techniques in Interactive content based image retreival .".1996

[4] Moshe M.Zloof " Query by Example" national computer conference, 1975.

[5] Arnold W.M. Smeulders, Marcel Worring, Simone Santini, Amarnath Gupta, and Ramesh Jain, "Content based image retrieval at the end of the early years."

[6] Stefano Berretti, Alberto Del Bimbo, and Pietro Pala, "Retrieval by Shape Similarity with Perceptual Distance and Effective Indexing"

[7] Yixin Chen James Z. Wang "Looking Beyond Region Boundaries" 2001

[8] Minakshi Banerjee 1, Malay K. Kundu "Edge based features for content based image retrieval" 0031-3203/2003

[9] DeokHwan Kim, ChinWan Chung "Qcluster: Relevance Feedback Using Adaptive Clustering for ContentBased Image Retrieval" SIGMOD 2003

[10] Sagarmay Deb Yanchun Zhang "An Overview of Content-based Image Retrieval Techniques" 2004 IEEE.

[11] Rouhollah Rahmani, Sally A. Goldman, Hui Zhang, John Krettek, and Jason E. Fritts "Localized Content Based Image Retrieval" MIR'05,

[12] Ying Liua, Dengsheng Zhanga, Guojun Lua,Wei-Ying Mab "A survey of content-based image retrieval with high-level semantics" 2006

[13] Giorgio Giacinto "A Nearest-Neighbor Approach to Relevance Feedback in Content Based Image Retrieval"

[14] Xiangli Xu, Libiao Zhang, Zhezhou Yu, Chunguang Zhou "Image Retrieval Using Multi-Granularity Color Features" ICALIP2008 IEEE.

[15] S. Nandagopalan, Dr. B. S. Adiga, and N. Deepak "A Universal Model for Content-Based Image Retrieval" DECEMBER 2008.

[16] Yu Xiaohong, Xu Jinhua "The Related Techniques of Content-based Image Retrieval" 2008

[17] Kambiz Jarrah, Ling Guan "Content-Based Image Retrieval via Distributed Databases" CIVR'08, July 7-9, 2008, Niagara Falls, Ontario, Canada. 2008 ACM.

[18] Zhi-Gang Fan, Jilin Li, Bo Wu, and Yadong Wu "Local Patterns Constrained Image Histograms for Image Retrieval" ICIP 2008 IEEE.

[19] Savvas A. Chatzichristofis and Yiannis S. Boutalis, Mathias Lux "Img(Rummager): An Interactive Content Based Image Retrieval System." 2009.

[20] Konstantinos Zagoris, Savvas A. Chatzichristofis, Nikos Papamarkos and Yiannis S. Boutalis, "img(Anaktisi): A Web Content Based Image Retrieval System" 2009

[21] Yihun Alemu, Jong-bin Koh, Muhammed Ikram, Dong-Kyoo Kim, "Image Retrieval in Multimedia Databases: A Survey" 2009.

[21] ZhiYong Zeng, ZhiQiang Yao, ShiGang Liu, "An Efficient and effective Image Representation for Region- Based Image Retrieval" ICIS 2009, November

[22] Sancho C Sebastine Bhavani Thuraisingham Balakrishnan Prabhakaran, "Semantic Web for Content Based Video Retrieval" 2009

[23] Christian Hartvedt, "Using Context to Understand User Intentions in Image Retrieval" 2010.

[24] Ning Ruan ,Ning huvang ,Wen "hongsemantic -based image retrieval in remote sensing archive :an ontology approach," .0-7803-9510-7/06 – 2006 IEEE

[26] Huan Wang, Song Liu, and Liang-Tien Chia ,"Does ontology help in image retrieval ?- A comparison between keyword , text ontology and multi modality ontology approaches."

[27] Joonwhoan lee , eunjong park " Fuzzy similarity – based emotional classification of color images" vol 13,no.5,oct2011.

[28] yue gao,meng wang,zheng-jun zha " less is more : efficient 3-D object retrieval with query view selection" vol 13, no.5,oct 2011

[29] Dhaval Metha, Diwakar,C.V>Jawahar " A Rule-Based Approach to Image Retrieval" IEEE2003.

[30] Feng Jing,Mingjing Li,Hong-Jiang Zhang,Bo Zhang "A Unified Framework for Image Retrieval Using Keyword and Visual features",IEEE 2005.

[31] Beng Chin Ooi, Kian-Lee Tan,Tat Seng Chua,Wynne Hsu "Fast Image Retrieval using color-spatial information"VLDB 1998.

Simulation of Unsteady Laminar Flow around a Circular Cylinder

Morteza Bayareh
Department of Mechanical Engineering, Young researchers Club, Lamerd Branch,
Islamic Azad University, Lamerd, Iran

Abstract
In this paper, unsteady laminar flow around a circular cylinder has been studied. Navier-stokes equations solved by Simple *C* algorithm exerted to specified structured and unstructured grids. Equations solved by staggered method and discretization of those done by upwind method. The mean drag coefficient, lift coefficient and strouhal number are compared from current work at three different Reynolds numbers with experimental and numerical values.

Keywords: Laminar flows, circular cylinder, lift, drag, Strouhal number.

1. INTRODUCTION

External flows past objects have been studied extensively because of their many practical applications. For example, airfoils are made into streamline shapes in order to increase the lifts, and at the same time, reducing the aerodynamic drags exerted on the wings. On the other hand, flow past a blunt body, such as a circular cylinder, usually experiences boundary layer separation and very strong flow oscillations in the wake region behind the body. Fornberg [1] did a numerical study of steady viscous flow past a circular cylinder at Reynolds numbers up to 300. Kim and Lee [2] investigated the flow around a circular cylinder under the influence of an electromagnetic force. The numerical results predict that the Lorentz force applied in the circumferential direction on the cylinder moves the separation point rearward, and reduces the drag. Catalano et al. [3] studied the flow around a circular cylinder at high Reynolds numbers using LES method. They showed that the LES solutions are more accurate than the RANS results. Hishida et al. [4] studied the dependency of Strouhal frequency with drag and lift on the non-dimensional pitch of square-pitched circular cylinder array. Alam and Zhou [5] presented the effect of the diameter of a cylinder and Reynolds number on time-averaged drag, rms drag, rms lift and Strouhal in the wake of a downstream cylinder. Behara and Mittal [6] investigated the transition of the wake of a circular cylinder via a stabilized finite element method for 150 < Re < 350. They showed that the transition from mode-A to mode-B vortex structure is gradual and not hysteric.
The present work aims to study the unsteady laminar flow around a circular cylinder using the commercial software FLUENT. The mean drag coefficient, lift coefficient and strouhal number are compared from current work at three different Reynolds numbers with experimental and numerical values.

2. GOVERNING EQUATIONS

The most important equations such as conservation of mass and momentum used by the software's solver are listed as follows:
Continuity equation:

$$\frac{\partial \rho}{\partial t} + \nabla . \rho v = 0 \tag{1}$$

Conservation of momentum:

$$\frac{\partial u_i}{\partial t} + u_j \frac{\partial u_j}{\partial x_j} = -\frac{1}{\rho}\frac{\partial p}{\partial x_i} + \frac{\partial}{\partial x_j}\left(\nu \frac{\partial u_i}{\partial x_j}\right) \tag{2}$$

3. RESULTS

The non-dimensional parameter describing the flow around a circular cylinder is Reynolds number:

$$Re = \frac{UD}{\nu} \tag{3}$$

where *D* is the diameter of the cylinder, *U* is the flow velocity, and *v* is the kinematic viscosity. The computational domain of the flow is shown in Figure 1.

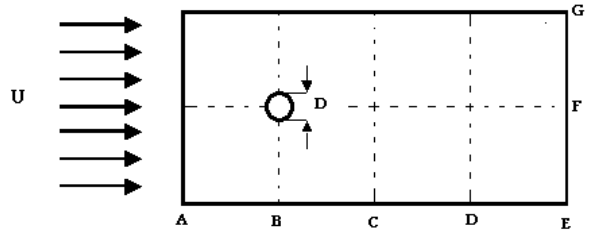

Figure 1. Computational domain of the flow (2D). AB=BC=CD=DE=EF=FG=10D

The cylinder was modeled in the software package GAMBIT. The geometry of the cylinder has been shown in figure 2 (two dimensional) and figure 3 (three dimensional). A fine mesh is needed in the closer regions of the cylinder.
The presence of the fluid viscosity slows down the fluid particles very close to the solid surface and forms a thin slow-moving fluid layer called a boundary layer. The flow velocity is zero at the surface to satisfy the no-slip boundary condition.

The flow regimes experienced with increasing the Reynolds number. In present work, we can see three regimes: *i*) Re < 5: no separation creeping flow. The separation first appears when *Re* becomes 5. *ii*) 5 < Re < 40: a fixed pair of symmetric vortices (figure 3). The length of this vortex formation increases with *Re*. *iii*) 40 < Re < 200: laminar vortex street (figure 4). The shedding is essentially two-dimensional.

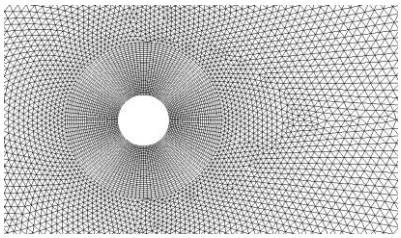

Figure 2. Geometry of the circular cylinder (2D).

The hydrodynamic driving forces exerted on a cylinder will be resolved into two components. The first is the drag force, which acts in the direction of the motion of the fluid. Drag is only force component that acts on a cylinder below Re = 40 because all flows in that regime are symmetrical with respect to the direction of the flow. Vortex instability and shedding in the regime: Re > 40 gives rise to an additional force component called lift, which is normal to both the flow direction and to the axis of the cylinder. The drag force is steady until vortex instability begins. Then it oscillates either periodically or randomly about zero.

Drag force refers to force which acts on a solid object in the direction of the relative flow velocity. This force can be determined using the following equation:

$$Drag = \frac{1}{2}\rho U^2 A C_d \tag{4}$$

Lift force is the component of the surface force that is perpendicular to the oncoming flow direction. This force can be determined using the following equation:

$$Lift = \frac{1}{2}\rho U^2 A C_L \tag{5}$$

Strouhal number can be determined using the following equation:

$$s = \frac{f_s d}{U_\infty} \tag{6}$$

f_s is frequency of the oscillation of the lift curve.

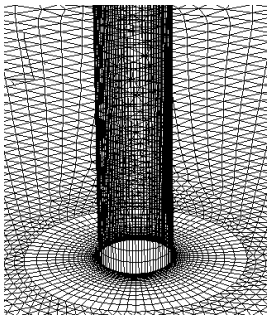

Figure 3. Geometry of the circular cylinder (3D).

In table 1, the mean drag coefficient, lift coefficient and strouhal number are compared from current work at three different Reynolds numbers with experimental values ([7]). The agreement with the measurements of Norberg [7] is reasonably good.

Table 1. Drag coefficient at three different Reynolds numbers

Re		Present work 3D	Present work 2D	Experimental results [7]	Numerical results [7]
40	C_D	1.4	1.5	1.4	1.5
100	C_D	1.48	1.6	1.2	1.29
	C_L	0.286	0.45	0.5	0.12–0.52
	S	0.18	0.18	0.18	0.17
500	C_D	1.4	1.52	1.06	1.25
	C_L	0.545	1.25	0.9	0.55 – 0.7
	S	0.203	0.227	0.21	0.21

4. CONCLUSIONS

In this paper, unsteady turbulent flow around an airfoil has been studied. Navier-stokes equations solved by Simple *C* algorithm exerted to specified structured and unstructured grids. The present work aims to simulate the flow around circular cylinder using the commercial software FLUENT. The mean drag coefficient, lift coefficient and strouhal number are compared from current work at three different Reynolds numbers with experimental and numerical values. ([7]). The agreement with the measurements of Norberg [7] is reasonably good

REFERENCES

1. B. Fornberg, 1980, "A numerical study of steady viscous flow past a circular cylinder", J. Fluid Mech., vol. 98, 819-855.
2. S. J. Kim and C. M. Lee, 2000, "Investigation of the flow around circular cylinder under the influence of an electromagnetic force", Experiments in Fluids, vol. 28, 252-260.
3. P. Catalano, M. Wang, G. Iaccarino and P. Moin, 2003, "Numerical simulation of the flow around a circular cylinder at high Reynolds numbers", International J. of Heat and Mass flow, vol. 24, 463-469.
4. H. Hishida, T. Adachi and H. Hishida, 2002, "dependency of strouhal frequency associated with drag and lift on the non-dimensional pitch of square-pitched circular cylinder array in two dimensional flow", computational fluid dynamics J., vol. 11, No. 3, 271-277.
5. M. M. Alam and Y. Zhou, 2007, "dependence of strouhal number, drag and lift on the ratio of cylinder diameters in a two tandem cylinder wake", 16 th Australasian fluid mechanics conference, 2-7 December, Gold Coast.
6. S. Behara and S. Mittal, 2010, "wake transition in flow past a circular cylinder", J. Phys. Fluids, vol. 22.
7. C. Norberg, , 2000, "*Flow around a circular cylinder : Aspects of fluctuating lift*", J. of fluids and structures ,15,459-469.

AN ANALYTICAL STUDY FOR THE PERFORMANCE ANALYSIS OF PROPAGATION MODELS IN WiMAX

Pallab Kanti Podder [1], Fahmida Islam[2], Dilip Kumar Sarker[3], Md. Galib Hasan [4], and Diponkar Kundu [5]

[1]Department of Information & Communication Engineering, Pabna Science & Technology University, Pabna, Bangladesh.
[2]Department of Computer Science & Engineering, The Peoples University of Bangladesh, Dhaka, Bangladesh.
[3,4,5] Department of Electrical & Electronic Engineering, Pabna Science & Technology University, Pabna, Bangladesh.

Abstract: In this paper, we compare and analyze six different path loss models (i.e. FSPL model, COST 231 Hata model, ECC-33 model, SUI model, Ericsson model and COST 231 Walfish-Ikegami model) in different receiver antenna heights in urban, suburban and rural environments in NLOS condition for WiMAX. We consider Bangladesh as three regions such: Urban, Suburban, flat area and use operating frequency 2.5 GHz. Our observation shows that none of a single propagation model is well suited for all environments. SUI model showed the lowest prediction in urban environment. ECC-33 model showed the heights path loss and also showed huge fluctuations due to change of receiver antenna height. COST-Hata model showed the moderate result and ECC-33 model showed the same path loss as like as urban environment because of the same parameters are used in the simulation. In flat or rural, COST 231 Hata model showed the lowest path loss.

Keywords: MATLAB, Path loss models, Propagation models, WiMAX.

1. Introduction

One of the technologies that can lay the foundation for the next generation (*fourth generation* [4G]) of mobile broadband networks is popularly known as "WiMAX." WiMAX, *Worldwide Interoperability for Microwave Access*, is designed to deliver wireless broadband bitrates, with *Quality of Service* (QoS) guarantees for different traffic classes, robust security, and mobility. The term “Mobile WiMAX” is used to describe wireless systems based on the IEEE Standard 802.16e-2005, which is an amendment to the IEEE standard 802.16-2004 and is the best
solution to provide BWA at same data rates offered by DSL etc. Broadband Wireless Access (BWA) systems have potential operation benefits in Line-of-sight (LOS) and Non-line-of-sight (NLOS) conditions, operating below 11 GHz frequency. During the initial phase of network planning, propagation models are extensively used for conducting feasibility studies. Propagation models are used for calculation of electromagnetic field strength for the purpose of wireless network planning during preliminary deployment. It describes the signal attenuation from transmitter to receiver antenna as a function of distance, carrier frequency, antenna heights and other significant parameters like terrain profile. There are numerous propagation models available to predict the path loss but they are inclined to be limited to the lower frequency bands (up to 2 GHz). The contribution to this paper undergoes the comparison and analysis of five path loss models which have been proposed for frequency at 2.5 GHz in urban and suburban and rural environments in different receiver antenna heights.

1.1 Related Studies

Models such as the Harald.T. Friis free space
model is used to predict the signal power at the receiver end when transmitter and receiver have line-of-sight condition. The classical Okumura model is used in urban, suburban and rural areas for the frequency range 200 MHz to 1920 MHz for initial coverage deployment. A developed version of Okumura model is Hata-Okumura model known as Hata model which is also extensively used for the frequency range 150 MHz to 2000 MHz in a build up area. Several performance evaluation and analysis have been presented in the literature. Comparison of path loss models for 3.5 GHz has been investigated by many researchers in many respects. In Cambridge, UK from September to December 2003, the FWA network researchers investigated some empirical propagation models [1] in different terrains as function of antenna height parameters. Another measurement was taken by considering LOS and NLOS conditions at Osijek in Croatia during spring 2007 [2]. Coverage and throughput prediction were considered to correspond to modulation techniques in Belgium [3]. September 1981, M. Hata, investigate some empirical formula for propagation loss in land mobile radio services [4] in Sweden. The Path loss models [5] have also been used for a comparison between these models. In this paper, different receiver antennas have been used during the measurement campaign and the results have been compared. We also describe various accurate path loss prediction methods [6] used both in rural and urban environments. The Walfisch-Bertoni and Hata models, which are both used for UHF propagation in urban areas, were chosen for a detailed comparison. The comparison shows that the Walfisch-Bertoni model, which involves more

parameters, agrees with the Hata model for the overall path loss. In Malaysia, May 2007, this paper deals with the performance of WiMAX networks in an Outdoor environment using the SUI channel models [7].

1.2 Aims and Objectives

Today the challenge is how to predict the path loss at the cellular frequency of 2.5 GHz. There are several empirical propagation models which can precisely calculate up to 2 GHz. But beyond 2 GHz,
there are few reliable models which can be referred for the WiMAX context. There are few proposed models [1]-[4], which focus on frequency range at 2.5 GHz out of which we base our analysis. In this paper, we compare and analyze path loss behavior for some proposed models at 2.5 GHz frequency band. Our research goal is to identify a suitable model in different environments by applying suitable transmitter and receiver antenna heights. Thus, a network engineer may consume his/her time by using our referred model for deploying the initial planning in different terrains.

2. Models for propagation under consideration

In our thesis, we analyze six different models and also consider free space path loss model which is most commonly used idealistic model. We take it as our reference model; so that it can be realized how much path loss occurred by the others proposed models.

2.1 Free Space Path Loss Model (FSPL)

In telecommunication, free-space path loss (FSPL) is the loss in signal strength of an electromagnetic wave that would result from a line-of-sight path through free space, with no obstacles nearby to cause reflection or diffraction. Free-space path loss is proportion to the square of the distance between the transmitter and receiver, and also proportional to the square of the frequency of the radio signal. The equation for FSPL is

$$\mathrm{FSPL} = \left(\frac{4\pi d}{\lambda}\right)^2 = \left(\frac{4\pi df}{c}\right)^2 \qquad (1)$$

Where:

λ is the signal wavelength (in meters), f is the signal frequency (in hertz), d is the distance from the transmitter (in meters), c is the speed of light in a vacuum, 2.99792458 × 10^8 meters per second.

This equation is only accurate in the far field; it does not hold close to the transmitter. If the separation d is continually decreased, eventually the received power appears greater than the transmitted power which is [obviously] impossible in reality, since free space is not an amplifier.

Free-space path loss in decibels a convenient way to express FSPL is in terms of dB:

$$\mathrm{FSPL(dB)} = 10\log_{10}\left(\left(\frac{4\pi}{c}\mathrm{df}\right)^2\right)$$
$$= 20\log_{10}(\mathrm{d}) + 20\log_{10}(\mathrm{f}) + 20\log_{10}\left(\frac{4\pi}{c}\right) \qquad (2)$$

where the units are same as before.

For typical radio applications, it is common to find f measured in units of MHz and d in km, in which case the FSPL equation becomes

$$\mathrm{FSPL\ (dB)} = 20\log_{10}(d) + 20\log_{10}(\mathrm{f}) + 32.45 \qquad (3)$$

For *d* in statute miles, the constant becomes 36.58.

2.2 cost 231 hata model

The Hata model is introduced as a mathematical expression to mitigate the best fit of the graphical data provided by the classical Okumura model to predict the path loss in the frequency range 1500 MHz to 2000 MHz. COST 231 Hata model is initiated as an extension of Hata model. The basic path loss equation for this COST-231 Hata Model can be expressed as:

$$\mathrm{PL} = 46.3 + 33.9\log_{10}(\mathrm{f}) - 13.82\log_{10}(\mathrm{h_b}) - \mathrm{ah_m} + (44.9 - 6.55\log_{10}(\mathrm{h_b}))\log_{10}\mathrm{d} + \mathrm{c_m} \qquad (4)$$

Where

d: Distance between transmitter and receiver antenna [km], f: Frequency [MHz], h_b: Transmitter antenna height [m].

The parameter c_m has different values for different environments like 0 dB for suburban and 3 dB for urban areas and the remaining parameter ah_m is defined in urban areas as:

$$\mathrm{ah_m} = 3.20(\log_{10}(11.75\mathrm{h_r}))^2 - 4.79, \quad \text{for } \mathrm{f} > 400\ \mathrm{MHz} \qquad (5)$$

The value for ah_m in suburban and rural (flat) areas is given as:

$$ah_m = (1.11\log_{10} f - 0.7)h_r - (1.5\log_{10} f - 0.8) \qquad (6)$$

Where the h_r is the receiver antenna height in meter.

2.3 Stanford University Interim (SUI) Model

IEEE 802.16 Broadband Wireless Access working group proposed the standards for the frequency band below 11 GHz containing the channel model developed by Stanford University, namely the SUI model. The base station antenna height of SUI model can be used from 10 m to 80 m. Receiver antenna height is from 2 m to 10 m. The cell radius is from 0.1 km to 8 km. The basic path loss expression of the SUI model with correction factors is presented as:

$$\mathrm{PL} = \mathrm{A} + 10\gamma \log_{10}\left(\frac{\mathrm{d}}{\mathrm{d_o}}\right) + \mathrm{X_f} + \mathrm{X_h} + \mathrm{S}$$
$$\text{For } \mathrm{d} > \mathrm{d_o} \qquad (7)$$

Where the parameters are

d: Distance between BS and receiving antenna [m], λ: Wavelength [m], d_o: 100 [m], d_o: 100 [m], X_f : Correction for frequency above 2 GHz [MHz], X_h : Correction for receiving antenna height [m], S: Correction for shadowing [dB], γ: Path loss exponent.

The parameter A is defined as

$$A = 20 \log_{10}\left(\frac{4\pi d_0}{\lambda}\right) \qquad (8)$$

And the path loss exponent γ is given by

$$\gamma = a - bh_b + \left(\frac{c}{h_b}\right) \qquad (9)$$

Where, the parameter h_b is the base station antenna height in meters. This is between 10 m and 80 m. The value of parameter $\gamma = 2$ for free space propagation in an urban area, $3 < \gamma < 5$ for urban NLOS environment, and $\gamma > 5$ for indoor propagation.

The frequency correction factor X_f and the correction for receiver antenna height X_h for the model are expressed in

$$X_f = 6.0 \log_{10}\left(\frac{f}{2000}\right) \qquad (10)$$

$$X_h = \begin{cases} -10.8 \log_{10}\left(\frac{h_r}{2000}\right), \text{for terrain type A and B} \\ -20 \log_{10}\left(\frac{h_r}{2000}\right), \text{for terrain type C} \end{cases} \qquad (11)$$

Where, f is the operating frequency in MHz, and h_r is the receiver antenna height in meter. For the above correction factors this model is extensively used for the path loss prediction of all three types of terrain in rural, urban and suburban environments.

2.4 Hata-Okumura extended model or ECC-33 Model

An extrapolated method is applied to predict the model for higher frequency greater than 3 GHz. In this model path loss is given by

$$PL = A_{fs} + A_{bm} - G_b - G_r \qquad (12)$$

A_{fs}: Free space attenuation [dB], A_{bm}: Basic median path loss [dB], G_b: Transmitter antenna height gain factor, G_r: Receiver antenna height gain factor.

These factors can be separately described and given by as

$$A_{fs} = 92.4 + 20\log_{10}(d) + 20 \log_{10}(f) \qquad (13)$$

$$A_{bm} = 20.41 + 9.83 \log_{10}(d) + 20 \log_{10}(f) + 9.56[\log_{10}(f)]^2 \qquad (14)$$

$$G_b = \log_{10}\left(\frac{h_b}{200}\right)\{13.958 + 5.8[\log_{10}(d)]^2\} \qquad (15)$$

When dealing with gain for medium cities, the G_r will be expressed in

$$G_r = [42.57 + 13.7 \log_{10}(f)][\log_{10}(h_r) - 0.585] \qquad (16)$$

For large city

$$G_r = 0.759h_r - 1.862 \qquad (17)$$

Where

d: Distance between transmitter and receiver antenna [km], f: Frequency [GHz], h_b: Transmitter antenna height [m], h_r: Receiver antenna height [m].

This model is the hierarchy of Okumura-Hata model.

2.5 COST 231 Walfish-Ikegami (W-I) Model

This model is a combination of J. Walfish and F. Ikegami model. This model is most suitable for flat suburban and urban areas that have uniform building height. The equation of the proposed model is expressed in:

For LOS condition

$$PL_{LOS} = 42.6 + 26\log_{10}(d) + 20\log_{10}(f) \quad (18)$$

And for NLOS condition

$$PL_{LOS} = \begin{cases} L_{FSL} + L_{rst} + L_{msd} \\ L_{fs} \end{cases}$$
for urban and suburban
$if\ L_{rst} + L_{msd} > 0$ (19)

Where
L_{FSL}= Free space loss, L_{rst}= Roof top to street diffraction, L_{msd}= Multi-screen diffraction loss.

Free space loss

$$L_{FSL}=32.45 + 20\log_{10}(d) + 20\log_{10}(f) \quad (20)$$

Roof top to street diffraction

$$L_{rst} = \begin{cases} -16.9 - 10\log(w) + 10\log(f) + 20\log(H_{mobile}) + L_{ori} \\ 0 \end{cases}$$
$H_{roof>H_{mobile}}$ (21)

where

$$L_{ori} = \begin{cases} -10 + 0.354\varphi \\ 2.5 + 0.075(\varphi - 35) \\ 4 - 0.114(\varphi - 55) \end{cases}$$
for $0 \le \varphi \le 35$
for $35 \le \varphi \le 55$
for $55 \le \varphi \le 90$ (22)

Note that

$$\Delta h_{mobile} = h_{roof} - h_{base}$$
$$\Delta h_{base} = h_{base} - h_{roof}$$

where

d: Distance between transmitter and receiver antenna [m], f: Frequency [GHz], w: Street width [m], φ: Street orientation angel w.r.t. direct radio path [degree].

In our simulation, we use the following data, i.e. building to building distance 50 m, street width 25 m, street orientation angel 30 degree in urban area and 40 degree in suburban area and average building height 15 m, base station height 30 m.

2.6 Ericsson Model

This model also stands on the modified Okumura-Hata model to allow room for changing in parameters according to the propagation environment. Path loss according to this model is given by

$$PL = a_0 + a_1.\log_{10}(d) + a_2.\log_{10}(h_b) + a_3.\log_{10}(h_b).\log_{10}(d) - 3.2(\log_{10}(11.75h_r)^2) + g(f) \quad (23)$$

Where $g(f)$ is defined by

$$g(f) = 44.49\log_{10}(f) - 4.78(\log_{10}(f))^2 \quad (24)$$

And parameters
f: Frequency [MHz], h_b: Transmission antenna height [m], h_r: Receiver antenna height [m].

3. SIMULATION ENVIRONMENT & DESIGN

For analyzing the performance of propagation models for WiMAX, we have used MATLAB software package. For evaluating and analyzing the performance of WiMAX propagation models I have used MATLAB simulation. A typical simulation model is shown in **Fig. 1**.

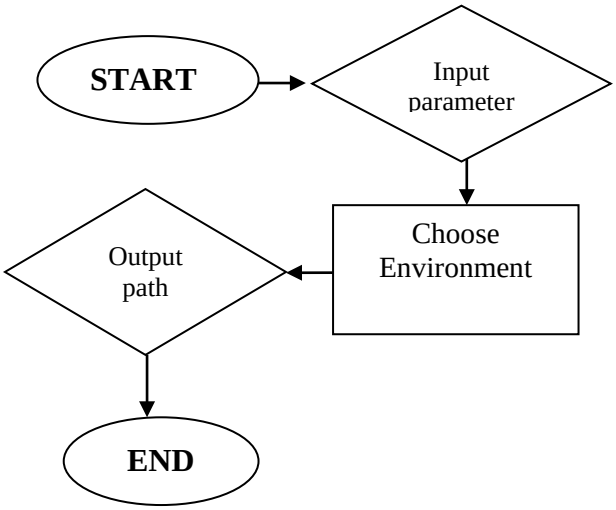

Fig. 1: Simulation process flow chart for three different environments.

Simulation Parameters: The following **Table 1** presents the parameters we applied in our simulation.

Table 1: Simulation parameters

Parameters	Values
Transmitter antenna height	40 m in urban and 30 m in suburban and 20 m in rural area
Receiver antenna height	3 m, 6 m and 10 m
Operating frequency	2.5 GHz
Distance between Tx-Rx	5 km
Building to building distance	50 m
Average building height	15 m
Street width	25 m
Street orientation angle	30^0 in urban and 40^0 in suburban
Correction for shadowing	8.2 dB in suburban and rural and 10.6 dB in urban area

4. Performance analysis & discussion

4.1 Analysis of simulation results in urban area

In our calculation, we set 2 different antenna heights (i.e. 3 m and 10 m) for receiver, distance varies from 250 m to 5 km and transmitter antenna height is 40 m. The numerical results for different models in urban area for different receiver antenna heights are shown in the **Fig. 2** and **Fig. 3**.

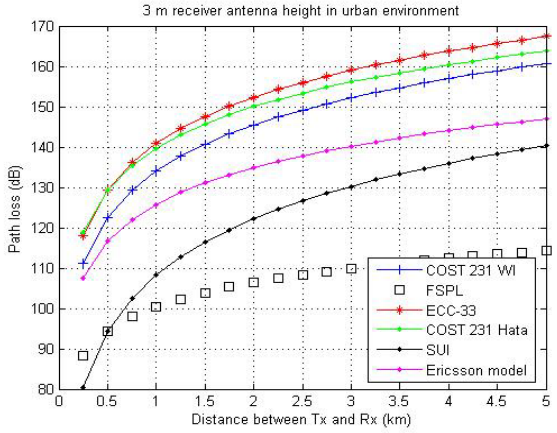

Fig. 2: Path loss in urban environment at 3 m receiver antenna height.

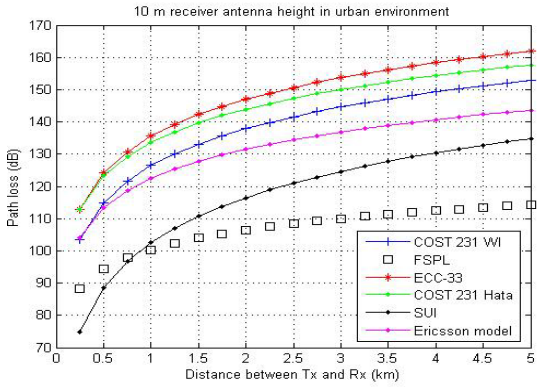

Fig. 3: Path loss in urban environment at 10 m receiver antenna height.

Our simulation result exhibits that SUI model showed the lowest prediction (128 dB to 121 dB) in urban environment. It also showed the lowest fluctuations compare to other models when we changed the receiver antenna heights. In that case, the ECC-33 model showed the heights path loss (156 dB) and also showed huge fluctuations due to change of receiver antenna height. In this model, path loss is decreased when increased the receiver antenna height. Increase the receiver antenna heights will provide the more probability to find the better quality signal from the transmitter. ECC-33 model showed the biggest path loss at 10 m receiver antenna height.

4.2 Analysis of simulation results in suburban area

In our calculation, we set 3 different antenna heights (i.e. 3 m and 10 m) for receiver, distance varies from 250 m to 5 km and transmitter antenna height is 30 m. The numerical results for different models in urban area for different receiver antenna heights are shown in the **Fig. 4** and **Fig. 5**.These represent us that the SUI model predict the lowest path loss (121 dB to 116 dB) in this terrain with little bit flections at changes of receiver antenna heights. Ericsson model showed the heights path loss (160 dB and 158 dB) prediction especially at 6 m and 10 m receiver antenna height. The COST-WI model showed the moderate result with remarkable fluctuations of path loss with-respect-to antenna heights changes. The ECC-33 model showed the same path loss as like as urban environment because of same parameters are used in the simulation.

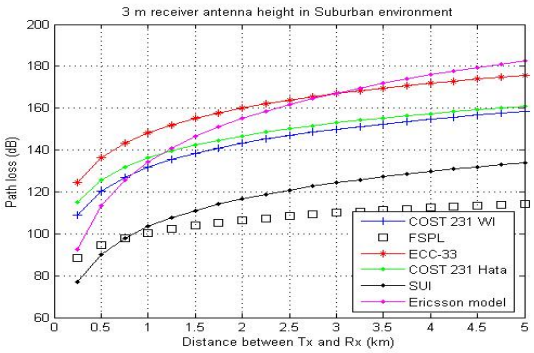

Fig. 4: Path loss in suburban environment at 3 m receiver antenna height.

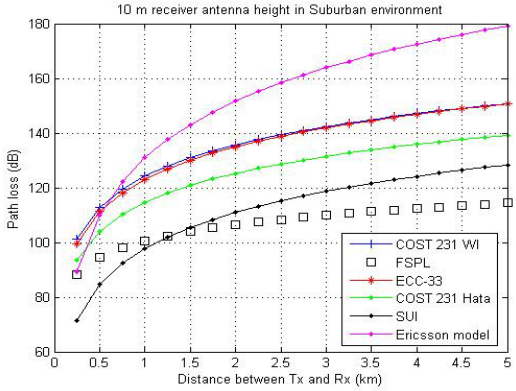

Fig. 5: Path loss in suburban environment at 10 m receiver antenna height.

4.3 Analysis of simulation results in flat area

we set 3 different antenna heights (i.e. 3 m and 10 m) for receiver, distance varies from 250 m to 5 km and transmitter antenna height is 20 m. COST 231 W-I model has no specific parameters for rural area, we consider LOS equation provided by this model The numerical results for different models in urban area for different receiver antenna heights are shown in the **Fig. 6** and **Fig. 7**.

In this environment COST 231 Hata model showed the lowest path loss (132 dB) prediction especially in 10 m receiver antenna height. COST 231 W-I model showed the flat results in all changes of receiver antenna heights. There are no specific parameters for rural area. In our simulation, we considered LOS equation for this environment (the reason is we can expect line of sight signal if the area is flat enough with less vegetation). Ericsson model showed the heights path loss (154 dB to 150 dB).

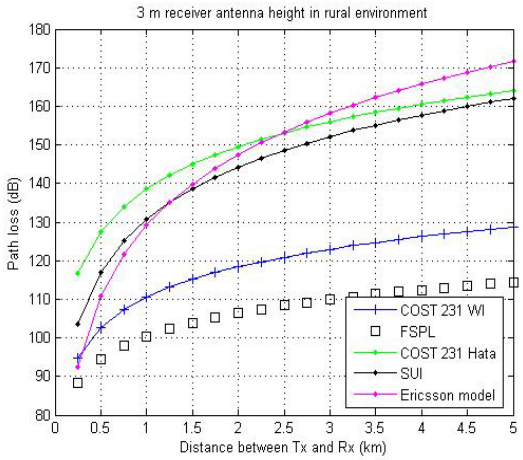

Fig. 6: Path loss in rural environment at 3 m receiver antenna height.

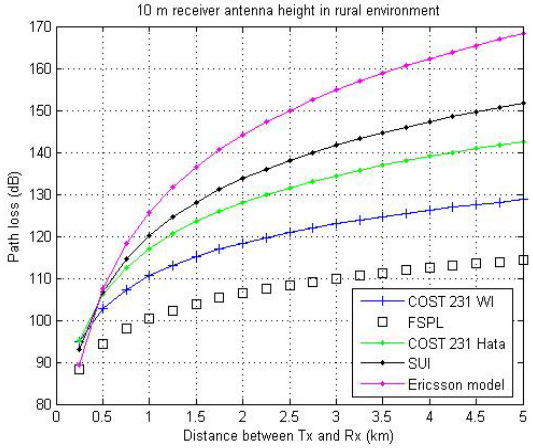

Fig. 7: Path loss in rural environment at 10 m receiver antenna height.

5. Conclusion

Our comparative analysis indicate that due to multipath and NLOS environment in urban and suburban area, SUI models experiences lowest path losses compare to flat area. In flat area COST-Hata model provide lowest path loss than SUI model at 10 m receiver antenna height. Moreover, we did not find any single model that can be recommended for all environments.

If we consider the worst case scenario for deploying a coverage area, we can serve the maximum coverage by using more transmission power, but it will increase the probability of interference with the adjacent area with the same frequency blocks. On the other hand, if we consider less path loss model for deploying a cellular region, it may be inadequate to serve the whole coverage area. Some users may be out of signal in the operating cell especially during

mobile condition. So, we have to trade-off between transmission power and adjacent frequency blocks interference while choosing a path loss model for initial deployment.

References

[1] V.S. Abhayawardhana, I.J. Wassel, D. Crosby, M.P. Sellers, M.G. Brown, "Comparison of empirical propagation path loss models for fixed wireless access systems," 61th IEEE Technology Conference, Stockholm, pp. 73-77, 2005.

[2] Josip Milanovic, Rimac-Drlje S, Bejuk K, "Comparison of propagation model accuracy for WiMAX on 3.5GHz," 14th IEEE International conference on electronic circuits and systems, Morocco, pp. 111-114. 2007.

[3] Joseph Wout, Martens Luc, "Performance evaluation of broadband fixed wireless system based on IEEE 802.16," IEEE wireless communications and networking Conference, Las Vegas, NV, v2, pp.978-983, April 2006.

[4] V. Erceg, K.V. S. Hari, M.S. Smith, D.S. Baum, K.P. Sheikh, C. Tappenden, J.M. Costa, C. Bushue, A. Sarajedini, R. Schwartz, D. Branlund, T. Kaitz, D. Trinkwon, "Channel Models for Fixed Wireless Applications," IEEE 802.16 Broadband Wireless Access Working Group, 2001.

[5] http://www.wimax360.com/photo/global-wimax-deployments-by [Accessed: June 28 2009]

[6] M. Hata, "Empirical formula for propagation loss in land mobile radio services," IEEE Transactions on Vehicular Technology, vol. VT-29, pp. 317-325, September 1981.

[7] Y.Okumura, "Field strength variability in VHF and UHF land mobile services," Rev. Elec. Comm. Lab. Vol. 16, pp. 825-873, Sept-Oct 1968.

[8] T.S Rappaport, Wireless Communications: Principles and Practice, 2n Ed. New delhi: Prentice Hall, 2005 pp. 151-152.

[9] Well known propagation model, [Online]. Available: http://en.wikipedia.org/wiki/Radio_propagation_model [Accessed: April 11, 2009]

[10] IEEE 802.16 working group, [Online]. Available: http://en.wikipedia.org/wiki/IEEE_802.16 [Accessed: April 11, 2009]

[11] Jeffrey G Andrews, Arunabha Ghosh, Rias Muhamed, "Fundamentals of WiMAX: understanding Broadband Wireless Networking", Prentice Hall, 2007.

2^n:1 Reversible Multiplexer and its Transistor Implementation

Praveen.B[1], Vinay Kumar S.B[2]

[1]System Engineer, Captronic Systems Pvt Ltd, Airport-Virthur Road,
Munekolalu, Marathahalli P.O Bangalore, Karnataka, India
[2]Faculty, ECE Department
School of Engineering and Technology, Jain University,
Jakkasandra Post, Kanakapura Taluk, Ramanagar District, Bangalore, Karnataka, India

Abstract:
The advantages of reversible logic systems and circuits have drawn a significant interest in recent years as a promising computing paradigm having applications in low power CMOS, quantum computing, nano technology, digital signal processing, computer graphics, cryptography and optical computing. In this paper, new reversible PV gate is proposed and the design of 2:1, 4:1 and 8:1 reversible multiplexer using the proposed reversible gate is discussed. Transistor implementation of proposed gate is done using virtuoso tool of cadence. Based on the result of the analysis, some of the trade-offs are made in the design to improve the efficiency.

Keywords- Basic reversible gates; Constant inputs; Reversible Multiplexer; Garbage; Gate count; Transistor count.

I. INTRODUCTION

The key components of communication systems are a multiplexer (Mux, parallel-to-serial converter) and a Demultiplexer (De-Mux, serial-to-parallel converter). In conventional computers, the computation carrying out is irreversible i.e. once logic block generates the output bits, the input bits are lost. But it is not in the case of reversible logic circuits. The classical set of gates such as AND, OR, and EXOR are not reversible as they are all multiple-input single output logic gates.

A gate is reversible if the gate's inputs and outputs have a one-to-one correspondence, i.e. there is a distinct output assignment for each distinct input. Therefore, a reversible gate's inputs can be uniquely determined from its outputs. Reversible logic gates must have an equal number of inputs and outputs [9]. Then the output rows of the truth table of a reversible gate can be obtained by permutation of the input rows. Reversible logic circuits have emerged as a promising technology in the field of information processing.

Irreversible hardware computation results in energy dissipation due to information loss [2]. According to the Landauer [6], traditional irreversible hardware computation inevitably leads to energy dissipation due to the loss of each one bit of information which dissipates an amount of KT ln(2) joules of energy, where K is the Boltzmann's constant and T is the absolute temperature at which computation is performed. This erasure is not done significantly and more power is dissipated for each erased bit. Power dissipation which leads to overheating is one of the major concerns in modern technologies. Thus, an alternative logic operation known as reversible logic came into existence, which does not erase information and also dissipate arbitrarily less heat [10].

Charles Bennett proposed a theoretical background which proved that reversible general purpose computing devices can be built [2, 3]. This gave rise to reversible logic circuits. Logical reversibility means that after finishing a computation, it is possible to retrace every step and reconstruct data which was used in every step. Thus, reversible logic circuits offer an alternative that allows computation with very small energy dissipation [17].

There is number of existing reversible gates in literature like Fredkin, Feynman and Toffoli gates etc. Experimental reversible chips and arithmetic circuits have been developed recently as well as magnetic, Josephson junction, nano-electronic and quantum implementations of reversible logic circuits have been proposed in different literatures [4-15]. Photon being the ultimate unit of information with unmatched speed and with data package in a signal of zero mass, the techniques of computing with light may provide a way out of the limitations of computational speed and complexity inherent in electronics computing. Different optical logic gates have already been proposed to perform irreversible logic function. But, reversible computation in a system can be performed if the system is composed of reversible gates. The well known 2x2 Feynman [14] gate operates as a controlled NOT (CNOT) if the control input of CNOT is set '0', the gate acts as a BUFFER gate; else, it acts as a NOT gate. The Feynman gate can be used as fan-out gate to copy a signal. Toffoli [20] and Fredkin gates are 3x3 reversible gates. Each of these gates is universal, i.e. any logical reversible circuit can be implemented using these gates.

II. BASIC REVERSIBLE LOGIC GATE

A set of reversible logic gates is needed to design reversible logic circuits. An N*N reversible logic gate can be represented as:

$$I_V = (I_1, I_2\ldots\ldots, I_N) \quad (1)$$
$$O_V = (O_1, O_2\ldots\ldots, O_N)$$

Where, I_v and O_v are inputs and output vectors. Consider following issues to perform synthesis of reversible gates and obtain optimization

- Garbage: Garbage is the number of outputs added to make an n-input k-output Boolean function ((n,k) function) reversible. In other sense, a reversible logic gate has an equal number of inputs and outputs (k*k) and all the outputs are not expected. Some of the outputs should be considered to make the gate reversible and those undesired outputs are known as garbage outputs. A heavy price is paid for every garbage outputs.
- Gate count: The number of reversible gates used to realize the function [11].
- Flexibility: This refers to the universality of a reversible logic gate in realizing more functions [12].
- Transistor Count: It denotes the effort needed, to realize a reversible circuit. The transistor count of a reversible gate is the number of transistors used in the gate [16].
- Critical path: Delay can be calculated in reversible logic based on the critical path. It is the longest path in the system to get the desired output [13].

Several reversible logic gates have been proposed. Among them a general New Toffoli Gate, NTG [8], New Gate, NG [5, 7], TKS Gate [18], TR gate [19] are discussed.

III. DESIGN OF REVERSIBLE MULTIPLEXER

We design the reversible circuit using dual-line pass-transistor logic [1] and monotone circuit. Boolean values X=1 and X=0 are denoted by (X,X)=(1,0) and (X,X)=(0,1), respectively. For example, an inverter is shown in Fig 1. It consists of a metal cross-over. Because of the monotone circuit, we set all initial values (X,X) = (0,0).

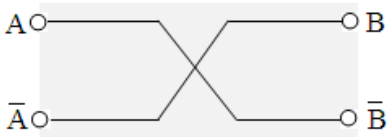

Figure.1. Reversible inverter

For the implementation of an on-off switch, we use a CMOS transmission gate which is a two-way switch shown in Figure. 2.

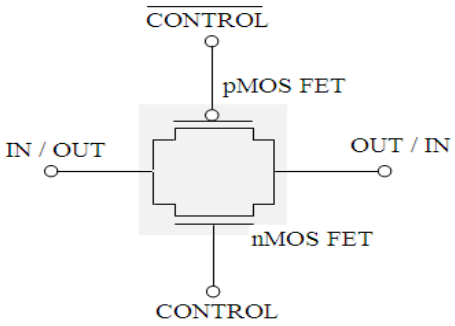

Figure..2. CMOS Transmission gate

IV. PROPOSED REVERSIBLE MULTIPLEXERS

A. 2:1 Reversible Multiplexer

A 3x3 reversible PV gate is proposed in order to function as the 2:1 reversible multiplexer producing two garbage bits. The inputs are S, A and B. Based on the selection input S, the corresponding message bits are passed on to the output 'Y'. Figure 3 depicts the symbolic representation of PV gate and Table I describes its truth table.

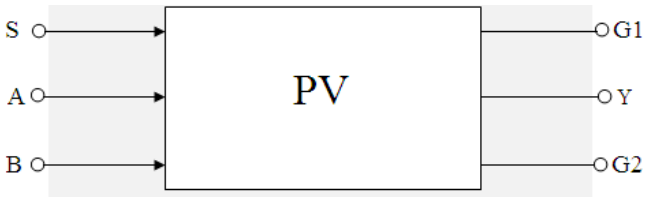

Figure.3. Reversible PV gate functioning as 2:1 reversible multiplexer

TABLE I. TRUTH TABLE OF REVERSIBLE PV GATE

S	*A*	*B*	*G1*	*Y*	*G2*
0	0	0	0	0	0
0	0	1	0	0	1
0	1	0	0	1	0
0	1	1	0	1	1
1	0	0	1	0	0
1	0	1	1	1	0
1	1	0	1	0	1
1	1	1	1	1	1

When the select input S=0, the output Y follows the input A, i.e Y=A, if the S=1, then the output Y follows the input B, i.e Y=B. 'G1' and 'G2' are the two garbage bits which is not required in multiplexing operation. However G1 follows the select input S, it may be used in additional circuits which requires the same input.

B. Design of 4:1 Reversible Multiplexer using reversible PV gate

Using the proposed reversible PV gate, 4:1 multiplexer can be designed as shown in Figure 4. This design requires three PV gates such that producing six garbage outputs. The Table II describes the truth table of 4:1 reversible multiplexer, the garbage outputs are discarded as it doesn't play a vital role in the multiplexing operation.

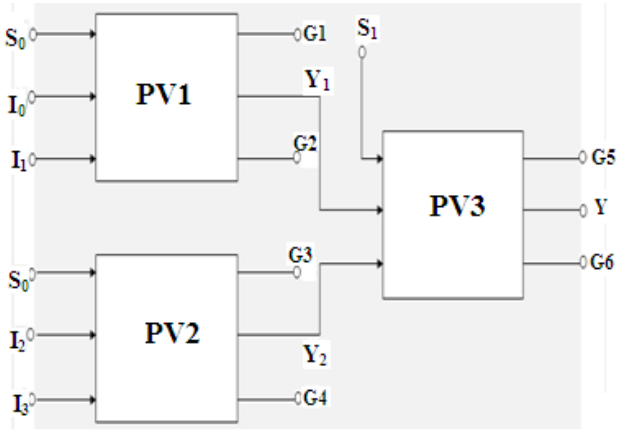

Figure.4. Design of 4:1 reversible multiplexer using PV gate

TABLE II. TRUTH TABLE OF REVERSIBLE 4:1 MULTIPLEXER

Select Inputs		**Output**
S_1	S_0	*Y*
0	0	I_0
0	1	I_1
1	0	I_2
1	1	I_3

The above truth table depicts there is no change in the functionality of 4:1 reversible multiplexer with respect to the irreversible multiplexer functionality. The equation for the output 'Y' is given as follows,

$$Y = \bar{S}_1\bar{S}_0I_0 + \bar{S}_1S_0I_1 + S_1\bar{S}_0I_2 + S_1S_0I_3$$

C. Design of 8:1 Reversible Multiplexer using reversible PV gate

Using the same proposed PV gate 8:1 reversible multiplexer also can be designed as shown in Figure 5 and Table III shows its truth table. This design uses seven PV gates producing 14 garbage outputs. In general we can design 2^n:1 reversible multiplexer where n is 1, 2, 3…n. For 2^n:1 reversible multiplexer (2^n-1) PV gates are required producing 2*(2^n-1) number of garbage outputs.

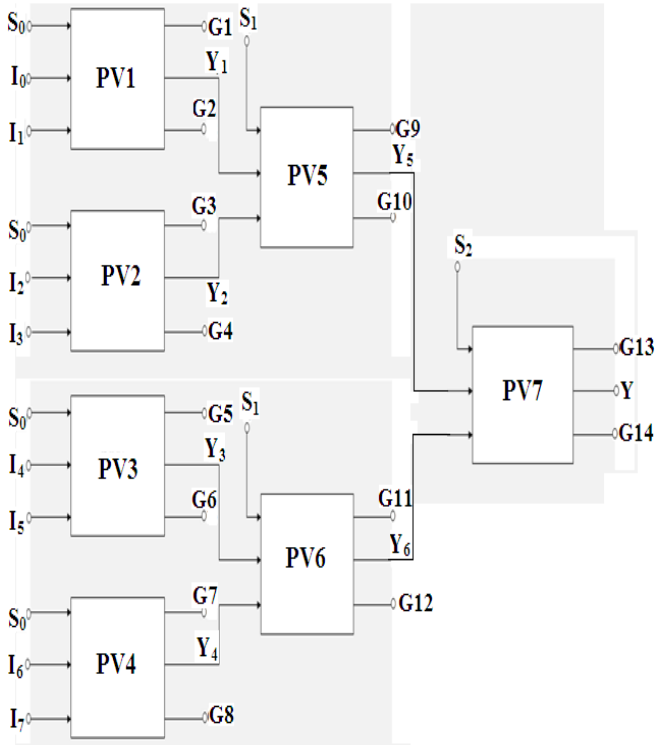

Figure.5. Design of 8:1 reversible multiplexer using PV gate

TABLE III. TRUTH TABLE OF REVERSIBLE 8:1 MULTIPLEXER

Select Inputs			Output
S_2	S_1	S_0	Y
0	0	0	I_0
0	0	1	I_1
0	1	0	I_2
0	1	1	I_3
1	0	0	I_4
1	0	1	I_5
1	1	0	I_6
1	1	1	I_7

$$Y = \bar{S}_2\bar{S}_1\bar{S}_0I_0 + \bar{S}_2\bar{S}_1S_0I_1 + \bar{S}_2S\bar{S}_0I_2 + \bar{S}_2S_1S_0I_3$$
$$+S_2\bar{S}_1\bar{S}_0I_4 + S_2\bar{S}_1S_0I_5 + S_2S_1\bar{S}_0I_6 + S_2S_1S_0I_7$$

V. IMPLEMENTATION OF PV GATE

The proposed reversible PV gate is realized using transistor implementation as described in Figure 6, Figure 7 and Figure 8. To construct one reversible PV gate five transistors are required. The required output 'Y' can be obtained using only two transistors however the other three transistors are required for calculating garbage outputs. To obtain output G1, a pass transistor is used for passing the selection input S to the output G1 as shown in Fig 8.

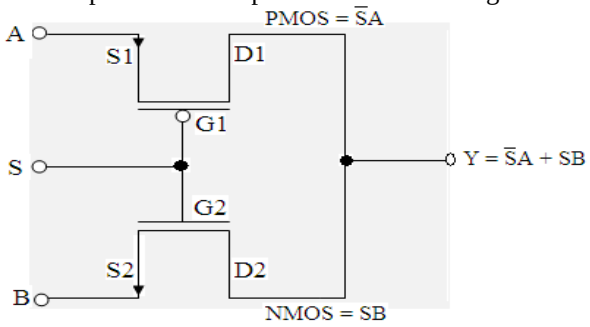

Figure.6. Circuit diagram for multiplexed output Y

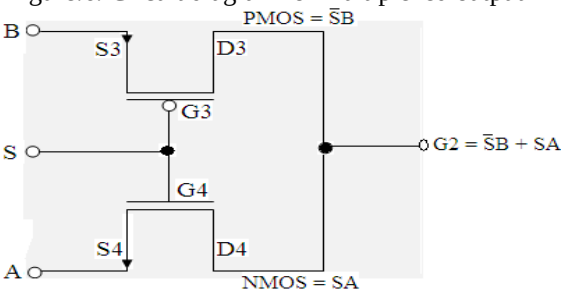

Figure.7. Circuit diagram for output G2

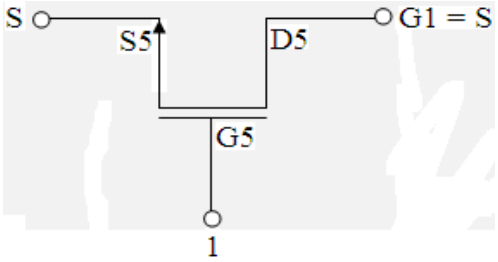

Figure.8. Circuit diagram for output G1

In Fig 6, when the selection input is 0, the pmos transistor will be ON while nmos will be off thus input A is passed to the output Y. If the selection input is 1, then nmos transistor will be conducting while pmos is in OFF state, passing input B to the output Y. Similar to output Y, output G2 is passed with input B when S=0 and input A when S=1.

VI. IMPLEMENTATION OF PV GATE

The proposed reversible PV gate is realized using the virtuoso tool of cadence. Spectre simulator of cadence is used to simulate the output. The simulations are performed using the 0.18uM technology. The circuit implementation of PV gate is shown in Figure 9. The input and output waveforms simulated for the PV gate is shown in Figure 10.

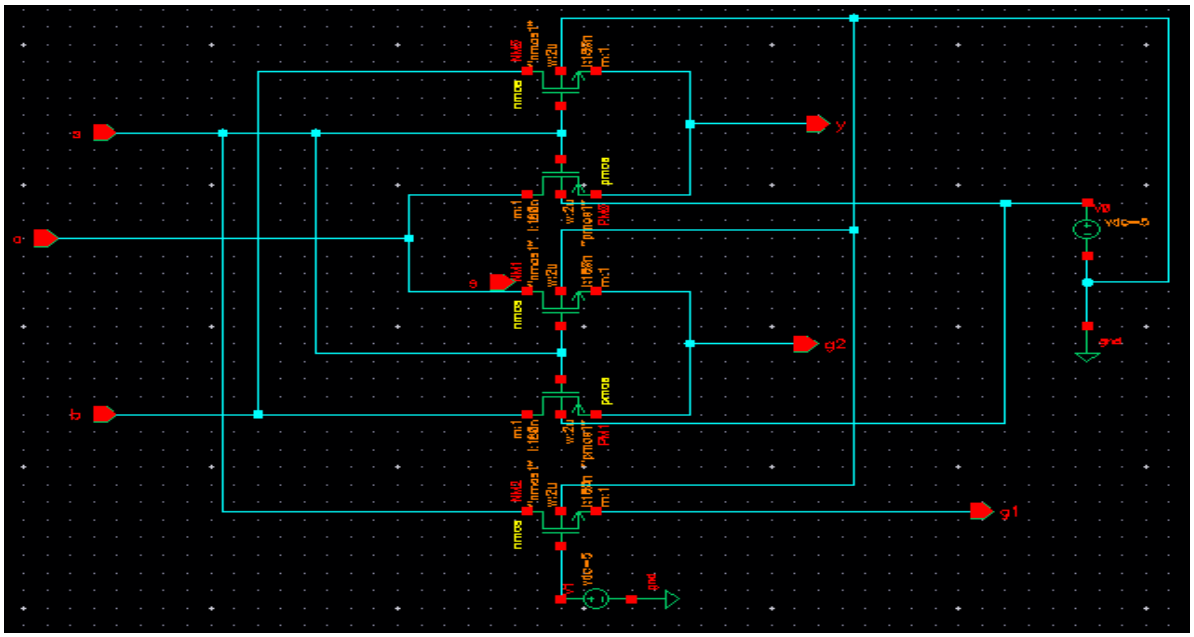

Figure.9. Transistor implementation of PV gate as 2:1 reversible multiplexer

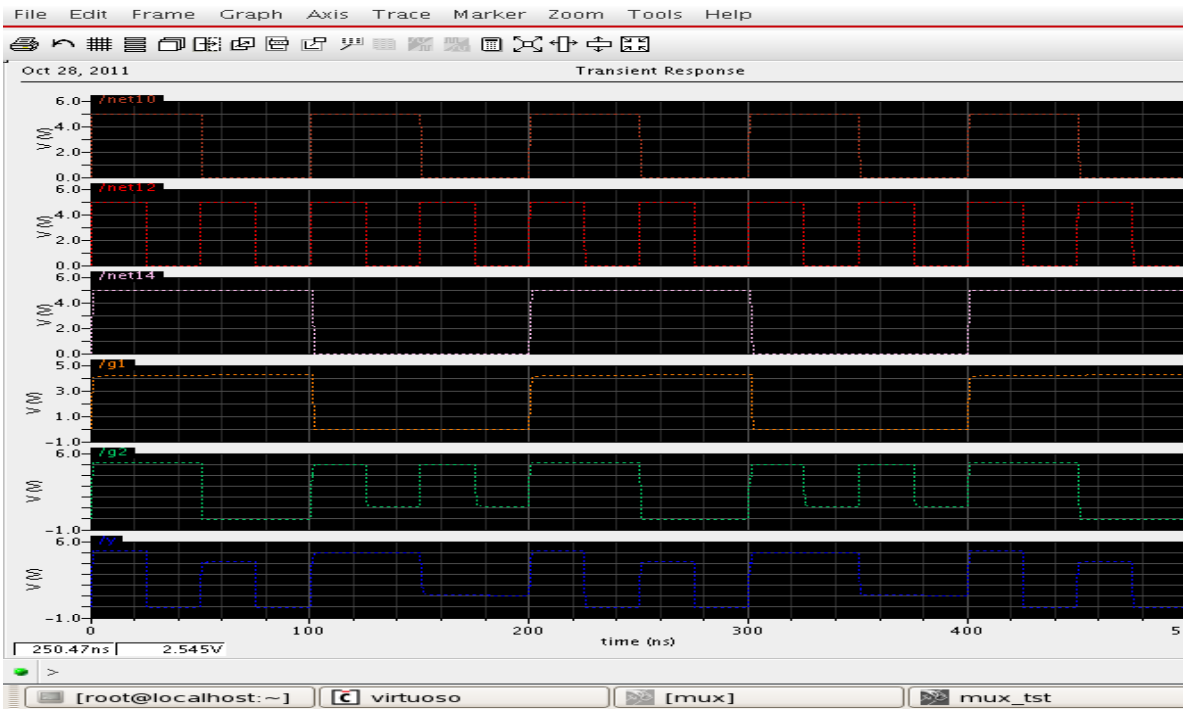

Figure.10. Simulation output of PV gate

VII. CONCLUSION

In this paper, the reversible multiplexer using PV gate is proposed and described. Simulation result and transistor implementation confirming described method is also presented in this paper. It is worth noting that the synthesis of reversible logic is different from irreversible logic synthesis. One of the major constraints in reversible logic is to minimize the number of reversible gates used, garbage outputs produced and usage of number of constant inputs. The proposed 2^n:1 reversible multiplexer requires (2^n-1) PV gates producing 2*(2^n-1) number of garbage outputs, where n is 1, 2, 3 … n.

References

[1] Alex De Vos, "Reversible computing", Progress in Quantum Electronics, 23, PP. 1-49, 1999.

[2] C.H. Bennett, 1973, Logical reversibility of computation, IBMJ, Research and Development, 17: 525 – 532.

[3] C.H. Bennett "The thermodynamics of computation – A Review", International Journal of Thearetical Physics, 21: 905-928, 1982.

[4] C.H. Bennett D.P. Di Vincenzo, "Quantum information and computation", Nature, 404, 247-255 (2000).

[5] Hasan Babu Hafiz Md., Md. Rafiqul Islam, Ahsan RajaChowdhury and Syed Mostahed Ali Chowdhury, 2003. On th realization of reversible full adder circuit. International Conference on Computer and Information Technology, Dhaka,Bangladesh, 2: 880-883.

[6] Landauer, R., 1961. Irreversibility and heat generation in the computing process,IBM J.Research and Development, 5 (3): 183-191.

[7] Md. M. H Azad Khan, Design of Full-adder with Reversible Gates, International Conference on Computer and Information Technology, Dhaka, Bangladesh, pp 515- 519, 2002

[8] Peres A., 1985. Reversible logic and quantum computers. Physical Review. A 32: 3266-

[9] Praveen B, Tilak B.G, Rashmi S.B, "A Novel High Speed Reversible Adder/Subtractor", Proceedings of the 3rd *International Conference on Computer Modelling and Simulations, ICCMS*, Jan 7-9, 2011.

[10] Praveen B, Rashmi S.B, Tilak B.G, "Transistor Implementation of Reversible PRT gates", *International Journal of Engineering Sceince and Technology*, ISSN: 09755462, Rec no: 2289-2297 Vol 3, issue 3, 2011, http://www.doaj.org/doaj?func=abstract&id=729234.

[11] Praveen B, Tilak B.G, Rashmi S.B, "An Optimised Design of 4-Bit Reversible Magnitude Comparator and Binary Subtractor ", © 2011 Published by *Elsevier Ltd*. Selection and/or peer-review under responsibility of GCSE 2011, GCSE 2011: 28-30 December 2011, Dubai, UAE.

[12] Praveen.B, Rashmi S.B and Tilak B.G, "A Novel Optimized Reversible BCD adder using reversible CL gate", Proceedings of the 3rd *International Conference on Computer Modelling and Simulations, ICCMS*, Jan 7-9, 2011.

[13] Rashmi S.B, Praveen B, and Tilak B.G., "Design of Optimized Reversible BCD Adder/Subtractor," *International Journal of Engineering and Technology* vol. 3, no. 3, pp. 230-234, 2011

[14] R Feynman, Quantum Mechanical Computers, Optical News (1985) 11-20.

[15] Maslov and G. Dueck, "Improved Quantum cost for n-bit Toffoli gates, Electronics letters 39(25) 1790-1791 (2003).

[16] Robert Wille, Rolf Drechsler "Towards a Design Flow for Reversible Logic", (9-13).

[17] Tilak B.G, Praveen.B and Rashmi S.B,"A New High Speed Universal Reversible Adder Gates", *International Conference on Demand Computing* nov 3-4, 2010.

[18] Thapliyal H., S. Kotiyal, M. B. Srinivas, 2006. Novel BCD adders and their reversible Logic Implementation for IEEE 754r format. Proceedings of the 19th International Conference on VLSI Design, 3-7 Jan 2006.

[19] Thapliyal H., N Ranganathan 2009."Design of efficient reversible subtractors based on a New novel gate"IEEE Computer society annual symposium on VLSI.

[20] Toffoli T, 1980, Reversible computing, Tech Memo MIT/LCS/TM-151, MIT Lab for computer science.

Author Information

Praveen B received Bachelor's Degree from Sri Bhagawan Mahaveer Jain College of Engineering, Visvesvaraya Technological University in 2011.

Currently he holds the position of System Engineer at Captronic Systems private limited, Bangalore. Since 2010, he has published more than 5 research papers most of them published in international journals and conference proceedings. His main research interests include Reversible logic circuits, Quantum computing, Low Power VLSI design and Embedded Systems.

Vinay Kumar S.B is an Faculty in the Department of Electronics and Communication Engineering, School of Engineering and Technology, Jain University, Bangalore.

He obtained his Bachelor degree in Electronics and Communication Engineering from Coorg Institute of Technology, ponnampet in 2009 and He obtained his Master degree M.tech in Signal Processing and VLSI, Jain University, Bangalore in 2012. His research interest includes Reversible Logic, VLSI, DSP, and Embedded Systems.

A Hybrid Approach for Web Service Selection

Mojtaba Khezrian[1], Wan M. N. Wan Kadir[2], Suhaimi Ibrahim[3], and Alaeddin Kalantari[4]

[1,2] Faculty of Computer Science and Information System, Universiti Teknologi Malaysia, Johor Bahru, Malaysia
[3,4] Advanced Informatics School, Universiti Teknologi Malaysia, Kuala Lumpur, Malaysia

Abstract – Web service selection which is specified to evaluate and select the best candidate from discovered Web services became one of the most significant topic in recent research on Service oriented Architecture (SOA). Indeed, current approaches are not sufficient enough to overcome Web service selection problems. Due to the nature of Web service selection, it is important to lead it to Multi Criteria Decision Making (MCDM). However, there are several MCDM methods such as AHP, ANP, TOPSIS and VIKOR. In this paper we propose a hybrid approach to solve Web service selection problem. First, we apply Analytical Hierarchy Process (AHP) to evaluate the weights of criteria instead of collect the weights directly from service consumer. In the next tread, we use VIKOR (VIšekriterijumsko KOmpromisno Rangiranje) to identify and rank the appropriate candidate services. Finally, in order to demonstrate the proposed method we have afforded an example using four criteria of QoS and five alternative services.

Keywords: Web Service, Web Service Selection, MCDM, AHP, VIKOR.

1. Introduction

Nowadays, web services are one of the most widely used groups of SOA and service computing. A lot of organizations and companies develop applications which are accessible through Internet. Therefore, the capability of selecting correctly and combining inter organizational and various services at runtime on the Web is an significant issue in the Web Service applications development [1].

One of the most significant current discussions in SOA is Service Selection which should evaluate discovered services and choose the best candidate from them. Web Service Selection is appears when there is a set discovered Web Services that can fulfill the user's requirements; one of these services should be selected to return back to service consumer [2].

When more than one Web Service which meets functional requirements is available, the Web Service Selection uses some criteria to select the best candidate service. It is essential that this selection is tailored to the users preferences while one user may have need of high quality another may require low price [3]. The value of non functional properties in these matching Web Services may be different, but essentially they should have minimum requirements. The selection criteria may have an interdependent relationship together.

A number of methods for decision making are addressed in Web Service Selection because of the complication that exists during the selection process. [4]. Two significant tasks in the process of using services are selection and ranking in which every solution for them is affected directly on description of services. During describing a service, three items have to be considered: behavior, functional, and nonfunctional. The non functional properties (QoS) of the services are used as criteria for selecting services.

On one hand, the majority of service selection techniques apply QoS and on other hand behavior of QoS based service selection, let researchers to lead service selection problem to Multi Criteria Decision Making (MCDM). There are some MCDM techniques that this paper presented VIKOR to solve service selection problem to identify best candidate service [5].

The VIKOR is a method for multi criteria optimization of complex systems. "It determines the compromise ranking-list, the compromise solution, and the weight stability intervals for preference stability of the compromise solution obtained with the initial (given) weights" [6]. Ranking and selecting from a set of alternatives in the presence of conflicting criteria is goal of this method. VIKOR addresses the multi criteria ranking index based on the particular measure of "closeness" to the "ideal" solution [7]. VIKOR is a useful method in Service Selection problem based on MCDM because it can be work on situation where the preference of user is not clarified at the beginning of selection process.

First of all the decision matrix is arranged based on QoS criteria and alternative services and the weights of each criterion will be gathered based on user preference then the VIKOR method will be applied. Consequently, based on the preference of service requester obtainable services will be ranked.

The remainder of this paper is structured as follows: Section 2 outlines the related works of the Web Service Selection based of MCDM; in Section 3 the proposed approach and applying on Service Selection are discussed; Section 4

illustrate the method by an arithmetic example; Section 5 is conclusion of this paper in which the future works for Web Service Selection are discussed.

2. Related Works

There are some Service Selection researches based MCDM [8], [9], [10], [11], [3], [12], [13], [14]. We investigate these researches based on some criteria such as User preference, Automation, Scalability, and aggregation function. These criteria are addressed in previous work [15].

Wang et al [8] present a model to select the exact web service based on user's preference. This model is a fuzzy decision making model that also will be used by independent third-party in an experimental QoS environment in the Internet to distinguish web service level for web service providers and lend a hand to requesters to make the right selection.

In order to assist service providers and requesters with consideration of their preferences, Huang in [9],[10] attempt to propose a method based on fuzzy group decision making with respecting to Similarity Aggregation Method (SAM). Although the Aggregation method in MCDM is addressed, aggregation function and user preference are missed in this research.

Kerrigan [3] presents a vision of Service Selection mechanisms in the WSMX that addressed the decision making in manual, automated, and hybrid selection methods. This paper did not address such criteria as aggregation function user preference and scalability in Service Selection mechanism.

Toma et al [12] proposes a multi criteria ranking approach for web services selection. First the ontological models are applied on non functional properties (QoS) then they used to specify the rules. These rules are evaluated by ranking method evaluates by a reasoning engine and finally a ranked list of services will be generated based on user preference. Also the scalability is addressed in this paper. But regarding the automation there is no information in this research.

For the selection of a logistic service provider (LSP) Ying et al [13] present a comprehensive methodology based on ANP and VIKOR. As it is an important aspect to choose the best logistics service provider for logistics management, it is divided two components. ANP is addressed to assure weight of criteria and in second division the VIKOR method is applied to solve MCDM problem.

Lo et al [14] apply fuzzy TOPSIS method for solving the service selection problem with respect of user's vision. First for estimating the weights of each criteria the linguistic terms stands for triangular fuzzy numbers are exploited then the fuzzy TOPSIS is applied to resolve the MCDM problem in service selection.

In this paper the AHP method is used to evaluate weights of criteria and VIKOR method is applied to resolve the service selection problem in view of decision making. In the research first the pair wise comparison matrix is arranged then we apply AHP to reach weights of criteria. Moreover, the decision matrix based on QoS criteria and a set of alternative services is generated and finally the VIKOR method is concerned.

3. Proposed Approach for Web Service Selection

In this section we proposed our approach. In this approach, as shown in Figure 1, first the weighting of criteria will be evaluated by the AHP and then for decision making we use the VIKOR method. The steps of our approach are shown in below:

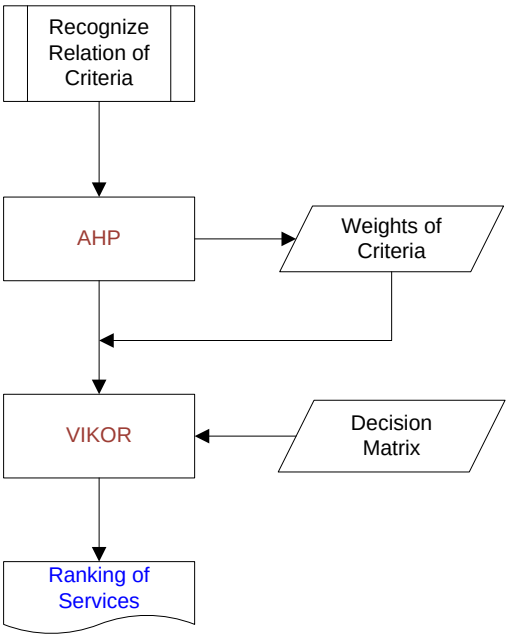

Figure 1 Process of the Proposed Approach

3.1. Weighting of Criteria by AHP

AHP is a process for developing a numerical score to rank each decision alternative based on how well each alternative meets the decision maker's criteria [16]. In this paper, we explain briefly how to apply AHP for finding the weighs of criteria and explaining of the formulas in more details is out of the scope of this paper. AHP is a pair wise comparison method that each criterion is comparing to each other and gets the score with respect to Table 1:

Table 1. Standard Preference Table

PREFERENCE LEVEL	NUMERICAL VALUE
Equally preferred	1
Equally to moderately preferred	2
Moderately preferred	3
Moderately to strongly preferred	4
Strongly preferred	5
Strongly to very strongly preferred	6
Very strongly preferred	7
Very strongly to extremely preferred	8
Extremely preferred	9

The criterion that has better level will get the numerical number mentioned in the table and the other will get the reciprocal of the value. To evaluate weights of criteria a matrix should be created; based on the definition the sample of matrix for three criteria is shown below:

	A	B	C
A	1	x	1/y
B	1/x	1	1/z
C	y	z	1

Figure 2: Matrix for evaluating weights of criteria

In the following the steps of AHP are described:

Step1: sum all the values in each column.
Step2: The values in each column are divided by the corresponding column sums.
Step3: Convert fractions to decimals and find the average of each row. This sum is corresponding to weight of the criterion of the row.

3.2. Decision Making by VIKOR

In this section we focus on how to apply VIKOR on Service Selection. VIKOR method is suitable for the system which the preferences of criteria are not clear at the beginning of system and it can compromise the result during the process of system.

To propose the method on service selection we suppose that there are *m* alternative services $(A_1, A_2, A_3, \ldots A_m)$ with respect of *n* criteria $(C_1, C_2, C$ which are used for evaluating the decision matrix:

$$d = \begin{array}{c} \\ A_1 \\ A_2 \\ \vdots \\ A_m \end{array} \begin{array}{c} \begin{array}{cccc} C_1 & C_1 & \cdots & C_1 \end{array} \\ \begin{bmatrix} X_{11} & X_{12} & \ldots & X_{1n} \\ X_{21} & X_{22} & \ldots & X_{2n} \\ \vdots & \vdots & & \vdots \\ X_{m1} & X_{m2} & \ldots & X_{mn} \end{bmatrix} \end{array}$$

The steps of VIKOR method on service selection are as follows:

Step 1. As the scales of each criterion are not equivalent the decision matrix should be normalized, while the scales of "Response time" and "Cost" are different. For this purpose VIKOR method uses linear normalization. In VIKOR method once the scale of criteria will be changed the result is stable because the linear normalization. In Eq. (1), (2) the normalization formulas are shown:

(1)

$$S_i = \sum_{j=1}^{n} w_j \left(\frac{X_j^* - X_{ij}}{X_j^* - X_j^-}\right)$$

And

(2)

$$R_i = \underset{j}{Max}\left[w_j \left(\frac{X_j^* - X_{ij}}{X_j^* - X_j^-}\right)\right]$$

Where $X_{i,j}\left(i = 1,2,3,\ldots, m \text{ and } j = 1,2,3,\ldots, n\right)$ are the elements of the decision matrix (alternative *i* respect to criteria *j*). are best and worst elements in criteria *j* respectively and represents the weights of criteria *j* (relative importance).

Step 2. Compute the index values. These index values are defined as:

(3)

$$Q_i = \begin{cases} \left[\frac{R_i - R^-}{R^+ - R^-}\right] & if\ S^+ = S^- \\ \left[\frac{S_i - S^-}{S^+ - S^-}\right] & if\ R^+ = R^- \\ \left[\frac{S_i - S^-}{S^+ - S^-}\right]v + \left[\frac{R_i - R^-}{R^+ - R^-}\right](1 - v) & Otherwise \end{cases}$$

Where

(4)

$$S^- = Min\, S_i\,, S^+ = Max\, S_i$$

And

(5)

$$R^- = Min\, R_i\,, R^+ = Max\, R_i$$

In the formula, *v* is introduced as a weight for the strategy of "the majority of criteria" (or "the maximum group utility"), whereas 1- *v* is the weight of the individual regret. The value of *v* lies in the range of 0_1 and these strategies can be compromised by *v*=0.5.

Step 3. The results are three ranking lists. By sorting the values S, R, and Q in decreasing order.

Step 4. Propose as a compromise solution the alternative which is the best ranked by the measure Q (minimum) if the following two conditions are satisfied:

***C1*. Acceptable advantage:**

$$Q(A^{(2)}) - Q(A^{(1}$$

Where $A^{(2)}$ is the alternative with second place in the ranking list by *Q*; DQ. *M* is the number of alternative services.

***C2*. Acceptable stability in decision making:** The alternative should also be the best ranked by *S* or/and *R*. A set of compromise solutions is proposed as follow, if one of the conditions is not satisfied:

Alternatives $A^{(1)}$ and $A^{(2)}$ if only the *C2* is not satisfied, or

Alternatives $A^{(1)}, A^{(2)},\ldots, A^{(M)}$ if the *C1* is not satisfied; $A^{(M)}$ is determined by the below relation for maximum *M*.

$$Q\left(A^{(M)}\right) - Q\left(A^{(1)}\right) \prec DQ$$

The service which has minimum value of Q is the most excellent alternative. The core ranking result is the compromise ranking list of alternative services, and the compromise solution with the "advantage rate"[6].

4. Illustrative Example

In this part, an example is concerned to illustrate the VIKOR method and how to apply it on service selection. We assume that there are five alternative services with respect to four criteria. These criteria are most popular criteria based on QoS and these are: *Response Time, Security, reliability, and Cost.* The relationship between the criteria and alternatives can be seen in Figure. 3:

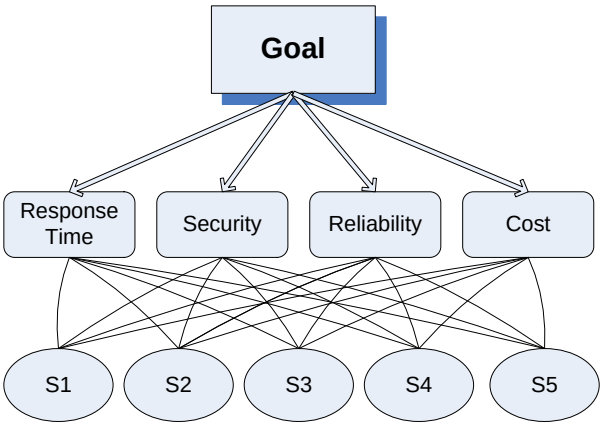

Figure 3. Relationship between Criteria and Services

There are some solutions to evaluate the weights of criteria: 1) from the feedback of service requester whom used the service before [15]; it calls Trust & Reputation method 2) it can be evaluate by some decision making method that in this research we apply AHP method. We do pair wise comparing between criteria and the below matrix is the result of the comparison with respect to Table 1.

Table 2. Pair wise Comparing Matrix

	R.T	Security	Reliability	Cost
R.T	1	1	3	2
Security	1	1	2	1
Reliability	1/3	1/2	1	1
Cost	1/2	1	1	1

Based on the above table we apply steps1-3 in section 3.1 and the weights of criteria are as follow:

$W_1 = 0.37; W_2 = 0.15; W_3 = 0.28; W_4 = 0.20$

In the second step we must apply VIKOR as a MCDM method. We assume that based on above example the data of five alternatives with respect of four QoS criteria is gathered and the decision matrix is prepared based on the example:

Table 3. Decision Matrix with reverence to the QoS Criteria

Criteria / Alternatives	Response Time	Security	Reliability	Cost
A1	0.590	0.255	0.665	0.135
A2	0.745	0.745	0.500	0.955
A3	0.410	0.665	0.745	0.410
A4	0.665	0.410	0.590	0.500
A5	0.135	0.745	0.865	0.335

Right now the necessary feeds for the VIKOR method is ready, so in the following based on given example, we show how VIKOR method can resolve a MCDM problem in area of Service Selection:

First S_i and R_i will be computed, but as some of criteria are negative (*Response Time, Cost*) and some are positive (*Security, Reliability*) the calculating and comparing these criteria together is complex effort, thus the decision matrix should be normalized, and the normalized matrix can be seen in Table 4:

Table 4. Normalized Decision Matrix

Criteria / Alternatives	Response Time	Security	Reliability	Cost
A1	0.746	1	0.548	0
A2	1	0	1	1
A3	0.451	0.163	0.329	0.335
A4	0.869	0.648	0.753	0.445
A5	0	0	0	0.244

Right now, the data in matrix are normalized and it means that there is no different between the type of criteria and all data are in same scale. In this situation there is possibility of comparing data together. After normalization, S_i and R_i can be calculated based on Eq. (1) , Eq. (2):

$$S_i = \begin{matrix} A_1 \\ A_2 \\ A_3 \\ A_4 \\ A_5 \end{matrix}\begin{bmatrix} 0.638 \\ 0.720 \\ 0.329 \\ 0.715 \\ 0.049 \end{bmatrix} \quad \& \quad R_i = \begin{matrix} A_1 \\ A_2 \\ A_3 \\ A_4 \\ A_5 \end{matrix}\begin{bmatrix} 0.280 \\ 0.370 \\ 0.167 \\ 0.321 \\ 0.049 \end{bmatrix}$$

Followed by the index values is computed but before that S^- , S^+ , R^- , and R^+ be supposed to calculate by Eq. (4) and Eq. (5). S^- is the minimum value and S^+ is the maximum value in table S also R^- and R^+ are minimum and maximum value in table R .

$$S^- = 0.049 , S^+ = 0.720 \quad \& \quad R^- = 0.049 , R^+ = 0.370$$

At this time based on the above matter the can be accessible. is the index value for ranking the alternatives; it can be calculated based on Eq. (3). Below the and are shown:

$$Q_i = \begin{matrix} A_1 \\ A_2 \\ A_3 \\ A_4 \\ A_5 \end{matrix}\begin{bmatrix} 0.799 \\ 1 \\ 0.392 \\ 0.920 \\ 0 \end{bmatrix} \quad \& \quad Q_{sorted} = \begin{matrix} A_5 \\ A_3 \\ A_1 \\ A_4 \\ A_2 \end{matrix}\begin{bmatrix} 0 \\ 0.392 \\ 0.799 \\ 0.920 \\ 1 \end{bmatrix}$$

Step4. In this part we check whether the *C1* and *C2* are satisfied? For this point, first we calculate the *DQ* then use the Eq. (6):

$$0.392 - 0 \geq 0.25$$

The *C1* is satisfied and *A3* has best situation in S_i and R_i so condition *C2* also is satisfied. At this time we can confirm that service alternative *A3* is the best option with respect to criteria of QoS and weight of them. The final ranking list is shown below:

$$A_5 \succ A_3 \succ A_1 \succ A_4 \succ A_2$$

5. Conclusion

In this paper, first we have studied the most prominent related researches and we propose a hybrid approach to support Web service selection. In our previous work [5], however, we have collected the weights of criteria directly from service requester. The evaluation of relative importance of weights of criteria has not been considered. In this paper, although, the data related to weights of criteria are gathered from user, we address AHP method for evaluation weighting of criteria instead of using the preference of service consumer without evaluation. Subsequently, the VIKOR method is addressed as a MCDM method to tackle service selection problem. Finally, the VIKOR method is applied step by step to overcome service selection problem in the view of MCDM. Moreover, in order to demonstrate how normalization of proposed method works and how it can be applied on service selection, we provide an example using QoS criteria and some other alternative services. The result shows that our approach can select the best and most related candidates.

Acknowledgment

This research is supported by Ministry of Higher Education (MOHE) Malaysia and RUG at Universiti Teknologi Malaysia (UTM) by Vot No. 00H68.

References

1. Tabatabaei, S.G.H., W.M.N.W. Kadir, and S. Ibrahim. *A comparative evaluation of state-of-the-art approaches for web service composition*. 2008. Sliema, Malta: Inst. of Elec. and Elec. Eng. Computer Society.

2. Pan, Z. and J. Baik, *A QOS ENHANCED FRAMEWORK AND TRUST MODEL FOR EFFECTIVE WEB SERVICES SELECTION*. Journal of Web Engineering, 2010. **9**(4): p. 327-346.

3. Kerrigan, M. *Web service selection mechanisms in the web service execution environment (WSMX)*. 2006: ACM.

4. Manish, G., S. Rajendra, and M. Shrikant, *Web Service Selection Based on Analytical Network Process Approach*, in *Proceedings of the 2008 IEEE Asia-Pacific Services Computing Conference*. 2008, IEEE Computer Society.

5. Khezrian, M., et al., *Service Selection based on VIKOR method.* International Journal of Research and Reviews in Computer Science, 2011. **2**(5).

6. Opricovic, S. and G.-H. Tzeng, *Compromise solution by MCDM methods: A comparative analysis of VIKOR and TOPSIS.* European Journal of Operational Research, 2004. **156**(Compendex): p. 445-455.

7. Opricovic, S., *Multicriteria optimization of civil engineering systems.* Faculty of Civil Engineering, Belgrade, 1998. **2**(1): p. 5-21.

8. Wang, P., et al. *A fuzzy model for selection of QoS-aware web services*. in *IEEE International Conference on e-Business Engineering, ICEBE 2006, October 24, 2006 - October 26, 2006*. 2006. Shanghai, China: Inst. of Elec. and Elec. Eng. Computer Society.

9. Huang, C.L., et al., *Applying Semi-Order Preference Model in Content-Based Service Discovery.* International Journal of Electronic Business, 2007. **5**(1): p. 48-58.

10. Huang, C.-L., K.-M. Chao, and C.-C. Lo. *A moderated fuzzy matchmaking for web services*. in *Fifth International Conference on Computer and Information Technology, CIT 2005, September 21, 2005 - September 23, 2005*. 2005. Shanghai, China: Institute of Electrical and Electronics Engineers Computer Society.

11. Mohammady, P. and A. Amid, *Integrated Fuzzy VIKOR and Fuzzy AHP Model for Supplier Selection in an Agile and Modular Virtual Enterprise Application of FMCDM on Service Companies.* The Journal of Mathematics and Computer Science, 2010. **4**(1): p. 413 - 434.

12. Toma, I., et al., *A multi-criteria service ranking approach based on non-functional properties rules evaluation.* Service-Oriented Computing–ICSOC 2007, 2007: p. 435-441.

13. Ying, L. and Z. Zhiguang. *Selection of Logistics Service Provider Based on Analytic Network Process and VIKOR Algorithm*. 2008: IEEE.

14. Lo, C.-C., et al. *Service selection based on fuzzy TOPSIS method*. in *24th IEEE International Conference on Advanced Information Networking and Applications Workshops, WAINA 2010, April 20, 2010 - April 23, 2010*. 2010. Perth, Australia: IEEE Computer Society.

15. Khezrian, M., et al. *An evaluation of state-of-the-art approaches for web service selection*. 2010: ACM.

16. Russell, R.S.a.T.I., Bernard W. , ed. *Operations Management* 2003: New Jersey.

Authors Information

Mojtaba Khezrian is currently a PhD candidate at Universiti Teknologi Malaysia. He received his BSc from IAU University of Iran (2007) and MSc from Universiti Teknologi Malaysia (2009). He is doing his research in the field of Software Engineering and Semantic Web Services. Software engineering, web services, semantic web and web intelligence are among his research interests. He intends to broaden his perspectives in interdisciplinary fields towards a career in software engineering and web engineering. Mojtaba Khezrian is the corresponding author and can be contacted at: m.khezrian@ieee.org.

Wan M.N. Wan Kadir is an Associate Professor in the Software Engineering Department, Faculty of Computer Science and Information Systems, UTM. He received his BSc from Universiti Teknologi Malaysia, MSc from UMIST and PhD in the field of Software Engineering from The University of Manchester. He has been an academic staff at Software Engineering Department for more than ten years, and he was the Head of the Department from 2005 to 2009. He is the Chairman of the 2nd Malaysian Software Engineering Conference (MySEC'06), and a member of pro-tem committee of Malaysian Software Engineering Interest Group (MySEIG). He serves as a Program Committee member of the 5th, 4th, and 3rd International Conference on Software Engineering Advances (ICSEA 2010, ICSEA 2009, ICSEA'08), the 15th and 16th Asia-Pacific Software Engineering Conference (APSEC 2009, APSEC 2008), the 5th and 4th International Conference on Software and Data Technologies (ICSOFT 2010, ICSOFT 2009), the 5th and 4th International Conference on Novel Approaches in Software Engineering (ENASE 2010, ENASE 2009), the 9th ACIS International Conference on Software Engineering, Artificial Intelligence, Networking, and Parallel/Distributed Computing (SNPD2008), and the 3rd and 4th Malaysian Software Engineering Conference (MySEC'07 and MySEC'08). Most of the proceedings are published by IEEE. His research interest covers various SE knowledge areas based on the motivation to reduce the cost of development and maintenance as well as to improve the quality of large and complex software systems

.

Suhaimi Ibrahim is an Associate Professor at the Centre for Advanced Software Engineering (CASE), Faculty of Computer Science and Information Systems, UTM. He is currently appointed as the Deputy Director of CASE and is involved in several short terms and National research schemes of software development, software testing and maintenance projects. He is an ISTQB certified tester of foundation level and currently being appointed as a board member of the Malaysian Software Testing Board. He is actively involved in syllabus and curriculum review of software engineering at the bachelor and post-graduate levels. His research interests include requirements engineering, web services, software process improvement and software quality.

Alaeddin Kalantari is currently a PhD student in AIS Lab at the Universiti Teknologi Malaysia. He received his MSc from Universiti Teknologi Malaysia (2009). He has proposed "A Security Framework to Support Enterprise Service Oriented Architecture (ESOA)" in his master project. He is pursuing his research in Service Oriented Architecture (SOA) and Semantic Web Services. The main area of his research is developing Semantic Web services specification based on Model-driven architecture (MDA).

Image Processing Software Package in Medical Imaging: A review

Nasrul Humaimi Mahmood, Ching Yee Yong, Kim Mey Chew and Ismail Ariffin
Bio-Medical Instrumentation and Electronics Research Group
Faculty of Electrical Engineering
Universiti Teknologi Malaysia
81310 UTM Johor Bahru, Johor, Malaysia

Abstract— MATLAB is at present among the best available technique for image processing. Medical images after digitalized processed can help reducing the number of false positives and they assist medical officers in deciding between follow-up and biopsy. This paper gives a survey of image processing algorithms that have been developed for detection of masses and segmentation techniques. 35 students from university campus participated in the Development of Biomedical Image Processing Software Package for New Learners Survey investigating the use of software package for processing and editing image. Composed of 19 questions, the survey built a comprehensive picture of the software package, programming language, workflow of the tool and captured the attitudes of the respondents. The result of this study shows that MATLAB is among the famous software package and this result is expected to be beneficial and able to assist users on effective image processing and analysis in a newly developed software package.

Keywords- MATLAB; image processing; image editting; software package.

1. Introduction

This paper details a project jointly funded by the *Dana Pembangunan Pengajaran (DPP)* and *Universiti Teknologi Malaysia* (UTM) to produce a survey of computer graphics and visualization tools in use in the medical image processing.

Image processing has moved into the mainstream, not only for the engineering world but also the society of general. Nowadays, personal computers are now able to handle a large amount of graphics and images with ease. The fast network system and modem transfer rate are able to transfer images just in a fraction of time. Image manipulation software becomes a general and common item on PC. As a result of this growth, image processing package had become a standard tool in the repertoire of the engineer.

This paper is divided into seven sections. The first section mainly introduces the whole study. It provides the general overview of the visualization tools in medical image processing. The second section includes the objectives of this study, which describes the aims that needed to be achieved. The third section discusses the background studies, literature review and the study implementation. A specification list of the computer environment and thorough discussion on the developmental tool or processing and analysis on various medical images will be explained in section 4 and 5. Finally, the last two sections contain the results, conclusions, future developments and possible enhancement and improvement on this study.

2. Problem Formulation

The hypothesized function of newly developed image processing software package is to provide the users with information about the ease of image processing of an image in order to deliver useful information through the analysis with connection to the theory of image information through processing. In this study, the practice item of image processing software package was focused on MATLAB application.

Several imperatives were identified to be addressed by the survey:

- To identify specific software packages in use together with the advantages and disadvantages of using these packages.
- To attempt to establish a dialog with software vendors to discuss how technological problems might be resolved.

Validity of measurement is very important as this argument need to be valid to the extent that conclusions and results drawn from the data collected do logically follow from them.

A wide variety of image processing techniques have been used in medical field for image analysis. This employs a large number of visual and physiological features, a fact which usually impedes the training process [1]. In this paper, an effective medical image processing for image processing is presented through survey result. Several aspects for example the speed of the processing and ease of use are considered while the processing is being done. This software package does not process only raw image for analysis, but also important in managing the image data effectively and providing scientific information about image characteristics.

3. Literature Review

Due to the rapid development of information technology, in turn, impacted significantly on the techniques for image processing techniques and implementing of survey processing systems. This main development has been shifted from mainframe system to PC platform. User now can easily perform all kind operations and processing techniques ranging from small scale to large scale statistical operations.

A number of software packages for the image processing and editing have emerged over the years. The different steps of image processing make each of the software packages differ with different relative strengths. Having the right software and appropriate processing techniques is necessary for guarantee for the successful processing of data.

In principle, all the data run through the same kind of cycle and the typical famous well-developed software packages for image processing are as follow:

A. *Adobe Photoshop*
A software used in teaching and research and was generally found to be useful and easy to use. Functionality for scanning and scanned image manipulation. Simple integration with other Adobe products.

B. *Adobe Illustrator*
It is the industrial standard software and works well with other graphics software. Not easily compatible with WORD and Windows PC users cannot easily send images to a non-graphics PC user.

C. *ImageTool*
ImageTool is a free package with powerful image processing capabilities. Its main use is image analysis and it is quite easy to use. Developed by UTHCSA, as will all freeware, *ImageTool* has no guaranteed future development and no direct support.

D. *LabView*
Its main use is to convert from one image file format to another. A large number of image formats are supported. Images can be increased or reduced in size. Image resolution may be altered in the preparation of images for importation into word-processing or desktop publishing packages.

E. *Paint Shop Pro*
It is used both in teaching and research. It is regarded as easy to use and useful. It is robust, good documentation and capable in conversion between different image file formats.

F. *ImageJ*
ImageJ is freeware. It is a free package with powerful image processing capabilities. The most used features of the software are image editing, processing, and enhancement.

G. *Image Prep*
A specialist graphics manipulation package which has proved to be very useful for converting and enhancing graphics images. Used for manipulation of scanned photographic images for research software generation.

H. *ERDAS Imaging*
A GIS package designed to plan for surface change such as urban development, transport planning and landscape planning. Useful but fairly difficult to use. Very hard to start off with, but once you have conquered the initial problems it becomes a lot easier.

I. *MATLAB*
Ease of customization and able to handle large matrices. Use of the language script to customize statistical tests and matrix manipulation.

J. *Microsoft Photo Editor*
A fairly easy and useful drawing package for drawing graphs within WORD documents used in preparation of teaching materials. Straight forward intuitive mouse-driven actions and the ease with which images could be embedded within WORD documents.

4. Methodologies

The survey was designed to support the imaging techniques community by fostering inter-institution communication and as an important first step toward determining effective ‘best practice’. It was also expected that camera and imaging systems developers would benefit by gaining in-depth understanding of the digital image processing needs of the imaging heritage

niche. Research laboratories, too, require the information sought by the survey to help guide them in determining where improvements are needed.

A number of steps were taken in order to realize these objectives and these including the design of a questionnaires framework, construction of the project web pages, the use of on-line social activity platform like facebook messaging, e-mail discussion groups, face-to-face interview and the development of a dedicated project discussion list.

A. Sample Size

Sample size and the method of collecting data from the respondents needed to be considered for this survey. 35 participants with a total sample size n=35 would have sufficient statistical power for statistical significance.

B. Data Collection Framework

The framework of the questionnaire is very simple and easy to understand. It was divided into 4 sections which are part 1 for demographic details, part 2 for quantitative questions, part 3 for qualitative questions and last part for open-ended questions.

The 19 questions of the survey took about half an hour to complete. That so many took the time to respond to the questions is testimony to a strong need and interest by imaging service providers for a better understanding of digital image processing. Participants included many of the major undergraduate students who had taken their image processing subject credit.

The full merits and limitations of particular software could only be fully established through the use of the software with real data, involving real questions and real problems. The design and size of the question within a subjective survey must be limited to promote respondents completion of the survey [2]. The survey was conducted through questionnaires distribution, World Wide Web Service online filling, email and facebook online activity platform. Subjects were also invited to make general observations and perspectives on the use and potential use of the image processing software tool techniques in their work. The result is mainly relies on human perception and is subjective by nature [3].

5. Results

The response rate to the questionnaires is mild and has been limited but not very disappointingly so. We have received over 35 completed questionnaires. Of these, almost 70% were completed the survey. Around 20-25% of the response rate to the questionnaires is considered good by some relevant literature suggestions [4].

Table 1 shows the frequency of coding with various types of programming languages. Result had recorded that most of the time, MATLAB and LabView are the main tools or languages for processing image then follow by C++, C# and Java. Due to the easiness of coding and image processing toolbox available in the platform, hence MATLAB and LabView are the famous choices for respondents. On opposition, all respondents definitely never use Python, R, Lua, Ruby and Perl as their processing tool for image processing.

When the respondents discussed about the use of MATLAB software in image processing, the software was described as being neither particularly easy nor difficult to use and it was viewed in high regard however. Descriptions were included that the software was specifically used for data analysis with customised procedures, matrix manipulation, data visualization, graphic image production and editing, and customization of statistical data using language script.

Nowadays, there are many types of different software products in the market that we can use to process images. Most of the products are well-developed and user may produce desired images within a few clicks. Table 2 shows the frequency of respondents of using these types of software products. In medical images wise, respondents still choosing MATLAB as their first choice following by Microsoft Photo Editor, Adobe Photoshop, LabView and ImageTool.

Although, MATLAB is not a well-developed image processing tool package like Adobe Photoshop and Microsoft Photo Editor, and also user need to code a few lines for processing process, but MATLAB still remain as the famous processing tool among all.

When we switch our discussion to rating an interesting piece of software if it were distributed as a ready-to-use package or source code as in Figure 1, respondents seems feeling likely on a ready-to-use package software due to the easiness and simple handling. They feel that it is easy for them to edit their photo according their needs without thinking or writing any code. But somehow, a ready-to-use software might not completely fulfil the user needs. Some respondents had commented that a source code package sometimes may save a lot of time for us especially who are not very familiar with the coding language but they also commented that understanding of the source code written by someone is not an easy task.

6. Discussions

A good image processing tool package is determined through five core capabilities: image utilities, image filtering and transformation, image compression, image analysis and programming and data analysis environment. User can easily rate any software package according the five core capabilities discussed above.

Besides, it is very important for a software package during the designing step. It should cover around four essential qualities: validity, reliability, impact and practicality. Validity is normally taken to be extent to which a processing can be shown to produce scores which are an accurate reflection of the image taken true level. Reliability concerns the extent to which processing results are stable, consistent and accurate, and therefore the extent to which they can be depended on for making decisions about the image processing. Impact concerns the effects, beneficial or otherwise, which an examination has on the processing using the package. Practically can be defined as the extent to which a processing is practicable in terms of the resources needed to produce and administer it [5].

The advantage of the development of image processing package over other is the ability of this processing tool to provide an effective and easy method for user. It is important to consider the processing in all the aspects including speed and quality.

Due to the speed and ease of use, MATLAB is highly recommended as the software for image processing. Users can rate a software package using above five major core capabilities.

MATLAB is a general numerical analysis and visualization environment. The underlying data structure in MATLAB is the matrices, and this structure lends itself well for image processing.

This processing tool also need be revised to make them more user-friendly, with a focus on issues such as layout, illustrations, message, information, and cultural appropriateness. It should provide full functionality for the entire processing cycle: authoring, scheduling, administering and rating. It is a premier and affordable personal computer-based image processing package for academia, government and business users.

7. Conclusion

Ethical issues had to be considered since the proposed survey required the involvement of human respondents. Ethical considerations are required during surveying human for their opinions and such considerations include: seeking permission of potential respondents for their involvement, explaining their level of involvement and responsibilities in the survey, providing some background so that they can make an informed decision based on their knowledge background and finally ensuring respondents of anonymity in the reporting of the project [2].

This survey attempted to raise an interest in MATLAB application in the medical image processing field. The survey results are fairly depressing and there is plenty of work to be done. In medical image field, not many visualization tools can be used and most of them are not easy being used. Hence, a creation of simple computer graphics such as histograms, bar charts and scatter plots by MATLAB package to manipulate and visualize matrices data is a need.

The project's web pages will continue beyond the completion of the survey, as will visualization tools.

In order to minimize the differences between variables, it is very important to standardize the procedures and instruments used in the survey due to variations in the way the research was carried out. Hence, solutions and procedures for providing consistent and interpretable results must be suggested, problems of defining observational variables and phrasing questions need to be outlined [2].

Further developments in each algorithm step are required to improve the overall performance of the computer-aided image processing in medical sciences.

ACKNOWLEDGEMENT

A project of this magnitude depends on the hard work and commitment of many professionals, and we are pleased to acknowledge their contributions. The authors are deeply indebted and would like to express our gratitude to the Universiti Teknologi Malaysia and *Dana Pembangunan Pengajaran* for supporting this study under Vote 08233.

REFERENCES

[1] Loui et al. (1990). "High-Speed Architectures for Morphological Image Processing", Nonlinear Image Processing, pp. 145-156.

[2] Sapsford, R. J. (1999). Survey Research. SAGE Publications Ltd, London. ISBN 9780761955283.

[3] Chakraborty, D. P. and Krupinski, E. A. (2003). "Medical Imaging 2003". San Diego, California, USA. Image perception, obeserver performance, and technology assessment. Volume 5034.

[4] Sapsford, R. and Jupp, V. (2006). Data Collection and Analysis. SAGE Publications Ltd, London. ISBN 9780761943631.

[5] Bourque, L. B. and Clark, V. A. (1992). "Processing Data". Quantitative Applications in the Social Sciences. Volume 85. SAGE Publications Ltd, London. ISBN 9780803947412.

TABLE I. FREQUENCY OF USING FOLLOWING PROGRAMMING LANGUAGES

Rate questions on a scale of 1 to 4.	Never	Occasionally	Frequently	Most of the time	Responses	Total	Mean	Standard deviation
How often do you use the following programming languages (%)	1	2	3	4				
C++	23	**57**	20	0	35	10	1.9714	0.6636
Python	**100**	0	0	0	35	10	1	0
Java	**86**	9	6	0	35	10	1.2	0.5314
C#	**63**	31	6	0	35	10	1.4286	0.6081
R	**100**	**0**	**0**	0	35	10	1	0
Lua	**100**	**0**	0	0	35	10	1	0
Ruby	**100**	**0**	0	0	35	10	1	0
Perl	**100**	0	0	0	35	10	1	0
MATLAB	9	20	**37**	34	35	10	2.9714	0.9544
LabView	29	**34**	29	6	35	10	2.1714	0.9544

TABLE II. FREQUENCY OF USING THE FOLLOWING SOFTWARE PRODUCTS

Rate questions on a scale of 1 to 4.	Never	Occasionally	Frequently	Most of the time	Response	Total	Mean	Standard deviation
How often do you use the following software products (%)	1	2	3	4				
Adobe Photoshop	14	**40**	29	17	35	8	2.4857	0.9509
Adobe Illustrator	**74**	17	6	3	35	8	1.3714	0.7311
Image Tool	**54**	20	26	0	35	8	1.7143	0.8599
LabView	31	29	**37**	3	35	8	1.2857	0.7101
Paint Shop Pro	**83**	9	6	3	35	8	2.1714	0.7470
Image J	11	**69**	11	9	35	8	1.0571	0.3381
Image Prep	**97**	0	3	0	35	8	1.0857	0.3735
ERDAS Imaging	**94**	3	3	0	35	8	2.6286	1.2623
MATLAB	9	17	**37**	**37**	35	8	1.0857	0.2840
Microsoft Photo Editor	29	17	17	**37**	35	8	1.0286	0.1690
OpenCV	**91**	9	0	0	35	8	3.0571	0.8382
VTK	**97**	3	0	0	35	8	2.4285	0.7778

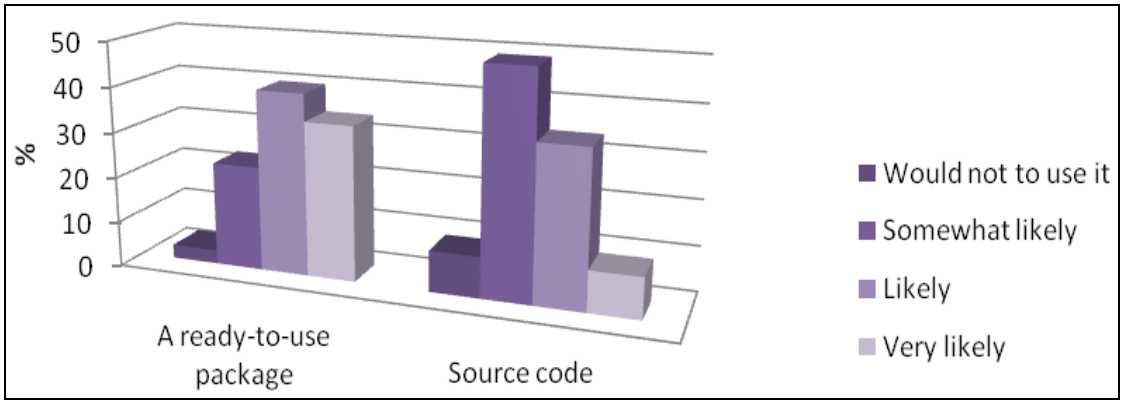

Figure 1. Comparison between a ready-to-use package and source code.

EXPERIMENTAL STUDY OF WASTE HEAT RECOVERY TECHNIQUE TO INCREASE EFFICIENCY AND TO DECREASE HAZARDOUS EMISSIONS IN CI ENGINE

[1] Mr. Janak Rathavi, [2] Mr. Amitesh Paul, [3] Dr. G.R. Selokar

[1]M.Tech. [Thermal Engineering] Student, Department of Mechanical Engg, Shri Satya Sai Institute of Science and Technology, Sehore, Madhya Pradesh

[2]Head of Department, Department of Mechanical Engg., Shri Satya Sai Institute of Science and Technology, Sehore, Madhya Pradesh

[3]Principal, Shri Satya Sai Institute of Science and Technology, Sehore, Madhya Pradesh

Abstract:

The quest for higher efficiencies has spurred the innovation of energy efficient technologies such as waste heat recovery. The recovery and utilization of waste heat not only conserves fuel, usually fossil fuel, but also reduces the amount of waste heat and greenhouse gases dumped to the environment. CI engines exchange approximately 30-40% of heat generated in the process of fuel combustion into useful mechanical work with the current available technology. The remaining heat is emitted to the environment through the exhaust gases (35%) and the engine cooling systems (31%). Experiment show that the boiling point of fossil fuels can be reduced by 50% by preheating. Large part of waste heat exhaust gases can be recovered by vaporizing the fuel through a small heat exchanger. This technical paper shows the experimental results for significant reduction of engine fuel consumption and hazardous emissions could be attained by recovering of exhaust heat by using self made Heat Exchanger. One of the most important issues is to develop an efficient heat exchanger which provides optimal recovery of heat from exhaust gases.

Key words: Emissions, Efficiency, Fuel consumption, Heat Exchanger, Waste Heat Recovery.

I: INTRODUCTION

Energy is an underlying driver of economic growth and social development. Human consumption of energy in the form of fossil fuels, primarily in developed countries, is altering the Earth's climate and has been a matter of great concern. While evidence suggests a need for both demand reduction through energy efficient engine and less harmful emissions.

The internal combustion engines have already become an indispensable and integral part of our present day life style, particularly in the transportation and agricultural sectors unfortunately the survival of these engines has, of late, been threatened due to the problems of fuel crisis and environmental pollution. Therefore, to sustain the present growth rate of civilization, a nonreplicable, clean fuel must be expeditiously sought.

Internal combustion engine convert about 25% to 35% of the chemical energy contained in the fuel into the mechanical energy. About 35% of the heat generated is lost to the cooling medium and the remaining heat is dissipated through the exhaust gases and other radiation losses. During the process of combustion the cylinder gas temperature reaches quite a higher value. A considerable amount of heat is transferred into walls of the combustion chamber. Therefore it is necessary to provide proper cooling specially to walls of the combustion chamber. Inside surface temperature of the cylinder walls will be maintained in ranges, which provides correct clearance between the parts and which promotes vaporization of fuel. After the combustion, heat is transferred to the walls of the combustion chamber, which is continuously removed (almost 30 to 35% of the total heat) by employing a cooling system [1].

While recent improvements in diesel engine design and calibration have greatly reduced both NOx and smoke emissions [2]–[4], there are still many alternatives being researched to improve the engine-out emission further. In recent years, a lot of attention has been focused on air pollution caused by automotive engines. Diesel engines have been particularly targeted for their production of oxides of nitrogen (NOx) and smoke emissions. NOx is formed at high rates when temperatures are high, whereas smoke is formed in fuel rich regions within the combustion chamber [5], [6]. Hence, it is essential to keep the peak cylinder temperature low in order to minimize NOx emission and also to allow for better fuel–air mixing thereby, reducing the smoke emission.

Homogeneous charge compression ignition (HCCI) is a combustion concept that constitutes a valid approach to achieve high efficiencies and low nitrogen oxides and particulate emissions in comparison with traditional compression ignition (CI) direct injection (DI) engines [7]. Although HCCI combustion was demonstrated about 20 years ago, only the recent advances made in airflow, fuel and exhaust gas recirculation (EGR) electronic control have made it feasible. HCCI has been successfully applied both to spark ignition (SI) and compression ignition (CI) engines, and proved to be fuel flexible

since it has been achieved with gaseous fuels such as propane or natural gas, as well as liquid fuels like traditional gasoline or diesel fuels. The HCCI process operates on the principle of having a lean, premixed, homogeneous charge that reacts and burns volumetrically throughout the cylinder as it is compressed by the piston [8].

From the previous research works [9]-[14] it is noticed that early injection, late injection and port fuel injection systems like Air assisted port injection with DI system (PCCI-DI) were used. It is well known that EGR [15]-[18] is a useful way to vary the cylinder gas temperature and the ignition timing could be delayed. In addition to that high levels of EGR and reduced compression ratio were demonstrated for simultaneous and substantial reduction of NOx and smoke emissions. In the above detailed methods the mixture was partially homogeneous. Hence the present system was developed to prepare a homogeneous mixture.

The present work deals with the study of performance, combustion and emission characteristics of diesel vapour combustion process in a DI diesel engine with mixture formation in heat exchanger- accumulator mechanism. In this investigation a stationary four stroke, single cylinder, direct injection diesel engine was modified to operate in dual mode- without diesel vapor mixture and with diesel vapor mixture formation of fuel. A heat exchanger-accumulator mechanism was used to vaporize the diesel fuel and catalytic cracking. It was mounted in the intake system to prepare the homogenous diesel vapour-air mixture. The experiments were conducted with diesel vapour induction with different injection timings. Experimental results obtained are compared with the base line readings. The results show that through this approach simultaneous and substantial reduction of NOx, fuel consumption and smoke emission can be achieved. Also it increases the efficiency of the engine.

II: EXPERIMENTAL WORK

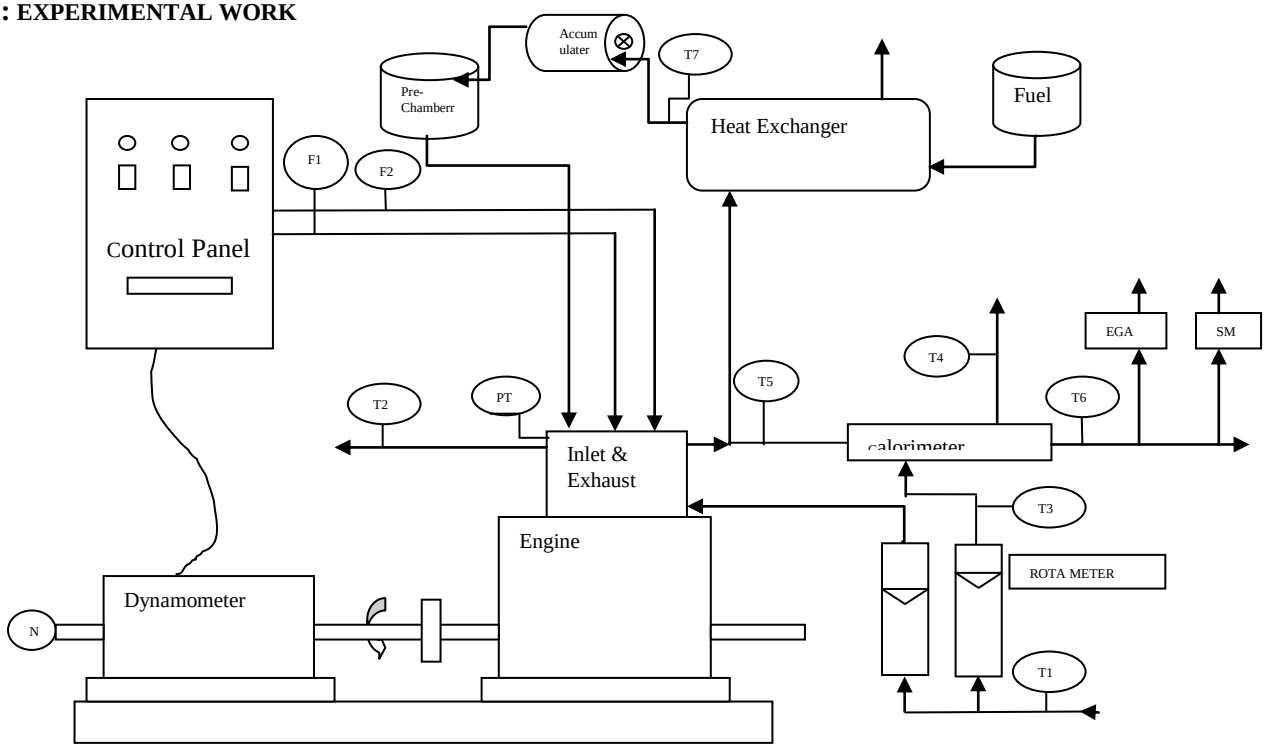

Figure 1: Schematic of the experimental set-up

T1, T3	Inlet Water Temperature	F1	Fuel Flow DP (Differential Pressure) unit
T2	Outlet Engine Jacket Water Temperature	F2	Air Intake DP unit
T4	Outlet Calorimeter Water Temperature	PT	Pressure Transducer
T5	Exhaust Gas Temperature before Calorimeter	N	RPM Decoder
T6	Exhaust Gas Temperature after Calorimeter	EGA	Exhaust Gas Analyzer (5 gas)
T7	Vaporised fuel Temperature after HE	SM	Smoke meter

Experiments were conducted on a modified single-cylinder, water-cooled, direct injection diesel engine developing 5.2 kW at 1500 rpm. Test rig is provided with necessary equipment and instruments for combustion pressure and crank angle

measurements with accuracy. The schematic diagram of the experimental set-up is shown in Figure 1 and Table 1 shows the test rig specifications.

Engine	4-stroke,single cylinder, constant speed, water cooled Diesel Engine
BHP	5.2 kW @ 1500 rpm
Bore x Stroke	87.5 x 110 mm
Compression Ratio	17.5 : 1
Connecting rod	234 mm
Dynamometer type	Eddy current with loading unit
Load Measurement	Strain gauge load cell
Water flow	Rota meter
Fuel and air	Differential pressure unit
Speed measurement	Rotary Encoder

Table 1:- Engine Test Rig Specification

Time taken for fuel consumption was measured with the help of a digital stopwatch with rotameter. Exhaust emission from the engine was measured with the help of gas analyzer, was used to measure the NOx (ppm), CO_2 (%) and UBHC (ppm) emissions in the exhaust. Smoke intensity was measured with the help of a Smoke meter. Fig. 2 shows the schematic of diesel fuel vaporizing heat exchanger.

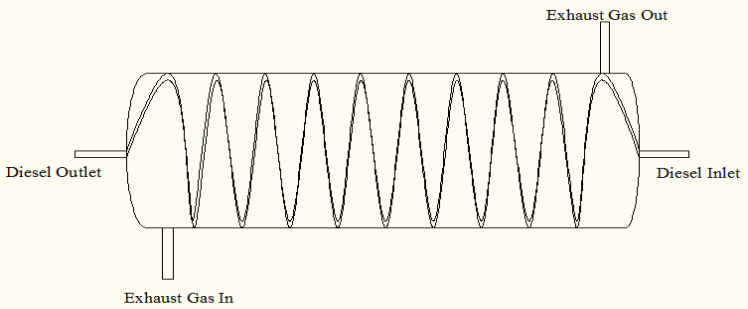

Figure 2: Schematic of Heat Exchanger

The Table 2 represents Specifications of the Heat exchanger.

Sr. No.	Particular	Dimension in mm
1	Diameter	420
2	Length	280
3	Thickness of the cylinder	2
4	Diameter of the copper pipe used	12
5	Length of the copper pipe	2000

Table 2:- Specification of Heat Exchanger

A liquid-gas accumulator is totally covered by the exhaust gases flow and inside the accumulator using catalysts. This is low temperature activating and material of the accumulator is copper which also acting as a catalysts. Both the end of accumulator have one way flapper check valve. One end is connected to the pre-chamber and another end is connected to the heat exchanger. The accumulator has 20mm inner shell diameter and 50mm of outer shell diameter. The accumulator was mounted in the intake manifold system to supply the diesel fuel in vapour form in the intake manifold and it was mixed with the air. The Figure 3 is the real picture of heat exchanger.

Figure 3: Real Picture of Heat Exchanger

III: PERFORMANCE CHARACTERISTICS

1) Brake Thermal Efficiency (BTE):

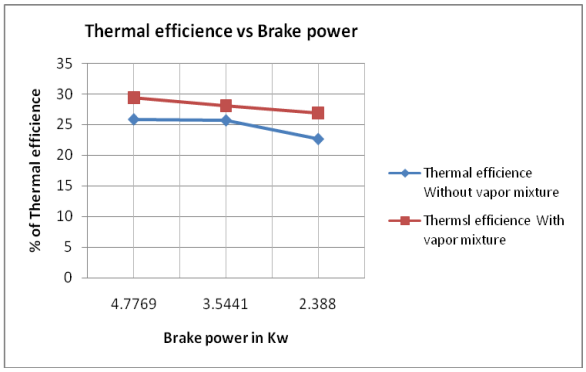

Figure 4: BTE variation of diesel and blend of diesel vapor mixture at 27^0 crank angle IT

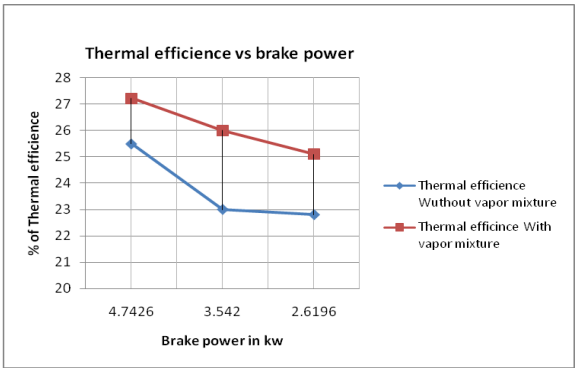

Figure 5: BTE variation of diesel and blend of diesel vapor mixture at 30^0 crank angle IT

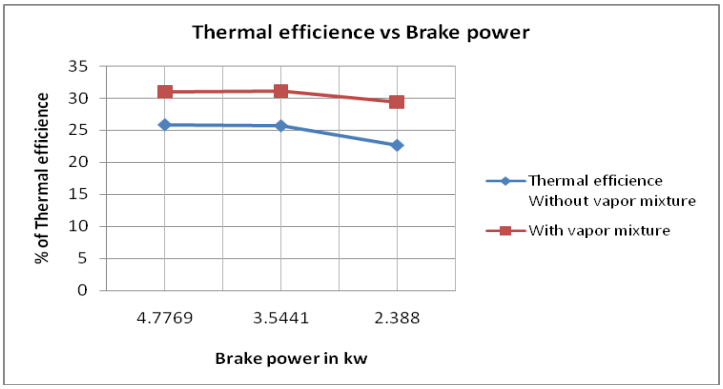

Figure 6: BTE variation of diesel and blend of diesel vapor mixture at 27^0 crank angle IT with DPS

Figure 4 to Figure 6 shows plotted graphs for the variations of Brake Thermal Efficiency with loads at different Injection Timing (IT) for without diesel vapour mixture and with diesel vapour mixture condition at constant flow rate of EGR (4%). It shown in Figure 4 that for 27^0 Injection Timing with respectively 100%, 75% and 50% loads the percentile increment of the brake thermal efficiency for 100% load is 15%, for 75% load is 13% and 50% load is 10% and for 30^0 Injection Timing shown in Figure 5, is 13.6%, 12.12% and 10.9% respectively with loads 100%, 75% and 50%. The third observation of the Brake Thermal Efficiency on 27^0 but the mixing of diesel vapour mixture fuel with air after pre-chamber Direct Port Supply

(DPS), thus percentile increment of the brake thermal efficiency with loads is 19.8%, 12.17%, and 14% respectively shown in Figure 6.

The trend of the graph for all injection timings remains same. The percentage increment of the brake thermal efficiency for 27^0 IT with DPS is more because of mixing of the charge potential is better than to other thus perfect combustion inside the chamber and reduce physical delay for combustion, thus increasing the peak pressure and less fuel consumption.

2) Brake Specific Fuel Consumption (BSFC):

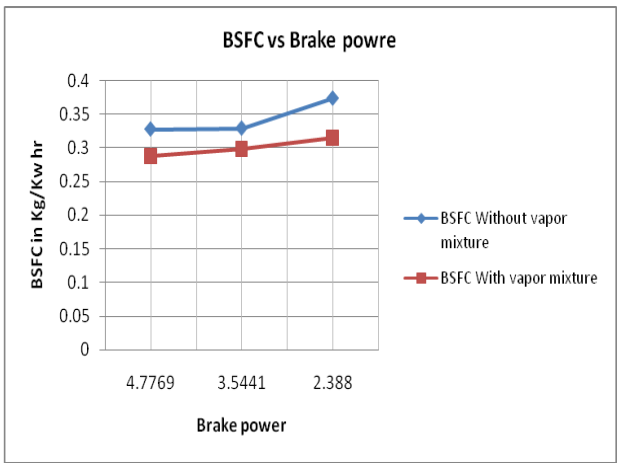

Figure 7: BSFC variation of diesel and blend of diesel vapor mixture at 27^0 crank angle IT

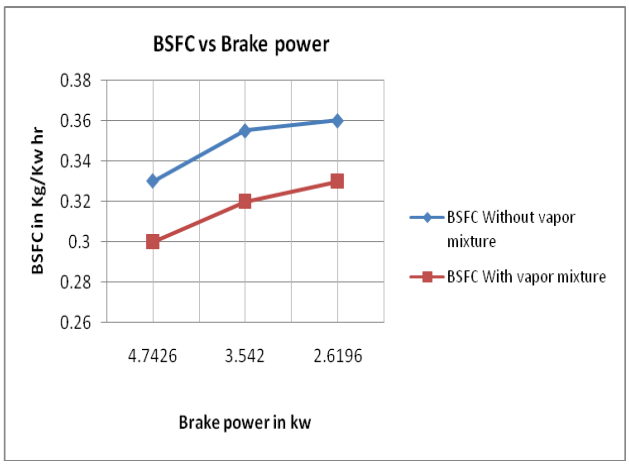

Figure 8: BSFC variation of diesel and blend of diesel vapor mixture at 30^0 crank angle IT

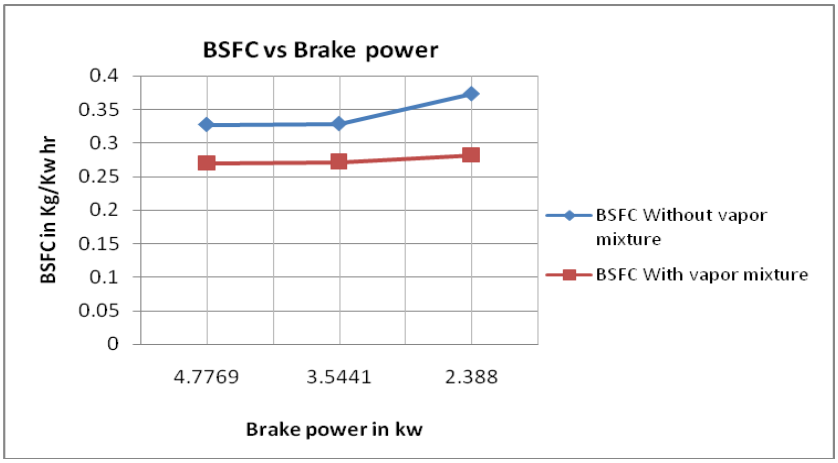

Figure 9: BSFC variation of diesel and blend of diesel vapor mixture at 27^0 crank angle IT with DPS

Observations provided the variation of brake specific fuel consumption as a function of load for diesel vapour mixture at different injection timing. The total bake specific fuel consumption estimated from the brake power output of the engine and it measures mass flow rate of the fuel. The total brake specific fuel consumption affected by mixing of the diesel vapour mixture as shown in Figure 7, 8 and 9 respectively. Percentage of load under dual fuel operation, the brake specific fuel consumption is comparable with normal diesel fuel operation at different injection timing. It is observed that as the % of load increases BSFC decreases by 5.44% for 27^0IT, 15% for 30^0 IT and 14% for 27^0 IT with DPS at 50% to 100% load. According to the trend of graph decrement of the brake specific fuel consumption is 30^0 and 27^0 with DPS, thus 30^0 is optimum condition for BSFC.

3) Exhaust Gas Temperature:

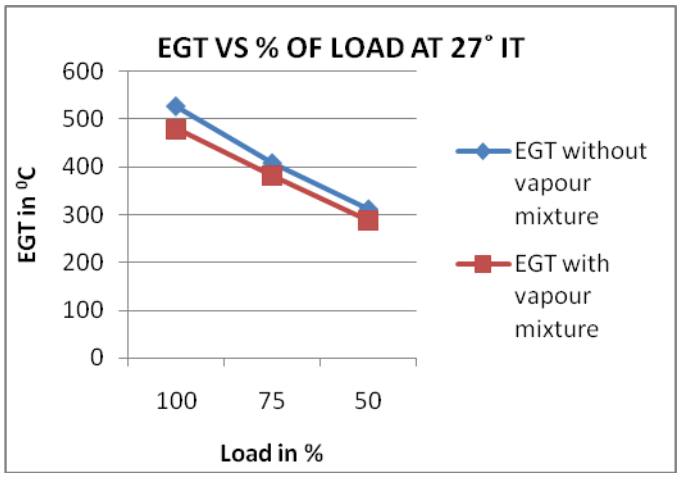

vapor mixture at 27^0 crank angle IT

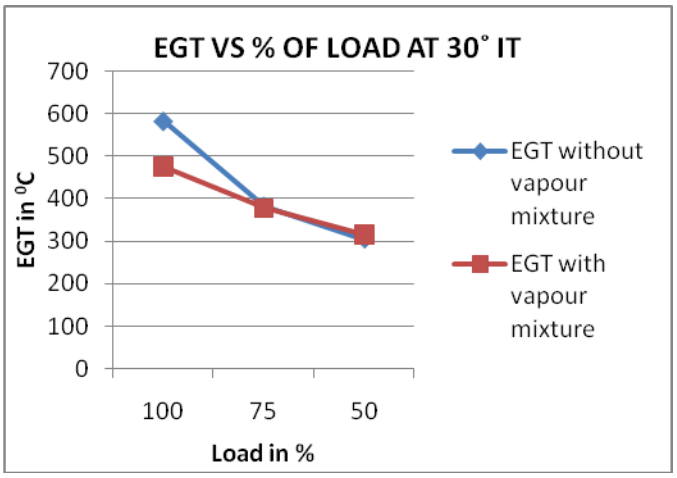

vapor mixture at 30^0 crank angle IT

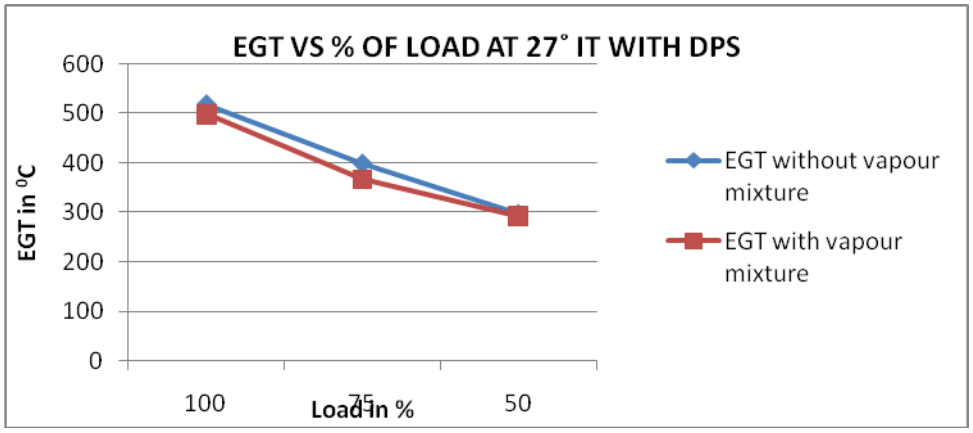

Figure 12: EGT variation of diesel and blend of diesel vapor mixture at 27^0 crank angle IT with DPS

It was found that exhaust gas temperature increase with the load. The effects of the exhaust gas temperature are shown in Figure 10, 11 and 12. From those charts it was also found that exhaust temperature decreases with diesel vapour mixture and EGR for all loads at different injection timing. Because of low temperature nitrogen oxide reduces and heat loss of the engine decreases.

Iv: emission characteristics

1) NO_X Emission:

The variation of NOx with load at different injection Timing for the diesel and diesel vapour mixture by varying load is shown in Figure 13, 14 and 15 respectively. It is observed that the NOx emission for standard diesel fuel has increases from 290ppm to 899ppm in 27^0 injection timing with load vary from 50% to 100% and for diesel vapour mixture NOx is increasing from 230ppm to 455ppm. It reduces 50% in comparison to standard diesel fuel. Same for 30^0 IT it is 679ppm to 1790 ppm for normal diesel and for diesel vapor mixture it is 594.25ppm to 880ppm. For $27^0$with DPS it is 483.75 to 894 for standard fuel and for diesel vapor mixture it is 305ppm to 635ppm respectively with 50% to 100% loads. NOx reduces by reducing the combustion temperature and reaching homogeneous charge of diesel vapor fuel and air inside the chamber and also affected by the 4.0% mixing of the EGR along with vapor mixture.

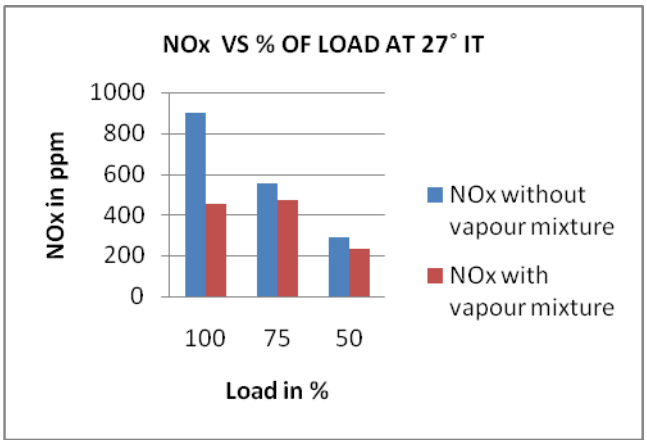

Figure 13: NOx variation of diesel and blend of diesel vapor mixture at 27^0 crank angle IT

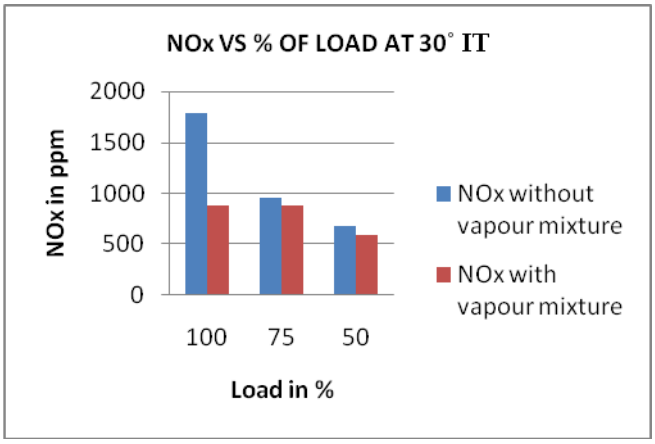

Figure 14: NOx variation of diesel and blend of diesel vapor mixture at 30^0 crank angle IT

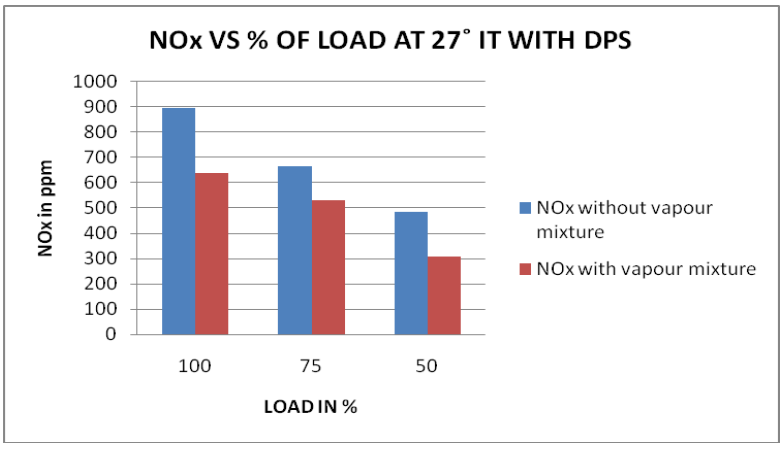

Figure 15: NOx variation of diesel and blend of diesel vapor mixture at 27^0 crank angle IT with DPS

2) Carbon Monoxide (CO) Emission:

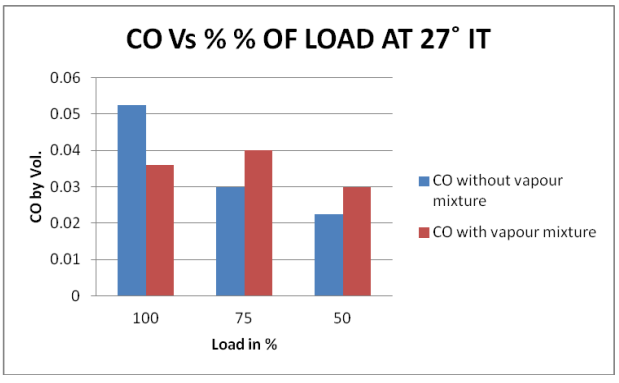

Figure 16: CO variation of diesel and blend of diesel vapor mixture at 27^0 crank angle IT

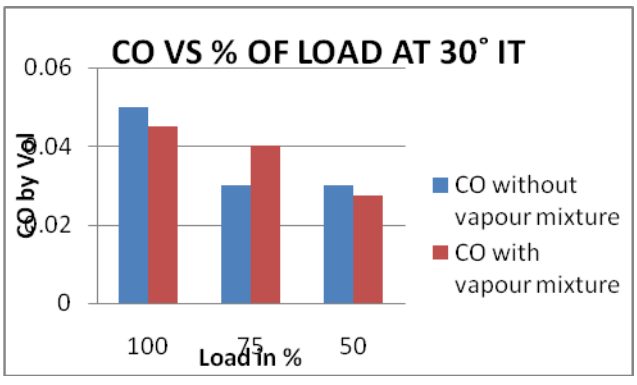

Figure 17: CO variation of diesel and blend of diesel vapor mixture at 30^0 crank angle IT

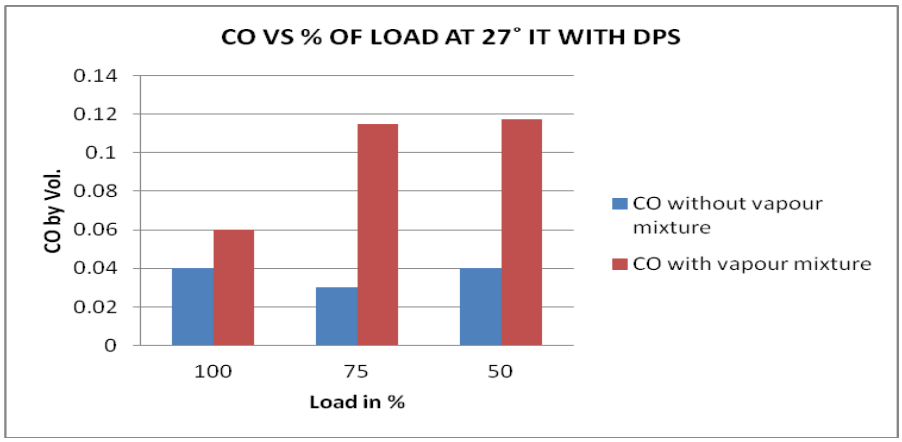

Figure 18: CO variation of diesel and blend of diesel vapor mixture at 27^0 crank angle IT with DPS

The CO emission with load at different injection timing is shown in Fig. 16, 17 and 18. It increases from 50% to 100% load for diesel fuel. It is observed that CO emissions are lower for diesel vapour mixture at 27^0 and 30^0 but its increasing in 27^0 with DPS. The CO emission reduces 20% at full load in 27^0 and 30^0 but it increases 30% in 27^0 DPS. This may be because of reducing the UHC according to increasing load and by mixing of the 4% of EGR along with diesel vapor mixture. It is also affected by lean mixture in combustion.

3) Un-burnt Hydro Carbon Emissions

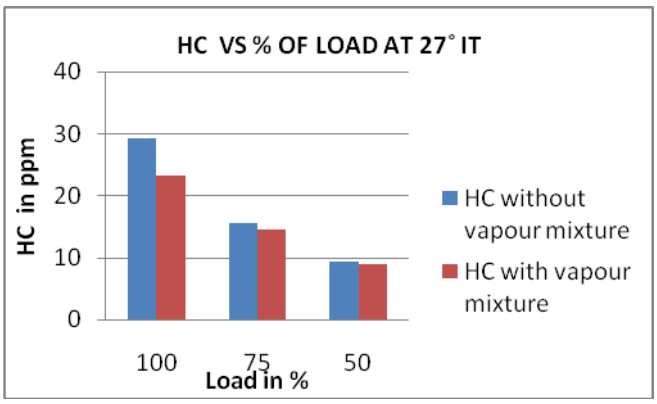

Figure 19: HC variation of diesel and blend of diesel vapor mixture at 27^0 crank angle IT

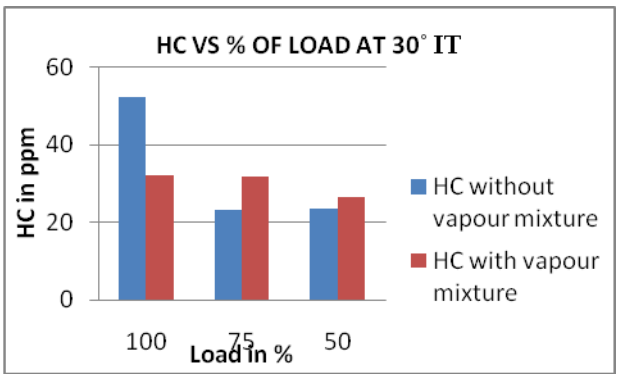

Figure 20: HC variation of diesel and blend of diesel vapor mixture at 30^0 crank angle IT

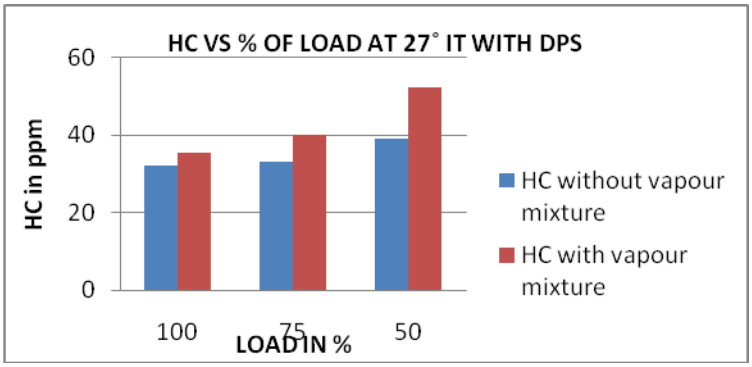

Figure 21: HC variation of diesel and blend of diesel vapor mixture at 27^0 crank angle IT with DPS

The variation of the HC emission with load at different injection timing as shown is Figure 19, 20 and 21. For standard diesel fuel HC emission at different injection timing 27^0,30^0 and 27^0 DPS is 9ppm to 29.25ppm, 23.5ppm to 52.5ppm and 39.2ppm to 32.5ppm respectively, as for the diesel vapour mixture it reduced in 27^0 and 30^0 injection timing but for 27^0 with DPS its increase with 50% load condition. This may because of mixing of EGR and constant flow and low temperature of the combustion chamber.

V: conclusion

The large amount waste heat is through exhaust which has high temperature is utilized to vaporizing the diesel fuel and mixed with intake air thus mixture getting homogeneity. This homogenous charge in compression ignition engine increases the combustion response and reducing the physical delay period so getting increment in combustion pressure develops more power.

1. Vaporizing of fuel by exhaust gas heat that means specific heat of the fuel is getting increases so less fuel consumption and perfect combustion carried out because the fuel gets ignited at multipoint, and thus no flame propagation in combustion chamber which causes less emission.
2. Brake thermal efficiency in the case of diesel vapor mixture, percentile increment of engine thermal efficiency is 15% at full load 27^0 injection timing, 13% at 30^0IT and 19.8% for 27^0DPS. In case of 27^0 DPS thermal efficiency is high with compared to other cases, it may because of perfect mixing of homogeneous charge and air fuel ratio.
3. Brake specific fuel consumption (BSFC):
   It is observed that as the % of load increases BSFC decreases by 5.44% for 20^0, 15% for 30^0 and 14% for 27^0 with DPS for 50% load to 100% load range. According to the graph trend it shows the decrement of brake specific fuel consumption for 30^0 and 27^0 with DPS. Thus 30^0 IT is optimum condition for BSFC.
4. NOx Emissions was reduced with diesel vapor mixture. It is because of reduced combustion temperature. It has reduced up to 50% at full load due to mixing 2.2% of EGR. At $27^0$with DPS the NOx is 894ppm to 635ppm and at 27^0 and 30^0 it is 899ppm to 455ppm, 1790pmm to 880ppm respectively.
5. Carbon monoxide (CO) is lower for diesel vapour mixture at 27^0 and 30^0 but its increases in 27^0 with DPS. The CO emission reduces about 20% at full load in 27^0 and 30^0 but it increases 30% in 27^0 DPS. This is because of insufficient oxygen inside the combustion chamber.
6. Here the opacity increases from 9% for 30^0, 10.34% for 27^0 and 13% for 27^0DPS injection timing. This is because EGR reduces availability of oxygen for combustion of fuel which results in incomplete combustion and increases formation PM. The smoke opacity for diesel vapour mixture is higher than diesel fuel.
7. The exhaust gas temperature is reduced because of reducing the NOx emission and cylinder pressure is increases 2 to 4 bar. Thus work output is increases and this results increased thermal efficiency.
8. Energy captured by this modification is 308.349KJ/hr from 20-30% exhaust gases.

Thus the advantage of diesel vapors combustion with the recovering the waste exhaust gas heat was utilized to get the benefits of low emissions and saving in fuel consumption through high efficiency at different load conditions.

Vi: references

[1] M L Mathur and R P Sharma, “INTERNAL COMBUSTION ENGINE”, first edition reprint, Danpat rai publication (p) Ltd. New Delhi India 2003.

[2] Sher E, Bar-Kohany T. Optimization of variable valve timing for maximizing performance of an unthrottled SI engine—a theoretical study. Energy 2002;27:757–75.

[3] Iwazaki K, Amagai K, Arai M. Improvement of fuel economy of an indirect injection (IDI) diesel engine with two-stage injection. Energy 2005;30:447–59.

[4] Papagiannakis RG, Hountalas DT. Combustion and exhaust emission characteristics of a dual fuel compression ignition engine operated with pilot diesel fuel and natural gas. Energy Convers Manage 2004;45:2971–87.

[5] Dec JE. Advanced compression ignition engines–understanding the incylinder processes. In: Proc. Combust. Inst, vol. 32; 2009. p. 2727–42.

[6] Akihama K, Takatori Y, Inagaki K, Sasaki S, Dean AM. Mechanism of the smokeless rich diesel combustion by reducing temperature, SAE paper no 2001-01-0655; 2001.

[7] Aceves SM, Flowers DL, Frias JM, Smith JR, Dibble R, Au M, Girard J., "HCCI combustion: analysis and experiments", SAE Paper, 2001–01–2077,2001

[8] Ryan TW, Callahan TJ, "Homogeneous charge compression ignition of diesel fuel", SAE Paper 961160, 1996

[9] Thring RH. Homogeneous-charge compression ignition (HCCI) engines. SAE Paper No 892068. Warrendale, PA: Society of Automotive Engineers Inc; 1989.

[10] Yanagihara H. Ignition timing control at Toyota ''unibus'' combustion system. A new generation of engine combustion processes for the future. In: Proceedings of the IFP international congress; 2001. p. 34–42.

[11] Shi Lei, Cui Yi, Peng Kangyao, chen Yuanyuan. Study of low emission homogeneous charge compression ignition (HCCI) engine using combined internal and external exhaust gas recirculation (EGR). Energy 2006;31:2665–76.

[12] Simescu Stefan, Fiveland Scott B, Dodge Lee G. An experimental investigation of PCCI-DI combustion and emissions in a heavy-duty diesel engine, SAE paper no 2003-01-0345.

[13] Ryan III TW, Callahan TJ. Homogeneous charge compression ignition of diesel fuel, SAE paper no 961160; 1996.

[14] Midlam-Mohler Shawn, Guezennec Yann, Rizzoni Giorgio. Mixed-mode diesel HCCI with external mixture formation. DEER 2003 Newport; August 26th 2003.

[15] Duret P, Gatellier B,Monteiro L, Zima P, Maroteaux D, Blundell D, et al. Progress in diesel HCCI combustion within the european space light project, SAE paper no 2004-01-1904; 2004.

[16] Stein J, Du¨ rnholz M, Wirbeleit F, Kopp C, Benz C. Homogeneous dieselmotorische verbrennung zur darstellung niedrigster emissionen. [Homogeneous diesel engine combustion for achieving minimum emissions]. In: 13th Aachen colloquium on vehicle and engine technology; 2004 www.iav.com.

[17] Puschmann Heike, Buchwald Ralf, Pannwitz Marcel, Sommer Ansgar. Homogeneous diesel combustion with external mixture formation by a cool flame vaporizer, SAE paper no 2006-01-3323; 2006.

[18] Maiboom Alain, Tauzia Xavier, He´ tet Jean-François. Experimental study of various effects of exhaust gasrecirculation (EGR) on combustion and emissions of an automotive direct injection diesel engine. Energy 2008;33:22–34.

Author's Addresses:

MR.JANAK RATHAVI
22, Shardanagar Society-2, 80 foot Road, Behind Madhuvan Pan Center, Wadhwan city-363035. Dist.: Surendranagar- (Gujarat)

MR. AMITESH PAUL
Shri Satya Sai Institute of Science and Technology, SH-18, Indore-Bhopal Road, Pachama, District: Sehore, M.P-466002

DR. G.R. SELOKAR
Shri Satya Sai Institute of Science and Technology, SH-18, Indore-Bhopal Road, Pachama, District: Sehore, M.P-466002